Dissecting Physiological Temperature Responses in Arctic Marine Microalgae

2025

Linda Rehder

Dissecting Physiological Temperature Responses in Arctic Marine Microalgae

Dissertation zur Erlangung des akademischen Grades eines Doktors der Naturwissenschaften

Dr. rer. nat

Am Fachbereich 2

Der Universität Bremen

Linda Rehder

Januar 2025

Kolloquium: 05.03.2025

Examination Committee

1. Examiner: Prof. Dr. Christian Wild
   University of Bremen

2. Examiner: Dr. Maren Striebel
   Carl von Ossietzky University of Oldenburg

1. Reviewer (and examiner): Prof. Dr. Björn Rost
   University of Bremen; Alfred-Wegener-Institute Bremerhaven, Helmholtz
   Center for Polar Marine Research

.

2. Reviewer: Prof. Dr. Elisa Schaum
   University of Hamburg

3. Reviewer (and examiner): Prof. Dr. Peter Kroth
   University of Constance

"Research is to see what everybody else has seen, and to think what nobody has thought."

(Albert Szent-Gyorgyi, Nobel Prize winner in medicine, 1937)

Acknowledgements/Danksagung

List of Abbreviations

AEF	Alternative electron flow
ADP	Adenosine diphosphate
AOX	Alternative oxidase
ATP	Adenosine triphosphate
BCP	Biological carbon pump
BPG	1,3-Bisphosphoglycerate
CCM	Carbon concentrating mechanism
CEF	Cyclic electron flow
Chl a	Chlorophyll a
Cyt	Cytochrome
DIC	Dissolved inorganic carbon
ETC	Electron transport chain
ETR	Electron transport chain
$FADH_2$	Flavin-adenine-dinucleotide
Fd	Ferredoxin
FNR	Flavoprotein-ferredoxin-NADP-reductase
FRRf	Fast repetition rate fluorometry
Fv/Fm	Maximum quantum yield of photosystem II
G3P	Glyceraldehyde-3-phosphate
I_k	Light acclimation index
LHC	Light harvesting complex
MIMS	Membrane-inlet mass-spectrometry
NAD(P)H	Nicotinamide adenine dinucleotide (phosphate)
OEC	Oxygen evolving complex
Phae	Phaeophytin
PMF	Proton motive force
POC	Particulate organic carbon
Pq	Plastoquinone
PQ	Photosynthetic quotient

PTOX	Plastid terminal oxidase
PSII or PSI	Photosystem I or II
PS680 or PS700	Reaction center of PSII or PSI
RCP	Representative concentration pathway
ROS	Reactive oxygen species
RQ	Respiratory quotient
RuBisCO	Ribulose-1,5-bisphosphat-carboxylase/-oxygenase
RuBP	Ribulose-1,5-bisphosphat
SST	Sea surface temperature
TCA	Tricarboxylic acid cycle
3PG	3-phospoglycerate
τ	PSII re-opening time
σ_{PSII}	Absorption cross section of the PSII antenna complex
a	Light use efficiency
μ	Specific growth rate

Table of Content

Summary

The Arctic Ocean is most prone to climate change, which exposes marine organisms to especially high degrees of ocean warming. Phytoplankton, the main primary producers of the Arctic Ocean, experience thermally induced changes in their physiology, and these impacts will likely propagate up the food web and have severe effects on marine biogeochemical cycling. The objective of this dissertation was to unravel how Arctic phytoplankton responds to different warming scenarios with a special emphasis on their underlying physiology. To achieve this, I used a combination of single-strain phytoplankton incubation experiments, including detailed physiological characterizations, and incubation experiments with natural Arctic phytoplankton communities to substantiate overarching temperature responses of phytoplankton physiology also on an ecologically more relevant level.

Publication I aimed to assess temperature response patterns of multiple functional traits in Arctic key phytoplankton species. To this end, I cultivated the centric diatom *Thalassiosira hyalina*, the mixotrophic picoeukaryote *Micromonas pusilla* and the ice-algae *Nitzschia frigida* over a temperature gradient from 0°C to 14°C and measured growth rates, biomass production, quotas of biomass and pigmentation as well as photophysiology. Next to surprisingly high optimal growth temperatures and maximal growth rates in all species, it was found that thermal sensitivities and optimal temperatures varied among species and functional traits. This resulted in distinct temperature response patterns of physiological processes such as cell division and biomass production, with their interplay ultimately shaping distinct temperature response patterns of biomass quotas.

Publication II aimed to identify hypothesized physiological imbalances between photosynthetic and respiratory sub-processes under warming. I further intended to understand how fundamental regulatory mechanisms adjust physiology to explain the high phenotypic plasticity of Arctic phytoplankton in response to increasing temperatures. To this end, I assessed photophysiological characteristics of photosystem II (PSII) as well as gas fluxes of $^{18}O_2$, $^{16}O_2$ and CO_2 corresponding to photosynthetic O_2 production and C-fixation as well as respiratory CO_2 release and O_2 consumption in *T. hyalina* at distinct temperatures (2°C, 6°C and 10°C) using fast repetition rate fluorometry (FRRf) and membrane-inlet mass-spectrometry (MIMS). I found two major regulatory strategies of *T. hyalina* to acclimate to increasing

temperatures. First, *T. hyalina* cells upregulated their light harvesting abilities to compensate for detrimental temperature effects on PSII efficiency, which made cells more prone to light-limitation. Thereby, cells were able to maintain their absolute electron transport rates per PSII, resulting in unchanged O_2 production. Second, I found that a metabolic coupling between chloroplasts and mitochondria was essential for cells to dissipate excess reductant towards mitochondrial processes, which was even more prominent under warming. In this situation, the plastidial reductants fueled the mitochondrial electron transport chain directly, which in turn resulted in a redox-mediated downregulation of the respiratory CO_2 release, which consequently maximized net biomass retention of the whole cell.

Finally, *Publication III* and *IV* aimed to understand how temperature affects phytoplankton physiology on the level of natural Arctic phytoplankton communities. To this end, communities from the open-ocean Fram Strait (*Publication III*) and a coastal fjord system in Svalbard (*Publication IV*) were incubated under similar temperature and light conditions as in *Publication II*. Biomass accumulation, O_2 fluxes of photosynthesis and respiration, photophysiology as well as community composition were assessed using a ship-going MIMS system or O_2 optodes, FRRf as well as rRNA 18s metabarcoding, respectively. Both communities exhibited a stimulated net biomass retention under warming scenarios, despite a lowered net O_2 production, due to strongly increasing respiratory O_2 consumption. These responses were not accompanied by distinct species shifts, e.g. towards more heterotrophic communities, indicating that the opposing temperature responses of O_2- and C-fluxes in the communities were likely a result of the same physiological regulatory mechanisms as observed in the single-strain experiment.

Findings from single-strain as well as community experiments strongly indicate that a metabolic coupling of chloroplasts and mitochondria is a fundamental mechanism across communities to plastically respond to ocean warming, that allows Arctic phytoplankton to thrive under increasing temperatures. In line with this, all *Publications* also revealed that optimal temperatures for growth and biomass production exceeded those in the present Arctic Ocean, suggesting a stimulation of biomass accumulation at least under moderate warming. Data of photophysiological assessments further signify synergistic beneficial effects on photosynthetic processes under a combined increase of temperature and light intensity, as it is projected for the future Arctic Ocean.

Zusammenfassung

Der Klimawandel zeigt sich besonders stark im Arktischen Ozean, sodass Meeresorganismen insbesondere hier einer starken Erwärmung ausgesetzt sind. Phytoplankton als die wichtigsten Primärproduzenten des Arktischen Ozeans erfahren folglich temperaturbedingte Veränderungen in ihrer Physiologie. Die daraus resultierenden Auswirkungen breiten sich potentiell über das Nahrungsnetz aus und können schwerwiegende Auswirkungen auf das gesamte Ökosystem haben. Ziel dieser Dissertation war es, zu untersuchen, wie arktisches Phytoplankton auf verschiedene Erwärmungsszenarien reagiert, wobei der Schwerpunkt dabei auf der zugrunde liegenden Physiologie lag. Ich habe Inkubationsexperimente mit einzelnen Phytoplankton Arten, sowie mit natürlichen arktischen Phytoplankton Gemeinschaften kombiniert, um übergreifende Temperaturreaktionen der Phytoplankton Physiologie sowohl im hochaufgelösten Prozessverständnis als auch in einem ökologisch relevanteren Kontext zu untersuchen.

In *Publikation I* habe ich die Temperaturabhängigkeit verschiedener funktioneller Eigenschaften in Arktischen Schlüsselarten untersucht. Dafür wurden die zentrische Kieselalge *Thalassiosira hyalina*, die mixotrophe Grünalge *Micromonas pusilla* und die Eisalge *Nitzschia frigida* über einen Temperaturgradienten von 0°C bis 14°C kultiviert und Messungen von Wachstumsraten, Produktionsraten, Biomasse- und Pigmentierungsquoten sowie Fotophysiologie wurden durchgeführt. Neben überraschend hohen optimalen Wachstumstemperaturen und maximalen Wachstumsraten bei allen Arten wurde festgestellt, dass die thermische Sensivität und die optimalen Temperaturen sowohl zwischen den Arten als auch zwischen den verschiedenen funktionellen Eigenschaften variieren. Dies führte zu unterschiedlichen Temperaturkurven oder -mustern bei physiologischen Prozessen, wie beispielsweise der Zellteilung und der Biomasseproduktion, wobei deren Zusammenspiel letztlich zu unterschiedlichen Konstellationen der Biomassequoten führte.

Publikation II zielte darauf ab, angenommene physiologische Dysbalancen zwischen fotosynthetischen und respiratorischen Teilprozessen unter Erwärmung zu beleuchten. Außerdem wurde untersucht, wie grundlegende Regulationsmechanismen eine physiologische Anpassung an höhere Akklimationstemperaturen ermöglichen, um die hohe phänotypische Plastizität von Arktischem Phytoplankton unter Erwärmung besser zu verstehen. Zu diesem Zweck

Zusammenfassung

wurden Messungen von fotophysiologischen Eigenschaften über Fluorometrie (FRRf) sowie von zellulären $^{18}O_2$-, $^{16}O_2$- und CO_2-Gasflüssen über Membran-Einlass-Massenspektrometrie (MIMS) durchgeführt, wodurch fotosynthetische O_2-Produktion und C-Fixierung sowie respiratorische CO_2-Freisetzung und O_2-Verbrauch in der Kieslealge *T. hyalina* bei verschiedenen Temperaturen quantifiziert werden konnten. Dabei konnten dabei wichtige Regulationsstrategien von *T. hyalina* zur Anpassung an steigende Temperaturen identifiziert werden. Zum einen steigert *T. hyalina* ihre Fähigkeit zur Lichternte, indem sie Antennenkomplexe des Lichterntekomplexes vergrößern. Dies kompensiert eine verringerte PSII-Effizienz, welche die Folge einer temperaturbedingten Lichtlimitierung war. Den Zellen wird so ermöglicht, ihre absoluten Elektronentransportraten pro PSII beizubehalten, was wiederum eine unveränderte O_2-Produktion erlaubt. Darüber hinaus, konnte eine metabolische Kopplung zwischen Chloroplasten und Mitochondrien bestätigt werden, welche überschüssige Reduktionsequivalente in mitochondriale Prozesse umleitet, um eine übermäßige Reduktion der Chloroplasten zu vermeiden. Dieser Mechanismus war besonders unter Erwärmung ausgeprägt und hatte zur Folge, dass die mitochondriale oxidative Phosphorylierung hauptsächlich über den Chloroplasten versorgt wurde. Folglich änderte sich die mitochondriale Redoxbalance und die CO_2-Freisetzung des Zitronensäurezyklus wurde minimiert, was wiederum eine Maximierung der Netto Produktion von Biomasse zur Folge hatte.

Die *Publikationen III* und *IV* zielten schließlich darauf ab zu verstehen, wie Temperatur die Physiologie von Phytoplankton auf einer höheren Ebene in natürlichen arktische Phytoplanktongemeinschaften beeinflusst. Dafür wurden Gemeinschaften aus der Framstraße (*Publikation III*) und einem Fjordsystem in Svalbard (*Publikation IV*) unter ähnlichen Temperatur- und Lichtbedingungen wie *in Publikation II* inkubiert. Biomasseakkumulation, O_2-Flüsse von Fotosynthese und Respiration, Fotophysiologie sowie die Artenzusammensetzung der Phytoplanktongemeinschaften wurden mit einem schiffseigenen MIMS-System bzw. O_2-Optoden, FRRf und rRNA 18s Metabarcoding untersucht. Beide Gemeinschaften wiesen unter Erwärmungsszenarien eine stimulierte Nettobiomasseretention auf, trotz einer geringeren Netto-O_2-Produktion, die auf einen stark zunehmenden respiratorischen O_2-Verbrauch zurückzuführen war. Diese Reaktionen gingen nicht mit deutlichen Artenverschiebungen einher, was darauf hindeutet, dass die gegensätzlichen Temperaturreaktionen der O_2- und C-Flüsse in den Gemeinschaften auf dieselben

physiologischen Regulationsmechanismen zurückzuführen sind, wie sie in *T. hyalina* beobachtet wurden.

Folglich deuten alle erhobenen Daten sowohl aus dem detaillierten Einzelartenexperiment als auch aus den Experimenten mit natürlichen Artengemeinschaften stark darauf hin, dass die metabolische Kopplung von Chloroplasten und Mitochondrien ein grundlegender Mechanismus von Arktischem Phytoplankton ist, um plastisch auf Ozeanerwärmung zu reagieren, und gegebenenfalls sogar davon zu profitieren. Im Einklang damit zeigten alle Publikationen auch, dass die optimalen Temperaturen für Wachstum und Biomasseproduktion grundsätzlich über denen im heutigen Arktischen Ozean liegen, was auf eine Stimulierung der Biomasseakkumulation zumindest unter moderater Erwärmung hindeutet. Die Daten der fotophysiologischen Untersuchungen deuten außerdem auf synergistische positive Effekte fotosynthetischer Prozesse bei einem kombinierten Anstieg von Temperatur und Lichtintensität hin, wie er für den Arktischen Ozean in der Zukunft prognostiziert wird.

1 Introduction

1.1. The Arctic Ocean under Climate Change

1.1.1. Global warming

The Earth´s temperature is controlled by solar incoming and outgoing longwave radiation. This balance depends on many factors, such as natural and anthropogenic greenhouse gases, atmospheric aerosols, surface albedo or land use patterns (Hartmann *et al.*, 1986; Liang, S *et al.*, 2019). Without natural greenhouse gases such as water vapor and CO_2, less of the outgoing longwave radiation would be absorbed in the atmosphere and surface temperatures would be as low as -18°C (Le Treut *et al.*, 2007). Since pre-industrial times, however, anthropogenic greenhouse gas emissions have drastically increased through fossil fuel combustion and land-use changes, resulting in the release of carbon dioxide (CO_2), which accounts for fossil emissions of ~10 Gt C yr^{-1}. These perturbations in the carbon cycle have caused the atmospheric CO_2 concentration to increase from ~280 ppm in 1850-1900 to ~420 ppm today (Friedlingstein *et al.*, 2023). As a consequence, the absorption of longwave radiation strongly increases, ultimately resulting in rising Earth´s surface air temperatures (Legg, 2021), which already experienced an average increase of 1.1°C compared to pre-industrial temperatures (Lee *et al.*, 2023).

Future projections of the increase of greenhouse gas concentrations are described by representative concentration pathway (RCP), which represent different emission scenarios (van Vuuren *et al.*, 2011). RCP2.6, for example, is a very stringent pathway of low emissions and high mitigation, so that global surface temperature increases until 2100 would be limited to 2°C compared to the average temperature in 1850-1900. RCP8.5, in contrast, represents the highest emission scenario without mitigation, were the average warming would exceed 4°C in the same time frame (Fig. 1a; Lee *et al.*, 2023). The magnitude of future warming highly depends on ongoing net anthropogenic greenhouse gas emissions, which are controlled by political decision making and global action (Harrison & Sundstrom, 2007; Weber, 2010).

The oceans are capable to take up ~3 Gt C yr^{-1} of fossil CO_2 emissions (Friedlingstein *et al.*, 2023), and by removing ~25% of the total anthropogenic emissions they function as a large CO_2 sink for the atmosphere. This results, however, in a shifted oceanic carbonate system with decreasing pH values (Fig. 1b), a phenomenon called ocean acidification and which especially affects calcifying organisms (Riebesell *et al.*, 2000;

Zeebe & Wolf-Gladrow, 2001; Doney *et al.*, 2009). Furthermore, large proportions (>90%) of the accumulated atmospheric heat are taken up by the oceans, which increases the sea surface temperatures (SSTs) and underlines their function as a strong buffer system on our climate (Fig. 1c; Lee *et al.*, 2023). The SSTs are rising slower than the air temperature, and yet, they already increased by 0.68 to 1.01°C since pre-industrial times and are projected to further rise by ~0.2°C on average per decade, depending on the RCP scenario.

In addition to long-term ocean warming, short-term extreme events, such as marine heatwaves, have become more frequent, longer-lasting and more intense during the past decades and are projected to expand under ongoing climate change (Fig. 1e; Hobday *et al.*, 2016). Marine heatwaves are discrete warming events of anomalously elevated temperatures for ≥ 5 days, which are driven by multiple factors, such as air-sea heat fluxes, ocean heat advection or large-scale climate variability (Oliver *et al.*, 2019).

The increase of SSTs has far-reaching effects on multiple other properties of the oceans: Sea levels are rising due to expanding water masses as well as melt of ice sheets and glaciers with strong impacts especially on densely populated coastal areas (Horwath *et al.*, 2021). With warming, hypoxic O_2 minimum zones expand, especially in tropical regions (Fig. 1d; Keeling *et al.*, 2010). A temperature-induced increase in oceanic stratification results in a shallower mixed layer depth, decreased nutrient availability as well as higher mean irradiance in the surface layer. A reduced vertical mixing, in turn, decreases the ability to take up atmospheric heat, which will result in an increase of weather extremes such as cyclones (Lee *et al.*, 2023). Furthermore, contrasts in oceanic salinity increase due to regionally higher evaporation or rainfalls, increased sea ice or glacial melt, i.e. high salinity regions become saltier and low salinity regions become fresher, which in turn further enhances stratification (Cheng *et al.*, 2020).

Ocean warming and the described indirect consequences will strongly affect marine organisms, e.g. in their metabolism and behavior. There are indications for poleward expansion of organisms such as Atlantic cod or North Atlantic phytoplankton (Dahlke *et al.*, 2018; Oziel *et al.*, 2020; Priest *et al.*, 2023), changes of phenology, i.e. the seasonal dynamics of biological life cycles, or increased risk of death and local extinction (Doney *et al.*, 2012). Additionally marine heatwaves expose organisms also

to fast changing temperature fluctuations, potentially pushing them temporarily beyond thermal limits (Frölicher *et al.*, 2018). Marine heatwaves also amplify the effects of enhanced stratification, e.g. changes in nutrient availability, which in combination with the extreme short-term warming can cause e.g. population shifts of marine species, mass mortality especially of non-motile species (Garrabou *et al.*, 2022) or exacerbation of harmful algae blooms (Trainer *et al.*, 2020). Consequently, these short- and long-term temperature increases can have cascading effects for the entire marine ecosystem, including various kinds of marine resources also relevant for human economy (Kumar *et al.*, 2012; Smith *et al.*, 2021).

Past and future changes in the ocean and cryosphere
Historical changes (observed and modelled) and projections under RCP2.6 and RCP8.5 for key indicators

Historical (observed) — Historical (modelled) — Projected (RCP2.6) — Projected (RCP8.5)
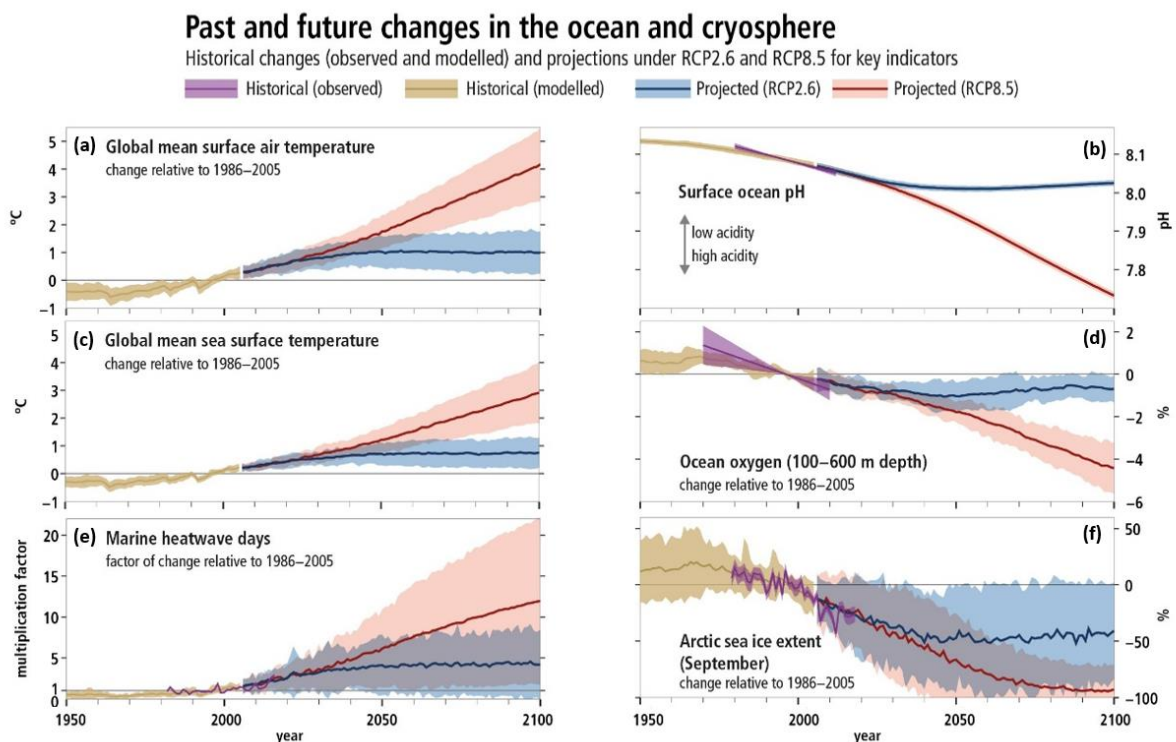
Fig 1. Changes of the ocean and cryosphere in the past corresponding to observed (purple) and modelled (yellow) data as well as in the future corresponding to the representing concentration pathways (RCP) 2.6 (blue) and 8.5 (red) relative to 1986-2000. (a) The global mean air temperature, the surface ocean pH, (c) global mean surface temperature, (d) ocean oxygen at a depth of 100-600 m, (e) days of marine heatwaves and (f) the Artic sea ice extent in September. Modified after Legg (2021).

1.1.2. The Arctic Ocean

The Arctic Ocean is the smallest, shallowest and northernmost of the five global oceans of our planet and comprises unique characteristics (Klenke & Schenke, 2002). It is almost completely land-locked, i.e. it is surrounded by coastal boundaries with only few major in- and outflows of water masses. Especially the coastal areas are directly

influenced by riverine and glacial freshwater run-off as well as mineral and trace metal discharge as numerous large rivers end in the Arctic Ocean (Carmack *et al.*, 2016; Solomon *et al.*, 2021). Furthermore, the light conditions in the Arctic are extreme due to the presence of polar day and night, i.e. 24h of daylight in summer and 24h of total darkness in winter, respectively. This forces especially primary producers to involve metabolic strategies to withstand months of darkness without phototrophic energy generation in winter (Berge *et al.*, 2015; Walter *et al.*, 2017; Hoppe *et al.*, 2024), but also to handle full daylight in summer. Large parts of the Arctic Ocean are covered by sea ice, which changes in its extent on seasonal time-scales but generally decreases by ~11% per decade due to climate change (Stroeve & Notz, 2018). Also the thickness of sea ice decreases, and thin first-year sea ice largely replaces thick multiyear sea ice (Kwok, 2018). This induces seasonal changes in salinity and also affects the light climate of the surface ocean layer.

The Arctic Ocean is one of the regions on our planet that is most prone to climate change, due to a decrease of the Arctic Oceans´ surface albedo, which is the proportion of incoming solar radiation reflected back to the atmosphere. Multi-year sea ice with snow coverage reflects up to 90%, while the open ocean reflects less than 20%, but absorbs a large fraction of radiation, which increases surface warming (Perovich & Polashenski, 2012). As a consequence, the ocean warming-induced decrease of sea ice extent and thickness amplify warming rates in the Arctic, which again results in stronger warming-induced effects on sea ice. This process is called polar amplification and is the driver behind the ~3-4-fold higher warming rates in the Arctic (Constable *et al.*, 2022; Rantanen *et al.*, 2022). Through diverse feedback loops, also other climate change drivers are thus more pronounced in polar areas, making the Arctic an ideal habitat to study climate change effects on marine ecosystems.

1.2. Phytoplankton and the biological carbon pump

1.2.1. Phytoplankton diversity

Phytoplankton are aquatic unicellular phototrophic organisms that significantly contribute to primary production and have evolved in multiple different taxonomic groups of eukaryotic microalgae such as diatoms, haptophytes, dinoflagellates or chlorophytes and prokaryotic cyanobacteria (Fig. 2; Simon *et al.*, 2009), all together composing at least 25,000 different species (Falkowski & Raven, 2013). Microalgae cover all aquatic ecosystems (limnic or marine) from polar to tropical waters, they can

live in pelagic, coastal or benthic ecosystems and can even thrive in extreme environments such as sea ice or snow habitats (Hoham & Remias, 2020; Niemi *et al.*, 2024). The different taxonomic groups of eukaryotic phytoplankton divide into various functional types, depending on their e.g. morphology or trophic mode (Litchman *et al.*, 2015; Chakraborty *et al.*, 2017). Phytoplankton can appear in diverse morphological shapes and their size ranges between <1 µm to <40 µm (Sournia, 1982; Chisholm, 1992; Naselli-Flores *et al.*, 2007). Many groups are moreover motile due to raphes or flagella, some form chains or colonies, and build silicate frustules or calcify (Visser & Kiørboe, 2006; Lana *et al.*, 2011; Van Donk *et al.*, 2011). Furthermore, many phytoplankton species are not necessarily exclusively photoautotrophic, but can also live mixotrophic or heterotrophic, i.e. they can also take up organic carbon and nutrients instead of relying only on photosynthesis (Mitra *et al.*, 2014; Stoecker *et al.*, 2017). All these different functions affect the impact of microalgae on biogeochemical cycling and ecosystem services.
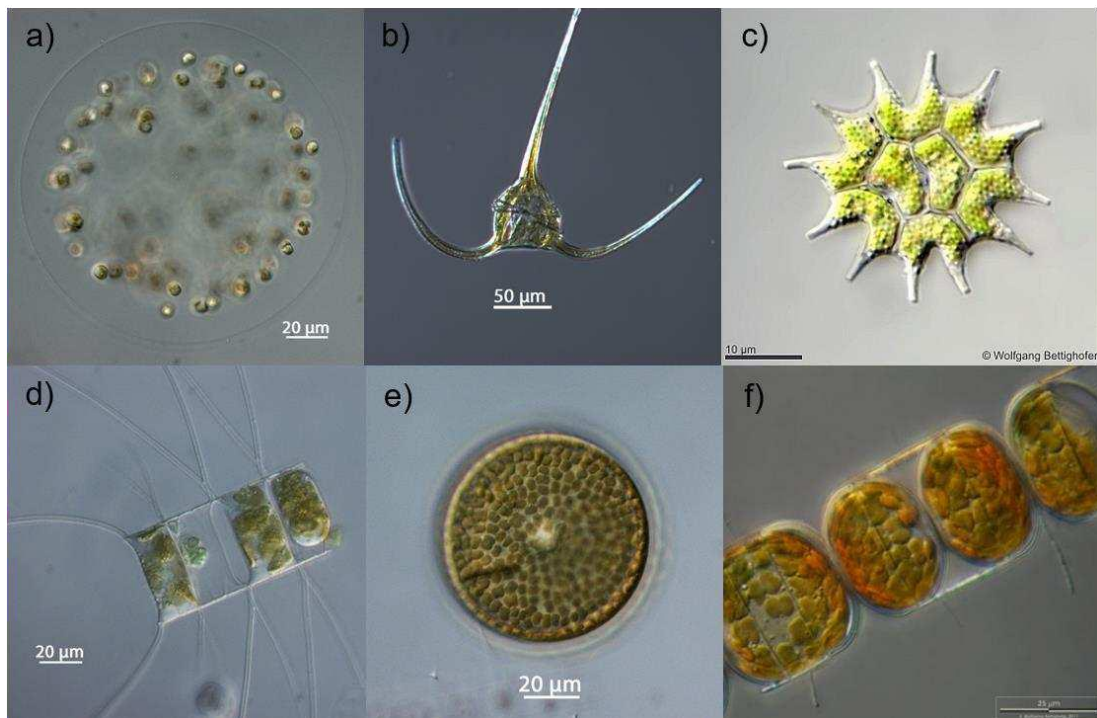
Fig 2. Some phytoplankton diversity. (a) *Phaeocystis globosa*, (b) *Tripos horridus*, (c), *Pediastrum boryanum* (d) *Chaetoceros decipiens*, (e) *Thalassiosira punctigera* and (f) *Melosira arctica*. Photos taken by Alexandra Kraberg (a, b, d, e) and Wolfgang Bettighofer (c, f).

One particularly successful and diverse group of phytoplankton are diatoms (*Bacillariophyceae*), which contain a characteristic silicate frustule (Martin-Jézéquel *et*

6

al., 2000; Falkowski & Raven, 2013). They often dominate bloom events and account for about 40% of the marine primary production, so that they are significant contributors to the marine biogeochemical cycles of carbon, nitrogen, phosphorus and silicate. Their success to compete over other phytoplankton groups is likely a result of comparably high intrinsic growth rates under nutrient replete conditions, a high physiological plasticity to respond to changing environmental conditions and their exalted light harvesting to biomass conversion efficiency (Wagner *et al.*, 2006; Lepetit *et al.*, 2022).

1.2.2. The biological carbon pump

Phytoplankton as primary producers are significant drivers of the biological carbon pump. While they only comprise about 1% of the total biomass, they account for about 50% of the global primary production (Field *et al.*, 1998). The biological carbon pump (Fig. 3) comprise a range of processes, which jointly contribute to the sinking and sequestration of photosynthetically fixed CO_2 in form of particulate organic carbon (POC) out of the euphotic zone into the deeper ocean and partly also the sediments (Volk & Hoffert, 1985; Le Moigne, 2019).

More precisely, atmospheric CO_2 equilibrates with the ocean following Henry´s law and contributes to the oceanic dissolved inorganic carbon (DIC) pool (1, Fig. 3), which is depending on physical and chemical properties of sea water such as temperature, salinity, alkalinity and pH, whereof the oceanic pH is vice versa also controlled by the CO_2 concentration (Zeebe & Wolf-Gladrow, 2001). DIC is consumed via the photosynthetic C uptake by phytoplankton in the euphotic zone (2, Fig. 3), i.e. phytoplankton use solar radiation, water (H_2O), as well as inorganic macronutrients, vitamins and trace metals to produce O_2 and take up C to build up POC (Field *et al.*, 1998; Falkowski *et al.*, 2000). This biomass provides the basis of the aquatic food webs, i.e. micro-zooplankton graze on phytoplankton (3, Fig. 3), which are, in turn, consumed by larger zooplankton, fish and large predators (e.g. Danielsdottir *et al.*, 2007; Napiórkowska-Krzebietke, 2017). In fact, the majority of phytoplankton biomass is taken up by grazers, so that its organic matter is converted back to CO_2 via respiration already in the upper ocean, or the biomass is converted to dissolved organic carbon (DOC) by fragmentation of POC due to sloppy feeding (4, Fig. 3).

About 5-25% of the POC built by photosynthesis, however, leaves the euphotic zone by sinking as fecal pellets or dead phytoplankton cells (5, Fig. 3; Iversen, 2023) and

the sinking velocity and thus efficiency can be accelerated by aggregate formation or mineral ballasting (Klaas & Archer, 2002; Iversen & Robert, 2015; Henson *et al.*, 2019; Le Moigne, 2019). During the sinking process, the detrital organic matter, also called marine snow, feeds bacteria or grazers that remineralize a large proportion of sinking biomass (6, Fig. 3; Carlson *et al.*, 2010). Thus, bacteria and other heterotrophs transform POC back to CO_2 and thus into the DIC pool again (7, Fig. 3), which is transported back to the surface ocean via mixing or upwelling. Ultimately, less than 1% of the POC that was formed by phytoplankton in the surface ocean reaches the deep ocean, where an even smaller proportion of carbon end up in sediments (Koeve, 2005), where it is potentially buried for time-scales over geological time-scales (8, Fig. 3). Due to the continuous CO_2 removal from the upper ocean by sinking of POC, atmospheric CO_2 can be taken up and stored in the ocean. In fact, model results showed that, if the biological pump would be turned off, atmospheric CO_2 levels would increase by about ~200 µatm (Watson & Liss, 1998).
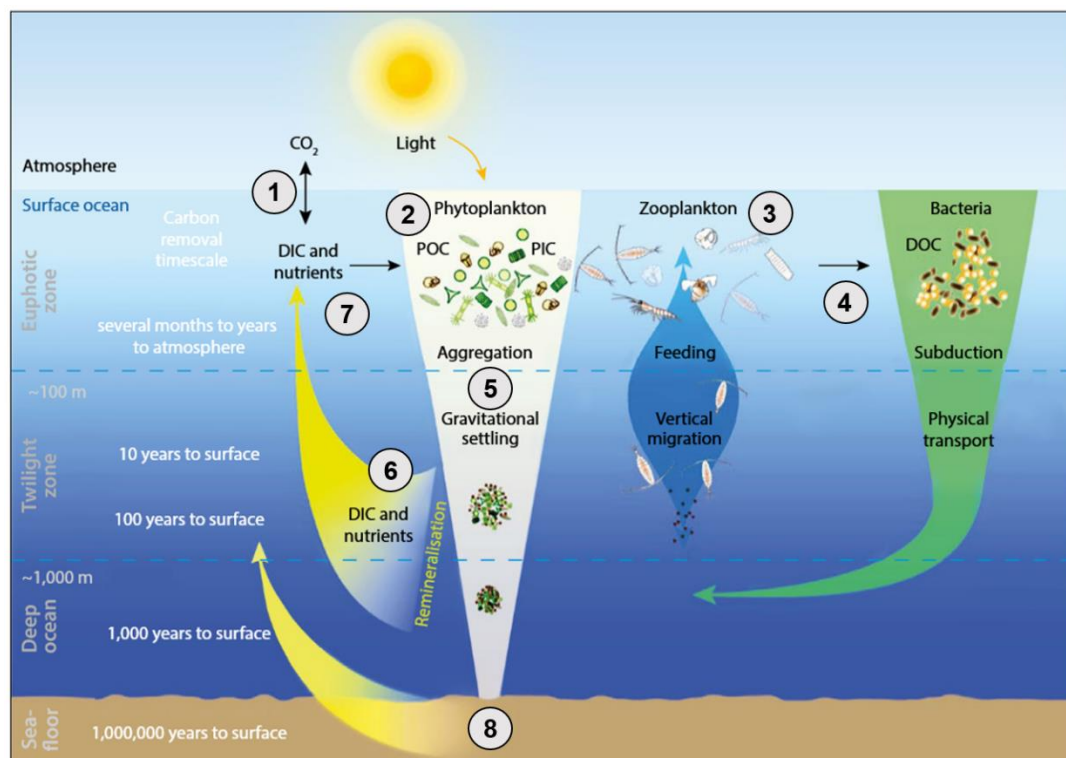
Fig 3. Simplified illustration of the biological carbon pump. Atmospheric CO_2 enters the ocean via diffusion (1) and is converted into particulate organic carbon (POC) by photosynthesis (2). Zooplankton grazes on the POC biomass (3) and contributes to the oceanic dissolved organic carbon pool via sloppy feeding (4). The POC biomass is sinking out of the photic zone (5) and is partly remineralized by heterotrophs (6). The resulting dissolved inorganic carbon (DIC) is transported back to the upper ocean by upwelling, where it contributes again to the surface DIC pool (7). A small fraction of sinking POC biomass reaches the sediments and is sequestered on geological time-scales (8). Modified after Gattuso *et al.* (2023).

1.2.3. Primary production in the Arctic

In contrast to projections of the global ocean, where primary production is described to decrease under ongoing climate change (Laufkötter *et al.*, 2015), the Arctic has been observed to increase in primary production over the past decades (Arrigo & van Dijken, 2015), and model projections show a further increase (Lewis et al., 2020). This increase is mainly attributed to prolonged growing seasons and larger sea ice-free habitats (Arrigo *et al.*, 2008). It is believed that the Barents Sea north of Norway, is indeed the most productive region of the Arctic Ocean because of its comparably low sea ice cover as well as high nutrient advection from the North Atlantic (Oziel *et al.*, 2020).

Primary production depends on light and nutrient availability but also temperatures, resulting in distinct seasonal succession patterns in temperate and polar oceans (Young & Schmidt, 2020). During winter, the phytoplankton biomass is typically low due to the absence of light in the polar night and the low temperatures. In this season, nutrients get replenished in the upper ocean due to recycling and mixing. In spring, the phytoplankton biomass starts to increase when temperature and light intensity are rising and nutrients are still ample. The phytoplankton biomass buildup maximizes during spring bloom events in late spring or early summer, which are typically terminated by either bottom-up-effects such as nutrient depletion and top-down-effects such as grazing (Assmy *et al.*, 2007). However, due to global warming, Artic phytoplankton phenology likely changes. Synergistic effects of increasing temperatures and light availability are, for instance, projected to cause an earlier initiation of spring bloom events with an accelerated phenology of 5 to 7 days per decade (Field & Barros, 2014; Rokitta *et al.*, 2023). Furthermore, phytoplankton spring bloom biomass is projected to reach higher peak biomass, but also to decline earlier in the season due to faster nutrient limitation (Kahru *et al.*, 2016; Chivers *et al.*, 2020; Rokitta *et al.*, 2023). Such changes will likely cause a restriction of first-order grazers such as copepods and fish larvae, which follow distinct annual cycles (Søreide *et al.*, 2010). Consequently, climate change-induced deviations in phytoplankton spring bloom phenology may cause temporal mismatches between primary production and grazing, which has ultimately far-reaching effects on the Arctic ecosystem trophodynamics, as well as the biological carbon pump (Rokitta *et al.*; Petrou *et al.*, 2016; Dezutter *et al.*, 2019). Such cascading effects will likely be most pronounced in

previously sea ice covered areas of the Arctic Ocean as here changes in temperature and light regime are expected to be most severe (Nicolaus *et al.*, 2012).

In addition to pelagic phytoplankton in the Arctic, also sea ice associated primary producers contribute to total Arctic primary production. Despite the fact that the decreasing sea ice thickness and increasing areas covered with melt ponds lead to increasing irradiance, which promotes primary production, remaining sea ice also functions as substrate for ice algae (Kirst & Wiencke, 1995). They attach to the sea ice and can also seed pelagic under ice blooms, as some species can grow in both habitats (Lund-Hansen *et al.*, 2020). Especially diatoms and the haptophyte *Phaeocystis* have been observed to thrive in ice covered surface waters and the marginal ice zone (Arrigo *et al.*, 2012; Assmy *et al.*, 2017), whereas other mixotrophic or heterotrophic species such as *Micromonas* or dinoflagellates can dominate the even less illuminated under ice communities in the high Arctic (Lee *et al.*, 2019). Under young sea, however, also potentially harmful haptophytes or dinoflagellates have been recently observed to dominate early spring bloom communities (Bruhn *et al.*, 2021; Søgaard *et al.*, 2021).

To understand how Arctic phytoplankton will respond to climate change and consequently will affect all higher trophic levels as well as carbon export, we need to elucidate their underlying physiology under future ocean conditions.

1.3. Phytoplankton Physiology

1.3.1. Photosynthesis

Archaea were the first organisms to use photosynthesis for anabolic metabolism (using hydrogen or hydrogen sulfide as reducing agent; Olson, 2006), while cyanobacteria were probably the first to perform oxygenic photosynthesis (i.e. water functions as the electron-donor; Buick, 2008). Cyanobacteria evolved during a time in which the atmosphere was anoxic and only became oxygenic due to their photosynthetic O_2 production. Nowadays, oxygenic photosynthesis can be performed not only by prokaryotic cyanobacteria, but also by eukaryotic plants and algae. Although, the general cell structure of prokaryotes and eukaryotes is substantially different, both contain thylakoid membranes to perform photosynthesis in a similar way (e.g. Vellai & Vida, 1999; Martin, 2017).

Photosynthesis in eukaryotic microalgae takes place in specialized organelles called chloroplasts (Boardman, 1977; Jensen & Leister, 2014), which consist of different membranes, an inner matrix called stroma and thylakoids that are often stacked up in grana or vesicles (Fig. 4; Flori *et al.*, 2017). Photosynthesis can be distinguished into two major processes: First, the photosynthetic light reactions, taking place in the thylakoid membrane, use light energy to generate reductants and energy-rich biochemicals in form of nicotinamide adenine dinucleotide phosphate (NADPH) and adenosine triphosphate (ATP). These are then used in the second part, the Calvin cycle, which takes place in the chloroplast stroma and fixes CO_2 into organic matter.

Because this dissertation focuses on physiological responses to ocean warming, important physiological sub-processes of phytoplankton are described in detail in the following.
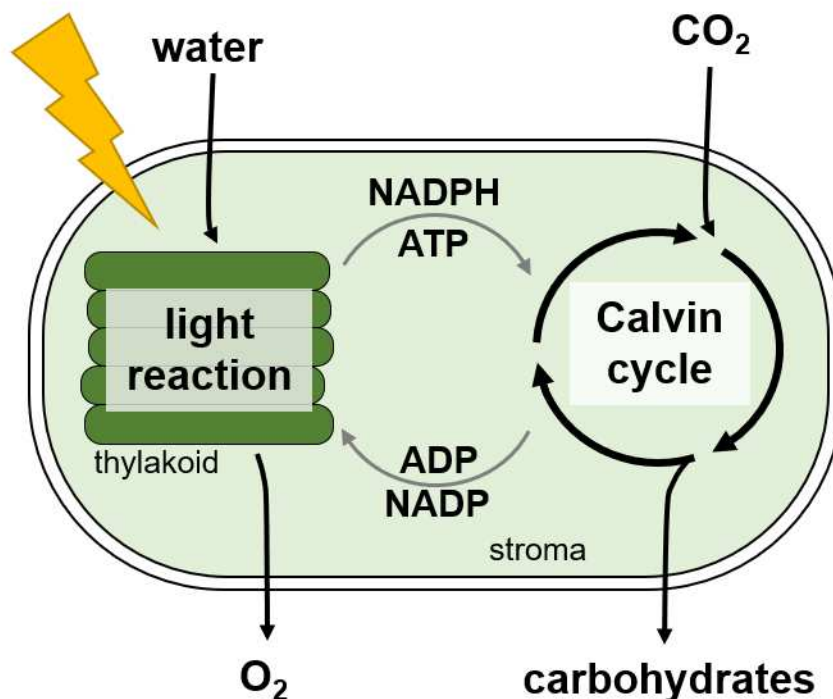
Fig 4. Simplified illustration of a chloroplast of a eukaryotic phototroph. Inside the thylakoids, the photosynthetic light reactions use solar radiation and water to produce O_2 and to generate NADPH and ATP to fuel the Calvin cycle. The Calvin cycle takes place in the stroma and takes up inorganic CO2 to build up organic C. Modified after Taiz and Zeiger (2006).

Introduction

The photosynthetic light reactions start with the process of light harvesting (1, Fig. 5; Cruz *et al.*, 2004; Lepetit *et al.*, 2022). Here, the light harvesting complexes (LHCs) of photosystem (PS) II consist of a number of proteins equipped with chlorophyll (Chl) molecules, surrounding the PSII reaction center (P680), which heterodimer of two distinct Chl molecules held by protein subunits D1 and D2 of the photosystem. The pigment composition of the light harvesting antenna are depending on the different functional groups of phototrophic organisms. While all groups contain Chl *a* as the core pigments, other important ones are, depending on the functional groups, Chl *b* or *c* as well as different carotenoids. These different pigments absorb photosynthetic active radiation of different absorption wavelength, whereas the maximum absorptions of PSII is at a wavelength of 680 nm. When excited by light energy, i.e. photons, the PS680 transfers an electron to pheophytin (Phae; 2, Fig. 5). The arising electron gap in P680 is then filled by photooxidation of water 3, (Fig. 5). This takes place at the oxygen-evolving-complex (OEC; a manganese and calcium containing enzyme complex), which is bound to PSII. Four photons need to be harvested to drive the oxidation of two H_2O molecules which split into four protons (H^+), and one O_2 molecule (Kok *et al.*, 1970). The O_2 is released as a by-product, whereas the H^+ build up a proton gradient inside the thylakoid lumen to later fuel an ATP-synthase for ATP generation.

The electrons are transferred further through to the acceptors Q_A and Q_B and passed on to the mobile electron carrier plastoquinone (PQ; 4, Fig. 5). PQ accepts two electrons from the Q_B site of PSII as well as two H^+ from the chloroplast stroma and thereby gets reduced into plastoquinol (PQH_2; 5, Fig. 5), which passes the electron on via the cytochrome-b_6/f-complex to plastocyanin (PC; 6, Fig. 5; Tikhonov, 2014). During this catalytic reaction, the two stromal H^+ from the PQ are translocated by the cytochrome-b_6/f-complex into the thylakoid lumen to also to support the electrochemical proton gradient. The reduced plastocyanin transfers the electrons to the reaction center of PSI (P700). P700 needs to be re-excited by excitons from light harvest, similar as in PSII (7, Fig. 5), to transfer the electrons via a series of membrane-bound iron-sulfur-proteins to soluble ferredoxin (Fd) and finally to the flavoprotein ferredoxin-NADP reductase (FNR), which mediates the transfer of an electron to $NADP^+ + H^+$, which is then reduced to NADPH (8, Fig. 5). NADPH functions as a generic electron donor for metabolism. The protons accumulated inside thylakoid lumen during the photosynthetic light reactions (9, Fig. 5) produce an electrochemical gradient, the so-called proton motive force (PMF; Mitchell, 1966). The PMF comprises both, a pH,

i.e. a chemical, as well as an electric gradient (Bailleul *et al.*, 2015; Lepetit *et al.*, 2022). It is exploited to generate ATP in the plastidial stroma by translocating H^+ through the membrane bound ATP-synthase (10, Fig. 5).
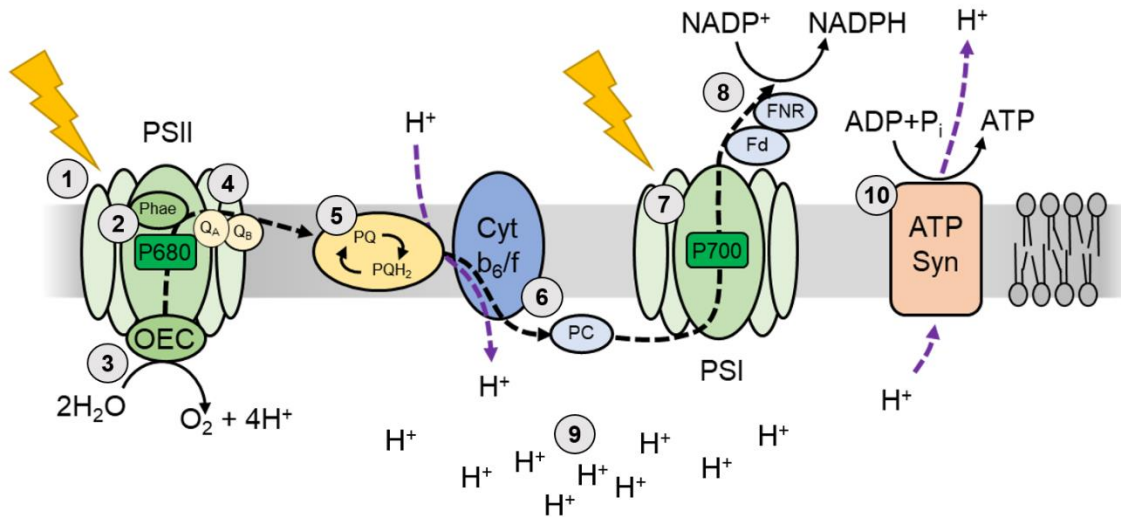
Fig 5. Schematic illustration of the photosynthetic light reactions, modified after Taiz and Zeiger (2006). Solar light is harvested by the light harvesting complex of photosystem II (PSII; 1), which excites the PSII reaction center (PS680) and electrons are transferred to phaeophytin (Phae; 2). The electron gap is filled by electrons from photolysis at the oxygen evolving complex (OEC; 3). Electrons are then passed through the electron transport chain (ETC) to PSI via the electron acceptors Q_A and Q_B (4), the plastoquinone pool (5), the cytochrome-b_6/f-complex and plastocyanin (6). At PSI (7), light harvesting re-excites the electrons and they are passed on towards the flavoprotein ferredoxin-NADP reductase (FNR; 8), where NADPH is generated. During the photosynthetic ETC, a proton gradient is built up inside the thylakoid membrane (9), which is exploited for ATP generation (10).

The generated molecules of NADPH and ATP are subsequently fueling the second part of photosynthesis, in which the Calvin cycle fixes CO_2 into organic precursors and thereby promotes the ongoing assimilation of organic carbohydrates. The Calvin cycle consists of three main phases, i.e. carboxylation, reduction and regeneration (Calvin, 1962; Kroth, 2015; Kroth & Matsuda, 2022).

During the carboxylation phase, the key photosynthetic enzyme ribulose-1,5-bisphosphat carboxylase/oxygenase (RuBisCO) catalyzes the assimilation of CO_2 into preexisting ribulose-1,5-bisphosphat (RuBP). The resulting fragile C_6-molecule breaks apart into two 3-phospoglycerate molecules (3-PG; 1, Fig. 6). In the reduction phase, the 3-PG molecules are phosphorylated by phosphoglycerate kinase with the use of the photochemically generated ATP, yielding 1,3-bisphosphoglycerate (1,3-BPG, 2,

Fig. 6). This compound undergoes a reductive dephosphorylation by glyceraldehyde-3-phosphate-dehydrogenase using the photochemically generated NADPH and yielding glyceraldehyde-3-phosphate (G3P; 3, Fig. 6), which is an aldose with 3 C-atoms. In the last, the regeneration phase, three RuBP molecules are formed by iterative transfer of C_2 and C_3 units from five generated G3Ps and a final phosphorylation that also uses photochemically generated ATP (4, Fig. 6). Thus, during the Calvin cycle, three molecules of each, CO_2 and RuBP are converted into six molecules of triosephosphates, of which only one can be called a net gain of C assimilation (5, Fig. 6), while the remaining five are required to regenerate the precursors RuBP. Thus, the net reaction of the Calvin cycle uses $3\ CO_2 + 3\ RuBP + 6\ NADPH + 9\ ATP$ to produce $1\ G3P + 6\ NADP^+ + 3\ H^+ + 9\ ADP + 6\ P_i + 3\ RuBP$ (Kroth & Matsuda, 2022).
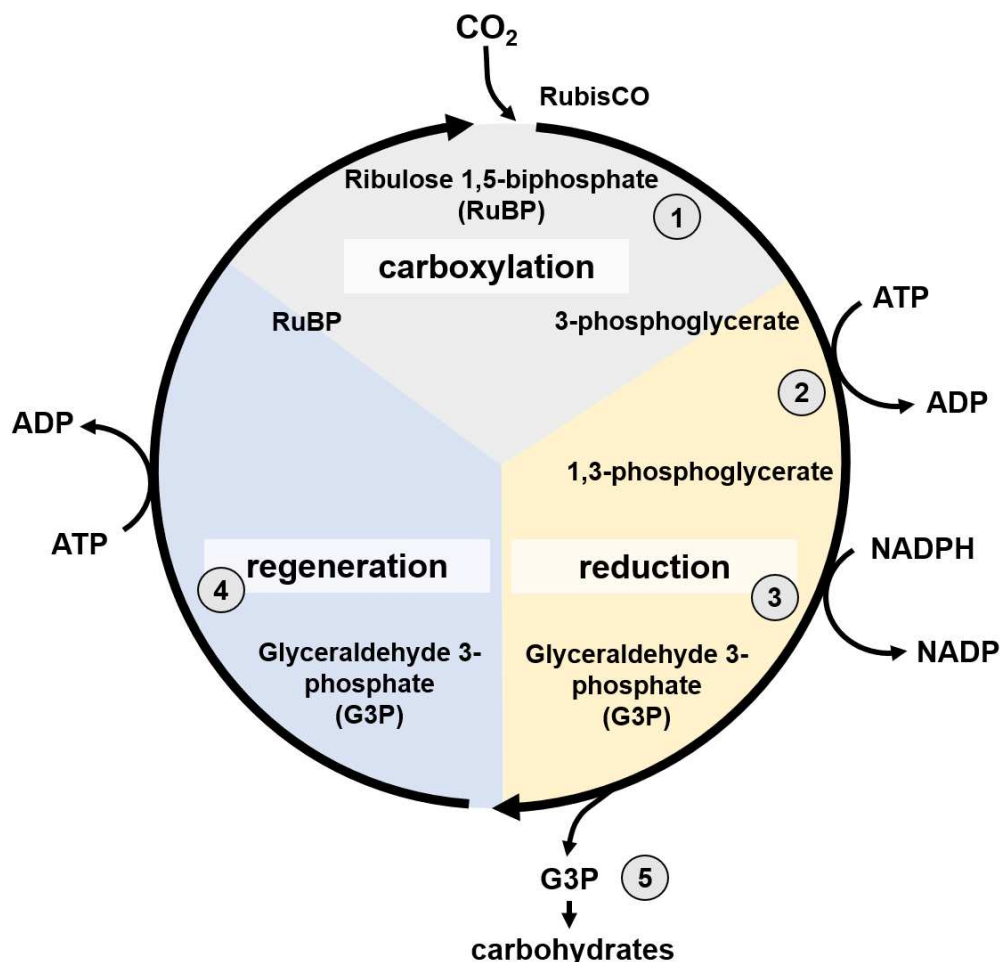
Fig 6. Schematic illustration of the Calvin cycle including catalytic reactions of the carboxylation phase, the reduction phase and the regeneration phase, modified after Taiz and Zeiger (2006). For a detailed description of the three phases, please see text.

RuBisCO can also catalyze an undesired oxygenation in a reaction called photorespiration (Bauwe *et al.*, 2010). Especially in aquatic photosynthesis, where CO_2 diffusion rates are 10,000-fold slower, and environments can therefore become completely CO_2 depleted, carbon concentrating mechanisms (CCMs) can prevent this oxygenation (Rokitta *et al.*, 2022). Many microalgae are known to have strong CCMs that enable cells to also take up bicarbonate (HCO_3^-), which is then converted into CO_2 by exploitation of the PMF. The inorganic C uptake in diatoms is typically facilitated by a high activity of carbonic anhydrase in most, if not all cell compartments, as well as membrane-bound HCO_3 transporters in all membranes (Tsuji et al., 2017). CO_2 is then accumulated in pyrenoidal structures inside chloroplasts, where it is used for RuBisCO in the Calvin cycle (Rokitta et al., 2022). CCMs are energy expensive, i.e. they consume parts of the generated PMF and have to ultimately increase internal CO_2 concentrations by up to 1000-fold compared to the ambient conditions (Raven et al., 2014).

As laid out, the Calvin cycle requires a stoichiometry output of the light reactions of at least 1.5 ATP:NADPH (Allen, 2002), which can increase due to the described CCM activity (Peltier *et al.*, 2010; Curien *et al.*, 2016). Lepetit *et al.* (2022), however, calculated based on the specific structure of plastidial ATP-synthase (Hahn *et al.*, 2018), that the linear electron flow during the photosynthetic light reactions as described above, only provides an ATP:NADPH ratio of 1.28, so that cells require a regulation of this stoichiometry. Therefore, cells modulate the coupling of electron transfer and proton pumping into the thylakoid lumen (Lepetit *et al.*, 2022). To increase the ATP relative to NADPH inside the chloroplasts, phototrophs often employ different routes of alternative electron flow (AEF; Fig. 7). First, cyclic electron flow (CEF; 1, Fig. 7) comprises a re-routing of electrons from PSI back towards the cytochrome-b_6f-complex without the reduction of FNR. Thus, proton pumping into the thylakoid lumen is enhanced, supporting the PMF, without further reductant generation (Alric, 2010; Larkum *et al.*, 2018). If the ATP yield cannot be increased any further, cells instead need to dissipate excess electrons or NADPH to balance the plastidial ATP:NADPH stoichiometry. To this end, they employ O_2 consuming processes, i.e. water-to-water-cycles (Curien *et al.*, 2016): The Mehler reaction (2, Fig. 7) comprises the reduction of O_2 to H_2O_2 at ferredoxin (Mehler, 1951; Asada, 2000), which necessitates a series of enzymatic reactions to detoxify resulting reactive oxygen species (ROS), and dissipate

15

electrons without NADPH generation. Another way to dissipate electrons without NADPH generation is the oxidation of PQ in the thylakoid membrane, catalyzed by the plastid terminal oxidase (3, PTOX; Fig. 7), which consumes O_2 and H^+ to dissipate electrons into H_2O molecules. As a third option, diatoms, green algae and plants can involve a metabolic coupling of chloroplasts and mitochondria (4, Fig. 7). Thereby, cells re-route excess plastidial NADPH to the cytoplasm and the mitochondria, possibly via the malate shuttle system (Strotmann & Murakami, 1976), (Bailleul *et al.*, 2015; Rehder *et al.*, 2023; Peltier *et al.*, 2024).
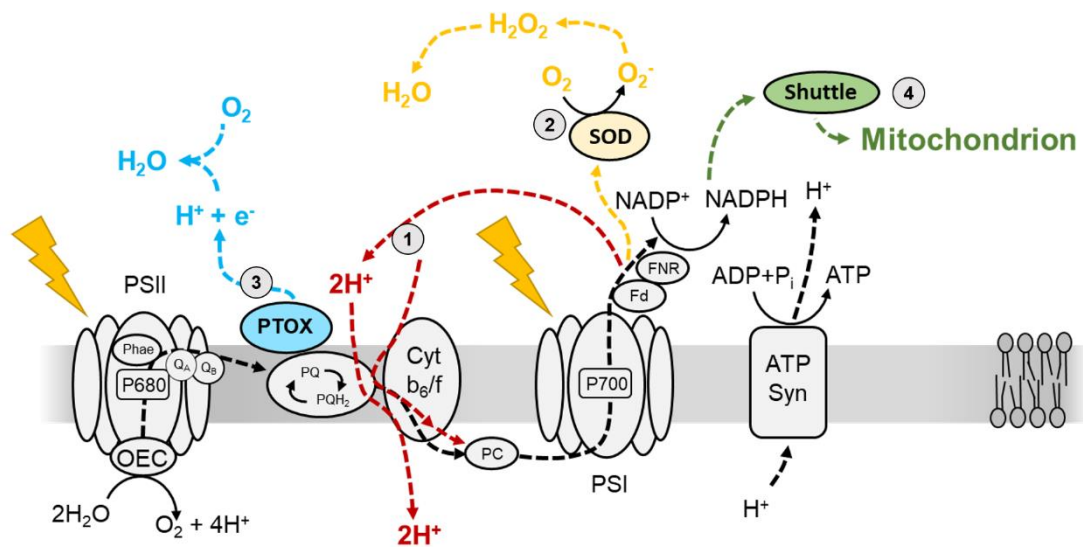
Fig 7. Schematic illustration of different routes of alternative electron flow to relatively increase the plastidial ATP:NADPH stoichiometry: (1) cyclic electron flow around photosystem I (red), (2) Mehler reaction (yellow), (3) plastid alternative oxidase (PTOX, blue) and (4) electron export form chloroplast to mitochondrion (green).

1.3.2. Mitochondrial respiration

Phytoplankton not only employ anabolic processes during their autotrophic photosynthesis, but also catabolic heterotrophic processes such as glycolysis and mitochondrial respiration in order to generate ATP to fuel cellular metabolism. Respiratory processes comprise primarily the TCA cycle that releases CO_2 and generates the reductant NADH, which fuels the respiratory electron transport chain (ETC) that consumes O_2 and establish a proton gradient for mitochondrial ATP generation, analog to the PMF of the plastid (Fig. 8; Raven & Beardall, 2016).

Glycolysis is a series of enzymatic reactions in the cytosol that break down sugars, prior produced during carboxylation, into pyruvate as well as ATP and NADH. The

pyruvate is then transported from the cytosol into the mitochondria, where the different respiratory processes take place. Here, the pyruvate molecules are oxidatively decarboxylated by pyruvate decarboxylase and bound to coenzyme A to form Acetyl-Coenzyme A, which is the first substrate of the respiratory TCA cycle. NADH and CO_2 are released.
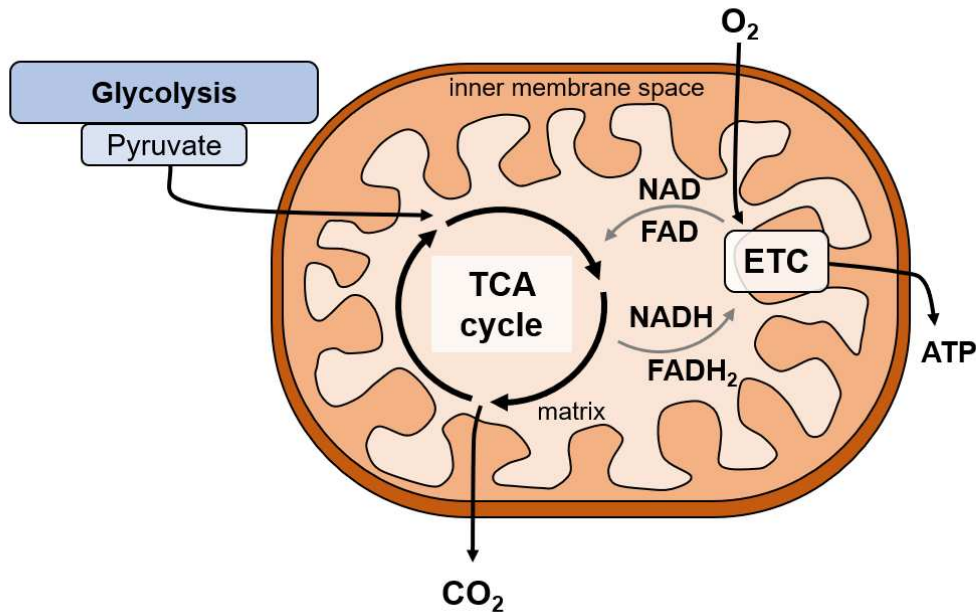
Fig 8. Simplified illustration of a mitochondrion. The tricarboxylic acid (TCA) cycle takes place in the mitochondrial matrix. It respires CO_2 and provides NADH and $FADH_2$ for the mitochondrial electron transport chain, which consumed O_2 and generates ATP. Modified after Taiz and Zeiger (2006).

The TCA cycle of eukaryotic phototrophs takes place in the mitochondrial matrix and encompasses a series of enzymatic reactions, starting with the combining of Acetyl-CoA and oxaloacetate by citrate synthase to build citrate (Fig. 9; Lowenstein, 1967; Krebs, 1970). Then, aconitase isomerizes citrate into isocitrate, which is oxidatively decarboxylated by isocitrate dehydrogenase, yielding 2-oxoglutarate. 2-oxoglutarate is then converted into succinyl-CoA by 2-oxoglutarate dehydrogenase under the release of CO_2 and NADH molecules. This is followed by a substrate-level phosphorylation of ADP to ATP, converting the succinyl-CoA into succinate by succinyl-CoA synthetase. Succinate is then oxidized by succinate dehydrogenase into fumarate, yielding flavin adenine dinucleotide ($FADH_2$). Fumarate, in turn, is hydrated by fumarase into malate, which is then as the last step of the TCA cycle oxidized by malate dehydrogenase back into oxaloacetate, whereas another NADH is generated.
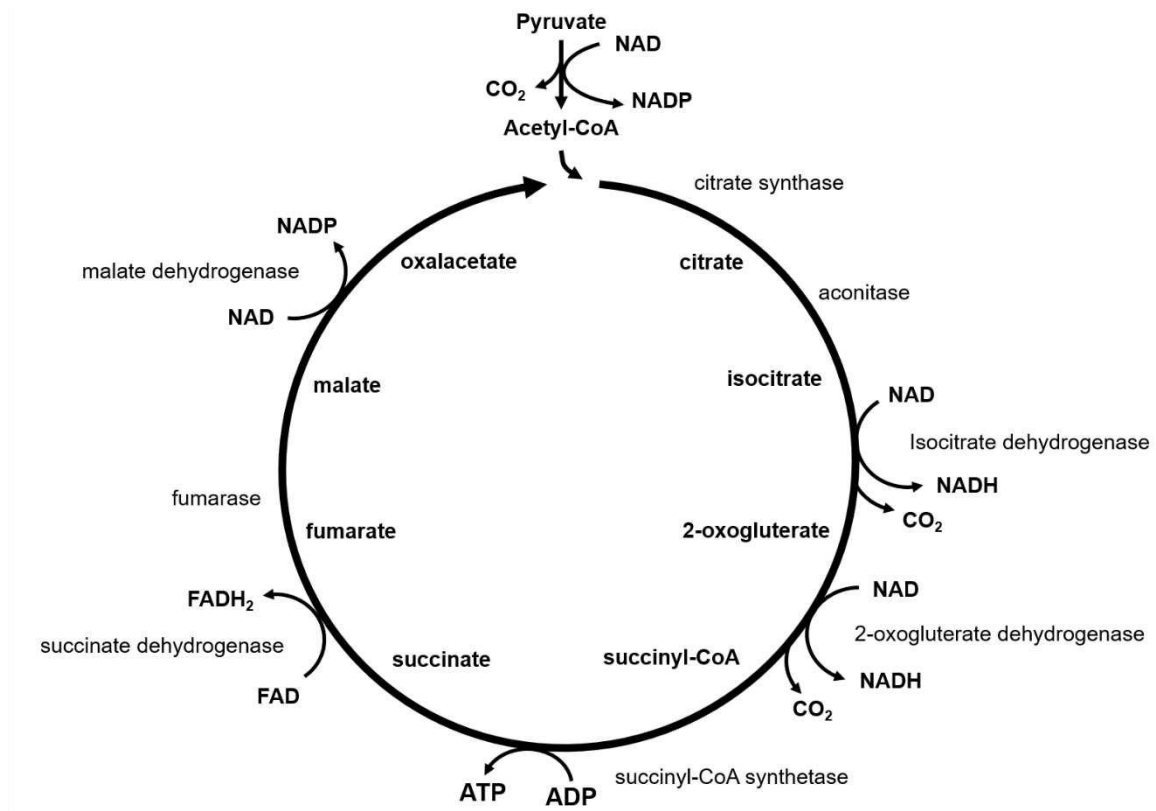
Fig 9. The enzymatic reactions of the tricarboxylic acid (TCA) cycle, in which CO_2 molecules are released, ATP consumed and NADP as well as $FADH_2$ to fuel the mitochondrial electron transport chain are generated. For further details, please see text, modified after Taiz and Zeiger (2006).

The reductants generated during the TCA cycle are typically fueled into the mitochondrial ETC (Fig. 10; Guo *et al.*, 2018). Here, complex I (NADH-dehydrogenase) accepts an electron directly from NADH (1, Fig. 10) and transfers it to the ubiquinone pool. Complex II (Succinate-dehydrogenase) is part of the TCA cycle and catalyzes the oxidation of succinate to fumarate with help of $FADH_2$ as a prosthetic group (2, Fig. 10), and donates the extracted electrons also to the ubiquinone pool (3, Fig. 10). Additionally, NAD(P)H from the matrix or inter membrane space can transfer electrons to the ubiquinone pool via rotenone-insensitive dehydrogenases (4, Fig. 10). The ubiquinone as a molecule is a carrier for reductant and protons, which, like plastidary PQ, diffuses freely inside the mitochondrial inner membrane and passes on the electrons to either complex III (Cytochrome bc_1 complex; 5, Fig. 10) or to an alternative oxidase (AOX; 6, Fig. 10). From complex III, electrons are transferred on via cytochrome c (Cyt c) to complex IV (Cytochrome C oxidase), where they reduce O_2 to H_2O (7, Fig. 10). During the transfer of electrons between complex I and complex IV, protons are translocated from the mitochondrial matrix to the inter membrane space at

each complex, thereby building up a proton gradient (8, Fig. 10). This proton gradient is then exploited by the ATP-synthase for mitochondrial ATP generation (9, Fig. 10). When electrons are passed on to AOX instead of to complex III, however, they are dissipated into the reduction of O_2 to H_2O, resulting in a lower H^+ translocation. While the AOX was under debate for a long time, it is now commonly agreed that its activity decrease cellular redox stress (Maxwell *et al.*, 1999), apparently increasing the cells´ ability to deal with abiotic stressors, such as high salinity, heat or nutrient limitation (Feng *et al.*, 2013; Murik *et al.*, 2019).
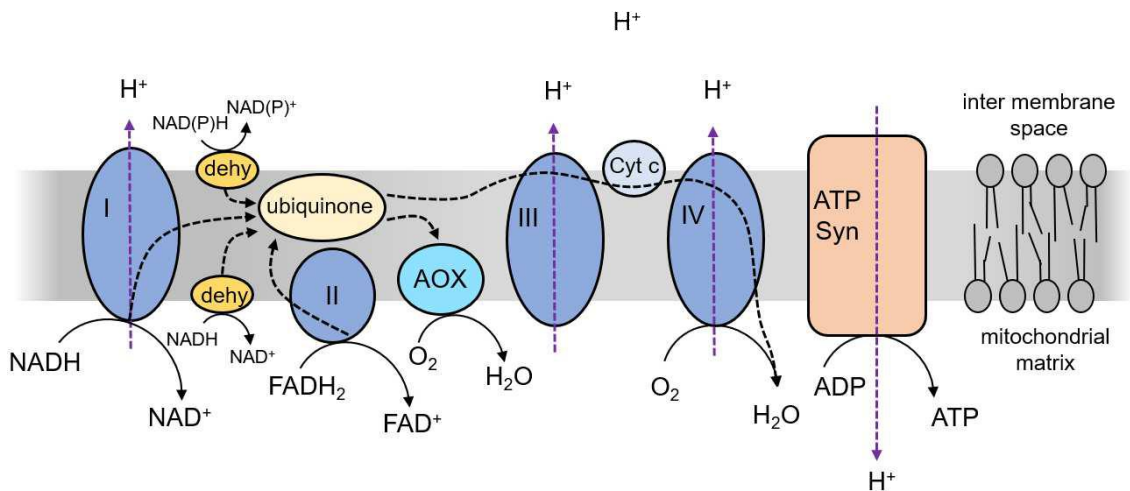
Fig 10. Schematic illustration of the respiratory electron transport chain and mitochondrial ATP generation, modified after Taiz and Zeiger (2006). Please see the text above for description.

1.3.3 Temperature effects on phytoplankton physiology

All these underlying physiological sub-processes of anabolic photosynthesis and catabolic respiration are driving cellular metabolism, and their integrated relative magnitudes ultimately control net cellular biomass buildup. These sub-processes are affected by all of the above-mentioned drivers of climate change, such as alterations in temperature, light, nutrients and CO_2 (Doney *et al.*, 2012; Constable *et al.*, 2022). Next to changes in light or nutrients, temperature has the potential to impact physiological sub-processes most profoundly. As a universal driver, temperature affects molecular movement and thus principally all physical and (bio)chemical processes involved in metabolism (Brown *et al.*, 2004; Pearle *et al.*, 2010). More precisely, temperature controls processes such as substrate diffusion rates, membrane fluidity, electron transport or enzyme activity, which ultimately also drive the physiology of photosynthesis and respiration (Raven & Geider, 1988).

It seems reasonable to assume that, depending on their nature, different underlying physiological processes are influenced by temperature to a different extent. While diffusion rates are basically purely physical and are directly driven by molecular movement (Brown *et al.*, 2004), temperature effects on membrane fluidity, for example, are more complicated. They depend on the degree of unsaturated fatty acids of membrane lipids (Los *et al.*, 2013), and the ability of the cells to change the composition in a given time. Under high temperatures, cells typically replace unsaturated fatty acids in membrane lipids with de-novo synthesized saturated fatty acids, which makes membranes more rigid and thereby compensate for a higher molecular motion under warming. Under low temperatures, however, cells require a larger degree of unsaturated fatty acids, facilitated by increased fatty acid desaturase activity to compensate for inhibited molecular movement. These acclimation responses help to maintain ion gradients and membrane-associated enzyme activity in diverse environmental settings (Thompson *et al.*, 1992; Murata & Los, 1997).

Enzyme activity is governed by the enzyme-specific kinetic properties like turnover rates as well as substrate affinity, which are both temperature sensitive. Enzymatic activity typically increases with temperature, following a pattern like the Arrhenius function. Thereby, the factor of rate stimulation in response to a 10°C temperature increase is termed the Q_{10} factor (Hegarty, 1973; Mundim *et al.*, 2020). In the photosynthetic key enzyme RuBisCO, Q_{10} factors typically range between ~2 to ~3 in plants (Sage, 2002), green algae (Devos *et al.*, 1998) and diatoms (Descolas-Gros & de Billy, 1987; Young *et al.*, 2015). After this exponential increase in response to temperature, enzyme activity reaches a plateau at the species-specific optimal temperature, beyond which the activity decreases again (Sharpe & DeMichele, 1977; Tang & Riley, 2024). The decline beyond optimal temperatures has for long been attributed heat-induced protein denaturation. This is not necessarily applicable, especially in polar phytoplankton, which can experience warming-induced declining process-rates already at temperatures below 10°C. Hobbs *et al.* (2013), therefore, proposed that instead of protein denaturation, rather the change in heat capacity of enzyme catalysis and differences in Gibbs free energy between ground state and transition state control the temperature dependency of enzymatic activity and cause a decline beyond optimal temperatures. Next to thermodynamic effects on enzyme kinetics, the availability or provision, respectively, of substrates within a cell or

compartment can change with temperature and affect enzymatic pathway output (Somero, 1978).

For RuBisCO, the carboxylation affinity decreases under warming and, vice versa, the oxygenation affinity increases (Galmés *et al.*, 2016; Hermida-Carrera *et al.*, 2016), while the ratio of $O_2:CO_2$ in seawater is also decreased by temperature (Zeebe & Wolf-Gladrow, 2001). These phenomena theoretically impact C-fixation and favor photorespiration, but phytoplankton typically employ efficient CCMs, which increase the CO_2 concentration at RuBisCO, thereby increasing carboxylation rates and suppressing the oxygenase activity. In polar phytoplankton, not only warm temperatures but also cold temperatures, often below the freezing-point, control enzyme activity due to cold inhibition. To compensate for low RuBisCO activity under low temperatures, some polar species have adapted by constitutively increasing their overall C-fixation machinery, specifically the protein concentration of RuBisCO. This adaptation enables them to achieve similarly high C-fixation rates as temperate species that thrive under much higher temperatures (Young *et al.*, 2015).

In phytoplankton, these different physical and (bio)chemical phenomena and their diverging temperature responses shape physiological sub-processes, which consequently also diverge in their temperature sensitivities, resulting in potentially diverging temperature response patterns (Baker *et al.*, 2016; Barton *et al.*, 2020). For example, growth rates, i.e. the cellular process of cell division, typically follow a unimodal optimal curve with a steady increase until a species- or strain-specific optimum and a sharp decline afterwards (Thomas *et al.*, 2012; Grimaud *et al.*, 2017). Photosynthetic and respiratory processes were described to follow a similar pattern, whereas they differ in their thermal sensitivity and/or optimal temperature: In many species, gross photosynthesis seems to be less stimulated by temperature than respiration on short-term time-scales (Barton *et al.*, 2020), which can decrease net carbon retention. As a consequence, cells are generally believed to experience a lowered carbon use efficiency (Padfield *et al.*, 2016) and thus also decreased biomass production under high temperatures (Atkinson *et al.*, 2003).

All physiological processes represent a large feedback system, and in the process of acclimation, cells attempt a fine-tuning of single sub-processes on a transcriptomic level in order to maintain metabolic homeostasis on the organismal level. On short-term time-scales, profound shifts of metabolic and redox balance can arise due to the

diverging thermal sensitivities of affected processes (Padfield *et al.*, 2016; Barton *et al.*, 2020). In these situations cells require antioxidative capacities and intensive physiological regulation to endure the time required for acclimation, otherwise the warming-induced oxidative stress increases and becomes lethal (Noctor & Foyer, 1998; Moreno *et al.*, 2024). Such physiological regulation can involve diverse AEFs as described above (see chapter 1.3.1; e.g. Curien *et al.*, 2016; Burlacot, 2023), changes in the stoichiometry of pigments and biomass, i.e. an up- or downregulation of LHCs (Geider, 1987; Thompson *et al.*, 1992), or photosystem abundances (PSII:PSI), as well as transcriptomic or proteomic regulation responses (Toseland *et al.*, 2013; Nikolova *et al.*, 2017). On even longer time-scales, phytoplankton evolves and adapts to higher temperatures, thereby potentially increasing their optimal growth temperature and photosynthetic capacity under previously supra-optimal temperatures (Schaum *et al.*, 2017; Hattich *et al.*, 2024).

On a community level, temperature affects physiological processes involved in primary production and respiration in single-strains, thereby affecting their individual fitness and competitive abilities. This can result in profound shifts in species composition and thus ecosystem functioning due to selection processes (Sommer *et al.*, 2015; Benedetti *et al.*, 2021; Ahme *et al.*, 2023). Poleward migration of more temperate species have already been observed in both, the Southern Ocean, where dinoflagellates and the coccolithophore *Gephyrocapsa huxleyi* increase (McLeod *et al.*, 2012), and the Arctic ocean, where the North Atlantic inflow promotes advection of temperate phytoplankton species, including *G. huxleyi* (Oziel *et al.*, 2020). Newly introduced species with a temperate thermal history may then be more competitive than polar ones under the ongoing ocean warming, possibly affecting the species composition and favoring the establishment of more temperate communities in (sub-) polar oceans (Giesler *et al.*, 2023). Furthermore, in temperate and Arctic phytoplankton communities, respiration is often more stimulated than photosynthesis (Hancke & Glud, 2004; Holding *et al.*, 2013; Coello-Camba *et al.*, 2015). As a consequence, warming may shift net autotrophic areas into net heterotrophic areas under climate change. This may result in decreased C export efficiency due to the decreased net primary production, which can become more prominent by increased surface layer remineralization (John *et al.*, 2014; Boscolo-Galazzo *et al.*, 2018).

1.3.4 Fast repetition rate fluorometry and membrane-inlet mass spectrometry to measure phytoplankton physiology

The temperature responses in phytoplankton physiology can be investigated and quantified by various complex physiological measurement techniques. For this dissertation, a combination of photophysiological assessments using fast repetition rate fluorometry (FRRf) and photosynthetic as well as respiratory gas flux measurements using membrane-inlet mass-spectrometry (MIMS) was applied. This allowed to disentangle multiple physiological sub-processes, which at times can mask each other, and to identify physiological imbalances between single processes in response to temperature changes and to answer how phytoplankton cells adjust their physiology as a compensation for upcoming imbalances.

FRRf comprises the induction and detection of Chl *a* fluorescence and can thus investigate photophysiological properties of a microalgal suspension by assessing e.g. the quantum yield efficiency, electron transfer rates, antenna size and non-photochemical quenching (Kolber *et al.*, 1998; Oxborough, 2012). These photophysical assessments are based on the premise that photosynthetically harvested light can take one of three competing pathways: It can either go into photochemistry, it can be dissipated as heat or re-emitted as fluorescence (Fig. 11a; Schuback *et al.*, 2021). Under the assumption of unchanged heat dissipation during the short induction time, the measured Chl fluorescence yield is inversely related to photochemistry. It is under control of the redox state of the first electron acceptor in PSII, the Q_A. If Q_A is reduced, the photosystem is in a "closed" state, i.e. no photochemistry can take place and further harvested light is re-emitted as fluorescence. Once the electron is passed on to the plastoquinone pool, the photosystem "opens" again and Q_A is ready to take up the next electron, which appears as a decrease of the re-emitted fluorescence signal. To measure this, the FRRf sends a series of high intensity, microsecond-long light flashlets into the sample to saturate PSII, followed by a relaxation phase of longer flashlets, in which electrons are passed on towards PSI, which induces a re-opening of PSII. During the saturation phase, proxies for maximum quantum yield of PSII, electron transfer rates, antenna sizes or non-photochemical quenching can be calculated, whereas the relaxation phase allows the estimation of PSII re-opening times (Fig. 11b).
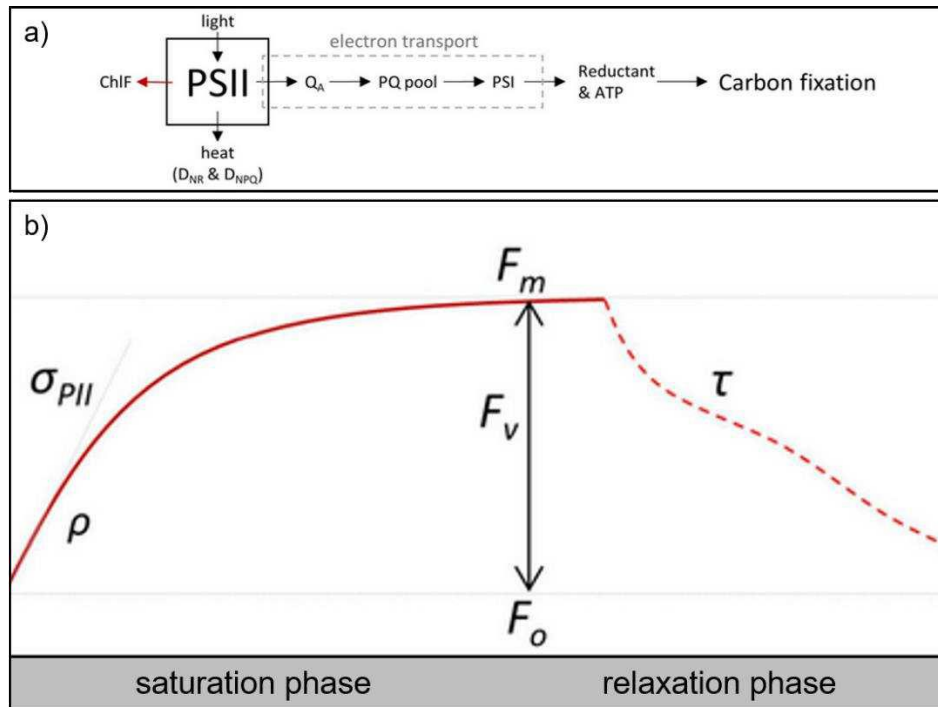
Fig 11. Conceptual illustration of the measurement principle of fast repetition rate fluorometry (FRRf). (a) demonstrates the three energy pathway of harvested light at photosystem (PS) II and (b) shows the chlorophyll a fluorescence signal of dark acclimated cells during the saturation and relaxation phase. Photophysiological parameters obtained from fluorescence signals are indicated as σ_{PSII} (absorption cross section of the antenna complex of PSII, F_m and F_0 (maximum and minimum fluorescence signals for calculations of maximum quantum yields of PSII) and τ (re-opening times of PSII). Modified after Schuback *et al.* (2021).

MIMS facilitates real-time measurements of O_2 and CO_2 concentrations in an enclosed microalgal suspension. A temperature-controlled cuvette system containing a continuously stirred algal suspension is connected to an inlet-system by a gas permeable polytetrafluorethylene (PTFE) membrane (Fig. 12). Dissolved gases such as O_2 and CO_2 transit the membrane and are led into the mass-spectrometer. After the gases have been ionized by electron-impact, a magnetic field then deflects, and thereby separates the ions depending on their masses to enable their independent quantification on ion-sensitive Faraday cups (Burlacot *et al.*, 2020). To increase the signals of O_2 and CO_2 relative to the background noise of e.g. water vapor, the inlet system can involve a cooling trap of below -80°C, facilitated e.g. by an ethanol-liquid nitrogen mixture or a Peltier cooling element, to freeze out water vapor before the gas stream enters the mass-spectrometer. The measured gas fluxes in the light correspond to net photosynthetic O_2 production and net CO_2 fixation during the Calvin cycle, whereas fluxes in the dark represent respiratory CO_2 release during the TCA cycle and O_2 consumption during the mitochondrial ETC .
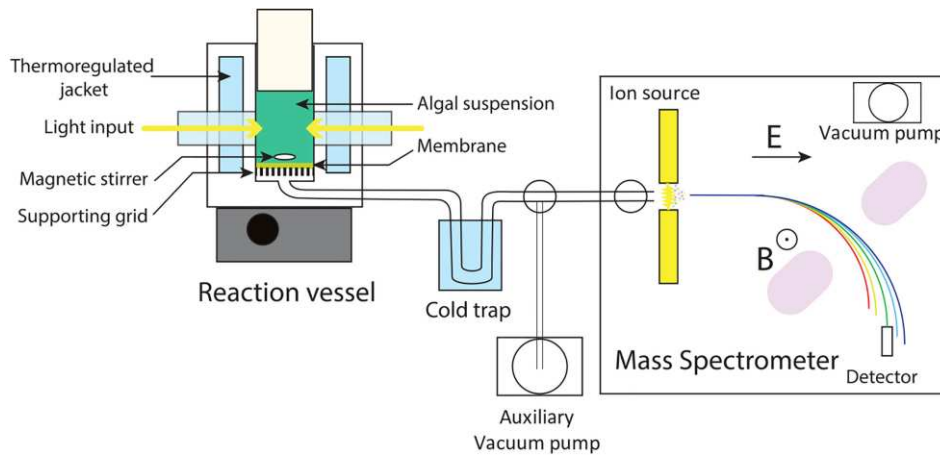
Fig 12. Schematic illustration of a membrane-inlet mass-spectrometer (MIMS) including a cuvette system (reaction vessel), a cold trap, a vacuum pump and the mass spectrometer (Burlacot *et al.*, 2020).

When using a stable- isotope mass-spectrometer, the presence of isotopically-labelled oxygen ($^{18}O_2$) enables to accurately distinguish between photosynthetic O_2 production ($^{16}O_2$ is produced from the splitting of $H_2^{16}O$) and respiratory O_2 consumption in the light ($^{18}O_2$ is taken up according to its relative proportion with respect to $^{16}O_2$) (Fig. 13; Fock & Sültemeyer, 1989). Thereby, this approach allows detailed investigations of O_2 consuming AEFs to understand physiological regulation mechanisms in phytoplankton, e.g. in response to different temperatures and light levels.
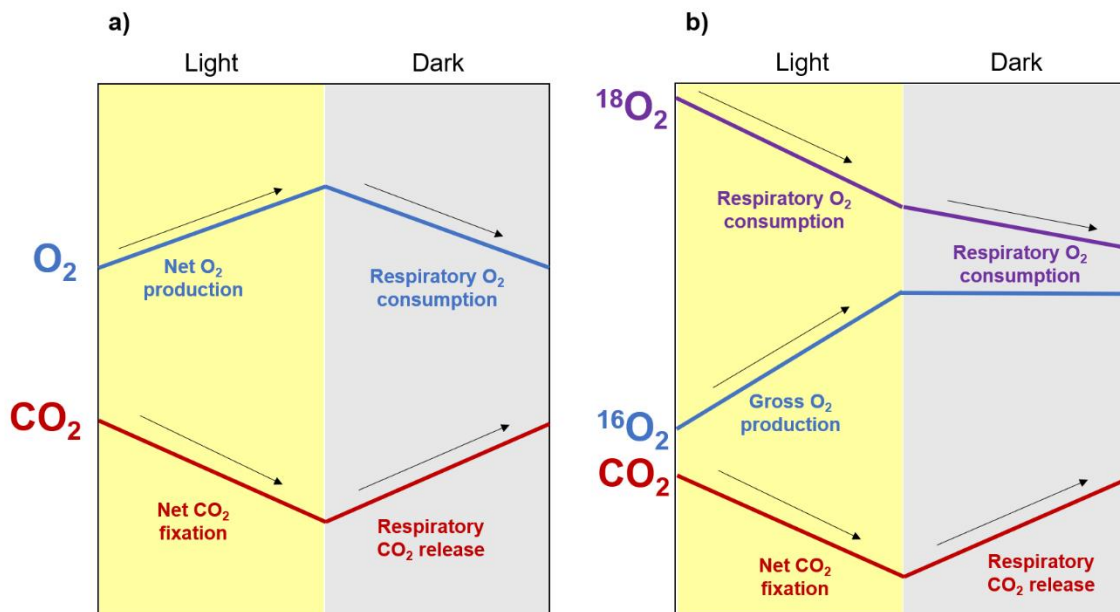
Fig 13. Schematic illustration of gas fluxes (O_2 and CO_2) corresponding to photosynthetic as well as respiratory sub-processes using an approach (a) without isotopic labelling or (b) with isotopic labelling of O_2 to distinguish between O_2 production and consumption in the light.

1.4. Objectives of this dissertation

As outlined above, temperature has the potential to affect multiple levels of phytoplankton physiology, which in turn can lead to shifts in natural phytoplankton communities with far-reaching consequences on ecosystem functioning and biogeochemical cycles. The objective of this dissertation is to unravel how Arctic phytoplankton responds to different warming scenarios with a special emphasis on their underlying physiology. Specifically, I aimed to

i. assess temperature response patterns of multiple functional traits in key Arctic phytoplankton species (*Publication I*).

ii. characterize underlying physiology to thereby identify imbalances between photosynthetic and respiratory sub-processes and to understand fundamental homeostatic mechanisms (*Publication II*).

iii. investigate the physiological reactions of natural Arctic phytoplankton communities under warming to verify the gained single-strain understanding on an ecologically more relevant level (*Publication III* and *IV*).

In *Publication I* the bloom-forming diatom *Thalassiosira hyalina,* the mixotrophic pico-eukaryote *Micromonas pusilla* and the ice-algae *Nitzschia frigida* were acclimated to temperatures ranging from 0°C and 14°C, and functional traits such as growth rates, production rates, quotas of biomass and pigmentation, as well as photophysiology were assessed to obtain respective temperature response patterns.

In *Publication II* physiological bottlenecks and key regulatory mechanisms were identified to understand how phytoplankton maintain a best-possible metabolic balance between different physiological processes to avoid detrimental temperature stress under warming. To this end, *T. hyalina* was acclimated to three distinct temperatures (sub-optimal, optimal and supra-optimal), and combined photophysiological and gas flux measurements using FRRf and MIMS (see chapter 1.3.4) were performed to characterize photosynthetic and respiratory sub-processes in detail.

To also understand temperature responses on a natural community level, I applied an incubation approach similar to *Publication II* to natural Arctic phytoplankton communities from the open-ocean central Fram strait (*Publication III*) as well as from a coastal fjord system in Svalbard (*Publication IV*). To this end, natural spring bloom communities were incubated at distinct temperatures and otherwise stable conditions,

and biomass accumulation, photosynthetic and respiratory O_2 fluxes (MIMS or O_2 optodes), photophysiology (FRRf) as well as community composition (18S rRNA metabarcoding) were assessed.

Because temperature responses highly depend on exposure time-scales, *Publication IV* did not only comprise stable temperature treatments over several weeks, but also short-term temperature fluctuations to assess Arctic phytoplankton responses under a simulated marine heatwave scenario.

1.5. List of publications and declaration of own contribution

(I) **Rehder, L.**, Rokitta, S.D., Hoppe, C.J.M., Buschmann, I., Jasper, L. and Rost, B. (2024). Different temperature sensitivities of key physiological processes lead to divergent trait response patterns in Arctic phytoplankton. Limnology and Oceanography, 69: 1845-1856. https://doi.org/10.1002/lno.12633 **Published.**

The experiments were planned together with the co-authors. The experiments were conducted by myself with contributions of IB and LJ. Data was analyzed by myself with contributions of SDR, CJMH and BR. The manuscript was written by myself with contributions of all co-authors.

(II) **Rehder, L.**, Rost, B., Kranz, S. and Rokitta, S.D Warming shifts plastidary-mitochondrial energy partitioning in the Arctic diatom *Thalassiosira hyalina*. **Under review at New Phytologist.**

The experiment was planned together with the co-authors. The experiment was conducted by myself. Data was analyzed by myself with contributions of all co-authors. The manuscript was written by myself with contributions of all co-authors.

Rehder, L., Ahme, A., Rokitta, S., Hoppe, C. and Rost, B. Warming stimulates biomass accumulation despite lowered net oxygen production in an Arctic phytoplankton community. **In preparation for submission.**

The experiment was planned together with the co-authors. The experiment was conducted by myself. Data was analyzed by myself with contributions of AA. The manuscript was written by myself with contributions of all co-authors.

(III) Wolf, K.K.E; Hoppe, C., **Rehder, L.**, Schaum, E., John, U. and Rost, B. (2024). Heatwave responses of Arctic phytoplankton communities are driven by combined impacts of warming and cooling. Sciences Advances. https://doi.org/10.1126/sciadv.adl590 **Published.**

The experiment was planned by KKEW with contribution of CJMH, ES and BR. The experiment was conducted by KKEW, CJMH and myself. Data was analyzed by KKEW with contributions of CJMH. The manuscript was written by KKEW with contributions of myself and the other co-authors.

2 *Publication I*

Different temperature sensitivities of key physiological processes lead to divergent trait response patterns in Arctic phytoplankton.

Published in Limnology and Oceanography

Rehder, L., Rokitta, S. D., Hoppe, C. J., Buschmann, I., Jasper, L., & Rost, B. (2024). Different temperature sensitivities of key physiological processes lead to divergent trait response patterns in Arctic phytoplankton. *Limnology and Oceanography*, *69*(8), 1845-1856.

Different temperature sensitivities of key physiological processes lead to divergent trait response patterns in Arctic phytoplankton

Linda Rehder [1*] Sebastian D. Rokitta [1], Clara J. M. Hoppe [1], Isabelle Buschmann [1,2],
Levke Jasper [1,3], Björn Rost [1,4]

[1]Marine Biogeosciences, Alfred Wegener Institute, Helmholtz Centre for Polar and Marine Research, Bremerhaven, Germany
[2]Department Biology I (Botany), Ludwig Maximilian University, Munich, Germany
[3]Plankton Ecology Lab, Institute for Chemistry and Biology of Marine Environments, Carl von Ossietzky University of Oldenburg, Wilhelmshaven, Germany
[4]Faculty of Biology and Chemistry, University of Bremen, Bremen, Germany

Abstract

Ocean warming is especially pronounced in the Arctic, and phytoplankton will face thermodynamically driven changes in their physiology, potentially pushing them beyond their thermal optimum. We assessed temperature responses of multiple functional traits over their entire thermal window (growth rates, quotas of particulate organic carbon, nitrogen, and chlorophyll *a*, as well as photophysiological parameters) in three different Arctic phytoplankton species (*Thalassiosira hyalina*, *Micromonas pusilla*, and *Nitzschia frigida*). Temperature response patterns in growth and biomass production rates indicated that all species exhibit wide thermal windows with highest rates at temperatures that exceed current polar temperatures. Species showed different temperature response patterns in cellular elemental quotas, which originate from the interplay of cell division and biomass production: These processes differ in their temperature sensitivity and optima, resulting in U-shaped, bell-shaped, or linear patterns of elemental quotas. Despite unaltered light intensity, higher temperatures increased light acclimation indices in all species while lifetimes of photosystem II reopening decreased in all species, suggesting that warming causes a transition from light saturation to light limitation. Our findings on temperature sensitivities of cell division and biomass production not only indicate that Arctic phytoplankton may benefit from moderate warming, but also highlight that meaningful interpretations of cellular quotas require a consideration of the underlying processes.

The Arctic is one of the regions most affected by climate change, with warming rates more than three times the global average (Rantanen et al. 2022). Alongside with rising mean temperatures, heatwaves have become more frequent, intense, and longer lasting in this region (Hobday et al. 2016; Cooley et al. 2022). Model simulations project further warming, especially in the ever-extending ice-free regions (Constable et al. 2022). In contrast to many other climate-related changes, like sea-ice decline or ocean acidification, warming itself has probably the most direct and potentially largest impact on polar species and ecosystems. Responses at the base of the ecosystems are hereby most relevant since changes in primary productivity are likely to propagate and amplify through the food web (Stock et al. 2014).

Phytoplankton and ice algae face many challenges in the Arctic Ocean. Being phototrophs, their growth is strongly controlled by light availability, but also the low temperatures prevailing in polar waters. Despite the absence of primary production during polar night, Arctic phytoplankton contributes significantly to global primary production (Van Leeuwe et al. 2018). Arctic sea-ice loss leads to deeper light penetration, longer growing seasons as well as an enlarged habitat for open ocean algae, which has been argued to drive substantial increases in net primary production (Ardyna and Arrigo 2020; Lewis et al. 2020). The earlier onset and accelerated biomass buildup due to altered light and temperature conditions may result in earlier phytoplankton spring blooms

Author Contribution Statement: Design of the research: LR, SR, CJMH, and BR. Conduct the research: LR, IB, and LJ. Data analysis: LR, SR, CJMH, IB, LJ, and BR. Drafting, revision, and editing of the manuscript: LR with contribution of all coauthors.

Rehder et al.   *Arctic phytoplankton thermal responses*

with higher peak biomass (Tedesco et al. 2019; Ardyna and Arrigo 2020; Rokitta et al. 2023), but also more prominent nutrient limitation over summer months (Wassmann and Reigstad 2011; Tremblay et al. 2015). While the aforementioned consequences of changes in the light regime are reasonably well understood and often used for projections, there are uncertainties with regard to the direct effects of warming on primary producers, specifically regarding optimal temperatures of different physiological processes.

As a universal driver, temperature affects all physical and (bio)chemical processes. Ectothermic organisms like phytoplankton are thus affected by temperature-induced changes of enzyme activity, membrane fluidity, or electron transfer rates, which are in turn reflected in processes underlying photosynthesis, respiration, nutrient assimilation, and cell division (Raven and Geider 1988; Falkowski et al. 1998). Typically, cell division (i.e., growth rate) as well as primary production follow an optimum curve (Thomas et al. 2012; Baker et al. 2016; Barton and Yvon-Durocher 2019), so that processes are stimulated by warming up to a certain optimum beyond which they sharply decline, for example, due to thermal inactivation of enzymes or increasing accumulation of reactive oxygen species (Moreno et al. 2024). Moreover, the temperature sensitivity of single physiological subprocesses likely differs, requiring readjustments of thermodynamically induced imbalances between those processes over the course of acclimation (Rehder et al. 2023). Since respiratory processes are often claimed to be more intensely stimulated than photosynthetic processes (Padfield et al. 2016; Barton et al. 2020), it is expected that ecosystems become more heterotrophic with warming (Hoppe et al. 2002; Hancke and Glud 2004; Holding et al. 2013). Furthermore, temperature was found to alter phytoplankton community composition (Hare et al. 2007; Kling et al. 2020; Ahme et al. 2023, 2024). In the Arctic, data from remote sensing, genetic field surveys, and sediment traps indeed suggest that species compositions shift from diatom-dominated toward *Phaeocystis*-dominated communities with warming (Nöthig et al. 2015; Soltwedel et al. 2016; Orkney et al. 2020), which will likely have substantial effects on food web dynamics and carbon export (Wiedmann et al. 2020; Assmy et al. 2023).

To understand the effect of ocean warming on phytoplankton, it is necessary to investigate how ecologically relevant phytoplankton species respond to temperature in different functional traits such as cell division, biomass production, or elemental stoichiometry. While previous studies focused mostly on growth rates over time scales of adaptation and evolution (Listmann et al. 2016; Schaum et al. 2017; Barton et al. 2023), we here focus on several traits and their physiological underpinnings on acclimation

time scales. To this end, we incubated *Thalassiosira hyalina*, a centric diatom that often dominates Arctic pelagic spring blooms (Hegseth and Sundfjord 2008), the picoeukaryote *Micromonas pusilla*, which substantially contributes to the largely mixotrophic winter community (Vader et al. 2015), and *Nitzschia frigida*, a typical ice-associated pennate diatom (Syvertsen 1991). We hypothesized that the investigated species occupy different thermal niches, according to their differences in habitat and seasonal distribution, and that functional traits exhibit different temperature sensitivities, which should become most prominent at the "edges" of their thermal windows.

Methods

Culturing

Strains of *T. hyalina* (KB3 SS5; Kongsfjord 2020), *M. pusilla* (CLP 1; Kongsfjord 2014) and *N. frigida* (UIO-542, Fram Strait 2019) were cultivated in triplicates in 0.2 μm sterile-filtered Arctic seawater (Salinity 32), which was enriched with vitamins and trace metals according to F/2 medium (Guillard and Ryther 1962). Nitrate, silicate, and phosphate were added in concentrations of 100, 100, and 6 μmol L^{-1}, respectively. Cells were grown as semi-continuous dilute batch cultures using custom-made 1-liter cylindric glass bottles. Cultures were aerated with air containing a pCO$_2$ of 400 μatm generated by a gas mixing system (CMG 2000, MCZ Umwelttechnik), in which CO$_2$-free air (< 1 ppm CO$_2$; Domnick Hunter) was mixed with pure CO$_2$ (Air Liquide). Acclimation temperatures ranged between 0°C and 14°C, depending on the species-specific thermal window that is defined as the temperature range in which cultures exhibit growth rates ≥ 0 d^{-1}. To ensure light saturation without photodamage, cell cultures were illuminated at 100 μmol photons m^{-2} s^{-1} (*T. hyalina* and *M. pusilla*) or 30 μmol photons m^{-2} s^{-1} (*N. frigida*, due to its association with sea-ice) in a 16:8 h light : dark cycle ensuring synchronized cell division. In the acclimations, cell concentrations remained low to ensure nutrient replete conditions and quasi-stable carbonate chemistry (pH drift < 0.05).

Cell division rate assessments and fitting of temperature responses

Before the start of the experiment, species were grown under the experimental treatment conditions at least for 10 generations, and full acclimation was confirmed by stable growth rates over at least 3 consecutive days. After acclimation was ensured, rate estimates were based on daily samplings, which took place about 4 h after the start of the photoperiod. Cell concentrations were determined using a cell counter (Beckmann-Coulter Multisizer III), and specific growth rates (i.e., using the base *e*) were calculated using the daily

increments of cell concentrations during the exponential growth phase according to the formula:

$$\mu = \frac{\ln(N_1) - \ln(N_0)}{t_1 - t_0} \tag{1}$$

where μ is the specific growth rate (d^{-1}), and N_0 as well as N_1 are the cell concentrations at the initial and final time points t_0 and t_1, respectively.

Temperature response curves of growth rates were fitted by least squares regression, applying the solver function of Microsoft Excel 2016 across all biological replicates per species at once. We hereby used the Eppley function (Eppley 1972) modified by Norberg et al. (2004) as the following:

$$\mu(T) = \left(1 - \left(\frac{T-z}{w}\right)^2\right) a e^{bT} \tag{2}$$

where w refers to the theoretical thermal niche width (later referred to as thermal window), z refers to the temperature where μ is equal to the Eppley function, and a and b are parameters of the Eppley function. This function was also used to derive the lower (T_{min}) and upper temperatures (T_{max}), beyond which the growth rate equals zero. Since the fit procedure yielded T_{min} values lower than the freezing point of seawater, we set this value to $-1.8°C$, in accordance with the freezing temperature of our sea water. The thermal window (T_{window}) was then calculated as the difference of T_{max} and T_{min}. The calculated optimal temperature (T_{opt}) was obtained via the derivative of Eq. 2 following:

$$T_{opt} = \frac{bz - 1 + \sqrt{\left(\frac{w}{2}\right)^2 b^2 + 1}}{b} \tag{3}$$

The calculated maximal growth rate (μ_{max}) was obtained from inserting T_{opt} into Eq. 2. Subsequently, we determined the temperature range where μ was $\geq 80\%$ of μ_{max} and highlighted this temperature range in each plot (Figs. 1–6) with a light green band.

Elemental composition and pigmentation

Sampling for cellular quotas of particulate organic carbon (POC) and nitrogen (PON) as well as of chlorophyll a (Chl a) was performed during exponential growth after acclimation for at least 10 d or seven generations. For the determination of POC and PON, cells were filtered onto precombusted (12 h, 500°C) glass fiber filters (GF/F, 0.7 μm nominal pore size, Whatman). After drying for at least 24 h, filters were submitted to elemental analysis (EuroVector EA 3000) using the flash combustion technique (Knap et al. 1996). Due to compromised PON analyses for *T. hyalina* and *M. pusilla*, only PON quotas of *N. frigida* could be obtained. POC production rates were calculated from POC quotas and specific growth rates per biological replicate following Morel (1987):

$$\text{POC production} = \mu \times \text{POC quota} \tag{4}$$

Chl a samples were filtered onto pre-combusted (12 h, 500°C) glass fiber filters (GF/F 0.7 μm, Whatman), shock-frozen in liquid nitrogen and stored at $-80°C$ until extraction. Filters were extracted overnight in 5 mL acetone (90%, Sigma-Aldrich), after cell disruption in a cell-mill (Precellys 24, Bertin). Then, extracts were centrifuged (4500 rpm for 7 min, Sigma 4K10) and Chl a concentration in the supernatant was determined using the fluorometric "acidification-method" (Turner Trilogy, Turner Designs; Knap et al. 1996). Samples of *N. frigida* were measured using a TD-700 Fluorometer (Turner Designs) after intercalibration of instruments. Ratios of Chl a : POC were subsequently calculated per biological replicate.

Chl a-based variable fluorescence

Photophysiological characteristics based on photosystem (PS) II variable fluorescence measurements were assessed using a fast repetition rate fluorometer (FRRf; FastOcean, Chelsea Technologies) combined with the FastAct2 Laboratory system (Chelsea Technologies). Light-emitting diodes were set to 450 nm emission wavelength to fully saturate all photosystems on short timescales. We used the FRRf in a single turn-over mode, in which the saturation phase comprised 100 (*T. hyalina*), 120 (*M. pusilla*), and 110 (*N. frigida*) flashlets, respectively, on a 2-μs pitch, and the relaxation phase comprised 40 flashlets on a 60-μs pitch. All measurements were conducted in a temperature-controlled cuvette at the respective acclimation temperature after dark acclimation for at least 15 min. Minimum Chl a fluorescence (F_0 and F'_0 for dark- and light-acclimated measurements, respectively) and maximum Chl a fluorescence (F_m and F'_m for dark- and light-acclimated measurements, respectively) were obtained from iteratively fitting the induction (Kolber et al. 1998) and the relaxation phase (Oxborough 2012). Photosynthesis–irradiance (PI) curves comprised eight light levels (5 min pre-acclimation at respective actinic light per light level; maximal light levels of $\sim 900 \mu$mol photons m^{-2} s^{-1}). Basic photophysiological parameters such as maximum quantum yields of PSII in the dark (F_v/F_m) and in the light, absorption cross section of PSII (σ_{PSII}), and life-time of PSII reopening (τ) were obtained using standard calculations (Genty et al. 1989; Maxwell and Johnson 2000; McKew et al. 2013; Schuback et al. 2017). Absolute electron transport rates (ETR) were obtained per light level according to Suggett et al. (2004) and Trimborn et al. (2017) and fitted in accordance to Rokitta and Rost (2012). ETRs at in situ irradiance of 30 or 100 μmol photons m^{-2} s^{-1}, light acclimation indices (E_k) and light use efficiencies (α; Supporting Information Table S1) were calculated accordingly. Non-photochemical quenching (NPQ) was calculated after McKew et al. (2013).

Data analysis

All data are shown as the mean of 3 biological replicates ± standard deviation (SD), if not stated otherwise. Least squares regression analyses of linear or quadratic functions were applied to verify the shapes of temperature response patterns of functional traits. Whenever temperature response patterns are described as "U-shaped," "bell-shaped," or "linear increased/decreased," trends are significant ($p \leq 0.05$). Results from regression fittings are reported in the Supporting Information (Tables S2–S4).

Results

Biological parameters

T. hyalina exhibited positive growth rates up to 12°C and presented a bell-shaped curve, with the highest measured growth rate of 1.4 ± 0.1 d^{-1} at 8°C (Fig. 1a). Between 2.5°C and 9°C, rates were ~ 1.0 d^{-1}, showing a wide plateau around the optimum. POC production rates followed a similar pattern with a maximum of 567 ± 56 pg C cell^{-1} d^{-1} at 8°C (Fig. 1a). POC quotas followed a U-shaped pattern over large parts of the investigated temperature range with maxima at 2.5°C (476 ± 12 pg C cell^{-1}) and 10°C (465 ± 26 pg C cell^{-1}; Fig. 1b). Chl *a* quotas followed a similar pattern as POC quotas (Fig. 1b). This resulted in largely unchanged Chl *a* : POC up to 8°C (~ 0.025 pg pg^{-1}; Fig. 1c), beyond which values increased to ~ 0.04 pg pg^{-1} (Fig. 1c).

M. pusilla exhibited positive growth rates up to 13°C and a symmetrical bell-shaped curve with a maximum rate of 1.0 ± 0.03 d^{-1} at 6°C (Fig. 2a). Production rates followed the same pattern with a maximum of 19.0 ± 2.0 pg C cell^{-1} d^{-1} at 6°C (Fig. 2a). POC quotas also followed a bell-shaped pattern similar to growth and production rates, with a maximum at 10°C (20 ± 2 pg C cell^{-1}; Fig. 2b). Chl *a* quotas (Fig. 2b), in turn, remained largely unchanged over the thermal window. Chl *a* : POC ratios varied between ~ 0.001 and 0.002 pg pg^{-1}

over the tested temperature range, with yet the highest values at or above 12°C (Fig. 2c).

N. frigida exhibited positive growth rates up to 11°C and a wide bell-shaped curve with a maximum of 0.52 ± 0.8 d^{-1} at 2.5°C (Fig. 3a). Since cells formed chains below 2.5°C (Supporting Information Fig. S1), we refrained from cellular normalizations for 0°C and 1.5°C data. POC production rates were highest at intermediate temperatures (70 ± 9 pg C cell^{-1} d^{-1} at 5.5°C; Fig. 3a) but declined beyond 8.5°C. POC quotas increased linearly with temperature from 129 ± 6 pg C cell^{-1} at 2.5°C to 366 ± 17 pg C cell^{-1} at 11°C (Fig. 3b). Chl *a* quotas (Fig. 3b) remained largely unchanged over the investigated temperature range. This resulted in a steep linear decrease of Chl *a* : POC ratio from 0.06 pg pg^{-1} at 2.5°C to 0.02 pg pg^{-1} at 11°C (Fig. 3c). POC : PON ratios, in turn, showed a steep linear increase from ~ 5 mol mol^{-1} at 2.5°C to ~ 15 mol mol^{-1} at 11°C (Fig. 3c).

To compare temperature responses between the three different species, data on growth rates were fitted using the Eppley–Norberg function (Norberg et al. 2004; Eq. 2). *T. hyalina* exhibited the highest calculated maximal growth rate (1.22 d^{-1}; Table 1), followed by *M. pusilla* (1.04 d^{-1}; Table 1). *N. frigida* exhibited lower calculated maximal rates (0.40 d^{-1}; Table 1). The derived optimal temperature for growth rate (T_{opt}) was highest in *M. pusilla* (7.6°C), followed by *T. hyalina* (7.0°C). For *N. frigida*, the derived optimal temperature was lower (4.3°C). The upper boundaries (T_{max}) were similarly high for *T. hyalina* and *M. pusilla* (~ 14°C), whereas *N. frigida* could only maintain growth up to ~ 11°C. Consequently, the thermal windows ranged between $\Delta 13$°C and $\Delta 16$°C (Table 1).

Photophysiology

T. hyalina exhibited generally high values for the photosystem II (PSII) quantum yield (F_v/F_m), with a bell-shaped curve in response to temperature and an optimum of ~ 0.65 at 6°C (Fig. 4a). The absolute electron transport rate at in situ

Fig. 1. Acclimation parameters of *Thalassiosira hyalina* at different temperatures. (**a**) Growth rates (black triangles) and POC production rates (gray circles), (**b**) particulate organic carbon quotas (POC; black triangles) and Chl *a* quotas (gray circles), and (**c**) ratios of Chl *a* : POC (black triangles). The green band defines the temperature range where μ is $\geq 80\%$ of the calculated μ_{max} and the dashed line indicates the measured optimal growth temperature. At 14°C, μ was ≤ 0 d^{-1}. Error bars denote standard deviation ($n = 3$), except for data where one or two replicates were lost ($n \leq 2$; empty symbols).

Rehder et al.   *Arctic phytoplankton thermal responses*
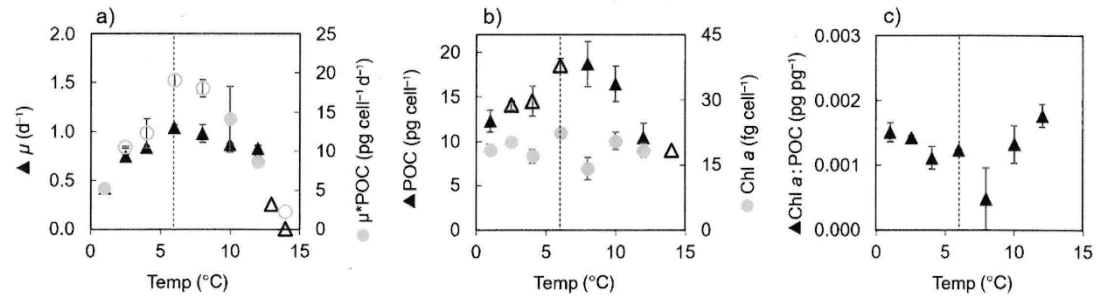
Fig. 2. Acclimation parameters of *Micromonas pusilla* at different temperatures. (**a**) Growth rates (black triangles) and POC production rates (gray circles), (**b**) particulate organic carbon quotas (POC; black triangles) and Chl *a* quotas (gray circles), and (**c**) ratios of Chl *a* : POC (black triangles). The green band defines the temperature range where μ is $\geq$ 80% of the calculated μ_{max}, and the dashed line indicates the measured optimal growth temperature. At 14°C, μ was $\leq$ 0 d^{-1}. Error bars denote standard deviation ($n = 3$), except for data where one or two replicates were lost ($n \leq 2$; empty symbols).
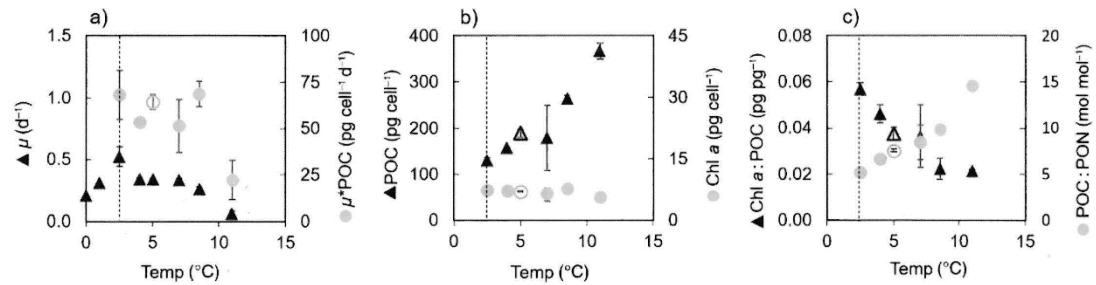
Fig. 3. Acclimation parameters of *Nitzschia frigida* at different temperatures. (**a**) Growth rates (black triangles) and POC production rates (gray circles), (**b**) particulate organic carbon quotas (POC; black triangles) and Chl *a* quotas (gray circles), and (**c**) ratios of Chl *a* : POC (black triangles) and POC : PON (gray circles). The green band defines the temperature range where μ is $\geq$ 80% of calculated μ_{max} and the dashed line indicates the measured optimal growth temperature. Error bars denote standard deviation ($n = 3$), except for data where one or two replicates were lost ($n \leq 2$; empty symbols).
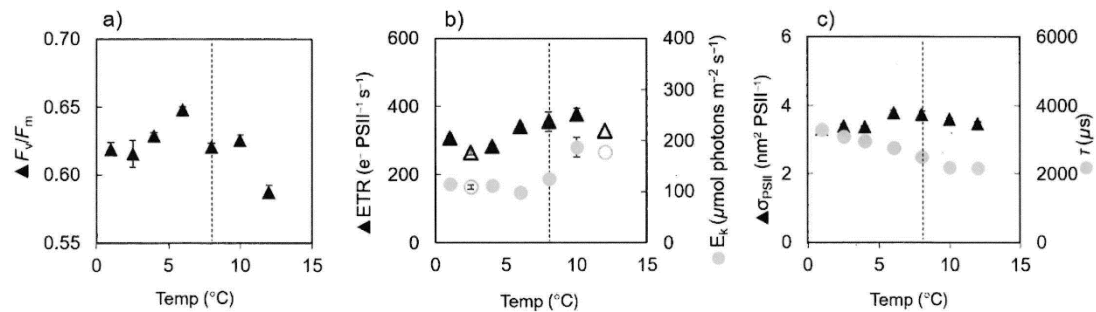
Fig. 4. Photophysiological parameters of *Thalassiosira hyalina* at different temperatures. (**a**) Photosystem II quantum yield (F_v/F_m; black triangles), (**b**) absolute electron transport rate under in situ irradiance (ETR; black triangles) and light acclimation index (E_k; gray circles), and (**c**) absorption cross section (σ_{PSII}; black triangles) and life time of PSII reopening (τ, gray circles). The green band defines the temperature range where μ is $\geq$ 80% of calculated μ_{max} and the dashed line indicates the measured optimal growth temperature. Error bars denote standard deviation ($n = 3$), except for data where one or two replicates were lost ($n \leq 2$; empty symbols).

1849

36
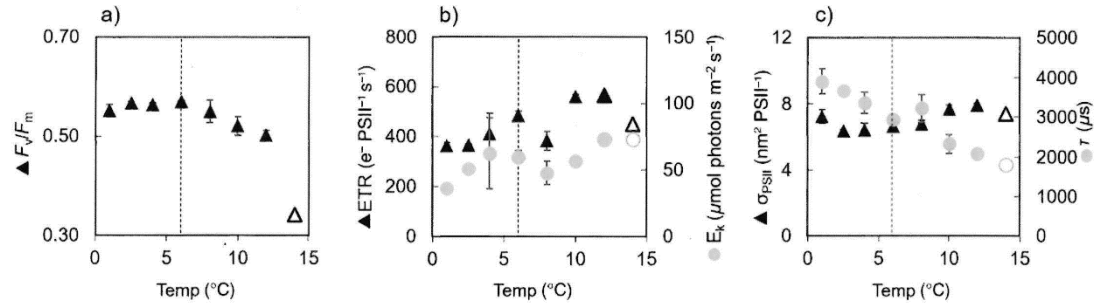
Fig. 5. Photophysiological parameters of *Micromonas pusilla* at different temperatures. (**a**) Photosystem II quantum yield (F_v/F_m; black triangles), (**b**) absolute electron transport rate under in situ irradiance (ETR; black triangles) and light acclimation index (E_k; gray circles), and (**c**) absorption cross section (σ_{PSII}; black triangle) and life time of PSII reopening (τ, gray circles). The green band defines the temperature range where μ is $\geq$ 80% of calculated μ_{max}, and the dashed line indicates the measured optimal growth temperature. Error bars denote standard deviation ($n = 3$), except for data where one or two replicates were lost ($n \leq 2$; empty symbols).

Fig. 6. Photophysiological parameters of *Nitzschia frigida* at different temperatures (**a**) photosystem II quantum yield (F_v/F_m; black triangles), (**b**) absolute electron transport rate under in situ irradiance (ETR; black triangles) and light acclimation index (E_k; gray circles), and (**c**) absorption cross section (σ_{PSII}; black triangle) and life time of PSII reopening (τ, gray circles). The green band defines the temperature range where μ is $\geq$ 80% of calculated μ_{max} and the dashed line indicates the measured optimal growth temperature. Error bars denote standard deviation ($n = 3$), except for data where one or two replicates were lost ($n \leq 2$; empty symbols).

irradiance (ETR) followed a bell-shaped curve between 2.5°C and 12°C with an optimum of ~ 400 e$^-$ PSII^{-1} s^{-1} at 10°C (Fig. 4b). The light acclimation index (E_k) remained constant until the optimal growth temperature at $\sim 110\,\mu$mol photons m^{-2} s^{-1}, but increased up to $\sim 190\,\mu$mol photons m^{-2} s^{-1} beyond (Fig. 4b). The absorption cross section (σ_{PSII}) followed a shallow bell-shaped curve similar to F_v/F_m with an optimum of ~ 3.8 nm^2 PSII^{-1} at 6°C (Fig. 4c). The lifetime of PSII reopening (τ) decreased linearly from ~ 3300 to $\sim 2200\,\mu$s over the investigated temperature range (Fig. 4c).

M. pusilla exhibited a wide bell-shaped curve for F_v/F_m with an optimum of 0.57 at 6°C (Fig. 5a), followed by a steep decline to 0.34 at 14°C. The ETR also followed a bell-shaped temperature response pattern with an optimum of ~ 600 e$^-$ PSII^{-1} s^{-1} at 10°C (Fig. 5b). E_k increased from ~ 35 to

$\sim 75\,\mu$mol photons m^{-2} s^{-1} (Fig. 5b). Except for lowest and highest investigated temperatures, σ_{PSII} followed a similar pattern, that is, it increased between 2.5°C and 12°C from ~ 6.4 to 7.9 nm^2 PSII^{-1}, and decreased to ~ 7.4 nm^2 PSII^{-1} at 14°C (Fig. 5c). τ decreased linearly from ~ 3900 to 1800 μs over the investigated temperature window (Fig. 5c).

N. frigida exhibited a decreasing trend in F_v/F_m with a plateau of ~ 0.59 between 2.5°C and 9°C (Fig. 6a). The ETR followed a bell-shaped temperature response pattern with an optimum of ~ 600 e$^-$ PSII^{-1} s^{-1} at 5°C (Fig. 6b). E_k increased until $\sim 220\,\mu$mol photons m^{-2} s^{-1} at 5°C and declined beyond (Fig. 6b). σ_{PSII} showed a subtle increase between 0°C and 7°C and remained more or less constant beyond (Fig. 6c). τ decreased linearly from ~ 4300 to 3000 μs over the investigated temperature window (Fig. 6c).

Rehder et al.   *Arctic phytoplankton thermal responses*

Discussion

High growth rates despite low temperatures

The three investigated species can be distinguished in two groups with regard to the width of their temperature windows and their maximal growth rates. *N. frigida* exhibited a comparably narrow thermal window (from < 0°C to 11°C, respectively; Fig. 3a; Table 1), which is in line with them occurring in the vicinity of sea-ice habitats (Assmy et al. 2017). Also, the obtained growth rates of *N. frigida* were comparably low with maximal rates of 0.54 d^{-1} (Fig. 3a).

T. hyalina and *M. pusilla* exhibited wider temperature windows in comparison *N. frigida* (< 1–12°C and 14°C, respectively; Figs. 1a, 2a; Table 1). This may reflect the strains originating from Kongsfjorden (Svalbard), which is influenced by warmer North Atlantic water masses and remains typically ice free (Payne and Roesler 2019; Tverberg et al. 2019). Both species also exhibited impressively high maximum growth rates of 1.4 d^{-1} (*T. hyalina*; Fig. 1a) and 1.02 d^{-1} (*M. pusilla*; Fig. 2a), which is in line with findings of previous studies on these isolates (Hoppe et al. 2018; Wolf et al. 2018, 2022). Such high growth rates at polar temperatures, which translate into more than 2.0 and 1.5 cell divisions per day, respectively, contradict the common notion of generally higher growth rates in warmer regions (Eppley 1972; Thomas et al. 2012). In fact, maximal growth rates observed in temperate *Thalassiosira* sp. and *Micromonas* sp. were in the same range or even lower at much higher temperatures but otherwise comparable nutrient and light conditions (Boyd et al. 2013; Baker et al. 2016; Demory et al. 2017). Consequently, the physiology of *T. hyalina* and *M. pusilla* must have evolved to compensate the thermodynamic challenges of high latitudes. One mechanism to achieve high growth rates under low temperatures could involve an upregulation of the C-fixation machinery (i.e., content of RuBisCO) as observed in a polar diatom (Young et al. 2015). Such remarkably high regulatory potential might be the foundation of the generally observed high plasticity of Arctic coastal phytoplankton assemblages (Hoppe et al. 2018) and particularly of *T. hyalina* (Wolf et al. 2018, 2022).

Table 1. Calculated optimal temperature for growth rate (T_{opt}), maximal temperature (T_{max}) as well as maximal growth rate (μ_{max}) at T_{opt} of *Thalassiosira hyalina*, *Micromonas pusilla*, and *Nitzschia frigida* according to Norberg et al. (2004). T_{window} denotes the total thermal scope, derived from $T_{max} - T_{min}$ (T_{min} was defined as −1.8°C, i.e., the freezing point of salt water at salinity 32).

Species	μ_{max} (d^{-1})	T_{opt} (°C)	T_{max} (°C)	T_{window} (Δ°C)
T. hyalina	1.22	7.0	14.5	16.3
M. pusilla	1.04	7.6	14.2	16.1
N. frigida	0.40	4.3	11.5	13.3

Interplay of cell division and biomass production rates shapes the response of biomass quotas

In contrast to the bell-shaped temperature response patterns observed in the growth rates of all species, other functional traits differed remarkably in their temperature responses. *T. hyalina* exhibited U-shaped thermal responses in their POC quotas over wide temperature ranges (Fig. 1b), which contrasts with the bell-shaped response curves of the growth rates: When growth rates were high, POC quotas were low and vice versa. This diverging pattern of the cellular POC quota is a result of the underlying physiological processes, namely cell division and biomass production. Even though, these underlying processes both followed a bell-shaped temperature response curve (Fig. 1a,b), they differ in their temperature sensitivities. More precisely, cell division is more temperature sensitive than biomass production in this species. As a consequence, cell division ceases faster than biomass production toward extreme temperatures, resulting in high POC quotas. Thus, the temperature responsiveness of cell division exerted a stronger control on elemental quotas than biomass production rates in *T. hyalina*. This phenomenon of U-shaped temperature responses of POC quotas was previously observed in the temperate phytoplankton *Phaeodactylum tricornutum*, *Pavlova lutheri*, and *Thalassiosira pseudonana* (Thompson et al. 1992; Atkinson et al. 2003; Carvalho and Malcata 2003).

M. pusilla not only exhibited bell-shaped temperature response patterns in growth and production rates similar as *T. hyalina*, but also exhibited a bell-shaped temperature response pattern in POC quotas (Fig. 2a,b). In this case, biomass production was more temperature sensitive and ceased earlier than cell division, leading to cells with lowered POC quotas at the edges of the temperature window. Thus, in this species, POC production exerted a stronger control on patterns of biomass quotas than cell division.

N. frigida also exhibited more or less bell-shaped temperature response patterns in both growth rates as well as biomass production rates. The optimum temperatures of these two processes were, however, distinct from each other, resulting in a linear increase of POC quotas with temperature (Fig. 3a,b). This finding is at odds with the common notion that high quotas reflect healthy cells. Our data, instead, show that high quotas are the result of gradually ceasing cell division while photosynthesis and subsequent biomass production are still maintained. PON quotas, however, were not increased in response to temperature in *N. frigida*, resulting in an increased POC : PON ratio of up to 15 mol mol^{-1} at 11°C (Fig. 3c). This indicates an enormous imbalance between net POC and PON production under rising temperatures with potential consequences on the nutritional value (Kwiatkowski et al. 2018; Boersma and Meunier 2020).

While the temperature response patterns of POC quotas differed remarkably between species, the principle of their emergence is generic for all species: Biomass quotas (here POC quotas) result from the interplay of the processes of cell

Fig. 7. Conceptualization of the interplay of growth rates (blue), POC production rates (orange) and POC quotas (gray), when POC quotas exhibit a (**a**) U-shaped temperature response, (**b**) bell-shaped temperature response or (**c**) linear temperature response.

division and biomass production (in this study calculated in accordance to Morel (1987)). While these two processes are largely independent and can differ in their temperature sensitivities, their combined effect and relation to each other determines the shape of the temperature response pattern of biomass quotas. Despite this comparably simple mechanistic relation, the interplay of these processes with different temperature response patterns (slope, width, and optimum temperature) manifests into diverse temperature response patterns of POC quotas. We have conceptualized these patterns in Fig. 7: If the temperature response pattern of the growth rate exhibits a steeper slope than the one of the POC production rate (i.e., cell division is more temperature sensitive than biomass production), POC quotas will exhibit a U-shaped temperature response pattern (Fig. 7a, *T. hyalina*). If the temperature response pattern of the growth rate exhibits a less steep slope than the one of POC production rate (i.e., the process of cell division is less temperature sensitive than biomass production), POC quotas will exhibit a bell-shaped temperature response pattern (Fig. 7b, *M. pusilla*). Different optimum temperatures for growth and POC production rates will result in linear trends in POC quotas (Fig. 7c, *N. frigida*). If temperature response patterns of growth rates and POC production rates were equal in shape and form, however, POC quotas would remain constant over the whole investigated temperature range (example not shown).

High temperatures cause profound shifts in photophysiology

In all species, the maximum potential quantum yield of photosystem II (F_v/F_m) was rather constant over large parts of the investigated temperature range, and only slightly decreased beyond the optimal growth temperatures (Figs. 4a, 5a, 6a). Thus, the functionality of the photosynthetic apparatus remained high over the investigated temperature range, even though cells experienced a slightly lowered efficiency under heat stress. The electron transport rate under in situ irradiance (ETR), however, followed a bell-shaped curve over large parts of the temperature window in all species

(Figs. 4b, 5b, 6b), similar to the rates of cell division and POC production. Despite species-specific differences in slope and width of the ETR temperature response, its optimal temperature seemed to be generally 1–3°C higher than the respective optimal temperatures of cell division and POC production. This proves the existence of diverging optimal temperatures in different photosynthetic subprocesses within one cell. The differences in temperature sensitivities between ETR and POC production, in turn, advocate arising imbalances between photosynthetic light-dependent and light-independent reactions toward the edges of the temperature window. More specifically, the discrepancies between "both sides of photosynthesis" cause an overreduction of the photosynthetic electron transport chain at temperature extremes, likely giving rise to oxidative stress. Future research should target compensatory mechanisms to deal with extreme temperatures.

In both pelagic species, the Chl a : POC ratio showed an increasing trend beyond optimal growth temperatures (Figs. 1c, 2c), indicating a relatively higher pigmentation per biomass. This can be caused by stronger changes in POC quotas than in Chl a quotas with temperature, but also shifts in light harvesting complexes or photosystem abundances are indicated. In *M. pusilla*, for instance, the absorption cross section of PSII (Fig. 5c) increased with temperature throughout the temperature range where μ is ≥ 80% of μ_{max} (i.e., the green band), indicating increased antenna sizes of the light harvesting complexes. In *T. hyalina*, we did not observe such an increase in PSII absorption cross section beyond optimal temperatures (Fig. 4c), but here the increased pigmentation per biomass might be explained by increased abundances of photosystems. Such a strategy, especially the upregulation of PSI, might additionally serve to dissipate the aforementioned overreduction at highest temperatures.

In contrast to the findings for the pelagic species, the ice alga *N. frigida* responded with a strong decrease of Chl a : POC ratios with increasing temperatures (Fig. 3c), which can be attributed to the massively increased POC quotas at high temperatures (Fig. 3b). This increase may be a result of the cells'

Rehder et al.   *Arctic phytoplankton thermal responses*

attempt to deal with temperature induced redox stress: Only *N. frigida* experienced an increase of nonphotochemical quenching (NPQ) at in situ light intensity under the highest temperature (Supporting Information Fig. S2), indicating overreduction. It was previously observed that other micro-algae reroute excess plastidary reductant into the mitochondria. This causes a shift in the redox state and throttles their citric acid cycle activity, which decreases the respiratory carbon loss (Bailleul et al. 2015; Curien et al. 2016), while maintaining the respiratory electron transport chain. This was especially pronounced under increased temperatures (Rehder et al. 2023) and might explain the here observed massive POC retention in *N. frigida* under high temperatures.

All three species showed a linear decrease in τ, reflecting a generally faster reopening of photosystem II with warming (Figs. 4c, 5c, 6c). This is in line with the response of temperate diatoms (Baker et al. 2016) as well as Arctic phytoplankton communities (Wolf et al. 2024) and possibly constitutes a generic feature of photosynthesis. Whether this is an acclimation response or merely a thermodynamic effect should be subject of future studies.

The here investigated species also showed a consistent increase in their fluorescence-based light acclimation indices (E_k) in response to warming until a certain threshold (Figs. 4b, 5b, 6b). E_k is the light intensity, at which photosynthesis transitions from light limitation (in situ light intensity $< E_k$) to saturation (in situ light intensity $> E_k$) (Behrenfeld et al. 2004). While it is known that E_k is affected by acclimation to different light levels (MacIntyre et al. 2002; Behrenfeld et al. 2008), our data show that the transition point from light limitation into light saturation is shifted to higher irradiances also with warming. In other words, high temperatures make cells more "light-limited" (as indicated by increasing E_k), thereby enabling them to exploit light intensities that would be saturating or even stressful under low temperatures (Behrenfeld et al. 2004). Despite this phenomenon being common among the investigated species, there were species-specific differences: *T. hyalina* and *N. frigida* kept E_k more or less constant up to their optimal growth temperatures, but experienced a strong increase beyond (Figs. 4b, 6b). Thereby, cells remained close to light saturation up to their temperature optimum, and only beyond, they transitioned abruptly into a thermally induced light limitation. *M. pusilla* experienced a gentle but steady increase of E_k over large parts of their thermal window (Fig. 5b). Thus, they gradually become more light-limited with warming so that the transition from light saturation at low temperature into light limitation at high temperature is smoother than in the other investigated species. Overall, phytoplankton likely benefit from a simultaneous increase of temperature and light, as these changes are projected for the large parts of the Arctic Ocean with ongoing climate change (Constable et al. 2022).

Conclusion and ecological implications

Different phytoplankton functional traits were found to differ substantially in their temperature response patterns. Particularly, physiological processes such as cell division, electron transport rates or biomass production rates generally followed optimal- or bell-shaped patterns, which differed in their optimal temperatures and/or slopes of increase or decrease. Resulting quotas such as Chl *a* and POC quotas, however, exhibited partially opposing response patterns between species, depending on the relation of their underlying physiological processes. This emphasizes the necessity for holistic assessments including multiple temperatures, species, and functional traits, all of which should then also be considered for biogeochemical modeling approaches or the evaluation of remote sensing data.

Generally, some of the investigated species not only exhibited impressively high growth rates, they also covered unexpectedly wide thermal windows with rather high optimal temperatures. Part of this may be attributable to the fact that isolates originated from the Fram Strait or Svalbard fjords and are thus influenced by varying contributions of warmer North Atlantic water. Consequently, these species may generally exhibit a higher phenotypic plasticity toward temperature than phytoplankton originating from the high Arctic. Nonetheless, all investigated species seem to live below their optimal growth temperatures in the present-day Arctic Ocean. Consequently, they will likely benefit from future ocean warming up to a certain species-specific (and potentially strain-specific) threshold. Our data on photophysiology moreover indicate a synergistic effect of irradiance and temperature, which both are predicted to increase in the Arctic due to enhanced sea-ice melt as well as thermally induced stratification. This would add further support to projections of nutrients becoming a dominant limiting factor for primary production in high-latitude marine ecosystems (Tremblay et al. 2015). In the future Arctic Ocean, phytoplankton spring blooms might be characterized by higher growth rates and biomass production, but thereby nutrients are depleted faster, resulting in more intense but shorter bloom events.

Data availability statement

The data supporting the findings of this study are openly available in the Pangea Database, https://doi.pangaea.de/10.1594/PANGAEA.968670.

References

Ahme, A., A. Von Jackowski, R. A. McPherson, K. K. Wolf, M. Hoppmann, S. Neuhaus, and U. John. 2023. Winners and losers of Atlantification: The degree of ocean warming affects the structure of Arctic microbial communities. Genes **14**: 623.

1853

40

Ahme, A., and others. 2024. Warming increases the compositional and functional variability of a temperate protist community. Sci. Total Environ. **926**: 171971.

Ardyna, M., and K. R. Arrigo. 2020. Phytoplankton dynamics in a changing Arctic Ocean. Nat. Clim. Change **10**: 892–903. doi:10.1038/s41558-020-0905-y

Assmy, P., and others. 2017. Leads in Arctic pack ice enable early phytoplankton blooms below snow-covered sea ice. Sci. Rep. **7**: 40850. doi:10.1038/srep40850

Assmy, P., and others. 2023. Seasonal plankton dynamics in Kongsfjorden during two years of contrasting environmental conditions. Prog. Oceanogr. **213**: 102996.

Atkinson, D., B. J. Ciotti, and D. J. Montagnes. 2003. Protists decrease in size linearly with temperature: ca. 2.5% C (−1). Proc. R. Soc. Lond. Ser. B Biol. Sci. **270**: 2605–2611.

Bailleul, B., and others. 2015. Energetic coupling between plastids and mitochondria drives CO_2 assimilation in diatoms. Nature **524**: 366–369.

Baker, K. G., C. M. Robinson, D. T. Radford, A. S. McInnes, C. Evenhuis, and M. A. Doblin. 2016. Thermal performance curves of functional traits aid understanding of thermally induced changes in diatom-mediated biogeochemical fluxes. Front. Mar. Sci. **3**: 44.

Barton, S., and G. Yvon-Durocher. 2019. Quantifying the temperature dependence of growth rate in marine phytoplankton within and across species. Limnol. Oceanogr. **64**: 2081–2091.

Barton, S., J. Jenkins, A. Buckling, C.-E. Schaum, N. Smirnoff, J. A. Raven, and G. Yvon-Durocher. 2020. Evolutionary temperature compensation of carbon fixation in marine phytoplankton. Ecol. Lett. **23**: 722–733. doi:10.1111/ele.13469

Barton, S., D. Padfield, A. Masterson, A. Buckling, N. Smirnoff, and G. Yvon-Durocher. 2023. Comparative experimental evolution reveals species-specific idiosyncrasies in marine phytoplankton adaptation to warming. Glob. Chang. Biol. **29**: 5261–5275.

Behrenfeld, M. J., O. Prasil, M. Babin, and F. Bruyant. 2004. In search of a physiological basis for covariations in light-limited and light-saturated photosynthesis 1. J. Phycol. **40**: 4–25.

Behrenfeld, M. J., K. H. Halsey, and A. J. Milligan. 2008. Evolved physiological responses of phytoplankton to their integrated growth environment. Philos. Trans. R. Soc. B Biol. Sci. **363**: 2687–2703.

Boersma, M., and C. L. Meunier. 2020. Zooplankton–phytoplankton interactions in a changing world, p. 28–52. *In* Zooplankton ecology. CRC Press.

Boyd, P. W., and others. 2013. Marine phytoplankton temperature versus growth responses from polar to tropical waters—Outcome of a scientific community-wide study. PLoS One **8**: e63091.

Carvalho, A. P., and F. X. Malcata. 2003. Kinetic modeling of the autotrophic growth of *Pavlova lutheri*: Study of the combined influence of light and temperature. Biotechnol. Prog. **19**: 1128–1135.

Constable, A. J., and others. 2022. Cross-chapter paper 6: Polar regions. *In* IPCC AR WGII. Cambridge Univ. Press.

Cooley, S., and others. 2022. Oceans and coastal ecosystems and their services. *In* IPCC AR6 WGII. Cambridge Univ. Press.

Curien, G., and others. 2016. The water to water cycles in microalgae. Plant Cell Physiol. **57**: 1354–1363.

Demory, D., and others. 2017. Temperature is a key factor in *Micromonas*–virus interactions. ISME J. **11**: 601–612. doi:10.1038/ismej.2016.160

Eppley, R. W. 1972. Temperature and phytoplankton growth in the sea. Fish. Bull. **70**: 1063–1085.

Falkowski, P. G., R. T. Barber, and V. Smetacek. 1998. Biogeochemical controls and feedbacks on ocean primary production. Science **281**: 200–206. doi:10.1126/science.281.5374.200

Genty, B., J.-M. Briantais, and N. R. Baker. 1989. The relationship between the quantum yield of photosynthetic electron transport and quenching of chlorophyll fluorescence. Biochim. Biophys. Acta Gen. Subj. **990**: 87–92. doi:10.1016/S0304-4165(89)80016-9

Guillard, R. R., and J. H. Ryther. 1962. Studies of marine planktonic diatoms: I. *Cyclotella nana* Hustedt, and *Detonula confervacea* (Cleve) Gran. Can. J. Microbiol. **8**: 229–239.

Hancke, K., and R. N. Glud. 2004. Temperature effects on respiration and photosynthesis in three diatom-dominated benthic communities. Aquat. Microb. Ecol. **37**: 265–281.

Hare, C. E., K. Leblanc, G. R. DiTullio, R. M. Kudela, Y. Zhang, P. A. Lee, S. Riseman, and D. A. Hutchins. 2007. Consequences of increased temperature and CO2 for phytoplankton community structure in the Bering Sea. Mar. Ecol. Prog. Ser. **352**: 9–16.

Hegseth, E. N., and A. Sundfjord. 2008. Intrusion and blooming of Atlantic phytoplankton species in the high Arctic. J. Mar. Syst. **74**: 108–119. doi:10.1016/j.jmarsys.2007.11.011

Hobday, A. J., and others. 2016. A hierarchical approach to defining marine heatwaves. Prog. Oceanogr. **141**: 227–238.

Holding, J. M., C. M. Duarte, J. M. Arrieta, R. Vaquer-Sunyer, A. Coello-Camba, P. Wassmann, and S. Agustí. 2013. Experimentally determined temperature thresholds for Arctic plankton community metabolism. Biogeosciences **10**: 357–370. doi:10.5194/bg-10-357-2013

Hoppe, C. J. M., C. M. Flintrop, and B. Rost. 2018. The Arctic picoeukaryote *Micromonas pusilla* benefits synergistically from warming and ocean acidification. Biogeosciences **15**: 4353–4365.

Hoppe, H.-G., K. Gocke, R. Koppe, and C. Begler. 2002. Bacterial growth and primary production along a north–south transect of the Atlantic Ocean. Nature **416**: 168–171. doi:10.1038/416168a

Rehder et al.   *Arctic phytoplankton thermal responses*

Kling, J. D., M. D. Lee, F. Fu, M. D. Phan, X. Wang, P. Qu, and D. A. Hutchins. 2020. Transient exposure to novel high temperatures reshapes coastal phytoplankton communities. ISME J. **14**: 413–424. doi:10.1038/s41396-019-0525-6

Knap, A., A. Michaels, A. Close, H. Ducklow, and A. Dickson. 1996. Protocols for the joint global ocean flux study (JGOFS) core measurements. JGOFS. Reprint of the IOC manuals and guides no. 29, UNESCO 1994, 19.

Kolber, Z. S., O. Prášil, and P. G. Falkowski. 1998. Measurements of variable chlorophyll fluorescence using fast repetition rate techniques: Defining methodology and experimental protocols. Biochim. Biophys. Acta Bioenergetics **1367**: 88–106.

Kwiatkowski, L., O. Aumont, L. Bopp, and P. Ciais. 2018. The impact of variable phytoplankton stoichiometry on projections of primary production, food quality, and carbon uptake in the global ocean. Global Biogeochem. Cycl. **32**: 516–528.

Lewis, K., G. Van Dijken, and K. R. Arrigo. 2020. Changes in phytoplankton concentration now drive increased Arctic Ocean primary production. Science **369**: 198–202.

Listmann, L., M. LeRoch, L. Schlüter, M. K. Thomas, and T. B. H. Reusch. 2016. Swift thermal reaction norm evolution in a key marine phytoplankton species. Evol. Appl. **9**: 1156–1164. doi:10.1111/eva.12362

MacIntyre, H. L., T. M. Kana, T. Anning, and R. J. Geider. 2002. Photoacclimation of photosynthesis irradiance response curves and photosynthetic pigments in microalgae and cyanobacteria 1. J. Phycol. **38**: 17–38.

Maxwell, K., and G. N. Johnson. 2000. Chlorophyll fluorescence—A practical guide. J. Exp. Bot. **51**: 659–668. doi:10.1093/jexbot/51.345.659

McKew, B. A., and others. 2013. The trade-off between the light-harvesting and photoprotective functions of fucoxanthin-chlorophyll proteins dominates light acclimation in *Emiliania huxleyi* (clone CCMP 1516). New Phytol. **200**: 74–85. doi:10.1111/nph.12373

Morel, F. M. 1987. Kinetics of nutrient uptake and growth in phytoplankton 1. J. Phycol. **23**: 137–150.

Moreno, H. D., S. Rokitta, N. Tremblay, M. Boersma, E. Groß, H. C. Klip, K. H. Wiltshire, and C. L. Meunier. 2024. Higher temperature, increased CO_2, and changing nutrient ratios alter the carbon metabolism and induce oxidative stress in a cosmopolitan diatom. Limnol. Oceanogr. **69**: 121–139. doi:10.1002/lno.12463

Norberg, E., G. Rogers, R. Goodling, J. Cooper, and P. Madsen. 2004. Genetic parameters for test-day electrical conductivity of milk for first-lactation cows from random regression models. J. Dairy Sci. **87**: 1917–1924.

Nöthig, E.-M., and others. 2015. Summertime plankton ecology in Fram Strait—A compilation of long- and short-term observations. Polar Res. **34**: 23349. doi:10.3402/polar.v34.23349

Orkney, A., T. Platt, B. E. Narayanaswamy, I. Kostakis, and H. A. Bouman. 2020. Bio-optical evidence for increasing *Phaeocystis* dominance in the Barents Sea. Philos. Trans. R. Soc. A Math. Phys. Eng. Sci. **378**: 20190357. doi:10.1098/rsta.2019.0357

Oxborough, K. 2012. FastPro8 GUI and FRRf3 systems documentation. Chelsea Technologies Group Ltd.

Padfield, D., G. Yvon-Durocher, A. Buckling, S. Jennings, and G. Yvon-Durocher. 2016. Rapid evolution of metabolic traits explains thermal adaptation in phytoplankton. Ecol. Lett. **19**: 133–142. doi:10.1111/ele.12545

Payne, C. M., and C. S. Roesler. 2019. Characterizing the influence of Atlantic water intrusion on water mass formation and phytoplankton distribution in Kongsfjorden, Svalbard. Cont. Shelf Res. **191**: 104005. doi:10.1016/j.csr.2019.104005

Rantanen, M., A. Y. Karpechko, A. Lipponen, K. Nordling, O. Hyvärinen, K. Ruosteenoja, T. Vihma, and A. Laaksonen. 2022. The Arctic has warmed nearly four times faster than the globe since 1979. Commun. Earth Environ. **3**: 168. doi:10.1038/s43247-022-00498-3

Raven, J. A., and R. J. Geider. 1988. Temperature and algal growth. New Phytol. **110**: 441–461.

Rehder, L., B. Rost, and S. D. Rokitta. 2023. Abrupt and acclimation responses to changing temperature elicit divergent physiological effects in the diatom *Phaeodactylum tricornutum*. New Phytol. **239**: 1005–1013.

Rokitta, S. D., and B. Rost. 2012. Effects of CO_2 and their modulation by light in the life-cycle stages of the coccolithophore *Emiliania huxleyi*. Limnol. Oceanogr. **57**: 607–618.

Rokitta, S. D., C. H. Grossmann, E. Werner, J. Moye, G. Castellani, E. M. Nöthig, and B. Rost. 2023. Future warming stimulates growth and photosynthesis in an Arctic microalga more strongly than changes in light intensity or pCO₂. Limnol. Oceanogr. **68**: 2789–2799.

Schaum, C. E., and others. 2017. Adaptation of phytoplankton to a decade of experimental warming linked to increased photosynthesis. Nat. Ecol. Evol. **1**: 0094. doi:10.1038/s41559-017-0094

Schuback, N., C. J. Hoppe, J. É. Tremblay, M. T. Maldonado, and P. D. Tortell. 2017. Primary productivity and the coupling of photosynthetic electron transport and carbon fixation in the Arctic Ocean. Limnol. Oceanogr. **62**: 898–921.

Soltwedel, T., and others. 2016. Natural variability or anthropogenically-induced variation? Insights from 15 years of multidisciplinary observations at the arctic marine LTER site HAUSGARTEN. Ecol. Indic. **65**: 89–102. doi:10.1016/j.ecolind.2015.10.001

Stock, C. A., J. P. Dunne, and J. G. John. 2014. Drivers of trophic amplification of ocean productivity trends in a changing climate. Biogeosciences **11**: 7125–7135. doi:10.5194/bg-11-7125-2014

Suggett, D. J., H. L. MacIntyre, and R. J. Geider. 2004. Evaluation of biophysical and optical determinations of light

absorption by photosystem II in phytoplankton. Limnol. Oceanogr. Methods **2**: 316–332.

Syvertsen, E. E. 1991. Ice algae in the Barents Sea: Types of assemblages, origin, fate and role in the ice-edge phytoplankton bloom. Polar Res. **10**: 277–288. doi:10.1111/j.1751-8369.1991.tb00653.x

Tedesco, L., M. Vichi, and E. Scoccimarro. 2019. Sea-ice algal phenology in a warmer arctic. Sci. Adv. **5**: eaav4830. doi:10.1126/sciadv.aav4830

Thomas, M. K., C. T. Kremer, C. A. Klausmeier, and E. Litchman. 2012. A global pattern of thermal adaptation in marine phytoplankton. Science **338**: 1085–1088. doi:10.1126/science.1224836

Thompson, P. A., M. x. Guo, P. J. Harrison, and J. N. Whyte. 1992. Effects of variation in temperature. II. On the fatty acid composition of eight species of marine phytoplankton 1. J. Phycol. **28**: 488–497.

Tremblay, J.-É., L. G. Anderson, P. Matrai, P. Coupel, S. Bélanger, C. Michel, and M. Reigstad. 2015. Global and regional drivers of nutrient supply, primary production and CO_2 drawdown in the changing Arctic Ocean. Prog. Oceanogr. **139**: 171–196.

Trimborn, S., S. Thoms, T. Brenneis, J. P. Heiden, S. Beszteri, and K. Bischof. 2017. Two Southern Ocean diatoms are more sensitive to ocean acidification and changes in irradiance than the prymnesiophyte *Phaeocystis antarctica*. Physiol. Plant. **160**: 155–170. doi:10.1111/ppl.12539

Tverberg, V., R. Skogseth, F. Cottier, A. Sundfjord, W. Walczowski, M. E. Inall, E. Falck, O. Pavlova, and F. Nilsen. 2019. The Kongsfjorden transect: Seasonal and inter-annual variability in hydrography, p. 49–104. *In* The cosystem of Kongsfjorden. Springer.

Vader, A., M. Marquardt, A. R. Meshram, and T. M. Gabrielsen. 2015. Key Arctic phototrophs are widespread in the polar night. Polar Biol. **38**: 13–21. doi:10.1007/s00300-014-1570-2

Van Leeuwe, M. A., and others. 2018. Microalgal community structure and primary production in Arctic and Antarctic sea ice: A synthesis. Elem. Sci. Anthrop. **6**: 4.

Wassmann, P., and M. Reigstad. 2011. Future Arctic Ocean seasonal ice zones and implications for pelagic-benthic coupling. Oceanography **24**: 220–231.

Wiedmann, I., E. Ershova, B. A. Bluhm, E.-M. Nöthig, R. R. Gradinger, K. Kosobokova, and A. Boetius. 2020. What feeds the benthos in the Arctic Basins? Assembling a carbon budget for the deep Arctic Ocean. Front. Mar. Sci. **7**: 224.

Wolf, K. K., C. J. Hoppe, and B. Rost. 2018. Resilience by diversity: Large intraspecific differences in climate change responses of an Arctic diatom. Limnol. Oceanogr. **63**: 397–411.

Wolf, K. K., S. D. Rokitta, C. J. Hoppe, and B. Rost. 2022. Pelagic and ice-associated microalgae under elevated light and pCO₂: Contrasting physiological strategies in two Arctic diatoms. Limnol. Oceanogr. **67**: 1895–1910.

Wolf, K. K. E., C. J. M. Hoppe, L. Rehder, C.-E. Schaum, U. John, and B. Rost. 2024. Heatwave responses of Arctic phytoplankton communities are driven by combined impacts of warming and cooling. Sci. Adv. **10**: eadl5904. doi:10.1126/sciadv.adl5904

Young, J. N., J. A. Goldman, S. A. Kranz, P. D. Tortell, and F. M. Morel. 2015. Slow carboxylation of Rubisco constrains the rate of carbon fixation during Antarctic phytoplankton blooms. New Phytol. **205**: 172–181.

Acknowledgments

Conflict of Interest

None declared.

3 *Publication II*

Warming shifts plastidary-mitochondrial energy partitioning in the Arctic diatom *Thalassiosira hyalina*

Warming alters energy partitioning between plastids and mitochondria in an Arctic diatom

Linda Rehder[1], Björn Rost[1,2], Sven Kranz[3] and Sebastian Rokitta[1]

[1]Marine Biogeosciences, Alfred-Wegener-Institute - Helmholtz Centre for Polar and Marine Research, Bremerhaven, Germany

[2]Faculty of Biology/Chemistry, University of Bremen, Bremen, Germany

[3]Department of BioSciences, Rice University, Houston, Texas, USA

Summary

- Temperature affects functional traits such as growth rates, biomass production or cellular quotas in Arctic phytoplankton to different degrees, likely resulting from diverging temperature sensitivities of underlying physiological key processes.

- We used membrane-inlet mass-spectrometry to measure $^{16}O_2$, $^{18}O_2$ and CO_2 fluxes to quantify O_2 production, C-fixation, CO_2 release and O_2 consumption, as well as fast repetition rate fluorometry to quantify quantum yield and electron transport in the Arctic diatom *Thalassiosira hyalina* under different warming scenarios.

- At higher temperatures, cells upregulate light harvesting abilities to compensate for a lower photosynthetic photosystem II efficiency, thereby maintaining O_2 production and thylakoid proton motive force (PMF). Resulting excess plastidial reductant is re-routed towards mitochondrial O_2 consumption, while the maintained PMF is used by the carbon concentrating mechanism under warming.

- As a consequence of reductant import, the mitochondrial citric acid cycle is suppressed, minimizing respiratory CO_2 loss despite stimulated O_2 consumption. This suggests that the optimization of the plastidial ATP:NADPH ratio is critical for

higher net biomass retention under warming. Our findings underline the necessity to interpret sub-processes of photosynthesis and respiration independently, and explain the often-observed enhanced biomass accumulation in a warmer Arctic Ocean.

Introduction

The Arctic Ocean is most prone to climate change, with warming rates being higher than the global average, especially in the Fram Strait area (Carvalho and Wang 2020; Constable, et al. 2022; Rantanen, et al. 2022). In addition to the general trend of rising mean sea surface temperatures, marine heatwaves (MHW) have notably increased in frequency, duration and intensity (Hobday, et al. 2016; Oliver, et al. 2019). Hence, the Arctic is already exposed to exceptional degrees of ocean warming, and model simulations project further temperature increases, especially in the extending sea-ice free regions. Since phytoplankton represent the base of the marine food web and contribute significantly to marine biogeochemical cycling (Falkowski, et al. 1998; Field, et al. 1998), their responses to warming have the potential to impact the entire Arctic ecosystem.

Temperature as a universal driver affects molecular movement and consequently all physical and (bio)chemical reactions (Brown, et al. 2004; Pearle, et al. 2010), including also those key processes involved in primary production. As single-celled phototrophic organisms, phytoplankton perform oxygenic photosynthesis to convert light energy into (bio)chemical energy (Falciatore, et al. 2022; Falkowski and Raven 2013). First, light harvesting takes place at pigmented antenna complexes in the thylakoid membrane of chloroplasts. The excitation energy harvested by pigment molecules is used to successively extract electrons from water, which are subsequently passed on to the photosynthetic electron transport chain (ETC) and ultimately lead to the generation of reductants [e$^-$], i.e. electron carriers like NADPH. With the flow of electrons along the ETC, a proton motive force (PMF) is established, which is later exploited for the generation ATP. Both, ATP and NADPH subsequently fuel the Calvin cycle, where the enzyme Ribulose-1,5-bisphosphate-carboxylase/-oxygenase (RuBisCO) catalyzes the fixation of carbon dioxide (CO_2) into organic biomass. The ATP:NADPH ratio created in the photosynthetic light reactions, however, is typically too low to drive the Calvin cycle alone (Allen, et al. 2005; Hahn, et al. 2018).

Alternative electron flows (AEFs) are therefore necessary to either increase the relative amount of ATP and/or to divert excess NADPH (Allen, et al. 2005; Curien, et al. 2016). AEFs comprise cyclic electron flow (CEF), which is known to be prominent in polar diatoms (Goldman, et al. 2015), oxygen (O_2) consuming water-to-water cycles, such as the Mehler reaction and the plastidial terminal oxidation (PTOX). The metabolic coupling of the chloroplast with other cellular compartments represent another mechanism, in which excess reductant from the plastid is dissipated to e.g. the cytoplasm and the mitochondria. All of these processes either support the PMF, and thus ATP production, or dissipate reductants in order to increase the ATP:NADPH ratio (e.g. Asada 2000; Bailleul, et al. 2015; Curien, et al. 2016; Lepetit, et al. 2022; Nawrocki, et al. 2019). Regarding temperature sensitivity, light harvesting is typically less sensitive than the use of ATP and NADPH in metabolic processes (Baker, et al. 1988; Raven and Geider 1988). Consequently, any temperature-dependent change in the biochemical consumption of ATP and NADPH will require physiological adjustments on multiple levels. Therefore, AEFs function as regulatory valves to maintain metabolic homeostasis inside the chloroplast and across cellular compartments, especially under stressful environmental conditions, as induced by e.g. increasing light intensities or temperatures.

Ecophysiological processes, including cell division, photosynthesis and respiration, are typically stimulated by elevated temperature as a result of accelerated diffusion rates, membrane fluidity and enzyme activity (Los, et al. 2013; Padfield, et al. 2016; Schuback, et al. 2017; Young, et al. 2015). However, temperature-induced changes are process-specific (e.g. Baker, et al. 2016; Barton, et al. 2020; Rehder, et al. 2024), and cells require physiological regulation, such as the above described AEFs, to overcome metabolic imbalances and to avoid detrimental temperature effects (Rehder, et al. 2023). Consequently, continuous adjustment of physiological processes is critical for phytoplankton to maintain metabolic homeostasis over the widest possible range of experienced temperatures. Arctic phytoplankton has evolved to be surprisingly plastic towards ocean warming (Hoppe, et al. 2018; Rehder, et al. 2024; Wolf, et al. 2024). Previous studies, for instance, found that many prominent Arctic phytoplankton species currently live well below their optimal temperatures and thus, it is expected that these organisms will benefit from moderate warming.

In this study, we hypothesized that Arctic phytoplankton modulate photosynthetic and respiratory processes to adjust to warmer temperatures, specifically their photophysiology as well as AEF operation. To resolve these regulatory efforts, we acclimated the Arctic diatom *Thalassiosira hyalina* to different temperatures (2°C, 6°C, 10°C) and measured photophysiological parameters as well as rates of $^{16}O_2$ evolution, $^{18}O_2$ uptake and CO_2 fluxes by means of fast repetition rate fluorometry (FRRf) and membrane-inlet mass-spectrometry (MIMS), respectively.

Methods

Phytoplankton cultivation

We cultured the Arctic diatom *Thalassiosira hyalina* (KB3 SS5, isolated 2021 in Svalbard, Norway) at 2°C, 6°C and 10°C in 0.2 µm sterile-filtered Arctic seawater (Salinity 31), enriched with vitamins and trace metals according to f/2 media (Guillard & Ryther, 1962). Nitrate, silicate and phosphate were added in concentrations of 100, 100 and 6 µmol L^{-1}, respectively. The irradiance was set to continuous light at 30 µmol photons $m^{-2}s^{-1}$ to mimic a polar day light climate. Cells were acclimated to experimental conditions for at least 7 generations as semi-continuous dilute batch cultures in aerated 2 L glass bottles (Schott Instruments) under continuous supply of humidified air (pCO2 of 400 µatm) generated in a gas mixing system (CGM 2000, MCZ Umwelttechnik, Bad Nauheim, Germany). To ensure temperature stability, culture bottles were submersed in temperature-controlled aquaria. Cell concentrations during cultivation never exceeded 8.000 cells mL^{-1} to ensure nutrient replete conditions and stable carbonate chemistry.

Growth, elemental composition and pigmentation

Specific growth rates were calculated from daily assessed cell concentrations obtained during the exponential growth phase, according to:

$$\mu = ((\ln(N_1) - \ln(N_0)))/(t_1 - t_0)$$

Eq. 1

where µ is the specific growth rate (d^{-1}), and N_0 as well as N_1 are the cell concentrations at the initial and final time points t_0 and t_1, respectively. Counting was performed with a cell-counter (Beckmann-Coulter Multisizer III, Fullerton, USA).

Particulate organic carbon (POC) samples were filtered onto pre-combusted (12h, 500°C) glass fiber filters (GF/F, 0.7 µm nominal pore size, Whatman). After drying for at least 24h at 60°C, filters were submitted to elemental analysis (EuroVector EA 3000) using the flash combustion technique (Knap et al., 1996). Chlorophyll *a* (Chl *a*) samples were filtered onto pre-combusted (12h, 500°C) glass fiber filters (GF/F, 0.7 µm, Whatman), shock frozen in liquid nitrogen and stored at -80°C until extraction. Chlorophyll was extracted overnight in 90% acetone (SIGMA-ALDRICH) with an additional cell disruption using a cell-mill (Precellys 24, Bertin). Extracts were centrifuged (13,000 rcf for 5 min, Sigma 4K10), and Chl *a* concentration in the supernatant was determined using the fluorometric 'acidification method' (Turner Triology Fluorometer, Turner Designs, Knap et al. (1996)).

Photophysiological parameters

Photophysiological characteristics of PSII were assessed by means of chlorophyll *a* variable fluorescence using a fast repetition rate fluorometer (FRRf; FastOcean, Chelsea Technologies) combined with the FastAct2 Laboratory system (Chelsea Technologies). Light-emitting diodes were set to 450 nm emission wavelength to fully saturate all PSII reaction centers on short timescales. We used the FRRf in single turnover mode, in which the saturation phase comprised 100 flashlets on a 2 µs pitch, and the relaxation phase comprised 40 flashlets on a 60 µs pitch. All measurements were conducted in a temperature-controlled cuvette at the respective acclimation temperature after dark acclimation for 45 min. Minimum Chl *a* fluorescence (F_0 and F' for dark- and light-acclimated measurements, respectively) and maximum Chl *a* fluorescence (F_m and F_m' for dark- and light-acclimated measurements, respectively) were obtained from iteratively fitting the induction phase (Kolber, et al. 1998), and re-opening times of PSII (τ) were obtained from iteratively fitting the relaxation phase (Oxborough 2012). FRRf measurements were performed in photosynthesis-irradiance (PI-) curves with 8 light levels (5 min pre-acclimation at respective actinic light per light level; maximum light levels of 720 µmol photons m^{-2} s^{-1}). Basic photophysiological parameters such as maximum quantum yields of PSII in the dark (F_v/F_m), the yields of non-regulated energy dissipation of PSII (Y(NO)), relative and absolute electron transport rates (rETR and absETR, respectively) at in-situ light intensity of 30 µmol photons m^{-2} s^{-1}, light acclimation indices (I_k) and absorption cross sections of PSII

(σ_{PSII}) were obtained using standard calculations (McKew, et al. 2013; Schuback, et al. 2017; Trimborn, et al. 2017).

Gas flux measurements

A membrane-inlet mass spectrometer (MIMS; Isoprime, GV Instruments, Manchester, UK) was used to measure i) photosynthetic O_2 production during light, ii) respiratory O_2 consumption during dark and light and iii) photosynthetic net C-fixation in the light and respiratory CO_2 release in dark. These rates were determined by measuring changes in gas concentrations of $^{16}O_2$, $^{18}O_2$ and CO_2 within concentrated suspension of each biological replicate. Calibrations followed the procedures described in Rokitta and Rost (2012) for $^{16}O_2$ and CO_2. To calibrate for $^{18}O_2$, a normal $^{16}O_2$ calibration was performed and the acceleration voltage of the mass-spectrometer was adjusted to redirect the $^{16}O_2$ beam to the $^{18}O_2$ detector. All fluxes were corrected for instrumental consumption of $^{16}O_2$ and $^{18}O_2$ under each temperature treatment. For $^{18}O_2$ consumption measurements, the assay medium was purged with N_2 gas overnight to remove all $^{16}O_2$. Subsequently, the medium was transferred into the MIMS cuvette and equilibrated with $^{18}O_2$ gas.

The bioassays were performed using a concentrated cell suspension. To this end, cells were concentrated by gentle filtration over polycarbonate filters (Isopore TSTP, 3 µm pore size, Merck, Darmstadt, Germany) and resuspended in O_2- and CO_2-free culture medium buffered to a pH_{NBS} of ~7.9 (50 mM 4-(2-hydroxyethyl)-1-piperazineethanesulfonic acid; HEPES). Subsequently, cells were transferred into the temperature- and light-controlled MIMS cuvette and spiked with $^{18}O_2$ reaching a final O_2 concentration of about 21%. Dissolved inorganic carbon (DIC) was added to the cuvette to yield typical concentration of seawater (about 2,200 µmol L^{-1}). Carbonic anhydrase was added (500 µg L^{-1} final concentration) to ensure instantaneous equilibration of the carbonate system. Using the CO_2:DIC ratios obtained in the calibrations, CO_2 traces were converted to total carbon fluxes. Flux measurements were performed in consecutive light-dark phases of ~3 min each, at two light intensities (30 and 150 µmol photons m^{-2} s^{-1}).

Calculations for net and gross rates of photosynthetic O_2 production (PS_{O2}), respiratory O_2 consumption in the dark ($R_{O2;dark}$) as well as respiratory O_2 consumption in the light followed Fock and Sültemeyer (1989). Subsequently, we subtracted mean $R_{O2;dark}$

51

rates from the respiratory O_2 consumption rates in the light to obtain gross light-driven O_2 consumptions ($R_{O2;light}$) per light level and temperature. Net C-fixation rates were obtained from CO_2 fluxes during the light phases, while rates of respiratory CO_2 release (R_{CO2}) were obtained from CO_2 fluxes during the dark phases. Gross rates of C-fixation (PS_{CO2}) were calculated by subtracting mean R_{CO2} rates from net C-fixation rates during light. After the assays, duplicate Chl *a* samples were taken from the cuvette to express the obtained rates based on Chl *a.* Assay data were based on 3-4 biological replicates. Photosynthetic and respiratory quotients (PQ and RQ, respectively) were calculated from gross rates as $PQ=PS_{O2}/PS_{CO2}$ and $RQ=R_{CO2}/R_{O2dark}$ in accordance with Rehder, et al. (2023).

**Statistical analysis**

All acclimation and photophysiological parameters are presented as the mean of four biological replicates ± standard deviation, if not stated otherwise. Data obtained from gas flux measurements are presented in three biological replicates ± standard deviation, except for the 2°C treatment (n=2). For acclimation and photophysiological parameters, normal distribution was tested using the Shapiro-Wilk-Test and equal variances were confirmed using the Welch test. We performed ANOVA followed by Tukey´s post-hoc test to test for significant differences using JASP statistics (Love, et al. 2019). The level of significance was set to $p \leq 0.05$.

Results

Growth, elemental composition and pigmentation
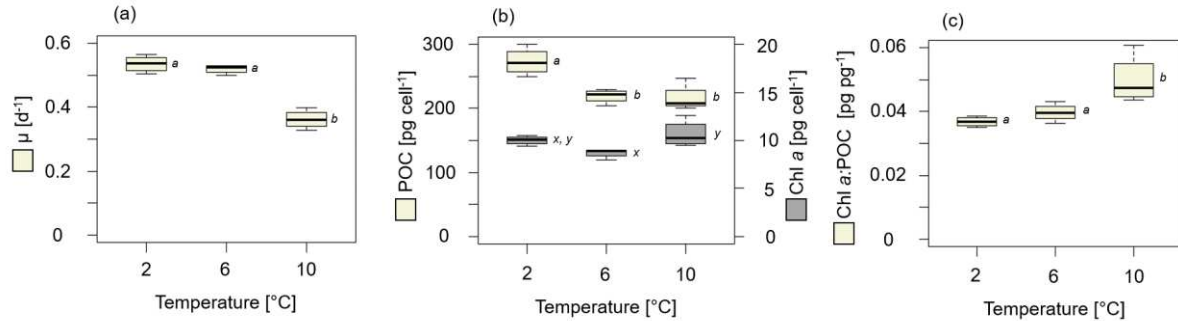
Fig 1. Acclimation parameters of *Thalassiosira hyalina* at 2°C, 6°C and 10°C. (a) growth rate (d^{-1}; beige), (b) particulate organic carbon (POC) quota (pg cell^{-1}; beige) and chlorophyll *a* (Chl *a*) quota (pg cell^{-1}; grey), and (c) Chl *a*:POC ratio (pg pg^{-1}; beige). Boxplots comprise 4 biological replicates and letters indicate significant differences (p ≤ 0.05).

Growth rates of *T. hyalina* were ~0.52 d^{-1} at 2° and 6°C and decreased significantly to 0.36 d^{-1} at 10°C (Fig. 1a). The particulate organic carbon (POC) quota was highest at 2°C, i.e. 270 pg cell^{-1} and decreased significantly to ~220 pg cell^{-1} at 6°C and 10°C (Fig. 1b). The chlorophyll *a* quota (Chl *a*) was lowest at 6°C and slightly increased from 8.7 pg cell^{-1} to 10.7 pg cell^{-1} at 10°C (Fig. 1b). The Chl *a*:POC ratio was maintained at ~0.038 pg pg^{-1} at 2°C and 6°C but increased significantly to 0.05 pg pg^{-1} at 10°C (Fig. 1c).

## Photophysiological measurements
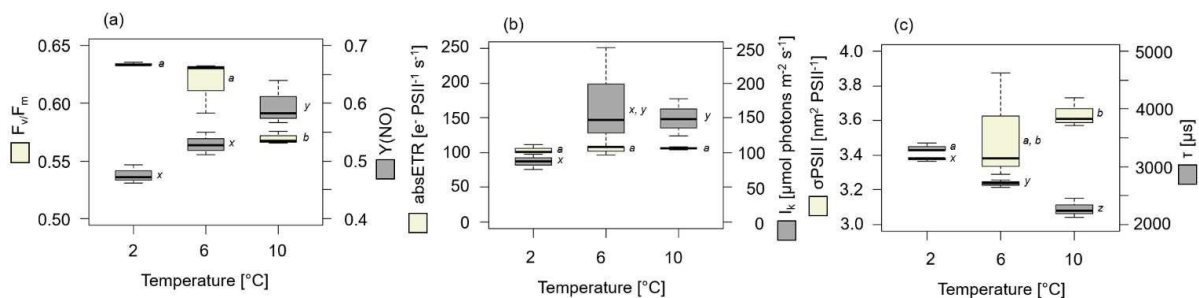
Fig 2. Photophysiological parameters obtained for *Thalassiosira hyalina* at 2°C, 6°C and 10°C. (a) photosystem II (PSII) quantum yield (F$_v$/F$_m$; beige) and the yield of non-regulated energy dissipation of PSII under in-situ light intensity (Y(NO); grey), (b) absolute electron transport rates under in-situ light intensity (absETR; e$^-$ PSII^{-1} s^{-1}; beige) and light acclimation indices (I$_k$; μmol photons m^{-2} s^{-1}; grey) and (c) absorption cross sections of PSII (σ$_{PSII}$; nm² PSII^{-1}; beige) and re-opening times of PSII (τ; μs; grey). Boxplots comprise 4 biological replicates and letters indicate significant differences (p ≤ 0.05).

53

T. hyalina exhibited a dark-adapted PSII quantum yield (F_v/F_m) of ~0.63 at 2°C and 6°C, which significantly decreased to 0.56 at 10°C (Fig. 2a). The yield of non-regulated energy dissipation of PSII (Y(NO)) under in-situ light intensity increased gradually from 0.47 at 2°C to 0.60 at 10°C (Fig. 2b). The absolute electron transport rate (absETR) under in-situ light intensity was maintained at 106 e^- $PSII^{-1}$ s^{-1} across all temperatures, and the light acclimation index (I_k) increased from ~85 µmol photons m^{-2} s^{-1} at 2°C to ~150 µmol photons m^{-2} s^{-1} at 10°C (Fig. 2b). The absorption cross section of PSII (σ_{PSII}) increased from 3.3 nm^2 $PSII^{-1}$ at 2°C to 3.6 nm^2 $PSII^{-1}$ at 10°C, and the re-opening time of PSII (τ) decreased significantly from 3320 µs at 2°C to 2270 µs at 10°C (Fig. 2c).

Gas flux measurements

Gross photosynthetic O_2 production rates (PS_{O2}) remained at ~60 µmol O_2 (mg Chl *a*)$^{-1}$ h^{-1} under in-situ light (30 µmol photons m^{-2} s^{-1}), irrespective of the acclimation temperature (Fig. 3a; dark green). Under high-light exposure (150 µmol photons m^{-2} s^{-1}), PS_{O2} was generally more than 2-fold higher than under in-situ light intensity and increased gradually with acclimation temperatures from 145 µmol O_2 (mg Chl *a*)$^{-1}$ h^{-1} at 2°C to 190 µmol O_2 (mg Chl *a*)$^{-1}$ h^{-1} at 10°C (Fig. 3b; dark green). Under in-situ light, gross photosynthetic C-fixation rates (PS_{CO2}) remained unchanged at ~33 µmol C (mg Chl *a*)$^{-1}$ h^{-1} at 2°C and 6°C, but decreased significantly to 20 µmol C (mg Chl *a*)$^{-1}$ h^{-1} at 10°C (Fig. 3a; light green). Under high-light exposure, PS_{CO2} was also 2-fold higher than under in-situ light intensity, but exhibited the same general pattern, i.e. similar values of 75 µmol C (mg Chl *a*)$^{-1}$ h^{-1} at 2°C and 6°C with a drop to 42 µmol C (mg Chl *a*)$^{-1}$ h^{-1} at 10°C (Fig. 3b; light green). Photosynthetic quotients (PQ) were ~2.0 at 2°C and 6°C, while they increased to 2.5 at 10°C under in-situ light intensity (Fig. S2).
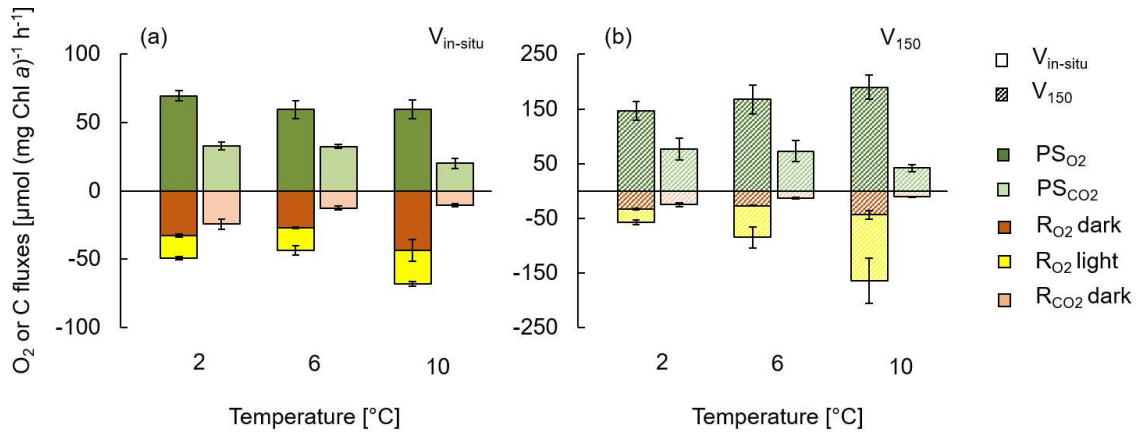
Fig 3. Physiological rates based on O_2 and C fluxes normalized to Chl *a* at 2°C, 6°C and 10°C acclimation temperatures of *Thalassiosira hyalina*. Gross photosynthetic O_2 production rates (PS_{O2}; dark green), gross photosynthetic C-fixation rates (PS_{CO2}; light green), respiratory O_2 consumption rates in the dark ($R_{O2;dark}$; dark orange) and in the light ($R_{O2;light}$; yellow) as well as respiratory CO_2 release rates (R_{CO2}) under (a) in-situ light intensity of 30 μmol photons m^{-2} s^{-1} ($V_{in-situ}$) and (b) 150 μmol photons m^{-2} s^{-1} (V_{150}). For illustration reasons, C fluxes are presented as negative values. Error bars denote standard deviation of 3 replicates (6°C and 10°C) or 2 replicates (2°C).

Respiratory O_2 consumption in the light ($R_{O2;light}$) was always higher than in the dark ($R_{O2;dark}$), irrespective of acclimation temperatures and light exposure. Under in-situ light intensities, $R_{O2;light}$ remained constant at 2° and 6°C (~16 μmol O_2 (mg Chl *a*)$^{-1}$ h^{-1}), but increased to 22 μmol O_2 (mg Chl *a*)$^{-1}$ h^{-1} at 10°C (Fig. 3a; yellow). Under high-light exposure, $R_{O2;light}$ experienced substantial increase from 25 μmol O_2 (mg Chl *a*)$^{-1}$ h^{-1} at 2°C up to 120 μmol O_2 (mg Chl *a*)$^{-1}$ h^{-1} at 10°C (Fig. 3b). $R_{O2;dark}$ remained constant at 2°C and 6°C (~30 μmol O_2 (mg Chl *a*)$^{-1}$ h^{-1}) and increased to 43 μmol O_2 (mg Chl *a*)$^{-1}$ h^{-1} at 10°C (Fig. 3a and b). Respiratory CO_2 release in the dark ($R_{CO2; dark}$) was highest at 2°C (24 μmol C (mg Chl *a*)$^{-1}$ h^{-1}) and decreased remarkably to 11 μmol C (mg Chl *a*)$^{-1}$ h^{-1} at 6°C and 10°C (Fig. 3a and b). As a consequence, respiratory quotients (RQs) decreased gradually from 0.7 to 0.2 between 2°C and 10°C (Fig. S2).

Discussion

Indications of increasing light limitation with warming

Overall cellular fitness, as often approximated by growth rates, did not benefit from the here tested degrees of warming. Instead, growth rates stayed constant at ~0.5 d^{-1} under the two lower temperatures (2°C and 6°C) and declined at the highest temperature of 10°C (Fig. 1a). In a previous study on the same *T. hyalina* strain using

a higher light intensity (100 µmol photons m^{-2} s^{-1}) but otherwise same conditions, a clear temperature optimum with peak growth rates of 1.4 d^{-1} was observed at 8 °C (Rehder, et al. 2024). In the current study, a thermal stimulation of cell division was suppressed likely due to the here prevalent light limitation (30 µmol photons m^{-2} s^{-1}). This is confirmed by light acclimation indices being consistently higher than the in-situ light intensity (I_k, Fig 2b). Interestingly, I_k increased further at higher temperatures, indicating that the limitation became even stronger with warming. This response is in agreement with studies on several temperate and Arctic phytoplankton species as well as natural communities (e.g. Mock and Hoch 2005; Rehder, et al. 2024; Wolf, et al. 2024). Hence, Arctic phytoplankton will likely benefit from a combined increase in temperature and light intensity, as it is projected for the future Arctic Ocean (e.g. Constable, et al. 2022).

Adjustments of light harvesting maintain homeostasis in light reactions

Photophysiological parameters suggest a lower efficiency of the light harvesting apparatus under increasing temperatures (Fig. 2). Specifically, the observed decrease in PSII quantum yield (F_v/F_m; Fig. 2a), the increased non-regulated energy dissipation of PSII (Y(NO); Fig. 2a) as well as the lower relative electron transport rates (rETR; Fig. S1) under in-situ light conditions indicate a decrease in photosynthetic performance. Despite of this, gas flux measurements indicate unchanged gross photosynthetic O_2 production (PS_{O2}) under all acclimation temperatures (Fig. 3a), which has also been observed in previous studies (e.g. Mock and Hoch 2005; Rehder, et al. 2023). Hence, it seems that cells are capable to adjust the photon harvest to water splitting. To facilitate this, cells increase their pigmentation per biomass (Chl *a*:POC; Fig. 1c) and specifically enlarge the antenna complexes of PSII (σ_{PSII}; Fig. 2c). As a consequence, absolute electron transport rates per PSII (absETR; Fig. 2b) were indeed maintained on a constant level, irrespective of the acclimation temperature. Thereby, cells ensure sufficient light harvesting to maintain water splitting of PSII on a quasi-constant level.

PSII re-oxidation times decreased under higher temperatures (τ; Fig. 2c), indicating a faster dissipation of reductant ([e^-]) into downstream sinks. However, cells were unable to fully exploit this higher efficiency in [e^-] transport, because under the here applied low-light conditions, the bottleneck of photosynthesis was not reductant-throughput in the first place, but rather the limited light harvesting. This emphasizes that the capacity

to adjust the light harvesting complex under changing acclimation temperatures is a central regulation strategy to maintain physiological homeostasis in photosynthetic light reactions.

Light-driven O_2 consumption increases with warming

The constant rates of gross PS_{O2} under all tested temperatures (Fig. 3a) suggest that the production of NADPH and ATP during the light reactions remains largely unchanged. This would also suggest that the Calvin cycle activity, i.e. gross photosynthetic C-fixation (PS_{CO2}), likewise remains unaffected by the here applied temperatures. Indeed, up to a moderate warming (6°C), cells were able to maintain the physiological rates of PS_{O2}, PS_{CO2} as well as respiratory O_2 consumption (both in light and darkness; $R_{O2;light}$ and $R_{O2;dark}$) at process-specific 'comfort rates'. This is in agreement with a previous study on the temperate diatom *Phaeodactylum tricornutum* (Rehder, et al. 2023) and indicates that the Arctic diatom *T. hyalina* follows the same strategy to keep physiological homeostasis, at least under moderate warming and the here tested light intensity.

The linear electron flow of the photosynthetic light reactions typically provides an excess of NADPH over ATP with regard to the stochiometric requirements of the Calvin cycle (Allen, et al. 2005; Curien, et al. 2016; Hahn, et al. 2018; Lepetit, et al. 2022). This necessitates alternative electron flows (AEF) to modulate the plastidial ATP:NADPH stoichiometry through re-routing [e⁻] from linear electron transport to cyclic electron flow (CEF) or to alternative O_2 consuming processes. While CEF increases the plastidial ATP and has been observed to be especially efficient in polar diatoms (Goldman, et al. 2015), our gas flux measurements rather indicate the involvement of at least one O_2 consuming AEF to dissipate NADPH, as signified by a 30% higher O_2 consumption rate in the light compared to the dark (Fig. 3a).

Such a light-driven O_2 consumption can originate from different [e⁻] consuming pathways associated with the photosynthetic electron transport, such as PTOX (Houille-Vernes, et al. 2011; Kuntz 2004; Peltier, et al. 2010), the Mehler reaction (Asada 2000; Curien, et al. 2016; Mehler 1951), as well as a re-routing of reductant from the chloroplast to the mitochondria (Bailleul, et al. 2015; Lepetit, et al. 2022; Peltier, et al. 2024). This metabolic coupling is well established in diatoms, green algae and land plants (Cardol, et al. 2003; Noctor, et al. 2004; Raghavendra and Padmasree

2003; Rehder, et al. 2023). In this mechanism, excess $[e^-]$ is exported from chloroplasts in the form of e.g. Malate and transported to the cytoplasm and the mitochondria (Heldt 1976; Kinoshita, et al. 2011; Strotmann and Murakami 1976). After $[e^-]$ has been transferred to compatible carriers, specifically NADH in the mitochondria, it partly fuels the respiratory ETC, where it is ultimately transferred to O_2 at complex IV or the alternative oxidase (Raven and Beardall 2003). The import of reductant causes a shift in the mitochondrial redox state, and as a consequence, the citric acid cycle that normally provides NADH during catabolic operation is suppressed (Igamberdiev 2020). Such regulation under elevated temperature has previously been observed in the temperate diatom *Phaeodactylum tricornutum* (Rehder, et al. 2023), and is here also reflected by the respiratory quotient (RQ) decreasing from 0.7 to 0.2 with warming (Fig. S2). Typically, mitochondria are thought to operate close to an RQ of 1, when respiring carbohydrates in a purely heterotrophic mode, in order to sufficiently provide reductant for respiratory ATP production (Kratz and Myers 1955). The low RQ observed in *T. hyalina* can only be achieved if NADH is utilized that is not originating from the citric acid cycle.

Under warming, increased efficiency of microalgal carbon concentrating mechanisms has been observed (CCMs; Li and Young 2023). A more efficient import of HCO_3^- into the thylakoid lumen under these conditions consumes more H^+ generated during the photosynthetic light reaction (Rokitta, et al. 2022), thereby partially consuming the PMF under increasing temperatures. Consequently, the lower net PMF, produced from a constant water splitting but lowered through the enhanced CCM activity, must result in a lower ATP:NADPH ratio, i.e. a higher excess of NADPH. As a consequence, under warming, even more NADPH has to be re-routed to the respiratory ETC, explaining the even stronger downregulation of the citric acid cycle under 6°C and 10°C, as signified by the lowered R_{CO2} and RQs (Figs. 3a, S2). These findings suggest that $[e^-]$ shuttling and redox-mediated control of mitochondrial activity are key elements in the physiological responses of microalgae to changing temperatures.

Imbalance of PS_{O2} and PS_{CO2} under strong warming

While the ratio of PS_{O2} to PS_{CO2} remained stable under moderate warming, reflected by a stable photosynthetic quotient of ~2.0 (PQ; Fig. S2), under strong warming, i.e. at 10°C, *T. hyalina* experienced a lowered PS_{CO2} despite maintained PS_{O2}, resulting in an imbalance of photosynthetic processes, reflected by a PQ of 2.5 (Fig. S2). In

addition, the decrease of growth rates and photosynthetic efficiency consistently indicates thermal stress at 10°C, which is in line with Rehder, et al. (2024). The decrease of PS_{CO2} may originate either from detrimental temperature effects on enzymes of the Calvin cycle (Hobbs, et al. 2013), or a further increased consumption of the PMF by a more active CCM under these conditions (Li and Young 2023). The latter should lower the ATP availability for the Calvin cycle, leading to lower PS_{CO2} despite unaltered PS_{O2}. If this was the case, high-light exposure should overcome this phenomenon. However, our gas flux measurements under 150 µmol photons m^{-2} s^{-1} still show a downregulated C-fixation while O_2 production was further stimulated under 10°C (Fig. 3b), so that a temperature stimulation of CCM activity cannot explain the decreased PS_{CO2}. Thus, a thermodynamic inhibition of the Calvin cycle enzymes is more likely to cause the lowered PS_{CO2}. This interpretation is in line with the general notion that processes involved in the photosynthetic light reactions are less temperature sensitive than those in the Calvin cycle (Raven and Geider 1988), and has previously been corroborated for different microalgae in response to strong warming (Baker, et al. 2016; Rehder, et al. 2024). Apparently, the thermal inhibition of the Calvin cycle contributes to the 'over-reduction' of the photosynthetic ETC under warming. This was also reflected in increased Y(NO) (Fig. 2a) and likely increases the demand for $[e^-]$ re-routing to the mitochondria. Indeed, the respiratory O_2 consumption in the light ($R_{O2;light}$) increased at 10°C, while the citric acid cycle activity remained at the same low level as under 6°C, reflected by unaltered R_{CO2} (Fig. 3a). As a consequence, cells exhibited an impressively low RQ of ~0.2 in the highest temperature treatment (Fig. S2). During the high-light exposure, this stimulation of $R_{O2;light}$ was even more pronounced, due to a massive over-reduction of the chloroplast (Fig. 3b). This highlights that the metabolic coupling of chloroplasts and mitochondria not only supports energy-partitioning under heat stress, but is also an important regulatory valve under high-light stress.

Conclusion

This study identified physiological bottlenecks under increasing temperature, and the compensatory measures taken by the Arctic diatom *T. hyalina*. Cells increased light harvesting to compensate for the lowered photosynthetic efficiency of PSII and the increasing light limitation under elevated temperatures. Thereby, they managed to

maintain electron transport rates, O_2 production and PMF, irrespective of the temperature treatment. Furthermore, cells increased the photosynthetic ATP:NADPH ratio by exporting plastidial reductant into the mitochondria. This fuels ATP synthesis and, importantly, suppressed the citric acid cycle. As a consequence, the net C retention can be maximized over a wide range of experienced temperatures. The outlined differential responses of O_2 and CO_2 fluxes can result in strongly diverging and unintuitive temperature response patterns: For instance, while Net C retention can be maintained under strong warming, net O_2 production, however can even become negative, due to massive stimulation of respiratory O_2 consumption in the light. This underlines the importance to assess O_2 and CO_2 fluxes independently. Whether this metabolic coupling also manifests in natural phytoplankton communities, needs to be explored in field experiments. Overall, the here described mechanisms allow for the surprisingly high plasticity of Arctic phytoplankton to deal with higher temperatures, and explain the stimulation of biomass accumulation under moderate warming. This will likely be even more prominent as sea ice retreat and increased stratification increase surface irradiance and thereby alleviate the temperature-induced light limitation.

Acknowledgements

Author contributions

All authors designed the study, L.R. performed the experiments, L.R. analyzed the data, all authors discussed data interpretation and L.R. wrote the manuscript with input of B.R, S.K. and S.R..

Data availability

The data that support the findings of this study are submitted to the Pangea data depository. Doi will be delivered at a later time point.

Competing interests

The authors declare no competing interests.

References

Allen A, Gillooly J, Brown J. 2005. Linking the global carbon cycle to individual metabolism. *Functional Ecology* 19(2): 202-213.

Asada K. 2000. The water–water cycle as alternative photon and electron sinks. *Philosophical Transactions of the Royal Society of London. Series B: Biological Sciences* 355(1402): 1419-1431.

Bailleul B, Berne N, Murik O, Petroutsos D, Prihoda J, Tanaka A, Villanova V, Bligny R, Flori S, Falconet D. 2015. Energetic coupling between plastids and mitochondria drives CO_2 assimilation in diatoms. *Nature* 524(7565): 366-369.

Baker KG, Robinson CM, Radford DT, McInnes AS, Evenhuis C, Doblin MA. 2016. Thermal Performance Curves of Functional Traits Aid Understanding of Thermally Induced Changes in Diatom-Mediated Biogeochemical Fluxes. *Frontiers in Marine Science* 3.

Baker NR, Long SP, Ort DR. 1988. Photosynthesis and temperature, with particular reference to effects on quantum yield. *Symposia of the Society for Experimental Biology* 42: 347-375.

Barton S, Jenkins J, Buckling A, Schaum C-E, Smirnoff N, Raven JA, Yvon-Durocher G. 2020. Evolutionary temperature compensation of carbon fixation in marine phytoplankton. *Ecology Letters* 23(4): 722-733.

Brown JH, Gillooly JF, Allen AP, Savage VM, West GB. 2004. Toward a metabolic theory of ecology. *Ecology* 85(7): 1771-1789.

Cardol P, Gloire G, Havaux M, Remacle C, Matagne R, Franck F. 2003. Photosynthesis and state transitions in mitochondrial mutants of *Chlamydomonas reinhardtii* affected in respiration. *Plant Physiology* 133(4): 2010-2020.

Carvalho KS, Wang S. 2020. Sea surface temperature variability in the Arctic Ocean and its marginal seas in a changing climate: Patterns and mechanisms. *Global and Planetary Change* 193: 103265.

Constable AJ, Harper S, Dawson J, Holsman K, Mustonen T, Piepenburg D, Rost B, Bokhorst S, Boike J, Cunsolo A 2022. Cross-chapter paper 6: polar regions. *IPCC AR WGII*: Cambridge University Press.

Curien G, Flori S, Villanova V, Magneschi L, Giustini C, Forti G, Matringe M, Petroutsos D, Kuntz M, Finazzi G. 2016. The water to water cycles in microalgae. *Plant and Cell Physiology* 57(7): 1354-1363.

Falciatore A, Bailleul B, Boulouis A, Bouly J-P, Bujaldon S, Cheminant-Navarro S, Choquet Y, de Vitry C, Eberhard S, Jaubert M. 2022. Light-driven processes: key players of the functional biodiversity in microalgae. *Comptes Rendus. Biologies* 345(2): 1-24.

Falkowski PG, Barber RT, Smetacek V. 1998. Biogeochemical Controls and Feedbacks on Ocean Primary Production. *Science* 281(5374): 200-206.

Falkowski PG, Raven JA. 2013. *Aquatic photosynthesis*: Princeton University Press.

Field CB, Behrenfeld MJ, Randerson JT, Falkowski P. 1998. Primary Production of the Biosphere: Integrating Terrestrial and Oceanic Components. *Science* 281(5374): 237-240.

Fock H, Sültemeyer D 1989. O_2 evolution and uptake measurements in plant cells by mass spectrometry. *Gases in plant and microbial cells*: Springer, 3-18.

Goldman JA, Kranz SA, Young JN, Tortell PD, Stanley RH, Bender ML, Morel FM. 2015. Gross and net production during the spring bloom along the W estern A ntarctic P eninsula. *New Phytologist* 205(1): 182-191.

Hahn A, Vonck J, Mills D, Meier T, Kuhlbrandt W 2018. Structure, mechanism, and regulation of the chloroplast ATP synthase. Science 360: eaat4318.

Heldt H 1976. Metabolite carriers of chloroplasts. *Transport in Plants III: Intracellular Interactions and Transport Processes*: Springer, 137-143.

Hobbs JK, Jiao W, Easter AD, Parker EJ, Schipper LA, Arcus VL. 2013. Change in Heat Capacity for Enzyme Catalysis Determines Temperature Dependence of Enzyme Catalyzed Rates. *ACS Chemical Biology* 8(11): 2388-2393.

Hobday AJ, Alexander LV, Perkins SE, Smale DA, Straub SC, Oliver EC, Benthuysen JA, Burrows MT, Donat MG, Feng M. 2016. A hierarchical approach to defining marine heatwaves. *Progress in Oceanography* 141: 227-238.

Hoppe CJM, Flintrop CM, Rost B. 2018. The Arctic picoeukaryote *Micromonas pusilla* benefits synergistically from warming and ocean acidification. *Biogeosciences* 15(14): 4353-4365.

Houille-Vernes L, Rappaport F, Wollman F-A, Alric J, Johnson X. 2011. Plastid terminal oxidase 2 (PTOX2) is the major oxidase involved in chlororespiration in *Chlamydomonas*. *Proceedings of the National Academy of Sciences* 108(51): 20820-20825.

Igamberdiev AU. 2020. Citrate valve integrates mitochondria into photosynthetic metabolism. *Mitochondrion* 52: 218-230.

Kinoshita H, Nagasaki J, Yoshikawa N, Yamamoto A, Takito S, Kawasaki M, Sugiyama T, Miyake H, Weber AP, Taniguchi M. 2011. The chloroplastic 2-oxoglutarate/malate transporter has dual function as the malate valve and in carbon/nitrogen metabolism. *The Plant Journal* 65(1): 15-26.

Kolber ZS, Prášil O, Falkowski PG. 1998. Measurements of variable chlorophyll fluorescence using fast repetition rate techniques: defining methodology and

experimental protocols. *Biochimica et Biophysica Acta (BBA)-Bioenergetics* 1367(1-3): 88-106.

Kratz WA, Myers J. 1955. Photosynthesis and Respiration of Three Blue-Green Algae. *Plant Physiol* 30(3): 275-280.

Kuntz M. 2004. Plastid terminal oxidase and its biological significance. *Planta* 218(6): 896-899.

Lepetit B, Campbell DA, Lavaud J, Büchel C, Goss R, Bailleul B 2022. Photosynthetic light reactions in diatoms. II. The dynamic regulation of the various light reactions. *The molecular life of diatoms*: Springer, 423-464.

Li M, Young JN. 2023. Temperature sensitivity of carbon concentrating mechanisms in the diatom *Phaeodactylum tricornutum*. *Photosynthesis research*: 1-11.

Los DA, Mironov KS, Allakhverdiev SI. 2013. Regulatory role of membrane fluidity in gene expression and physiological functions. *Photosynthesis research* 116(2): 489-509.

Love J, Selker R, Marsman M, Jamil T, Dropmann D, Verhagen J, Ly A, Gronau QF, Šmíra M, Epskamp S, et al. 2019. JASP: Graphical Statistical Software for Common Statistical Designs. *Journal of Statistical Software* 88(2): 1 - 17.

McKew BA, Davey P, Finch SJ, Hopkins J, Lefebvre SC, Metodiev MV, Oxborough K, Raines CA, Lawson T, Geider RJ. 2013. The trade-off between the light-harvesting and photoprotective functions of fucoxanthin-chlorophyll proteins dominates light acclimation in *Emiliania huxleyi* (clone CCMP 1516). *New Phytologist* 200(1): 74-85.

Mehler AH. 1951. Studies on reactions of illuminated chloroplasts: I. Mechanism of the reduction of oxygen and other hill reagents. *Archives of Biochemistry and Biophysics* 33(1): 65-77.

Mock T, Hoch N. 2005. Long-Term Temperature Acclimation of Photosynthesis in Steady-State Cultures of the Polar Diatom *Fragilariopsis cylindrus*. *Photosynthesis research* 85(3): 307-317.

Nawrocki WJ, Bailleul B, Picot D, Cardol P, Rappaport F, Wollman F-A, Joliot P. 2019. The mechanism of cyclic electron flow. *Biochimica et Biophysica Acta (BBA)-Bioenergetics* 1860(5): 433-438.

Noctor G, Dutilleul C, De Paepe R, Foyer CH. 2004. Use of mitochondrial electron transport mutants to evaluate the effects of redox state on photosynthesis, stress tolerance and the integration of carbon/nitrogen metabolism. *Journal of experimental botany* 55(394): 49-57.

Oliver EC, Burrows MT, Donat MG, Sen Gupta A, Alexander LV, Perkins-Kirkpatrick SE, Benthuysen JA, Hobday AJ, Holbrook NJ, Moore PJ. 2019. Projected marine heatwaves in the 21st century and the potential for ecological impact. *Frontiers in Marine Science* 6: 734.

Oxborough K. 2012. FastPro8 GUI and FRRf3 systems documentation. *Chelsea Technologies Group Ltd, West Molesey, UK*.

Padfield D, Yvon-Durocher G, Buckling A, Jennings S, Yvon-Durocher G. 2016. Rapid evolution of metabolic traits explains thermal adaptation in phytoplankton. *Ecology Letters* 19(2): 133-142.

Pearle P, Collett B, Bart K, Bilderback D, Newman D, Samuels S. 2010. What Brown saw and you can too. *American Journal of Physics* 78(12): 1278-1289.

Peltier G, Stoffel C, Findinier J, Madireddi SK, Dao O, Epting V, Morin A, Grossman A, Li-Beisson Y, Burlacot A. 2024. Alternative electron pathways of photosynthesis power green algal CO_2 capture. *The Plant Cell* 36(10): 4132-4142.

Peltier G, Tolleter D, Billon E, Cournac L. 2010. Auxiliary electron transport pathways in chloroplasts of microalgae. *Photosynthesis research* 106(1): 19-31.

Raghavendra AS, Padmasree K. 2003. Beneficial interactions of mitochondrial metabolism with photosynthetic carbon assimilation. *Trends in Plant Science* 8(11): 546-553.

Rantanen M, Karpechko AY, Lipponen A, Nordling K, Hyvärinen O, Ruosteenoja K, Vihma T, Laaksonen A. 2022. The Arctic has warmed nearly four times faster than the globe since 1979. *Communications Earth & Environment* 3(1): 168.

Raven JA, Beardall J 2003. Carbohydrate metabolism and respiration in algae. *Photosynthesis in algae*: Springer, 205-224.

Raven JA, Geider RJ. 1988. Temperature and algal growth. *New Phytologist* 110(4): 441-461.

Rehder L, Rokitta SD, Hoppe CJ, Buschmann I, Jasper L, Rost B. 2024. Different temperature sensitivities of key physiological processes lead to divergent trait response patterns in Arctic phytoplankton. *Limnology and Oceanography*.

Rehder L, Rost B, Rokitta SD. 2023. Abrupt and acclimation responses to changing temperature elicit divergent physiological effects in the diatom *Phaeodactylum tricornutum*. *New Phytologist* 239(3): 1005-1013.

Rokitta SD, Kranz SA, Rost B. 2022. Inorganic carbon acquisition by aquatic primary producers. *Blue Planet, Red and Green Photosynthesis: Productivity and Carbon Cycling in Aquatic Ecosystems*: 81-132.

Rokitta SD, Rost B. 2012. Effects of CO_2 and their modulation by light in the life-cycle stages of the coccolithophore *Emiliania huxleyi*. *Limnology and Oceanography* 57(2): 607-618.

Schuback N, Hoppe CJ, Tremblay JÉ, Maldonado MT, Tortell PD. 2017. Primary productivity and the coupling of photosynthetic electron transport and carbon fixation in the Arctic Ocean. *Limnology and Oceanography* 62(3): 898-921.

Strotmann H, Murakami S 1976. Energy transfer between cell compartments. *Transport in Plants III: Intracellular Interactions and Transport Processes*: Springer, 398-416.

Trimborn S, Thoms S, Brenneis T, Heiden JP, Beszteri S, Bischof K. 2017. Two Southern Ocean diatoms are more sensitive to ocean acidification and changes in irradiance than the prymnesiophyte *Phaeocystis antarctica*. *Physiologia Plantarum* 160(2): 155-170.

Wolf KKE, Hoppe CJM, Rehder L, Schaum C-E, John U, Rost B. 2024. Heatwave responses of Arctic phytoplankton communities are driven by combined impacts of warming and cooling. *Science Advances*.

Young JN, Goldman JA, Kranz SA, Tortell PD, Morel FM. 2015. Slow carboxylation of Rubisco constrains the rate of carbon fixation during Antarctic phytoplankton blooms. *New Phytologist* 205(1): 172-181.

4 *Publication III*

Warming stimulates biomass accumulation despite lowered net oxygen production in an Arctic phytoplankton community

In preparation for submission

Warming stimulates biomass accumulation despite lowered net oxygen production in an Arctic phytoplankton community

Linda Rehder[1], Antonia Ahme[2], Clara J. M. Hoppe[1], Sebastian Rokitta[1], and Björn Rost[1, 3]

[1]Marine Biogeosciences, Alfred Wegener Institute, Helmholtz Centre for Polar and Marine Research, Bremerhaven, Germany

[2]Ecological Chemistry, Alfred Wegener Institute, Helmholtz Centre for Polar and Marine Research, Bremerhaven, Germany

[3]Faculty of Biology/Chemistry, University of Bremen, Bremen, Germany

Abstract

The Arctic Ocean is exposed to exceptional climate change with higher warming rates than the global average. As the main Arctic primary producers, phytoplankton are profoundly affected by warming, and recent studies revealed that key physiological processes differ in their temperature responses. However, these processes have rarely been assessed on a community level, impairing our understanding of how they upscale to ecologically relevant settings. Therefore, we here exposed a natural Arctic phytoplankton community from the marginal ice zone of the Fram Strait to different degrees of warming (2°C, 6°C and 9°C) and assessed biomass accumulation, community composition (18s rRNA metabarcoding), photophysiology (fast repetition rate fluorometry) as well as photosynthesis and respiration rates (membrane-inlet mass spectrometry). Growth rates were consistently stimulated by higher temperatures, implying increased net biomass accumulation with warming. Assessments of photosynthetic and respiratory O_2 fluxes, however, showed a strongly downregulated net O_2 production and increased dark respiration under elevated temperatures. As these opposing trends in O_2-based and C-based assessments of photosynthesis were not accompanied by major functional species shifts, we propose that the observed phenomenon is of fundamental physiological nature. These findings

68

are in line with a recent study on Arctic diatom monocultures, arguing for a warming-induced metabolic coupling of chloroplasts and mitochondria, which results in lowered respiratory CO_2 loss and thereby increased biomass retention despite the decreased net O_2 production. Our findings underline the necessity to interpret O_2- and CO_2-based processes of photosynthesis independently, and suggest increased phytoplankton biomass accumulation in a warmer Arctic Ocean.

Introduction

The Arctic Ocean is especially impacted by climate change with warming rates being much higher than the global average (Constable *et al.*, 2022; Rantanen *et al.*, 2022) This exceptionally strong warming is caused by feedbacks between the decreasing sea-ice extent and the concomitantly decreasing surface albedo, a process known as "Arctic amplification" (Lee, 2014; Goosse *et al.*, 2018; Pistone *et al.*, 2019). Furthermore, the intrusion of North Atlantic water masses via the West Spitzbergen current is intensifying since the beginning of the 20th century (Ingvaldsen *et al.*, 2021; Tesi *et al.*, 2021). This process, named "Atlantification", not only increases the influence of warm water masses, but also promotes the advection and northward expansion of Atlantic organisms (Oziel *et al.*, 2017; Neukermans *et al.*, 2018; Wassmann *et al.*, 2019; Oziel *et al.*, 2020), which may be more competitive than Arctic ones in a warming habitat. Additionally, marine heatwaves are projected to increase in frequency, duration and intensity, further exposing marine organisms to stronger short-term temperature fluctuations (Hobday *et al.*, 2016; Oliver *et al.*, 2019).

As the main primary producers, phytoplankton provide the base of the marine food web and play a significant role in marine biogeochemical cycling of carbon and other elements (Field *et al.*, 1998; Falkowski *et al.*, 2000). Due to a shift from thick multiyear to thin first-year sea ice as well as faster seasonal sea ice melting, the light climate below the sea ice changes, likely stimulating under-ice phytoplankton blooms if nutrient regimes permit. Additionally, the declining sea ice cover leads to more open water habitats and extended growing season for pelagic phytoplankton under warming (Lewis *et al.*, 2020; Rokitta *et al.*, 2023). As a consequence, overall Arctic primary production has already increased over the past decades and is projected to be further

stimulated in the future (Arrigo *et al.*, 2008; Kwiatkowski *et al.*, 2018; Ardyna & Arrigo, 2020; Constable *et al.*, 2022; Oziel *et al.*, 2024).

Next to changes in light, phytoplankton are influenced by environmental factors such as temperature, nutrients and CO_2 availability, all of which are modified by climate change (Rost *et al.*, 2008; Doney *et al.*, 2012; Cooley *et al.*, 2022). As a universal driver, temperature affects molecular movement and thereby principally controls all physical and biochemical processes (Brown et al., 2004; Pearle et al., 2010). More specifically, temperature variations induce changes of enzyme activity, membrane fluidity, substrate diffusion or electron transport rates, which lead to stimulated or inhibited metabolic processes such as photosynthesis, respiration, nutrient assimilation or cell division in phytoplankton (Raven & Geider, 1988). Phytoplankton cell division rates, for example, are typically stimulated by warming up to a species- or strain-specific optimal temperature, but sharply decline beyond because oxidative stress increases (Moreno *et al.*, 2024) and elevated temperatures become detrimental for the process of cell division (Thomas *et al.*, 2012; Grimaud *et al.*, 2017). For Arctic phytoplankton, it has recently been shown that other physiological processes within the same cell (e.g. photosynthetic electron transport or biomass production) can have their own specific 'temperature response patterns', causing much of the high phenotypic variations that phytoplankton exhibit under various constellations of environmental drivers (Rehder *et al.*, 2024).

While temperature effects on single phytoplankton strains are comparably well understood (e.g. *Publication II*; Baker *et al.*, 2016;; Barton *et al.*, 2020; Giesler *et al.*, 2023; Rehder *et al.*, 2024), the responses of natural phytoplankton communities to warming can be rather complex: Their bulk primary production is not only affected by temperature effects on each species' (or even strains') physiology, but also selection for better adapted species can cause profound changes in phytoplankton community composition and thus affect overall metabolic activity (Hillebrand *et al.*, 2012; Hoppe *et al.*, 2018b; Ahme *et al.*, 2023; Ahme *et al.*, 2024). As a consequence, community shifts can possibly amplify but also buffer temperature effects, driven by combined selection on a strain-specific (Wolf *et al.*, 2018) and species-specific level (Hoppe *et al.*, 2018b). For both, monocultures and natural communities, it was found that respiratory O_2 consumption is generally more stimulated by warming than photosynthetic O_2 production (Brown *et al.*, 2004; Lopez-Urrutia *et al.*, 2006),

suggesting a shift towards higher heterotrophy in the future (Hoppe *et al.*, 2002; Boscolo-Galazzo *et al.*, 2018). Furthermore, physiological assessments of phytoplankton monocultures showed diverging temperature responses between respiratory CO_2 loss and respiratory O_2 consumption as a result of physiological interaction between chloroplasts and mitochondria (*Publication II*; Igamberdiev, 2020;; Lepetit *et al.*, 2022; Rehder *et al.*, 2023; Peltier *et al.*, 2024).

Here, we studied the responses of a natural Arctic phytoplankton community to low (2°C), intermediate (6°C) and high temperatures (9°C). Next to bulk parameters integrated over several days, we employed membrane-inlet mass-spectrometry to quantify photosynthetic and respiratory O_2 fluxes as well as fast repetition rate fluorometry to assess photophysiology at the end of the experiment. Furthermore, we used 18S rRNA metabarcoding to assess the community composition and identify potential functional shifts within the community, e.g. more heterotrophic or Atlantic species with warming.

Methods

Sampling site and incubation

An Arctic phytoplankton community was sampled in the central Fram Strait from the chlorophyll *a* (Chl *a*) maximum at 11 m depth, in a region that was covered by sea ice at the time of sampling (Hausgarten station IV; 79°03.834 N, 4°11.465 E). The water was collected through the Teflon inflow system of the research vessel Polarstern during the PS136 campaign on 31st May 2023 (water temperature: -0.7°C, salinity: 31 PSU) and pre-filtered through a 200 µm mesh to exclude meso-zooplankton. Filtered sea water (0.2 µm pore size) from the same location and depth was enriched with macronutrients (100 µmol L^{-1} nitrate, 100 µmol L^{-1} silicate, 6 µmol L^{-1} phosphate) as well as trace metals and vitamins (F/2 medium; Guillard et al. 1962) to dilute the initial phytoplankton community to a Chl *a* concentration of ~2.7 µg L^{-1} and to ensure nutrient replete conditions. For the same reason, a second dilution was done after 6 days of incubation. Algal cultures were incubated as biological triplicates in 5 L glass bottles (Schott instruments, Mainz, Germany) at low (2°C, equivalent to mean SSTs for this region and season; Soltwedel *et al.*, 2016), intermediate (6°C) and high (9°C) temperatures (Rantanen *et al.*, 2022) for a duration of 12 to 14 days. Irradiance was

set to 30 µmol photons m^{-2} s^{-1} under continuous illumination, and cultures were continuously and gently aerated with environmental air from outside the ship to avoid sedimentation.

Growth rates, elemental composition and pigmentation

Chl *a* concentration in the incubations were monitored at least every other day. To this end, 70-150 ml of each community incubation was filtered on glass fiber filters (GF/F; 0.7 µm nominal pore size, Whatman, UK) and stored at -80°C until extraction. Filters were extracted overnight in 5 mL acetone (90%, SIGMA-ALDRICH, St. Louis, USA), after cell disruption in a cell-mill (Precellys 24, Bertin, Montigny-le-Bretonneu, Germany). Then, the extract was centrifuged (4500 rpm for 7 min, Sigma 4K10, Osterode, Germany) and the Chl *a* concentration in the supernatant was determined using the fluorometric 'acidification-method' (Turner Trilogy, Turner Designs San Jose, USA; Knap et al. 1996.

Particulate organic carbon (POC) was measured at the start of the experiment, after six days and at the end of the experiment. To this end, cells were filtered onto pre-combusted (12h, 500°C) GF filters (0.7 µm nominal pore size, Whatman, UK). After drying for at least 24h, filters were measured on an elemental auto-analyzer (EuroVector EA 3000, Pavia, Italy) using the flash combustion technique (Knap et al., 1996).

The Chl *a* concentration or POC concentration per community incubation over time were used to calculate specific Chl *a*-based (μ_{Chla}) or POC-based (μ_{POC}) accumulation rates, respectively (Eq. 1):

$$\mu = \frac{\ln(N_1) - \ln(N_0)}{t_1 - t_0} \qquad \text{(Eq. 1)}$$

where µ is the specific growth rate (d^{-1}), and N_0 as well as N_1 are the Chl *a* or POC concentrations at the initial and final time points t_0 and t_1, respectively. For growth rate calculations, only Chl *a* and POC concentrations after the dilution at day 6 were considered.

Physiological assays

Photosynthetic and respiratory rates were measured by assessing O$_2$ fluxes during consecutive light and dark phases using a custom-made membrane-inlet mass

spectrometer (MIMS). The applied MIMS system is based on a Pfeiffer QMG220 Prisma Plus (pressure at ion source during measurements was ~$5*10^{-6}$ mbar; Asslar, Germany), which couples to a custom-built, water cooled 8 mL cuvette through a PTFE membrane (0.01 µm pore size; Reichelt Chemietechnik, Heidelberg, Germany). O_2 in the seawater can permeate the membrane and enter the inlet, following its steep chemical gradient. Gasses are passed along a modified pulse-tube cooler (PXE 100, AIM, Heilbronn, Germany) that provides a 170 cm² metal freezing surface (-95°C) to facilitate efficient cryodistillation. O_2 signals were calibrated following Rokitta and Rost (2012). O_2 consumption of the instrument was assessed by measuring the O_2 and Argon (Ar) decline over time in assay medium without biological activity. Based on the obtained correlation between O_2 and Ar in the calibration (R^2 >0.95), Ar signals were used to account for the concentration-dependent abiotic O_2 consumption during biological measurements (Tab. S2).

Assays were performed at the end of the experiment (T_{fin}). To this end, cells were concentrated by gentle filtration over polycarbonate filters (Isopore TSTP, 3 µm nominal pore size; Merck, Darmstadt, Germany) in a reverse filtration unit and resuspended in culture medium buffered to a pH_{NBS} of 8.0 (50 mM 4-(2-hydroxyethyl)-1- piperazineethanesulfonic acid; HEPES). Subsequently, cells were transferred into the temperature- and light-controlled MIMS cuvette, and after signal- and temperature-stabilization (~20 min) during darkness, photosynthesis-vs-irradiance (PI-) assays were performed in consecutive light–dark phases with increasing light intensities (0, 35, 60, 70, 135 µmol photons m^{-2} s^{-1}). While net photosynthetic rates (NP) and dark respiratory rates (DR) were obtained from O_2 fluxes directly observed during the light and dark phases, respectively, gross photosynthetic rates (GP) were calculated by subtracting the mean dark respiration rates from the net photosynthesis rates (GP = NP - DR). After each measurement, Chl *a* samples were collected from the cuvette in duplicates and analyzed as described above, for normalization to Chl *a*. Chl *a*:POC ratios of the same day were used to express physiological rates normalized to POC.

Photophysiological characteristics based on the variable fluorescence of photosystem II (PSII) were assessed using a fast repetition rate fluorometer (FRRf; FastOcean, Chelsea Technologies, West Molesey, UK) combined with the FastAct2 Laboratory system (Chelsea Technologies, West Molesey, UK) at the same timepoints and in accordance to the same assay concept as described above. Light-emitting diodes were

set to 450 nm emission wavelength. We used the FRRf in single turnover mode, in which the saturation phase comprised 60 flashlets on a 2 µs pitch, and the relaxation phase comprised 15 flashlets on a 90 µs pitch. All measurements were conducted in a temperature-controlled cuvette at the respective acclimation temperature after dark acclimation for 45 min. Minimum Chl *a* fluorescence (F0 and F'0 for light- and dark-acclimated measurements, respectively) and maximum Chl *a* fluorescence (Fm and F'm for light- and dark-acclimated measurements, respectively) were obtained from iteratively fitting the induction phase (Kolber *et al.*, 1998), and PSII re-opening times were obtained from iteratively fitting the relaxation phase (Oxborough, 2012). FRRf measurements were performed in photosynthesis-irradiance (PI-) curves of 8 light levels (5 min pre-acclimation at respective actinic light; maximum light level of ~300 µmol photons m^{-2} s^{-1}). Basic photophysiological parameters such as maximum quantum yields of PSII (F_v/F_m), relative electron transport rates ($rETR_{exp}$) at 30 photons m^{-2} s^{-1} (incubation irradiance), light acclimation indices (I_k) and absorption cross sections of PSII (σ_{PSII}) were obtained using standard calculations (Genty *et al.*, 1989; Maxwell & Johnson, 2000; Schuback *et al.*, 2017).

Community composition

Protist community composition was assessed through 18S rRNA metabarcoding. To this end, 500 mL of each community incubation was filtered onto polycarbonate filters (0.8 µm nominal pore size, Nucleopore, Whatman, Maidstone, UK) and stored at -20°C until extraction. DNA extraction was performed using the NucleoSpin Soil extraction kit according to the manufacturer's protocol (Macherey-Nagel GmbH, Düren, Germany) before normalization to 5 ng/µL. Using the forward primer GCG GTA ATT CCA GCT CCA A and reverse primer ACT TTC GTT CTT GAT, amplicons of the variable region 4 of the 18S rRNA gene including an Illumina tail were generated based on the standard protocol for amplicon library preparation (16S Metagenomic Sequencing Library Preparation, Part #15044223 Rev. B. Illumina, San Diego, CA, USA). Indexing of single samples was performed using the Nextera XT Index Kit v2 Set A primers (Illumina, San Diego, CA, USA). Resulting libraries were pooled and sequenced on a MiSeq sequencer (Illumina, San Diego, CA, USA), with the outcome of 300 base pair paired-end gene amplicon reads, which were demultiplexed by the integrated "Generate FASTQ" workflow. Primer removal was performed with v2.8 cutadapt (Martin, 2011) and quality-trimming, denoising, paired-end merging and chimera-

removal were conducted using the v1.18 DADA2 package (Callahan *et al.*, 2016). The resulting amplicon sequence variants (ASVs) were taxonomically annotated using the reference database PR2 (v5.0.1; Guillou *et al.*, 2012).

Samples with a sequencing depth below the 5 % quantile and ASVs identified as metazoans, fungi, plastids or nuclei were removed. A sufficient sequencing depth of all samples was confirmed via rarefaction. Trophic mode was assigned based on the categorizations by Adl *et al.* (2019). To analyze species composition data, all samples were scaled to the lowest depth through ranked subsampling (Beule & Karlovsky, 2020) before the replicates were merged to produce pie charts. For beta-diversity analyses, pairwise dissimilarity matrices were generated using Aitchinson distances and then visualized with a principal components analysis (PCA) based on the recommendations by (Gloor *et al.*, 2017).

Statistical analysis

All parameters are presented as the mean of the biological replicates, if not stated otherwise. For all data, normal distribution was confirmed using the Shapiro-Wilk-Test and equal variances were tested using the Welch test. We performed an ANOVA with subsequent Tukey post-hoc tests to identify significant differences using JASP statistics. The level of significance was set to $p \leq 0.05$.

18s rRNA data did not allow statistical analyses due to the loss of one biological replicate at 2°C.

Results

Acclimation responses and physiological assays
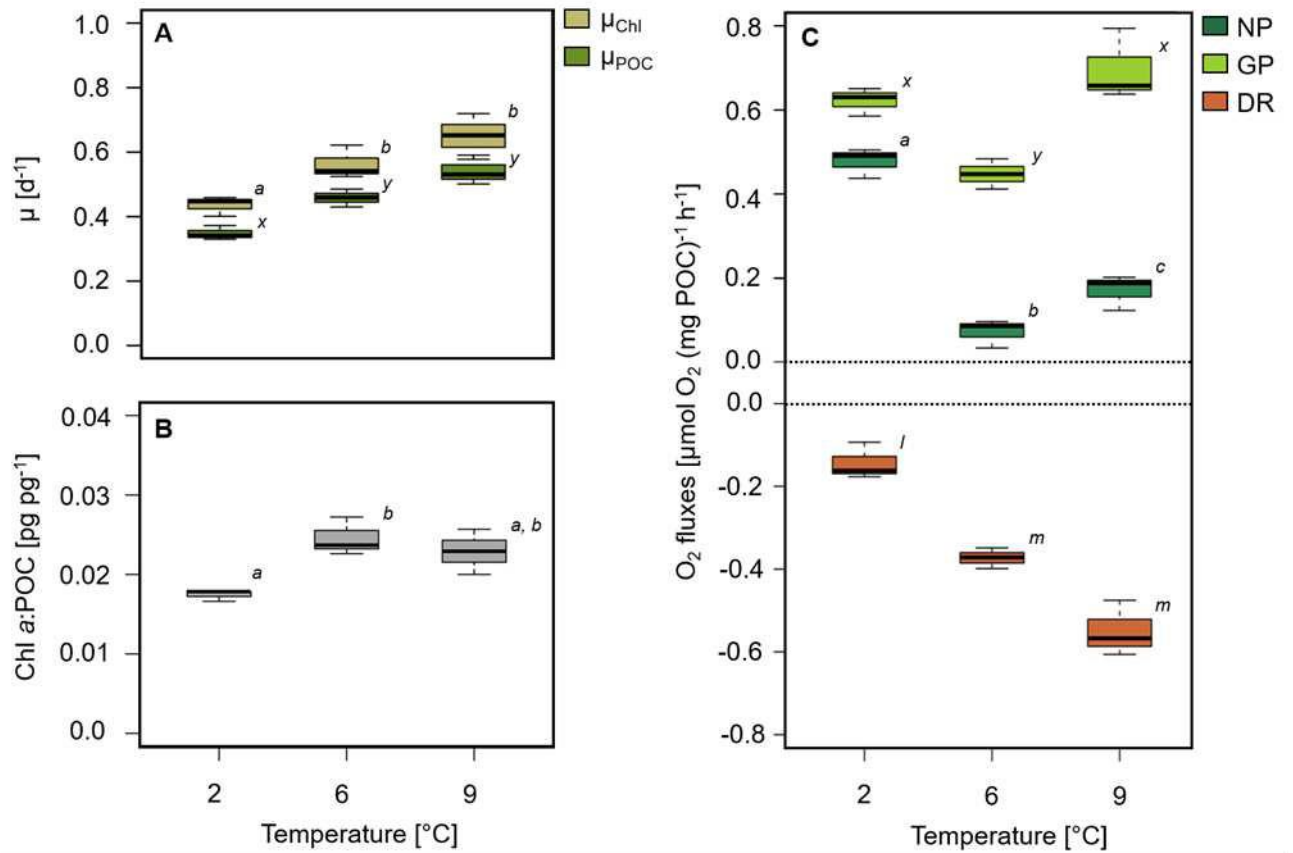
Fig 1. Acclimation responses (A, B) and physiological assays (C) of the communities at the end of the experiment (t_{fin}) at 2°C, 6°C and 9°C. (A) Growth rates based on chlorophyll *a* (Chl *a*; μ_{Chl}; olive) and growth rates based on particulate organic carbon (POC; μ_{POC}; dark olive), (B) ratios of Chl *a*:POC after at the end of the incubation (t_{fin}; grey) and (C) net photosynthetic rates (NP; dark green), gross photosynthetic rates (GP; green) and dark respiratory rate (DR, orange). Boxplots display the mean of three biological replicates (n = 3) and letters indicate significant differences (p ≤ 0.05).

Chl *a*-based growth rates (μ_{Chla}) were lowest at 2°C with ~0.45 d^{-1} and increased gradually to ~0.55 d^{-1} at 6°C and to ~0.65 d^{-1} at 9°C (Fig. 1A). POC-based growth rates (μ_{POC}) also increased gradually with temperature from 0.35 d^{-1} at 2°C to 0.46 d^{-1} at 6°C and 0.54 d^{-1} at 9°C (Fig. 1A). The Chl *a*:POC ratio of the in-situ phytoplankton community was ~0.012 pg pg^{-1} (SI). At the end of the experiment, Chl *a*:POC was 0.017 pg pg^{-1} at 2°C and increased to 0.023 pg pg^{-1} at 6°C and 9°C (Fig. 1B).

Net photosynthetic rates (NP; Fig. 2C) were highest at 2°C (0.48 µmol O_2 mg C a^{-1} h^{-1}) but significantly lowered at 6°C and 9°C (0.07 and 0.17 µmol O_2 mg C^{-1} h^{-1},

respectively). Dark respiratory rates (DR; Fig. 2C) were lowest at 2°C (0.13 μmol O_2 (mg C)$^{-1}$ h^{-1}) and increased consistently to 0.37 and 0.49 μmol O_2 mg C^{-1} h^{-1} at 6 and 9°C, respectively. Gross photosynthetic rates (GP, Fig. 2C), were maintained between 0.45 and 0.6 μmol O_2 mg C^{-1} h^{-1} across all temperatures. However, GP was significantly lower at 6°C than in the other treatments.

Tab 1. Photophysiological parameters obtained by Chl *a* variable fluorescence measurements (FRRf). Maximum quantum yield efficiency of PSII (Fv/Fm), relative electron transport rates at incubation irradiance (rETR$_{exp}$), maximum relative electron transport rates (rETR$_{max}$) and light acclimation indices (I$_k$) at 2°C, 6°C and 9°C. Values display the mean of 3 biological replicates ± SD (n = 3), except for 9°C, where one replicate was lost due to instrumental error (n = 2).

Temp [°C]	Fv/Fm	rETR$_{exp}$	rETR$_{max}$	Ik [μmol photons m^{-2} s^{-1}]
2°C	0.57 ± 0.01	16 ± 1	72 ± 27	117 ± 48
6°C	0.56 ± 0.01	14 ± 1	73 ± 19	138 ± 52
9°C	0.50 ±0.01	11 ± 1	106 ± 10	279 ± 63

Maximum quantum yield of PSII (F$_v$/F$_m$) reached similar values of 0.57 and 0.56 at 2 and 6°C and decreased to 0.50 under 9°C (Tab. 1). Relative electron transport rate under experimental intensity (rETR$_{exp}$) decreased consistently from ~16 at 2°C to ~14 at 6°C and to ~11 at 9°C. Maximum electron transport rates (rETR$_{max}$) remained similarly high at 2°C and 6°C with a value of ~72 and increased to ~106 at 9°C (Tab. 1). The light acclimation indices (I$_k$) of the incubated communities were ~120 μmol photons m^{-2} s^{-1} in the 2°C and ~140 μmol photons m^{-2} s^{-1} in the 6°C treatment, while the value was remarkably increased to ~280 photons m^{-2} s^{-1} at 9°C.

Community composition
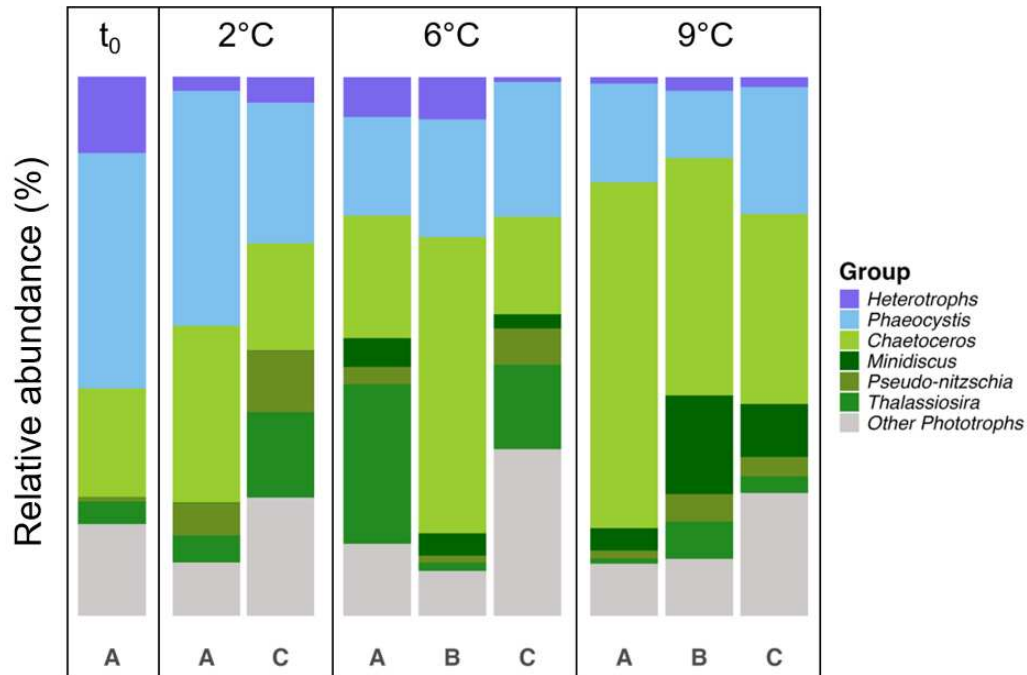
Fig 2. Relative species composition per temperature treatment at t_0 and t_{fin} (2°C, 6°C, 9°C), based on the ASV data. Diatoms are colored in different shades of green.

At the end of the experiment, the main genera of phytoplankton were *Phaeocystis*, *Chaetoceros*, *Thalassiosira* and *Pseudo-Nitzschia*, irrespective of the temperature treatment (Fig. 2). Over the applied experimental temperature gradient, the relative abundance of *Phaeocystis* generally decreased with warming, whereas the relative abundance of diatoms generally increased. *Chaetoceros* was the dominant diatom genus in all temperature treatments. Across temperature treatments, heterotrophs had generally low relative abundances (<10%), with the lowest one at 9°C (<5%).

Discussion

Warming induced a shift from *Phaeocystis towards* diatoms

Despite a rather high variation within treatment replicates, which together with the low number of biological replicates did not allow for statistical testing, we observed a trend of a warming-induced dominance shift in the phytoplankton communities (Fig. 2). The relative abundance of *Phaeocystis* gradually decreased with warming, while the relative abundance of diatoms, especially *Chaetoceros*, gradually increased. Such a decreasing trend of *Phaeocystis* abundance under increasing temperatures has also been observed in another incubation study on phytoplankton communities from the Fram strait (Ahme et al. 2023), whereas field data from sediment traps and remote sensing indicate long-term phytoplankton composition shifts from diatoms towards *Phaeocystis* dominance in this region (Nöthig *et al.*, 2015; Soltwedel *et al.*, 2016; Orkney *et al.*, 2020). Based on the experimental data from temperature manipulations, however, we would argue that the observed increase in *Phaeocystis* dominance over the past decades in the Fram strait may rather be a result of other environmental drivers than temperature.

Biomass accumulation increases with warming

Irrespective of whether they were based on changes in Chl *a* or POC, growth rates increased gradually with warming, indicating a faster biomass accumulation (Fig. 1A). This temperature-dependent stimulation in growth is in line with other findings on Arctic natural phytoplankton communities (Sugie *et al.*, 2020; Ahme *et al.*, 2023; Wolf *et al.*, 2024) and Arctic phytoplankton monocultures (Pančić *et al.*, 2015; Coello-Camba & Agustí, 2017; Hoppe *et al.*, 2018a; Wolf *et al.*, 2018; Rehder *et al.*, 2024), in which several species exhibited optimal growth temperatures substantially higher than what they typically experience in their natural habitat. This demonstrates that many Arctic phytoplankton species currently live below their optimal growth temperature, and thus, their biomass accumulation rates will likely increase in response to warming, provided that nutrients are not limiting.

Oxygen fluxes suggest opposing trend to biomass accumulation response

While growth rate data signified a stimulated biomass accumulation with warming, the MIMS-based measurements of photosynthesis and respiration suggested an apparently opposing trend (Fig. 1B): Gross photosynthetic O_2 production per biomass,

79

a proxy for the light reactions that provide chemical energy for C assimilation, was largely maintained across the applied temperature gradient, indicating an overall unaltered potential for C-assimilation. Simultaneously, the respiratory O_2 consumption, a proxy for the activity of the mitochondrial electron transport chain, was gradually stimulated with temperature (Fig 1B). As a result, net photosynthetic rates were significantly lowered at high temperatures. At first sight, this suggests that phytoplankton metabolism becomes more "heterotrophic" with warming, which should, however, also result in a lowered net C-assimilation, i.e. biomass accumulation.

Such temperature responses of gross photosynthesis and respiration have previously been observed in temperate as well as Arctic phytoplankton (Hancke & Glud, 2004; Barton *et al.*, 2020; Wolf *et al.*, 2024). Some studies found that warming can promote compositional shifts in a plankton community from rather autotrophic towards more mixo- or heterotrophic species, which should increase community respiration (Hancke & Glud, 2004; Holding *et al.*, 2013; Coello-Camba *et al.*, 2015). In our study, however, we can exclude this possibility, as we did not detect a relative increase of hetero- or mixotrophic species with warming (Fig. 2).

Organellar reductant exchange may explain the diverging temperature responses

Overall, our data implies that the tested Arctic phytoplankton community became more productive with warming from a "C-based point of view" as reflected by the increased biomass accumulation rates (Fig. 1A), but also more heterotrophic from an "O_2-based point of view", indicated by the lowered net photosynthetic O_2 production rates (Fig. 1B). This pattern appears somewhat counterintuitive, since O_2- and CO_2-based photosynthetic and respiratory processes are typically thought to be closely connected as they provide reductant for each other. In fact, many studies interpret them to be interchangeable or at least easily convertible into each other.

This opposing temperature response in O_2- and CO_2-based rates has also been observed recently in diatom monoculture experiments (*Publication II*; Rehder *et al.*, 2023), in which especially the respiratory CO_2 release and O_2 consumption diverged substantially under elevated temperatures. This can be attributed to the ability of phytoplankton to independently re-adjust single physiological processes in response to warming. More precisely, under high temperatures, diatoms have been found to be

80

able to export excess reductant from the chloroplasts to the mitochondria to fuel the respiratory O_2 consumption and thus mitochondrial ATP production. As a physiological feedback, this alternative electron source for mitochondrial respiration leads to a downregulation of the citric acid cycle activity and thus lowered respiratory CO_2 loss, which ultimately enhances net C-retention. Even though we cannot directly refer to detailed single cell physiology in a community experiment, our data as well as a similar experiment on Arctic phytoplankton by Wolf *et al.* (2024) both showed theses diverging temperature responses in net O_2 and CO_2 fluxes, which strongly advocates for a similar physiological regulation with downregulated respiratory CO_2 loss and thus increased carbon retention on a community level.

Such regulation pattern could indeed be a more fundamental response to increasing temperatures and is thus rather prevalent in natural phytoplankton communities. The proposed mechanism would also add an explanation as to why observed photosynthetic quotients vary far beyond what theory predicts (Trentman *et al.*, 2023) with far-reaching implications for oceanographic methods that assess carbon fluxes based on oxygen data.

Warming enables photophysiology to exploit higher light levels

Photophysiological assays proved phytoplankton communities to be light limited in all temperature treatments as light acclimation indices (I_k) always exceeded irradiances in the acclimation (Tab. 1). The degree of limitation, however, became even stronger with warming, as indicated by the increase in I_k, which is in line with previous findings on temperature responses of Arctic phytoplankton (*Publication II*; Behrenfeld *et al.*, 2008; Rehder *et al.*, 2024; Wolf *et al.*, 2024). The relative electron transport rates under experimental irradiance ($rETR_{exp}$) were gradually downregulated with warming (Tab. 1), indicating an overall lowered efficiency of PSII. This response is likely attributed to the increasing light limitation, and experiments on Arctic monocultures showed that this decrease of rETR can be partially compensated by a physiological upregulation of the light harvesting machinery (*Publication II*). The elevated Chl *a*:POC ratios (Fig. 1C), which originate from Chl *a*-based accumulation rates being slightly higher than POC-based ones (Fig. 1A), indicate such an upregulation of light harvesting abilities with warming also in our communities. One may argue the relatively increased pigmentation per biomass could originate from the temperature-induced shifts in the community composition, but Hoppe, CJM *et al.* (2024) observed no major effects from such shifts

on Chl *a*:POC ratios. Thus, a physiological upregulation of pigmentation per biomass with warming likely causes the increased Chl *a*:POC ratios. Such a response has also been described in several studies (e.g. Thompson *et al.*, 1992; Baker. *et al.*, 2016; Rehder *et al.*, 2024; Wolf *et al.*, 2024), and is therefore likely a fundamental regulatory mechanism to compensate for the temperature-induced light limitation.

While warming challenges the photophysiology in terms of the increasing light limitation, it also enables phytoplankton to exploit higher irradiances and thus obtain overall higher rates, as indicated by strongly increasing maximum relative electron transport rates (rETR$_{max}$, Tab. 1) at 9°C. Consequently, Arctic phytoplankton may likely benefit from a combined increase of temperature and irradiance, as it is projected for large parts of the Arctic Ocean due to sea ice decline and increased stratification (Constable *et al.*, 2022).

Conclusion and ecological implications

Warming was found to stimulate growth and biomass accumulation at temperatures far beyond what Arctic phytoplankton currently experience in their natural habitats. This does not only underline that Arctic phytoplankton currently live below their optimal growth temperatures (see also Rehder et al. 2024), but also that they will likely benefit from ocean warming, provided that nutrients are not limiting. Thus, Arctic phytoplankton may also remain reasonably competitive towards advected phytoplankton species from the North Atlantic and still thrive under moderate warming scenarios. Despite the stimulated biomass accumulation, which indicates higher net C retention rates, net O_2 production was substantially lowered with warming. This shows that different physiological processes of photosynthesis and respiration can strongly diverge in their temperature responses, underlining the necessity to interpret O_2- and CO_2-fluxes individually. As a consequence, Arctic phytoplankton communities may provide less O_2 per biomass in a warmer future Ocean, but yet they still increase their net C-fixation and consequently also their provision of food for the pelagic and deep-sea environments. Photophysiological data, furthermore, suggest that this stimulation of biomass accumulation will even be more prominent under a combined increase of temperature and light, as it is projected for the future Arctic Ocean.

Acknowledgements

Author contributions

All authors designed the study, L.R. performed the experiments, L.R. analyzed the data with contributions of A.A., all authors discussed data interpretation and L.R. wrote the manuscript with input of A.A., C.J.M.H., S.R. and B.R..

Data availability

The data that support the findings of this study are submitted to the Pangea data depository. Doi will be delivered at a later time point.

Competing interests

The authors declare no competing interests.

References

Adl SM, Bass D, Lane CE, Lukeš J, Schoch CL, Smirnov A, Agatha S, Berney C, Brown MW, Burki F, et al. 2019. Revisions to the Classification, Nomenclature, and Diversity of Eukaryotes. *Journal of Eukaryotic Microbiology* 66(1): 4-119.

Ahme A, Happe A, Striebel M, Cabrerizo MJ, Olsson M, Giesler J, Schulte-Hillen R, Sentimenti A, Kühne N, John U. 2024. Warming increases the compositional and functional variability of a temperate protist community. *Science of The Total Environment*: 171971.

Ahme A, Von Jackowski A, McPherson RA, Wolf KK, Hoppmann M, Neuhaus S, John U. 2023. Winners and losers of Atlantification: the degree of ocean warming affects the structure of Arctic microbial communities. *Genes* 14(3): 623.

Ardyna M, Arrigo KR. 2020. Phytoplankton dynamics in a changing Arctic Ocean. *Nature Climate Change* 10(10): 892-903.

Arrigo KR, van Dijken G, Pabi S. 2008. Impact of a shrinking Arctic ice cover on marine primary production. *Geophysical Research Letters* 35(19).

Baker KG, Robinson CM, Radford DT, McInnes AS, Evenhuis C, Doblin MA. 2016. Thermal Performance Curves of Functional Traits Aid Understanding of Thermally Induced Changes in Diatom-Mediated Biogeochemical Fluxes. *Frontiers in Marine Science* 3.

Barton S, Jenkins J, Buckling A, Schaum C-E, Smirnoff N, Raven JA, Yvon-Durocher G. 2020. Evolutionary temperature compensation of carbon fixation in marine phytoplankton. *Ecology Letters* 23(4): 722-733.

Behrenfeld MJ, Halsey KH, Milligan AJ. 2008. Evolved physiological responses of phytoplankton to their integrated growth environment. *Philosophical Transactions of the Royal Society B: Biological Sciences* 363(1504): 2687-2703.

Beule L, Karlovsky P. 2020. Improved normalization of species count data in ecology by scaling with ranked subsampling (SRS): application to microbial communities. *PeerJ* 8: e9593.

Boscolo-Galazzo F, Crichton KA, Barker S, Pearson PN. 2018. Temperature dependency of metabolic rates in the upper ocean: A positive feedback to global climate change? *Global and Planetary Change* 170: 201-212.

Brown JH, Gillooly JF, Allen AP, Savage VM, West GB. 2004. Toward a metabolic theory of ecology. *Ecology* 85(7): 1771-1789.

Callahan BJ, McMurdie PJ, Rosen MJ, Han AW, Johnson AJA, Holmes SP. 2016. DADA2: High-resolution sample inference from Illumina amplicon data. *Nature Methods* 13(7): 581-583.

Coello-Camba A, Agustí S. 2017. Thermal Thresholds of Phytoplankton Growth in Polar Waters and Their Consequences for a Warming Polar Ocean. *Frontiers in Marine Science* 4.

Coello-Camba A, Agustí S, Vaqué D, Holding J, Arrieta JM, Wassmann P, Duarte CM. 2015. Experimental Assessment of Temperature Thresholds for Arctic Phytoplankton Communities. *Estuaries and Coasts* 38(3): 873-885.

Constable AJ, Harper S, Dawson J, Holsman K, Mustonen T, Piepenburg D, Rost B, Bokhorst S, Boike J, Cunsolo A 2022. Cross-chapter paper 6: Polar regions. *IPCC AR WGII*: Cambridge University Press.

Cooley S, Schoeman D, Bopp L, Boyd P, Donner S, Ito S-i, Kiessling W, Martinetto P, Ojea E, Racault M-F 2022. Oceans and coastal ecosystems and their services. *IPCC AR6 WGII*: Cambridge University Press.

Doney SC, Ruckelshaus M, Emmett Duffy J, Barry JP, Chan F, English CA, Galindo HM, Grebmeier JM, Hollowed AB, Knowlton N. 2012. Climate change impacts on marine ecosystems. *Annual review of marine science* 4: 11-37.

Falkowski P, Scholes RJ, Boyle E, Canadell J, Canfield D, Elser J, Gruber N, Hibbard K, Högberg P, Linder S, et al. 2000. The Global Carbon Cycle: A Test of Our Knowledge of Earth as a System. *Science* 290(5490): 291-296.

Field CB, Behrenfeld MJ, Randerson JT, Falkowski P. 1998. Primary Production of the Biosphere: Integrating Terrestrial and Oceanic Components. *Science* 281(5374): 237-240.

Genty B, Briantais J-M, Baker NR. 1989. The relationship between the quantum yield of photosynthetic electron transport and quenching of chlorophyll fluorescence. *Biochimica et Biophysica Acta (BBA) - General Subjects* 990(1): 87-92.

Giesler JK, Harder T, Wohlrab S. 2023. Microbiome and photoperiod interactively determine thermal sensitivity of polar and temperate diatoms. *Biology Letters* 19(11): 20230151.

Gloor GB, Macklaim JM, Pawlowsky-Glahn V, Egozcue JJ. 2017. Microbiome datasets are compositional: and this is not optional. *Frontiers in Microbiology* 8: 2224.

Goosse H, Kay JE, Armour KC, Bodas-Salcedo A, Chepfer H, Docquier D, Jonko A, Kushner PJ, Lecomte O, Massonnet F, et al. 2018. Quantifying climate feedbacks in polar regions. *Nature Communications* 9(1): 1919.

Grimaud GM, Mairet F, Sciandra A, Bernard O. 2017. Modeling the temperature effect on the specific growth rate of phytoplankton: a review. *Reviews in Environmental Science and Bio/Technology* 16(4): 625-645.

Guillou L, Bachar D, Audic S, Bass D, Berney C, Bittner L, Boutte C, Burgaud G, de Vargas C, Decelle J, et al. 2012. The Protist Ribosomal Reference database (PR2): a catalog of unicellular eukaryote Small Sub-Unit rRNA sequences with curated taxonomy. *Nucleic Acids Research* 41(D1): D597-D604.

Hancke K, Glud RN. 2004. Temperature effects on respiration and photosynthesis in three diatom-dominated benthic communities. *Aquatic Microbial Ecology* 37(3): 265-281.

Hillebrand H, Burgmer T, Biermann E. 2012. Running to stand still: temperature effects on species richness, species turnover, and functional community dynamics. *Marine Biology* 159(11): 2415-2422.

Hobday AJ, Alexander LV, Perkins SE, Smale DA, Straub SC, Oliver EC, Benthuysen JA, Burrows MT, Donat MG, Feng M. 2016. A hierarchical approach to defining marine heatwaves. *Progress in Oceanography* 141: 227-238.

Holding JM, Duarte CM, Arrieta JM, Vaquer-Sunyer R, Coello-Camba A, Wassmann P, Agustí S. 2013. Experimentally determined temperature thresholds for Arctic plankton community metabolism. *Biogeosciences* 10(1): 357-370.

Hoppe CJM, Flintrop CM, Rost B. 2018a. The Arctic picoeukaryote *Micromonas pusilla* benefits synergistically from warming and ocean acidification. *Biogeosciences* 15(14): 4353-4365.

Hoppe CJM, Wolf KK, Schuback N, Tortell PD, Rost B. 2018b. Compensation of ocean acidification effects in Arctic phytoplankton assemblages. *Nature Climate Change* 8(6): 529-533.

Hoppe CJM, Wolf KKE, Cottier F, Leu E, Maturilli M, Rost B. 2024. The effects of biomass depth distribution on phytoplankton spring bloom dynamics and composition in an Arctic fjord. *Elementa: Science of the Anthropocene* 12(1).

Hoppe H-G, Gocke K, Koppe R, Begler C. 2002. Bacterial growth and primary production along a north–south transect of the Atlantic Ocean. *Nature* 416(6877): 168-171.

Igamberdiev AU. 2020. Citrate valve integrates mitochondria into photosynthetic metabolism. *Mitochondrion* 52: 218-230.

Ingvaldsen RB, Assmann KM, Primicerio R, Fossheim M, Polyakov IV, Dolgov AV. 2021. Physical manifestations and ecological implications of Arctic Atlantification. *Nature Reviews Earth & Environment* 2(12): 874-889.

Knap A, Michaels A, Close A, Ducklow H, Dickson A. 1996. Protocols for the joint global ocean flux study (JGOFS) core measurements. *JGOFS, Reprint of the IOC Manuals and Guides No. 29, UNESCO 1994* 19.

Kolber ZS, Prášil O, Falkowski PG. 1998. Measurements of variable chlorophyll fluorescence using fast repetition rate techniques: defining methodology and experimental protocols. *Biochimica et Biophysica Acta (BBA)-Bioenergetics* 1367(1-3): 88-106.

Kwiatkowski L, Aumont O, Bopp L, Ciais P. 2018. The impact of variable phytoplankton stoichiometry on projections of primary production, food quality, and carbon uptake in the global ocean. *Global biogeochemical cycles* 32(4): 516-528.

Lee S. 2014. A theory for polar amplification from a general circulation perspective. *Asia-Pacific Journal of Atmospheric Sciences* 50(1): 31-43.

Lepetit B, Campbell DA, Lavaud J, Büchel C, Goss R, Bailleul B 2022. Photosynthetic light reactions in diatoms. II. The dynamic regulation of the various light reactions. *The molecular life of diatoms*: Springer, 423-464.

Lewis K, Van Dijken G, Arrigo KR. 2020. Changes in phytoplankton concentration now drive increased Arctic Ocean primary production. *Science* 369(6500): 198-202.

Lopez-Urrutia A, San Martin E, Harris RP, Irigoien X. 2006. Scaling the metabolic balance of the oceans. *Proceedings of the National Academy of Sciences* 103(23): 8739-8744.

Martin M. 2011. Cutadapt removes adapter sequences from high-throughput sequencing reads. *2011* 17(1): 3.

Maxwell K, Johnson GN. 2000. Chlorophyll fluorescence—a practical guide. *Journal of experimental botany* 51(345): 659-668.

Moreno HD, Rokitta S, Tremblay N, Boersma M, Groß E, Klip HC, Wiltshire KH, Meunier CL. 2024. Higher temperature, increased CO_2, and changing nutrient ratios alter the carbon metabolism and induce oxidative stress in a cosmopolitan diatom. *Limnology and Oceanography* 69(1): 121-139.

Neukermans G, Oziel L, Babin M. 2018. Increased intrusion of warming Atlantic water leads to rapid expansion of temperate phytoplankton in the Arctic. *Global Change Biology* 24(6): 2545-2553.

Nöthig E-M, Bracher A, Engel A, Metfies K, Niehoff B, Peeken I, Bauerfeind E, Cherkasheva A, Gäbler-Schwarz S, Hardge K, et al. 2015. Summertime plankton ecology in Fram Strait—a compilation of long- and short-term observations. *Polar Research* 34(1): 23349.

Oliver EC, Burrows MT, Donat MG, Sen Gupta A, Alexander LV, Perkins-Kirkpatrick SE, Benthuysen JA, Hobday AJ, Holbrook NJ, Moore PJ. 2019. Projected marine heatwaves in the 21st century and the potential for ecological impact. *Frontiers in Marine Science* 6: 734.

Orkney A, Platt T, Narayanaswamy BE, Kostakis I, Bouman HA. 2020. Bio-optical evidence for increasing Phaeocystis dominance in the Barents Sea. *Philosophical Transactions of the Royal Society A: Mathematical, Physical and Engineering Sciences* 378(2181): 20190357.

Oxborough K. 2012. FastPro8 GUI and FRRf3 systems documentation. *Chelsea Technologies Group Ltd, West Molesey, UK*.

Oziel L, Baudena A, Ardyna M, Massicotte P, Randelhoff A, Sallée J-B, Ingvaldsen RB, Devred E, Babin M. 2020. Faster Atlantic currents drive poleward expansion of temperate phytoplankton in the Arctic Ocean. *Nature Communications* 11(1): 1705.

Oziel L, Gürses Ö, Torres-Valdes S, Hoppe C, Rost B, Danek C, Juhls B, Voelker C, Koldunov N, Wang Q. 2024. Climate Change and terrigenous inputs decrease the efficiency of the future Arctic Ocean's biological carbon pump.

Oziel L, Neukermans G, Ardyna M, Lancelot C, Tison JL, Wassmann P, Sirven J, Ruiz-Pino D, Gascard JC. 2017. Role for A tlantic inflows and sea ice loss on shifting phytoplankton blooms in the Barents Sea. *Journal of Geophysical Research: Oceans* 122(6): 5121-5139.

Pančić M, Hansen PJ, Tammilehto A, Lundholm N. 2015. Resilience to temperature and pH changes in a future climate change scenario in six strains of the polar diatom *Fragilariopsis cylindrus*. *Biogeosciences* 12(14): 4235-4244.

Peltier G, Stoffel C, Findinier J, Madireddi SK, Dao O, Epting V, Morin A, Grossman A, Li-Beisson Y, Burlacot A. 2024. Alternative electron pathways of photosynthesis power green algal CO2 capture. *The Plant Cell* 36(10): 4132-4142.

Pistone K, Eisenman I, Ramanathan V. 2019. Radiative Heating of an Ice-Free Arctic Ocean. *Geophysical Research Letters* 46(13): 7474-7480.

Rantanen M, Karpechko AY, Lipponen A, Nordling K, Hyvärinen O, Ruosteenoja K, Vihma T, Laaksonen A. 2022. The Arctic has warmed nearly four times faster than the globe since 1979. *Communications Earth & Environment* 3(1): 168.

Rehder L, Rokitta SD, Hoppe CJ, Buschmann I, Jasper L, Rost B. 2024. Different temperature sensitivities of key physiological processes lead to divergent trait response patterns in Arctic phytoplankton. *Limnology and Oceanography*.

Rehder L, Rost B, Rokitta SD. 2023. Abrupt and acclimation responses to changing temperature elicit divergent physiological effects in the diatom Phaeodactylum tricornutum. *New Phytologist* 239(3): 1005-1013.

Rokitta SD, Grossmann CH, Werner E, Moye J, Castellani G, Nöthig EM, Rost B. 2023. Future warming stimulates growth and photosynthesis in an Arctic microalga more strongly than changes in light intensity or pCO_2. *Limnology and Oceanography* 68(12): 2789-2799.

Rokitta SD, Rost B. 2012. Effects of CO_2 and their modulation by light in the life-cycle stages of the coccolithophore *Emiliania huxleyi. Limnology and Oceanography* 57(2): 607-618.

Rost B, Zondervan I, Wolf-Gladrow D. 2008. Sensitivity of phytoplankton to future changes in ocean carbonate chemistry: current knowledge, contradictions and research directions. *Marine Ecology Progress Series* 373: 227-237.

Schuback N, Hoppe CJ, Tremblay JÉ, Maldonado MT, Tortell PD. 2017. Primary productivity and the coupling of photosynthetic electron transport and carbon fixation in the Arctic Ocean. *Limnology and Oceanography* 62(3): 898-921.

Soltwedel T, Bauerfeind E, Bergmann M, Bracher A, Budaeva N, Busch K, Cherkasheva A, Fahl K, Grzelak K, Hasemann C, et al. 2016. Natural variability or anthropogenically-induced variation? Insights from 15 years of multidisciplinary observations at the arctic marine LTER site HAUSGARTEN. *Ecological Indicators* 65: 89-102.

Sugie K, Fujiwara A, Nishino S, Kameyama S, Harada N. 2020. Impacts of Temperature, CO2, and Salinity on Phytoplankton Community Composition in the Western Arctic Ocean. *Frontiers in Marine Science* 6.

Tesi T, Muschitiello F, Mollenhauer G, Miserocchi S, Langone L, Ceccarelli C, Panieri G, Chiggiato J, Nogarotto A, Hefter J. 2021. Rapid Atlantification along the Fram Strait at the beginning of the 20th century. *Science Advances* 7(48): eabj2946.

Thomas MK, Kremer CT, Klausmeier CA, Litchman E. 2012. A global pattern of thermal adaptation in marine phytoplankton. *Science* 338(6110): 1085-1088.

Thompson PA, Guo Mx, Harrison PJ, Whyte JN. 1992. Effects of variation in temperature. II. On the fatty acid composition of eight species of marine phytoplankton 1. *Journal of Phycology* 28(4): 488-497.

Trentman MT, Hall Jr. RO, Valett HM. 2023. Exploring the mismatch between the theory and application of photosynthetic quotients in aquatic ecosystems. *Limnology and Oceanography Letters* 8(4): 565-579.

Wassmann P, Slagstad D, Ellingsen I. 2019. Advection of mesozooplankton into the northern Svalbard shelf region. *Frontiers in Marine Science* 6: 458.

Wolf KK, Hoppe CJ, Rost B. 2018. Resilience by diversity: Large intraspecific differences in climate change responses of an Arctic diatom. *Limnology and Oceanography* 63(1): 397-411.

Wolf KKE, Hoppe CJM, Rehder L, Schaum C-E, John U, Rost B. 2024. Heatwave responses of Arctic phytoplankton communities are driven by combined impacts of warming and cooling. *Science Advances*.

5 *Publication IV*

Heatwave responses of Arctic phytoplankton communities are driven by combined impacts of warming and cooling

Published in Science Advances

Wolf, K. K., Hoppe, C. J., Rehder, L., Schaum, E., John, U., & Rost, B. (2024). Heatwave responses of Arctic phytoplankton communities are driven by combined impacts of warming and cooling. *Science Advances*, *10*(20), eadl5904.

ECOLOGY

Heatwave responses of Arctic phytoplankton communities are driven by combined impacts of warming and cooling

Klara K. E. Wolf[1,2,3]*, Clara J. M. Hoppe[3], Linda Rehder[3], Elisa Schaum[1], Uwe John[3,4], Björn Rost[3,5]

Marine heatwaves are increasing in frequency and intensity as climate change progresses, especially in the highly productive Arctic regions. Although their effects on primary producers will largely determine the impacts on ecosystem services, mechanistic understanding on phytoplankton responses to these extreme events is still very limited. We experimentally exposed Arctic phytoplankton assemblages to stable warming, as well as to repeated heatwaves, and measured temporally resolved productivity, physiology, and composition. Our results show that even extreme stable warming increases productivity, while the response to heatwaves depends on the specific scenario applied and is not predictable from stable warming responses. This appears to be largely due to the underestimated impact of the cool phase following a heatwave, which can be at least as important as the warm phase for the overall response. We show that physiological and compositional adjustments to both warm and cool phases drive overall phytoplankton productivity and need to be considered mechanistically to predict overall ecosystem impacts.

INTRODUCTION

In a warming climate, extreme events such as marine heatwaves are becoming more frequent, intense, and longer-lasting (*1*). They often expose species to conditions beyond their tolerance thresholds with far-reaching consequences on entire ecosystems (*2*). Impacts of marine heatwaves include shifts in community composition, mass mortality of species, and severe biodiversity loss, up to the collapse of regional fisheries (*3*). In the Arctic, marine heatwaves have already increased in number over the past decades (*4*), and impacts are expected to increase further as temperatures rise and sea ice declines (*5*, *6*).

A broader understanding of the ecological impacts of marine heatwaves is still missing and so far limited to opportunistic observations of large-scale and long-term events (*7*) with a focus on higher trophic levels such as fish. For areas north of the Arctic circle, however, observations on marine heatwaves and their impacts hardly exist to date (*8*), and only very few recent ones have been described for Antarctica (*9*). To our knowledge, the northernmost warm water events for which direct biological impacts were recorded are in the Bering Sea, the Gulf of Alaska 2016 (*10*, *11*), and the North Atlantic 2012 (*12*), all of which reported northward shifts of species and changed migration patterns. The few described cases for changes at the lower trophic levels comprise shifts in phytoplankton species abundance and composition, including occurrences of toxic algal blooms (*13*, *14*). These changes propagated up the foodweb and led to shifts in important zooplankton species, eventually causing mass starvation or intoxication of higher trophic levels (*10*, *15*).

While there is little data on the responses of phytoplankton to heatwaves to date, general temperature effects on growth and other physiological processes are well described. Maximum growth rates are expected to generally increase with temperature (*16*, *17*), while warming beyond the optimum usually induces stress and decreases rates again (*18*). These temperature dependencies are typically derived from the responses of long-term acclimated laboratory strains, and it has been shown that they do not necessarily predict short-term responses under fluctuating temperature dynamics (*19*, *20*). Depending on the optimum ranges of an organism and time frames of exposure, variable temperature conditions can have negative impacts on phytoplankton productivity (*21*, *22*), e.g., because acclimation and selection act into different directions in warm and cool phases. Especially when exposed to extremely low or high temperatures, variability can also be beneficial and provide opportunities for physiological recovery or evolutionary rescue (*23*, *24*).

Interactions with other environmental and ecological factors in natural environments make variable temperature responses even harder to predict. Modeling and observations generally suggest that marine heatwaves cause a decline in primary productivity at lower latitudes, while productivity increases at higher latitudes (*10*, *25*, *26*). These opposing patterns are strongly connected not only to regional nutrient backgrounds but also to temperature-driven changes in nutrient and light availability due to increased stratification (*3*, *25*, *27*, *28*). Heatwaves at low latitudes often intensify nutrient limitation and decrease overall productivity, while heatwaves in comparably nutrient-rich high-latitude regions are expected to intensify blooms. This has indeed been observed in satellite-based chlorophyll *a* (Chl *a*) data in Antarctica (*29*), but high-resolution observations of the lower trophic levels during heatwaves are still lacking (*25*), especially for polar regions. The same is true for process understanding of phytoplankton responses to heatwaves, which is urgently needed to enable better predictions.

Experiments can provide answers to more targeted mechanistic questions regarding heatwave responses. The few existing studies on phytoplankton are yet difficult to compare because of very different experimental setups, ecological complexity, geographic regions, and measured parameters, and often do not specifically resolve the time period after a heatwave, i.e., when temperatures return to baseline conditions. Accordingly, they deliver very different results, ranging

[1]Institute of Marine Ecosystem and Fishery Science, University of Hamburg, Hamburg, Germany. [2]Environmental Genomics, University of Konstanz, Konstanz, Germany. [3]Alfred Wegener Institute Helmholtz Centre for Polar and Marine Research, Bremerhaven, Germany. [4]Helmholtz Institute for Functional Marine Biodiversity (HIFMB), Oldenburg, Germany. [5]FB2, University of Bremen, Bremen, Germany.
*Corresponding author. Email: klara.wolf@uni-konstanz.de

from detrimental [e.g., (*30*, *31*)] to beneficial effects on productivity or biomass production [e.g., (*32*)], and from strong stability to high sensitivity in taxonomic composition and diversity (*24*, *33–35*). This illustrates that responses to heatwaves are complex and need to be tested in view of their specific context, such as their seasonal and regional settings. One study has investigated polar phytoplankton under heatwaves by exposing isolated genotypes of an Antarctic diatom to heatwaves scenarios, finding increased mortality with increasing intensity and duration of heat exposure under nutrient limitation (*31*). Among the tested genotypes, however, they found large intraspecific variability, suggesting that, in an entire dynamic community, response variability is going to be even more relevant.

The aim of this study was to characterize the response of phytoplankton communities to elevated stable temperatures and to investigate whether such general temperature responses can help to anticipate responses to heatwaves of the same temperature range. We exposed triplicates of natural spring communities from coastal Svalbard (Norway) for 2 to 3 weeks to stable temperature treatments (2°, 6°, and 9°C), where 2°C acted as a control treatment, as well as to repeated 5-day heatwaves of differing intensities [HW6° and HW9°C; Fig. 1]. By excluding grazers and ensuring nutrient replete and stable light conditions, we focused on the effect of temperature only. To understand the dynamics and mechanisms during changing temperature regimes, we explicitly investigated the different phases of a heatwave toward their impact on the community. At several time points (t1 to t4), we measured an extensive set of parameters, including growth and productivity assays, stoichiometry, photophysiology, as well as species and intraspecific population composition. With this study, we deliver a rare record of the implications of heatwave scenarios for the most important traits of Arctic primary producers.

RESULTS AND DISCUSSION
In the following, we will first present and discuss the responses to the stable temperature treatments in terms of their time-integrated outcomes, followed by the assessment of their temporal dynamics and their compositional development. Next, we will focus on the responses in the heatwave treatments and contrast those findings to the ones obtained from stable temperature treatments. Last, we will discuss what mechanistic understanding we have gained regarding heatwave responses and ecological implications arising from our

findings. We would like to mention initially that, toward the end of the experiment, biofilm formation inside all incubation bottles could be observed (see details in Materials and Methods). While this potentially biased species composition toward benthic species, we are confident that it did not change overall outcomes or conditions of the incubations (e.g., light or nutrient regime).

Even strongly elevated temperature stimulates community productivity
Growth rates increased with increasing temperatures under stable conditions. This was observed using weighted means to integrate over the entire experiment [linear mixed model (lme) for growth: $P < 0.001$; Fig. 2A and table S1] but also at time resolution (Fig. 3A, see below). The other two productivity measures, net primary productivity (NPP; ^{14}C-based) and gross primary productivity (GPP; O_2-based), also showed increasing trends with temperature (lme NPP: $P = 0.02$, GPP: $P = 0.15$; Fig. 2A and table S1). For growth and NPP, even the scale of increase with warmer temperatures was similar (6°C growth: +17%, NPP: +34% and 9°C growth: +30%, NPP: +31%). GPP increased at a higher mean rate (6°C: +41% and 9°C: +75%), but rates were also more variable (Fig. 2A). Although these three rate measurements have different units, and are based on different assumptions and potential biases by unaccounted processes (e.g., potential light and bacterial respiration in GPP), they consistently show similar positive trends with warming up to 9°C. While this is not unexpected in view of general knowledge on temperature effects on growth rates [e.g., (*16*)], it is impressive considering that we exposed communities to fairly extreme scenarios for high-latitude organisms and for a spring community at this specific location (see fig. S11). Growth rates yielded a Q10 value of 1.45 (±0.01) all the way up to 9°C. This value is close to Q10 estimates of the global average for phytoplankton (*36*), which include a large proportion of temperate species. This suggests that the sampled Svalbard community could indeed remain competitive compared to invading Atlantic species over the here tested temperature range. Our results also support the literature showing that many polar phytoplankton species live well below their optimum growth temperature (*37–39*).

The stimulatory effects of warming on productivity were observed despite even stronger increases in dark respiration relative to 2°C (6°C: +130%, 9°C: +300%, lme: $P < 0.001$; Fig. 2A and table S1). This is in line with studies showing that respiration is more sensitive
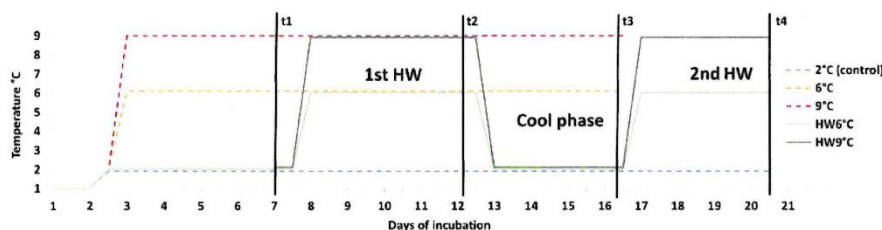
Fig. 1. Experimental design. Overview of the temperature treatments (legend) and sampling and dilution points (t1 to t4) of the experiment. Three stable temperature treatments exposed phytoplankton communities to 6° and 9°C for 16 days and 2°C for 20 days. The two heatwave treatments (HW6°C and HW9°C) exposed communities to two consecutive 5-day heatwaves at 6° and 9°C, respectively, with a 3-day cool phase at 2°C in between and ran for a total of 20 days. Because of this design, the final time points are only directly compared between the heatwave treatments and stable 2°C at day 20 (t4) and between all stable treatments at day 16 (t3).
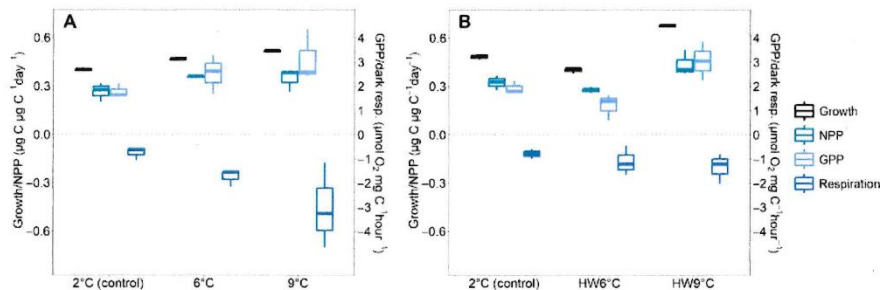
Fig. 2. Weighted means over time of rate measurements. Growth (based on POC), NPP (based on ^{14}C assays), GPP, and dark respiration (based on O_2 evolution assays) as weighted means over the time of the experiment. (**A**) Stable temperature treatments up to day 16. (**B**) Heatwave treatments and stable 2°C up to day 20.
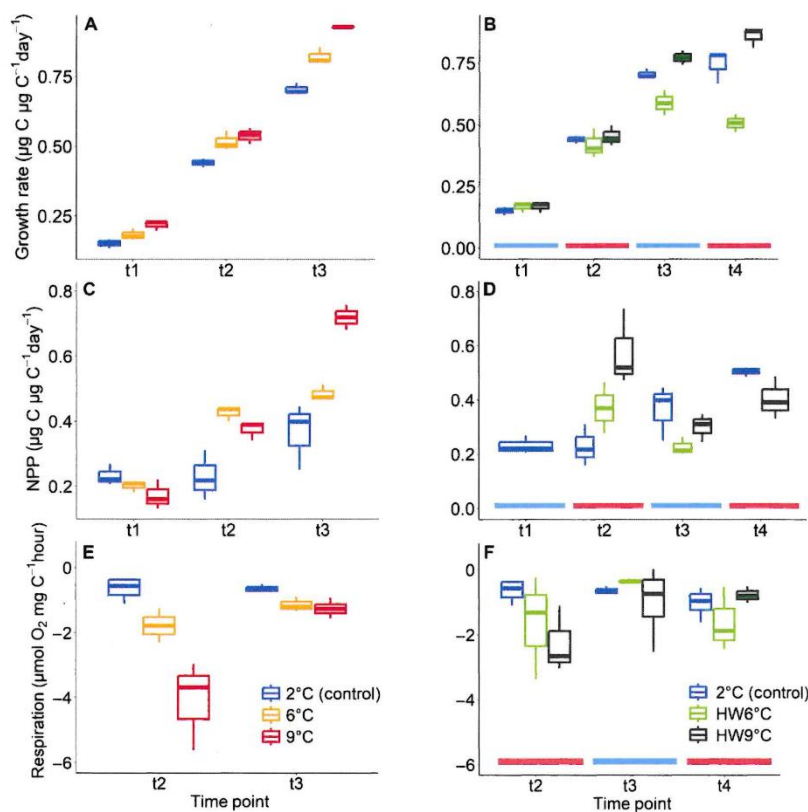
Fig. 3. Time-resolved measurements. Growth rate (**A** and **B**), NPP (**C** and **D**), and dark respiration (**E** and **F**) at time resolution for the stable [(A), (C), and (E)] and the heatwave treatments [(B), (D), and (F)]. Blue and red lines at the bottom of the heatwave plots indicate where time points followed a cool or warm phase. NPP values for the heatwave treatments at t1 were adopted from the 2°C control treatment, NPP measurements of HW6°C at t4 were lost due to technical problems. Rates of O_2 evolution were only measured from t2 onward because biomass was too low for accurate rate assessments before.

Wolf *et al.*, *Sci. Adv.* **10**, eadl5904 (2024)   17 May 2024

3 of 11

94

to temperature change than photosynthesis in phototrophs [e.g., (40, 41)] but is probably partly influenced by the fact that our community measurements comprise not only phytoplankton respiration but also heterotrophic organisms (here mainly bacteria). Nevertheless, we assume that primary producers were likely the dominant O_2 consumers, which is corroborated by the largely congruent patterns of O_2-based community GPP and ^{14}C-based phototrophic NPP (Fig. 2).

The overall Chl a:POC ratio in the communities increased with temperature in the stable treatments (lme Chl a:POC: $P = 0.002$; fig. S1A and table S1), which is in line with a number of experimental studies (30, 42–44). At the same time, however, electron transport rates at in situ light (isETR) showed a trend for lower values with increasing temperature (lme: $P = 0.058$; fig. S1C and table S1). Usually, the photosynthetic machinery is accelerated by warming, supported here by a trend of shorter reoxidation time at PSII (tau; fig. S1E), which enables higher productivity if sufficient light can be harvested. The decrease in electron transport at PSII (isETR) under warming may thus have been compensated by more reaction centers, reflected in the increase in Chl a:POC. This reorganization would make cells more flexible to opportunistically exploit higher light intensities when turnover rates in the Calvin cycle are accelerated by higher temperatures. Otherwise, responses in photophysiology were relatively minor, even during abrupt temperature ramps (fig. S7).

Time-resolved growth and productivity rates showed an increasing trend in all treatments over time (Fig. 3A). This is to be expected even in ambient treatments since the phytoplankton community adjusts increasingly to laboratory conditions, physiologically as well as by increasing contributions of fast-growing species under the replete nutrient and stable light conditions. In line with the time-integrated results (Fig. 2A), the temporal development of growth rates in the stable temperature treatments showed consistently larger increases at higher temperatures [linear model (lm) growth, 2°C slope = 0.055 day^{-1}; 6°C slope = 0.063 day^{-1}; 9°C slope = 0.07 day^{-1}; table S2]. A similar development over time was visible in productivity measures (Fig. 3C and table S2), but not in respiration rates (Fig. 3E): In the 2°C treatment, dark respiration remained remarkably unchanged over the course of the experiment (lm on respiration without significant slope; table S2), apparently already being sufficiently acclimated to these temperatures before that time point. In the stable warm treatments, however, respiration rates were notably higher than those at 2°C early on [t2: 6°C: +173%, 9°C: +527%, analysis of variance (ANOVA): $P = 0.003$; table S2] and then decreased to values closer to 2°C at the last time point (t4: 6°C: +78%, 9°C: +94%, ANOVA $P = 0.02$; table S2), suggesting a slow but substantial acclimation effect.

Next to physiological acclimation, sorting between species and strains can also contribute substantially to the overall response patterns (45). The experiment started off with a diverse pre–spring bloom community (figs. S2 and S3) dominated by diatoms, alongside dinoflagellates, haptophytes (Phaeocystis), and green algae (Micromonas). Note that community composition was assessed from 18S ribosomal RNA (rRNA) gene metabarcoding and is thus only meaningful concerning relative abundances within samples. By the end of the experiment, diatoms dominated all communities independently of the treatment [71 to 92% of taxonomically assigned amplicon sequence variants (ASVs)]. At the final time point, the species composition between the stable temperature treatments was

distinct (PERMANOVA: $P = 0.003$; Fig. 4). Unexpectedly, dominant taxa were largely identical across treatments despite the large temperature differences, consisting mainly of the genera Navicula, Fragilariopsis, Thalassiosira, Nitzschia, and Skeletonema (fig. S3). The similarity between the treatments suggests that the majority of species retained similar competitive ranking to each other under stable temperature conditions between 2° and 9°C, suggesting a high resilience in species composition over the here tested temperature range. This resilience toward stable warming scenarios has been previously described for phytoplankton communities from different Arctic regions, which were furthermore concomitantly challenged with changes in carbonate chemistry and light levels (46).

Overall, the observed differences between our stable temperature treatments were much larger in bulk ecophysiological responses than in composition. We therefore conclude that changes in traits such as productivity were likely caused by physiological adjustments of the dominant members of the community in parallel, rather than by fundamental compositional changes. Our findings thus hint toward more general, cross-species physiological response patterns under stable warming.

Heatwave responses are not predictable from stable temperature responses

In contrast to communities in the stable temperature treatments, responses to the heatwave treatments were much less linear and intuitive. Despite the stimulating effects at stable 6°C, the treatment with 6°C heatwaves (HW6°C) yielded overall lower productivity estimates than the stable 2°C treatment (growth: −17%, NPP: −14%, GPP: −37%; Fig. 2B). In the 9°C heatwave treatment (HW9°C), however, all productivity measures showed increased trends when integrated over time (growth: +43%, NPP: +35%, GPP: +59%; Fig. 2B) and even surpassed the rates at stable 9°C. Although unexpected, these trends are supported by three independent measurement
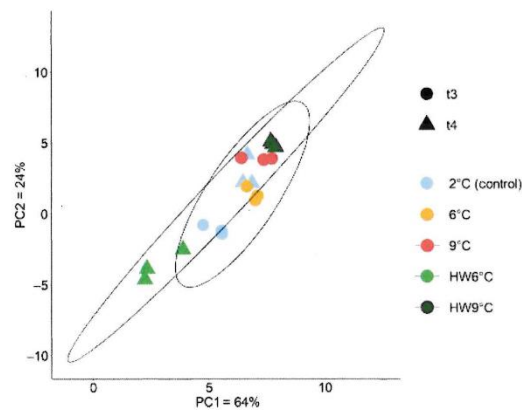
Fig. 4. Species composition at the end of the experiment. Similarity of proportional species composition at the final time points of the experiment (stable treatments at t3 = 16 days and HWs at t4 = 20 days). The plot is based on a principal components (PCA) analysis of Aitchinson distances between 18S gene metabarcoding results of the three replicates of all treatments.

techniques, depicting different biological aspects of productivity (biomass buildup, C fixation, and O_2 production). The responses in respiration rates were more similar to the stable temperature exposures and showed increased trends in both heatwave treatments (Fig. 2B). Nonetheless, viewed in concert with the stable temperature treatments, the detrimental responses in the HW6°C treatment are especially puzzling. To understand the fundamental differences between the two heatwave treatments, it proved necessary to consider the different warm and cool phases separately over time.

In both heatwave treatments, it was not the warming itself that had the largest influence on biomass buildup. In fact, growth rates remained not only similar to those in stable 2°C during the initial phase but also even during the first heatwave (t2), i.e., in the first 5 days after temperature increased (Fig. 3B). Significant treatment differences in growth appeared only at the end of the cool phase (ANOVA growth t3: $P = 0.002$; table S2) and then continued to increase throughout the second heatwave (ANOVA t4: $P < 0.001$): While HW6°C communities showed substantially slower growth than 2°C control (second HW: −32%, Tukey's test t4: $P = 0.003$; table S2), HW9°C communities grew faster (second HW: +15%, Tukey's test t4: $P = 0.07$). In the NPP measurements, both heatwave communities showed increased rates at the end of the first heatwave already (ANOVA t2: $P = 0.02$; Fig. 3D), although this increase was significant only in HW9°C (+151%, Tukey's test: $P = 0.02$; table S2). In the following cool phase (t3), net productivity of both heatwave communities tended to decrease to rates even below those observed at stable 2°C (t3 + t4, ANOVA not significant), with especially low rates in the HW6°C communities (Fig. 3D). Thus, in both productivity parameters, the heatwave communities showed the biggest divergence during the first cool phase (t3).

Respiration rates were only successfully recorded from day 11 onward (t2, after the first heatwave) but still show interesting temporal developments (Fig. 3F). During heatwave exposure, effects on respiration were similar in HW6°C and HW9°C and even to those in the stable treatments, although measurements yielded higher variability, causing differences not to be significant. During the first heatwave (t2), respiration increased in both heatwave treatments relative to 2°C (HW6°C: +152%, HW9°C: +248%). During the consecutive cool phase (t3), respiration fell back to levels at 2°C for both heatwave treatments and afterward, increased only in HW6°C during the second heatwave (t4, +58% compared to the 2°C control), but not in HW9°C (−24%). The trend of decreased respiration over time, which was observed in the stable warm treatments and in HW9°C, hints toward acclimation rather than stress accumulation through warm phases. Here, our data differ from findings on Antarctic diatom strains, where mortality was higher in cultures with repeated heat exposure (*31*).

Note that some of the differences in the dynamics of productivity might be caused by the fact that assay-based assessments (NPP, GPP, and respiration) display immediate responses of cells at a specific acclimation state, while growth rates represent an integrated signal of biomass produced over several days, which was formed by cells with potentially different physiological states during the process of acclimation. In HW6°C communities, the combination of lower NPP during the first heatwave (t2) and the cool phase (t3), along with the higher respiration during the second heatwave (t4), may thus have led to the overall decreased growth in this treatment, which started to be visible after the cool phase (t3). In HW9°C, on the other hand, the community had very high NPP rates during the

first heatwave (t2), which may have carried over into the cool phase in the form of higher cell fitness or storage compounds. These "stored gains" (*24*) could have enabled increased growth even during the cool phase and, lastly, also an overall higher performance over the entire course of the experiment.

All treatments had distinct species compositions at the final time point, as described by their beta-diversities (PERMANOVA: $P < 0.001$; Fig. 4 and table S3). Their richness, however, as well as their dominant species were similar (figs. S2 and S3 and table S3). The notable exception was HW6°C, where the dominant genera differed from all other treatments (Fig. 4 and fig. S2): Here, *Navicula* was much less abundant than in any other treatment, while *Thalassiosira* and *Fragilariopsis* were more dominant. HW6°C was also the only treatment where a larger fraction of Chlorophyta (9% *Micromonas*) remained in the community. Because HW6°C communities were taxonomically distinct from all other treatments, and they were also unique in their lowered productivity and growth, it is likely that here compositional changes played a larger part in the overall response than for the other treatments. A closer look at the most dominant genera at the final time points reveals that some genera appeared to generally profit more or less from the applied treatments (fig. S4). Some profited from stable warming, such as species of *Fragilariopsis* and *Nitzschia*, while species of *Thalassiosira* and *Micromonas* declined under warming conditions. Fluctuating conditions as in the heatwaves, on the other hand, seemed to favor species of *Fragilariopsis*, as well as *Thalassiosira* in the intermediate heatwave, but not *Nitzschia*, indicating that also species dominance, here demonstrated by genera, can be poorly predicted from stable warming.

To also follow the intraspecific population composition, we used microsatellite PoolSeq barcoding [MPB; (*47*)] on one key diatom species, *Thalassiosira hyalina*, throughout the experiment. In addition to shifts between taxa, lineage sorting among diverse genotypes of the same species could be a powerful way of adaptation apart from physiological acclimation (*37, 48*). On the basis of the allelic composition of both tested microsatellite loci, however, no directional shifts over time or among the treatments at the final time points were observed (fig. S6B). While the genus *Thalassiosira* decreased in abundance in all warmer treatments (fig. S6A), *T. hyalina* was likely even extinct at the final time point in the stable 9°C treatment as it was not detectable by MPB anymore. Overall, it does not appear that genotypic shifts within the species played a role in these communities.

Similar to the temporal development of growth rates, shifts in species composition of HW6°C also appeared during the cool phase (t3; fig. S5). Communities started to become distinctly different between treatments by the end of the first heatwave (t2, PERMANOVAs on beta-diversity t2 to t4 with $P < 0.05$; table S3). At this time point, communities in HW6°C were most similar to those at stable 2°C, while communities in HW9°C resembled those at stable 6°C (fig. S5). After the cool phase (t3), however, HW9°C communities approached the composition of stable 2°C again, while HW6°C shifted into a "new direction" and decreased in growth from then on. When comparing the two heatwave treatments, it is also notable that HW9°C communities remained more diverse after the first heatwave than HW6°C communities (t2; fig. S3), where some species relevant for buffering negative responses in the following cool phase may have been lost. Especially in fluctuating treatments, maintenance of higher diversity throughout a heatwave may provide a better basis for coping with the subsequent cool and warm phases.

The interplay between warm and cool phases determines the overall heatwave response

The unexpected outcomes of the two heatwave treatments (Fig. 2) can only be explained by taking both, the warm and cool phases into account, as well as their interplay. Ecologically motivated heatwave experiments often report carryover effects and low recovery of phytoplankton composition after a warm phase [e.g., (32, 49)], but more mechanistic studies classically focus on the high-temperature phase [e.g., (30, 50)]. Little attention has been paid to physiological responses during the phase when temperatures return to more ambient levels [but see (31)], although this may interrupt an ongoing acclimation process and respectively start a new one in an opposite direction. Our overall data on ecophysiological and taxonomic changes suggest that a cool phase following a heatwave can be at least as decisive a driver as the warm phase itself. A cool phase can even act as an additional stressor rather than a relief to organisms and change compositional trajectories as argued above for the case of HW6°C. Similar seemingly "counterintuitive" responses were also described on a physiological level for phytoplankton by Rehder *et al.* (43), who found abrupt temperature decreases to cause transient imbalances in subcellular processes that can be even larger than those caused by warming. Temperature optima of polar species are often found above ambient temperatures (37, 39), which may contribute to this effect, but the physiological impacts of cooling have to our knowledge rarely been investigated.

While compositional changes played an unexpectedly minor role in the majority of our treatments, it likely had a considerable impact on the responses of HW6°C, especially from the cool phase on. This example illustrates how small selective shifts at one time point may translate into large effects on productivity and composition later on, an aspect especially hard to foresee for exponentially growing organisms under fluctuating conditions. During the different temperature phases of a heatwave scenario, natural communities are likely confronted with opposing acclimation and selection pressures, which can shift or reduce the diversity during one phase in a way that is decisive for the next. While most dominant taxa in our study appear to have similarly large plastic ranges in their stable temperature response, fluctuations can apparently change this picture, unless heatwave-like fluctuations become the "new normal" and species' abilities to withstand fluctuations are what is being selected for in a future ocean.

Ecological implications of heatwave responses may be unexpectedly large and complex

The implications of physiological rate changes in exponentially proliferating organisms are often not easy to grasp but are ultimately the drivers of bloom dynamics and biogeochemical cycling (51–53). For better illustration, we calculated theoretical biomass accumulation based on growth rates for each of our treatments without dilution (i.e., as in a bloom modeled without loss terms; fig. S8). After 14 days of stable warm temperatures, biomass production would thus be stimulated by +280% at 6°C and +560% at 9°C compared to 2°C. After 20 days with two 5-day heatwaves (i.e., 10 days warm and 10 days cold), communities would have experienced a smaller increase under 9°C heatwaves compared to stable 2°C (+60%) and a large decrease under heatwaves of 6°C (−86%). Of course, this upscaling exercise applies vast simplifications, e.g., it does neither account for potential resource limitation nor loss terms such as sinking or grazing. Although effects of heatwaves on grazing are still not

well understood (54) and likely depend on many concomitant factors, first evidence from longer heatwaves hints toward an increase in zooplankton abundance through reduced top-down control by forage fish during warm phases (55, 56). Our data nevertheless demonstrate the large potential ecological implications of bottom-up changes in biomass buildup of the observed scale over a bloom situation, underlining the need for a better understanding of these short-term temperature events. Especially if compositional changes between taxonomic groups appear, as in HW6°C with a larger relative abundance of Chlorophyta compared to diatoms, impacts on biogeochemistry and trophic transfer efficiency along the food chain can be expected (57). Whether these taxonomic shifts are a cause or an effect of the observed physiological responses cannot not be distinguished from this study. Further physiological studies on single species under heatwaves might help to shed light on this question, but here, compositional shifts were apparently driven more by the fluctuation of temperature than its absolute value. This in mind, note that responses to fluctuating temperature are not independent of the thermal history and the optimal temperatures of different species, which is why elevated future mean temperatures likely also have an effect on heatwave responses (58).

The overall increased Chl *a*:POC ratio at higher temperatures in photosynthetically dominated communities could also have important implications. A systematic influence of temperature on Chl *a*:POC ratios, as also suggested by physiological theory (59), could have large implications for modeled biomass predictions because observations of altered primary production are often based on Chl *a* as proxy for phytoplankton biomass. Effects of elevated temperature on phytoplankton biomass in the field [e.g., (29)] could thus be overestimated. Furthermore, NPP measurements, which are usually normalized to Chl *a*, would be inconsistent with C-based estimates at different temperatures. An illustration of this effect can be found in fig. S9, where NPP results of the present study are shown normalized to C and Chl *a*, with very different trends due to the shifts in underlying Chl *a*:POC ratios under different treatments.

Lastly, please note that this study was designed to single out and understand the effects of temperature alone on Arctic phytoplankton communities. To achieve a complete assessment of heatwave and temperature effects in a realistic context, interactions with other bottom-up factors such as nutrients and light but also top-down impacts such as grazing should be included. Nutrient regimes are likely very crucial for heatwave responses of phytoplankton, especially as they are expected to change alongside with warming (2) and can drive species composition and response sensitivity in systematic ways (3, 60). More specifically, heatwaves themselves can impede nutrient supply through stratification (25), and nutrient limitation was found to lower the temperature optimum for phytoplankton growth, making them more prone to heat stress (24, 60, 61). In the Arctic, temperature-nutrient interactions are thus likely most relevant during summer when heatwaves and nutrient-limitation coincide. Such mechanistic understanding will be necessary to identify the most important drivers and to disentangle the complex interactions between them.

In conclusion, we found that stable warming strongly increased growth and productivity in spring phytoplankton communities from Svalbard, although the temperatures were far above organisms' thermal history at this location (see fig. S11). Responses to short-term heatwaves proved less intuitive as they were driven by a complex interplay of warming and cooling effects, and shifts in community

composition and physiology were carried over from one temperature phase to the next. Notably, response differences and shifts in composition became especially apparent during cool phases and were not necessarily larger at more extreme heatwave temperatures. Our study shows that temperature increases can cause positive or negative effects on productivity, depending on whether exposure takes place uniformly or oscillates as a heatwave and includes cool phases. Therefore, our knowledge on responses under stable warming cannot simply be transferred to anticipate effects of heatwave scenarios, which consist of warming and cooling. Better predictions on heatwave responses require improved mechanistic understanding and will depend on the properties of temperature fluctuation itself (intensity and reoccurrence, as well as duration of the temperature exposure). The cool phase after a heatwave appears to have a decisive impact, which is at least as big as the effect of the warm phase, and should receive more scientific attention in the future.

MATERIALS AND METHODS

Initial sampling and culturing conditions

Initial phytoplankton assemblages were sampled in April 2021 from the Kongsfjord, Svalbard, Norway (mid-fjord station KB3, 78°55′N, 11°56′E), in a pre–spring bloom setting. Seawater temperature was −0.1°C, Chl a concentration was 0.15 µg liter^{-1}, while nitrate, phosphate, and silicate concentrations were 10.5, 0.7, and 5.0 µM, respectively. Seawater was pumped up from a depth of 19 m using a monsoon pump (Mega-Thyphoon, Proactive Environmental Products; flow rate, approximately 4 liters min^{-1}) and directly filled into 4-liter polycarbonate incubation bottles (Nalgene) after passing through a 100-µm nylon mesh to remove large grazers from the community. To ensure homogenous filling while drifting with the boat, all culture bottles were filled halfway first before starting to fill them completely. From the same location, depth, and day, 300 liters of seawater was pumped up, prefiltered (0.2 µm), and stored in the dark and cold (2°C) for dilutions throughout the experiment.

The incubation bottles were then directly transferred to a temperature-controlled room at the Kings Bay AS Marine Laboratory, Svalbard, where they were exposed to constant 24-hour daylight of 31 ± 0.8 photons m^{-2} s^{-1} using a full-spectrum white Mobile LED Illumination System (CLF PlantClimatics GmbH). Light conditions were chosen in accordance with average in situ conditions at that time of the year (last sunset in mid-April) at a depth of 10 to 20 m (according to own measurements on site). For additional temperature control, bottles were placed inside five Plexiglas aquaria, in which water temperatures were adjusted using immersion thermostats (JULABO GmbH) and monitored throughout the experiment using a temperature logger (Almemo 2890, Ahlborn). The incubation bottles were continuously sparged (approximate flow rate of 100 ml/min) with ambient air delivered through sterile 0.2-µm air filters to keep cells in suspension and carbonate chemistry stable.

To ensure exponential growth of the phytoplankton communities throughout the experiment and to avoid nutrient limitation owing to high cell densities, cultures were diluted to ~2 µg Chl a liter^{-1} (mean 1.8 ± 0.04 µg liter^{-1}) after each sampling time point, i.e., at three to four time points throughout the experiment (Fig. 1, t1 to t4, and fig. SI12). After each dilution, nutrients were added to reach values slightly above natural concentrations (averages: 17 µM NO$_3$, 3 µM PO$_4$, and 15 µM SiO$_2$). At the initial time point, NO$_3$ was accidentally added in excess in all treatments, reaching 65 to 85 µM. Throughout

the experiment, nutrients were sampled approximately every 2 days, directly measured using a QuAAtro39 analyzer (Seal Analytical Limited) on site, and refilled when running low. Toward the end of the experiment, there were a few time points when nutrients reached potentially limiting conditions (<8 µM NO$_3$) in the fasted growing treatments (e.g., t3 in stable 9°C and t4 in HW9°C), periods that were yet always short in time, at the very end of the experiment (for more details, see fig. S13) and not in all biological replicates, which showed nevertheless very similar responses. We therefore do not see evidence for nutrient conditions affecting the communities in a crucial way.

Experimental design and time frames

Directly after the initial sampling, all 15 culture bottles were incubated in the laboratory at 1.5°C for an initial adjustment phase for 2.5 days (Fig. 1), after which they were transferred in random triplicates to one of the five different temperature treatments: stable 2°C, acting as a control treatment (1.96° ± 0.3°C), stable 6°C (5.8° ± 0.2°C), stable 9°C (8.81° ± 0.1°C), and two heatwave treatments, each with two consecutive 5-day heatwaves, with a 3.5-day cool phase in between (2.0° ± 0.2°C; Fig. 1). In treatment HW6°C, both heatwaves were set to 6°C (5.94° ± 0.03°C), and in treatment HW9°C, heatwaves were set to 9°C (8.87° ± 0.3°C). For the initial 5 days at 2°C (up to dilution time point 1), there were only three heatwave replicates, which were then split up after the first dilution into six bottles for HW6°C and HW9°C. All temperature transitions were reached by a 1°C per hour temperature ramp by either increased heating of the thermostats or addition of ice to the aquaria under continuous mixing.

Throughout the course of the experiment, the incubation bottles accumulated biofilms on their inside surfaces (benthic diatoms, dominated by *Navicula* sp.). The extent of biofilm formation was approximately congruent with the growth rates in the different treatments, with stable 9°C and HW9°C having the strongest biofilm, followed by stable 6°C, and HW6°C and the 2°C control treatment with the weakest biofilm. Because the cultures were diluted regularly, and the surface growth was strongest on the bottom side of the bottles, the biofilms never reached an extent interfering with the experimental conditions (e.g., light reduction). At the last dilution time point for each treatment (day 16 for 6° and 9°C and day 20 for the others), we gently removed those biofilms with a magnetic stirrer from the bottle surfaces, followed by rinsing the bottle with hot water, distilled water, and cooled growth medium before aliquots of the treatment were lastly reinoculated into temperature-adjusted medium again. Despite our efforts, all cultures showed strongly decreased performance after this procedure (see fig. S10), which is why we decided to remove subsequent data from our analysis, leaving a total duration of 16 days for 6° and 9°C (t3) and 20 days (t4) for the other treatments. The final time point for the heatwave treatments was thus the end of the second heatwave, not comprising the final cooling phase. Next to monitoring of nutrients and Chl a content every other day, sampling for a range of parameters took place just before each dilution of the culture bottles by gentle filtration (<200 mbar) of water samples in a 5°C room at low light or by conducting dedicated assays (see below).

Growth and elemental composition

Specific growth rates µ (day^{-1}) between sampling/dilution time points were calculated on the basis of measured Chl a and particulate

organic carbon (POC) concentrations at the dilution time points (t1 to t4; Fig. 1). We applied an exponential growth function to the respective values with $\mu = \ln(Nt) - \ln(N0)/\Delta t$, where Nt is the value at the time of sampling (e.g., t4), $N0$ is the value after the last dilution (e.g., t3), and Δt is the time passed in days between those time points. $N0$ was calculated from the measured value just before dilution (e.g., t2), and the exact volume the bottle was diluted by in milliliters.

For determination of total Chl *a*, 100 to 200 ml of water sample were filtered gently (<200 mbar) and under cold conditions onto precombusted (15 hours, 500°C) glass-fiber filters (GF/F, Whatman, United Kingdom). Chl *a* samples were immersed in cold 90% acetone and shredded with glass beads (0.5 to 1 mm in diameter) in a homogenizer (Precellys Evolution, Bertin Technologies, France), before being extracted overnight at −20°C. Chl *a* concentrations were measured fluorometrically (Trilogy, Turner Designs, United States), including an acidification step (1 M HCl) to determine phaeopigments (62).

Samples for POC and particulate organic nitrogen were taken in the same way as those for Chl *a*. Filters were directly frozen at −20°C and later acidified and dried overnight at 60°C before elemental analysis was performed using a gas chromatograph CHNS-O elemental analyzer (Euro EA 3-,000, HEKAtech). All raw values were corrected by the mean of blank filters ($n = 6$) handled alongside the sampling process.

Species and population composition
Species composition was assessed by 18S rRNA metabarcoding. In the same filtration setup as described above, 400 to 500 ml of samples was filtered on 0.8-µm PC filters (Nucleopore, Whatman, United Kingdom), and immersed in 650 µl of preheated extraction buffer [SL1 of the NucleoSpin Soil extraction kit (see below) at 50°C] to be stored at −20°C until further analysis. After thawing and cell disruption with a MagNa Lyser (Roche Diagnostics, Switzerland), DNA extraction was performed according to the manufacturer's protocol using the NucleoSpin Soil extraction kit (Macherey-Nagel GmbH, Germany). Amplicon libraries of the V4 region (18S rRNA gene) were generated using the standard 16S Metagenomic Sequencing Library Preparation protocol (16S Metagenomic Sequencing Library Preparation, part no. 15044223 Rev. B. Illumina, United States) using the forward primer CCAGCASCYGCGGTAATTCC and reverse primer ACTTTCGTTCTTGAT (63). Single samples were indexed using the Nextera XT Index Kit v2 primers (Illumina, United States) and pooled for sequencing on a MiSeq sequencer (Illumina, United States). Results were demultiplexed, and FASTQ sequence files were generated using the Generate FASTQ workflow of the MiSeq sequencer software, yielding a total of ~10 × 10^6 raw amplicons. Primers were removed with cutadapt v2.8 (64), and further processing of the sequence data was performed using the DADA2 R package v1.18 (65). Reads were trimmed [forward reads after 240 to 260 base pairs (bp) and reverse reads after 200 to 210 bp] and denoised before paired-end reads were merged (minimum overlap 50 bp and no mismatches), and predicted chimeras were removed, yielding a total of ~6.8 × 10^6 filtered amplicons (table S4). Taxonomic assignment of the resulting ASVs was performed using the reference databases PR2 (v4.12.0). For downstream analyses in the software R (version 4.3), nonphototrophic taxa were removed, as well as ASVs with a count of less than 10 reads in replicate sample means. Sequencing depth was checked using rarefaction curves, and raw data were normalized using a scaling with ranked subsampling procedure (srs) for further analysis.

Intraspecific population composition of the diatom *T. hyalina* was assessed via MPB, following the protocol as described by Wolf *et al.* (47). The sample (500 to 700 ml) was filtered on 10-µm PC filters (Nucleopore, Whatman, United Kingdom) and immersed in 650 µl of warm extraction buffer to be stored at −20°C until further analysis. DNA was extracted and applied in triplicate in a first-stage amplicon polymerase chain reaction (PCR) with the microsatellite primers ThKF3 and ThKF7. PCR products were visualized on an agarose gel, and bands at the approximate size of the microsatellite sequences were manually excised and purified (PCR Clean-up Kit, Macherey-Nagel, Germany). Single samples were indexed using the Nextera XT Index Kit v2 primers (Illumina, United States) and pooled for sequencing on a MiSeq sequencer (Illumina, United States). Demultiplexing and FASTQ sequence generation were performed using MiSeq Reporter software, yielding a total of 7 × 10^6 raw amplicons for ThKF3 and 10 × 10^6 for ThKF7. Amplicon contingency tables were constructed for each primer set using an in-house modified metabarcoding analysis pipeline, including cropping, trimming, merging, and truncating amplicons, as well as several feature filters for quality control (filtered amplicons ThKF3: 2.4 × 10^6 and ThKF7: 3 × 10^6). Resulting amplicon contingency tables were then further filtered for correct microsatellite sequences and minimum abundance, and amplicon numbers were standardized. The analysis of the processed data was performed using principal components analyses (PCAs) of all analyzed samples, as well as sample distance matrices.

Physiological assays
Photophysiological parameters were measured via variable Chl *a* fluorescence of photosystem II (66) using a fast repetition rate fluorometer (FRRf, FastOcean PTX; Chelsea Technologies, United Kingdom) in combination with a FastAct Laboratory system (Chelsea Technologies). Temperatures inside the measurement chamber were adjusted by continuously pumping water of the respective aquarium into the FastAct chamber around the cuvette. Samples were dark-acclimated for >15 min before each measurement. Because it was not possible to run full photosynthesis-irradiance (PI) curves for all replicates on a single day, we measured samples of each bottle in a reduced PI protocol, collecting repeated measurements after 10 min of exposure to no light, experimental light (~30 µmol m^{-2} s^{-1}), and oversaturating light levels (~600 µmol m^{-2} s^{-1}) to inflict a light stress response. This allowed us to retrieve a basic set of parameters for all replicates, including Fv/Fm, connectivity of photosystems, and reoxidation time at PSII (tau) from dark-acclimated samples as well as isETR at experimental light levels (67, 68). In addition, we recorded immediate photophysiological responses in the HW9°C treatment during the phases of warming and cooling of both heatwaves. When temperatures were increased/decreased at 1°C hour^{-1}, at each step, a fresh sample was dark-acclimated and measured ~15 min after the temperature change with the reduced PI protocol as above. This yielded four "temperature ramps" from 2° to 9°C and the reverse.

NPP was measured in duplicate by 24-hour incubation with a NaH^{14}CO$_3$ spike (53.1 mCi mmol^{-1} or 2.109 megabecquerel mol^{-1} stock; PerkinElmer) under the respective treatment conditions. We used the same protocol as in Hoppe *et al.* (46). In short, 20-ml aliquots were incubated after addition of 10 µCi NaH^{14}CO$_3$ (specific

activity of 0.5 μCi ml^{-1}). Total amounts of added NaH^{14}CO$_3$ (DPM$_{100\%}$) and blank values (DPM$_{0\%}$) were determined through 0.5-ml aliquots that were immediately added to 1 M NaOH and 6 M HCl, respectively. DPM$_{100\%}$ samples were measured after 2 hours, and DPM$_{0\%}$ samples were handled alongside the experimental samples. After 24 hours, incubated samples were filtered onto GF/F filters, acidified with 0.5 ml of 1 M HCl, and left to degas overnight. Ten milliliters of scintillation cocktail were added (Ultima Gold AB, PerkinElmer), and samples were vortexed and left to stand in the dark for approximately 12 hours before counting on the liquid scintillation counter (DPM$_{sample}$) using an automatic quench correction and a counting time of 5 min. NPP [μg C (μg Chl a)$^{-1}$ day^{-1}] was calculated as $NPP = ([DIC] \times (DPM_{sample} - DPM_{0\%}) \times 1.05)/(DPM_{100\%} \times t \times [Chl\ a])$, where $[DIC]$ and $[Chl\ a]$ denote the concentrations of dissolved inorganic carbon and Chl a in the sample, respectively. DPM$_{sample}$ denotes the disintegrations per minute (DPM) in the samples, DPM$_{0\%}$ and DPM$_{100\%}$ are the DPM of the blank and total amount of NaH^{14}CO$_3$, and t is the duration of the incubation. The value of 1.05 was used to correct for fractionation against ^{14}C relative to ^{12}C (69). Since, in all treatments, the Chl a:POC ratio increased during the first 10 days of the experiment (fig. S1A), likely due to acclimation to the stable but low light intensities in the experimental setup, we normalized NPP to POC instead of Chl a. Chl a–specific rates were converted to C-specific rates by using the measured Chl a:POC ratio for each replicate bottle at the respective time point.

Measurements of O$_2$ evolution were performed in discrete assays in 20-ml gas-tight glass vials equipped with oxygen and temperature sensor spots, in combination with a Firesting-PRO station (PyroScience, Germany). Two samples of each biological replicate were incubated headspace-free for 24 hours under experimental conditions inside the water tanks (alongside the respective ^{14}C-based assay vials), one in the light and one in darkness. The O$_2$ concentrations in each vial were measured at a start and end time point for >10 min until the signal was stable while gently mixing the sample using a small magnetic stirrer. One additional replicate per measurement day was incubated under constant O$_2$ logging as a technical control. All sensors were two-point calibrated at 0 and 100% atmospheric O$_2$ for each temperature. O$_2$ calibrations (0%) and temperature calibrations were performed before the start of the experiment by adding sodium sulfate to distilled water until saturation. Calibrations (100%) were performed once before and once during the experiment (t3) for each temperature in seawater. Temperature-corrected O$_2$ values were read out at a mean of 2 min after the measurement stabilized at the beginning and endpoint. The difference of these two values were then divided by the exact incubation time to derive rates of net O$_2$ evolution per hour, which was then normalized to the initial Chl a concentration of the sample. GPP was calculated by adding the rate of respiration measured in the dark to the net O$_2$ evolution measured in light. Outlier values were identified using Dixon's test ($P < 0.1$) and excluded from further analysis (5 of 94 measurements). Measurements at time point 1 were discarded for all treatments because biomass was too low to produce meaningful signals. Because of the variability in Chl a:POC ratios throughout the experiment, we transformed all productivity measurements to rates per POC rather than Chl a using the ratio of the closest time point where both parameters were measured.

Because assays were time-consuming and some instrumentation hardware was limited (O$_2$ optode setups and FRRf), some of the assays had to be performed a day before or after the dilution time points (t1 for 6° and 9°C: 1 day before and t2 to t4 2°C: 1 day after). In those cases, all assay measurements were started on the same day, alongside which additional Chl a samples were analyzed, and Chl a:POC ratios of the respective time point were applied for biomass normalization.

Statistical analysis

Since heatwave and stable warm treatments were running for different time frames (16 and 20 days), only their trends and not their absolute values can be directly compared. Therefore, they are depicted in separate graphs along with the 2°C control treatment after the respective time. To assess treatment effects across the entire experiment, we estimated the cumulative responses as weighted means of all time points for all parameters, thus integrating the overall effect throughout the experiment rather than only taking the final measurements into account. We did this by calculating a weighted mean of all time points according to the number of days passed between them. For statistical testing, we used linear mixed-effect models (lme4 R package version 1.1.3) on data from all time points, with treatment as fixed effect and time and replicate as random effects. A null model was run on the same data without treatment as fixed effect. The treatment was reported as having a significant effect if the comparison of the two models (ANOVA) yielded a significant result, and χ^2, degrees of freedom, and P value were reported. Post hoc tests were performed using pairwise comparisons of estimated marginal means (emmeans package, version 1.8.7), and Bonferroni correction was applied to control for multiple testing. Model assumptions of linearity and homoscedasticity were verified for each dataset. To meet these assumptions, respiration rate data and growth rates of the heatwave treatments were log-transformed before analysis.

For the time-resolved data, we used one-way ANOVAs to identify differences between treatments at specific time points in question or between time points within a treatment (e.g., in response to temperature change). For a further analysis of the separate treatments, we used Tukey's post hoc tests. Furthermore, we used linear models (lm) for regression analysis over several time points. Also here, model assumptions of linearity and homoscedasticity were verified in each case.

To analyze species composition data, srs-normalized asv data were used for composition plots showing the top five genera (fig. S2) and to calculate species richness and Shannon index as measures of alpha-diversity (fig. S3). Note that community composition was based purely on 18S rRNA gene metabarcoding, which is not a strictly quantitative measure and can be subject to quantitative distortions. Since all treatments contained largely the same genera at the respective time points, however, results contain meaningful information on relative abundance dynamics. Following Gloor et al. (70), beta-diversity was estimated through pairwise dissimilarity matrices using Aitchison distances, i.e., the Euclidean distance of centered log-ratio–transformed raw data and was visualized through PCA. Treatment differences were tested by PERMANOVA analysis.

To assess the effects of different treatments in a bloom setting, responses were also compared as upscaled biomass buildup of the initial community (fig. S8). This theoretical biomass buildup was calculated on the basis of the POC content of the phytoplankton community at t0 and then modeled for each replicate using an exponential growth function and the respective growth rate over the days of incubation from one time point to the next. This result was then

SCIENCE ADVANCES | RESEARCH ARTICLE

used as the base for the next time point and, therefore, yielded exponential accumulation until the end of the experiment.

Supplementary Materials
This PDF file includes:
Figs. S1 to S13
Tables S1 to S4
References

REFERENCES AND NOTES
1. E. C. J. Oliver, M. T. Burrows, M. G. Donat, A. Sen Gupta, L. V. Alexander, S. E. Perkins-Kirkpatrick, J. A. Benthuysen, A. J. Hobday, N. J. Holbrook, P. J. Moore, M. S. Thomsen, T. Wernberg, D. A. Smale, Projected marine heatwaves in the 21st century and the potential for ecological impact. *Front. Mar. Sci.* **6**, 364 (2019).
2. S. Cooley, D. Schoeman, L. Bopp, P. Boyd, S. Donner, D.Y. Ghebrehiwet, S.-I. Ito, W. Kiessling, P. Martinetto, E. Ojea, M.-F. Racault, B. Rost, and M. Skern-Mauritzen, 2022: Oceans and Coastal Ecosystems and Their Services. In: Climate Change 2022: Impacts, Adaptation and Vulnerability. Contribution of Working Group II to the Sixth Assessment Report of the Intergovernmental Panel on Climate Change [H.-O. Pörtner, D.C. Roberts, M. Tignor, E.S. Poloczanska, K. Mintenbeck, A. Alegría, M. Craig, S. Langsdorf, S. Löschke, V. Möller, A. Okem, B. Rama (eds.)]. Cambridge University Press, Cambridge, UK and New York, NY, USA, pp. 379–550, doi:10.1017/9781009325844.005.
3. L. A. Arteaga, C. S. Rousseaux, Impact of Pacific Ocean heatwaves on phytoplankton community composition. *Commun. Biol.* **6**, 263 (2023).
4. B. Huang, Z. Wang, X. Yin, A. Arguez, G. Graham, C. Liu, T. Smith, H. M. Zhang, Prolonged marine heatwaves in the Arctic: 1982–2020. *Geophys. Res. Lett.* **48**, e2021GL095590 (2021).
5. T. L. Frölicher, E. M. Fischer, N. Gruber, Marine heatwaves under global warming. *Nature* **560**, 360–364 (2018).
6. A. Barkhordarian, D. M. Nielsen, D. Olonscheck, J. Baehr, Arctic marine heatwaves forced by greenhouse gases and triggered by abrupt sea-ice melt. *Commun. Earth Environ.* **5**, 57 (2024).
7. T. L. Frölicher, C. Laufkötter, Emerging risks from marine heat waves. *Nat. Commun.* **9**, 650 (2018).
8. A. J. Constable, S. Harper, J. Dawson, K. Holsman, T. Mustonen, D. Piepenburg, and B. Rost, 2022: Cross-Chapter Paper 6: Polar Regions. In: Climate Change 2022: Impacts, Adaptation and Vulnerability. Contribution of Working Group II to the Sixth Assessment Report of the Intergovernmental Panel on Climate Change [H.-O. Pörtner, D.C. Roberts, M. Tignor, E.S. Poloczanska, K. Mintenbeck, A. Alegría, M. Craig, S. Langsdorf, S. Löschke, V. Möller, A. Okem, B. Rama (eds.)]. Cambridge University Press, Cambridge, UK and New York, NY, USA, pp. 2319–2368, doi:10.1017/9781009325844.023.
9. M. P. Latorre, C. M. Iachetti, I. R. Schloss, J. Antoni, A. Malits, F. de la Rosa, M. De Troch, M. D. Garcia, X. Flores-Melo, S. I. Romero, M. N. Gil, M. Hernando, Summer heatwaves affect coastal Antarctic plankton metabolism and community structure. *J. Exp. Mar. Biol. Ecol.* **567**, 151926 (2023).
10. L. M. Cavole, A. M. Demko, R. E. Diner, A. Giddings, I. Koester, C. M. L. S. Pagniello, M.-L. Paulsen, A. Ramirez-Valdez, S. M. Schwenck, N. K. Yen, M. E. Zill, P. J. S. Franks, Biological impacts of the 2013–2015 warm-water anomaly in the Northeast Pacific: Winners, losers, and the future. *Oceanography* **29**, 273–285 (2016).
11. J. E. Walsh, R. L. Thoman, U. S. Bhatt, P. A. Bieniek, B. Brettschneider, M. Brubaker, S. Danielson, R. Lader, F. Fetterer, K. Holderied, The high latitude marine heat wave of 2016 and its impacts on Alaska. *Bull. Am. Meteorol. Soc.* **99**, S39–S43 (2018).
12. K. E. Mills, A. J. Pershing, C. J. Brown, Y. Chen, F.-S. Chiang, D. S. Holland, S. Lehuta, J. A. Nye, J. C. Sun, A. C. Thomas, R. A. Wahle, Fisheries management in a changing climate: Lessons from the 2012 ocean heat wave in the Northwest Atlantic. *Oceanography* **26**, 191–195 (2013).
13. R. M. McCabe, B. M. Hickey, R. M. Kudela, K. A. Lefebvre, N. G. Adams, B. D. Bill, F. M. D. Gulland, R. E. Thomson, W. P. Cochlan, V. L. Trainer, An unprecedented coastwide toxic algal bloom linked to anomalous ocean conditions. *Geophys. Res. Lett.* **43**, 10366–10376 (2016).
14. D. M. Anderson, E. Fachon, R. S. Pickart, P. Lin, A. D. Fischer, M. L. Richlen, V. Uva, M. L. Brosnahan, L. McRaven, F. Bahr, K. Lefebvre, J. M. Grebmeier, S. L. Danielson, Y. Lyu, Y. Fukai, Evidence for massive and recurrent toxic blooms of Alexandrium catenella in the Alaskan Arctic. *Proc. Natl. Acad. Sci. U.S.A.* **118**, e2107387118 (2021).
15. D. A. Smale, T. Wernberg, E. C. J. Oliver, M. Thomsen, B. P. Harvey, S. C. Straub, M. T. Burrows, L. V. Alexander, J. A. Benthuysen, M. G. Donat, M. Feng, A. J. Hobday, N. J. Holbrook, S. E. Perkins-Kirkpatrick, H. A. Scannell, A. Sen Gupta, B. L. Payne, P. J. Moore, Marine heatwaves threaten global biodiversity and the provision of ecosystem services. *Nat. Clim. Change* **9**, 306–312 (2019).
16. J. E. Bissinger, D. J. Montagnes, J. Sharples, D. Atkinson, Predicting marine phytoplankton maximum growth rates from temperature: Improving on the Eppley curve using quantile regression. *Limnol. Oceanogr.* **53**, 487–493 (2008).
17. R. W. Eppley, Temperature and phytoplankton growth in the sea. *Fish. Bull.* **70**, 1063–1085 (1972).
18. M. J. Angilletta, Thermal adaptation: A theoretical and empirical synthesis (Oxford Univ. Press, 2009).
19. M. J. Cabrerizo, E. Marañón, Temperature fluctuations in a warmer environment: Impacts on microbial plankton. *Fac. Rev.* **10**, 9 (2021).
20. X. Wang, F. Fu, P. Qu, J. D. Kling, H. Jiang, Y. Gao, D. A. Hutchins, How will the key marine calcifier Emiliania huxleyi respond to a warmer and more thermally variable ocean? *Biogeosciences* **16**, 4393–4409 (2019).
21. J. R. Bernhardt, J. M. Sunday, P. L. Thompson, M. I. O'Connor, Nonlinear averaging of thermal experience predicts population growth rates in a thermally variable environment. *Proc. Natl. Acad. Sci. U.S.A.* **285**, 20181076 (2018).
22. P. Qu, F. X. Fu, J. D. Kling, M. Huh, X. Wang, D. A. Hutchins, Distinct responses of the nitrogen-fixing marine cyanobacterium Trichodesmium to a thermally variable environment as a function of phosphorus availability. *Front. Microbiol.* **10**, 1282 (2019).
23. C. E. Schaum, A. Buckling, N. Smirnoff, D. J. Studholme, G. Yvon-Durocher, Environmental fluctuations accelerate molecular evolution of thermal tolerance in a marine diatom. *Nat. Commun.* **9**, 1719 (2018).
24. P. Siegel, K. G. Baker, R. Low-Décarie, R. J. Geider, Phytoplankton competition and resilience under fluctuating temperature. *Ecol. Evol.* **13**, e9851 (2023).
25. H. Hayashida, R. J. Matear, P. G. Strutton, Background nutrient concentration determines phytoplankton bloom response to marine heatwaves. *Glob. Chang. Biol.* **26**, 4800–4811 (2020).
26. K. M. Noh, H.-G. Lim, J.-S. Kug, Global chlorophyll responses to marine heatwaves in satellite ocean color. *Environ. Res. Lett.* **17**, 064034 (2022).
27. A. Sen Gupta, M. Thomsen, J. A. Benthuysen, A. J. Hobday, E. Oliver, L. V. Alexander, M. T. Burrows, M. G. Donat, M. Feng, N. J. Holbrook, S. Perkins-Kirkpatrick, P. J. Moore, R. R. Rodrigues, H. A. Scannell, A. S. Taschetto, C. C. Ummenhofer, T. Wernberg, D. A. Smale, Drivers and impacts of the most extreme marine heatwave events. *Sci. Rep.* **10**, 19359 (2020).
28. W. K. Zhan, Y. Zhang, Q. Y. He, H. G. Zhan, Shifting responses of phytoplankton to atmospheric and oceanic forcing in a prolonged marine heatwave. *Limnol. Oceanogr.* **68**, 1821–1834 (2023).
29. S. Montie, M. S. Thomsen, W. Rack, P. A. Broady, Extreme summer marine heatwaves increase chlorophyllain in the Southern Ocean. *Antarct. Sci.* **32**, 508–509 (2020).
30. E. Feijão, C. Gameiro, M. Franzitta, B. Duarte, I. Caçador, M. T. Cabrita, A. R. Matos, Heat wave impacts on the model diatom Phaeodactylum tricornutum: Searching for photochemical and fatty acid biomarkers of thermal stress. *Ecol. Indicators* **95**, 1026–1037 (2018).
31. T. Samuels, T. A. Rynearson, S. Collins, Surviving heatwaves: Thermal experience predicts life and death in a Southern Ocean diatom. *Front. Mar. Sci.* **8**, 343 (2021).
32. T. Soulié, F. Vidussi, S. Mas, B. Mostajir, Functional stability of a coastal Mediterranean plankton community during an experimental marine heatwave. *Front. Mar. Sci.* **9**, 831496 (2022).
33. N. Filiz, U. Işkın, M. Beklioğlu, B. Öğlü, Y. Cao, T. A. Davidson, M. Søndergaard, T. L. Lauridsen, E. Jeppesen, Phytoplankton community response to nutrients, temperatures, and a heat wave in shallow lakes: An experimental approach. *Water* **12**, 3394 (2020).
34. J. D. Kling, M. D. Lee, F. Fu, M. D. Phan, X. Wang, P. Qu, D. A. Hutchins, Transient exposure to novel high temperatures reshapes coastal phytoplankton communities. *ISME J.* **14**, 413–424 (2020).
35. M. Remy, H. Hillebrand, S. Flöder, Stability of marine phytoplankton communities facing stress related to global change: Interactive effects of heat waves and turbidity. *J. Exp. Mar. Biol. Ecol.* **497**, 219–229 (2017).
36. C. T. Kremer, M. K. Thomas, E. Litchman, Temperature- and size-scaling of phytoplankton population growth rates: Reconciling the Eppley curve and the metabolic theory of ecology. *Limnol. Oceanogr.* **62**, 1658–1670 (2017).
37. I. W. Bishop, S. I. Anderson, S. Collins, T. A. Rynearson, Thermal trait variation may buffer Southern Ocean phytoplankton from anthropogenic warming. *Glob. Chang. Biol.* **28**, 5755–5767 (2022).
38. M. K. Thomas, C. T. Kremer, C. A. Klausmeier, E. Litchman, A global pattern of thermal adaptation in marine phytoplankton. *Science* **338**, 1085–1088 (2012).
39. A. Coello-Camba, S. Agustí, Thermal thresholds of phytoplankton growth in polar waters and their consequences for a warming polar ocean. *Front. Mar. Sci.* **4**, 168 (2017).
40. S. Barton, J. Jenkins, A. Buckling, C.-E. Schaum, N. Smirnoff, J. A. Raven, G. Yvon-Durocher, Evolutionary temperature compensation of carbon fixation in marine phytoplankton. *Ecol. Lett.* **23**, 722–733 (2020).
41. D. Bozzato, T. Jakob, C. Wilhelm, Effects of temperature and salinity on respiratory losses and the ratio of photosynthesis to respiration in representative Antarctic phytoplankton species. *PLOS ONE* **14**, e0224101 (2019).

SCIENCE ADVANCES | RESEARCH ARTICLE

42. K. G. Baker, C. M. Robinson, D. T. Radford, A. S. McInnes, C. Evenhuis, M. A. Doblin, Thermal performance curves of functional traits aid understanding of thermally induced changes in diatom-mediated biogeochemical fluxes. *Front. Mar. Sci.* **3**, 44 (2016).

43. L. Rehder, B. Rost, S. D. Rokitta, Abrupt and acclimation responses to changing temperature elicit divergent physiological effects in the diatom Phaeodactylum tricornutum. *New Phytol.* **239**, 1005–1013 (2023).

44. P. A. Thompson, M.-X. Guo, P. J. Harrison, Effects of variation in temperature. I. On the biochemical composition of eight species of marine phytoplankton. *J. Phycol.* **28**, 481–488 (1992).

45. S. Collins, A. Gardner, Integrating physiological, ecological and evolutionary change: A Price equation approach. *Ecol. Lett.* **12**, 744–757 (2009).

46. C. J. M. Hoppe, N. Schuback, D. Semeniuk, K. Giesbrecht, J. Mol, H. Thomas, M. T. Maldonado, B. Rost, D. E. Varela, P. D. Tortell, Resistance of Arctic phytoplankton to ocean acidification and enhanced irradiance. *Polar Biol.* **41**, 399–413 (2018).

47. K. K. E. Wolf, C. J. M. Hoppe, F. Leese, M. Weiss, B. Rost, S. Neuhaus, T. Gross, N. Kühne, U. John, Revealing environmentally driven population dynamics of an Arctic diatom using a novel microsatellite PoolSeq barcoding approach. *Environ. Microbiol.* **23**, 3809–3824 (2021).

48. K. K. E. Wolf, E. Romanelli, B. Rost, U. John, S. Collins, H. Weigand, C. J. Hoppe, Company matters: The presence of other genotypes alters traits and intraspecific selection in an Arctic diatom under climate change. *Glob. Chang. Biol.* **25**, 2869–2884 (2019).

49. L. I. Seifert, G. Weithoff, M. Vos, Extreme heat changes post-heat wave community reassembly. *Ecol. Evol.* **5**, 2140–2148 (2015).

50. I. E. Huertas, M. Rouco, V. López-Rodas, E. Costas, Warming will affect phytoplankton differently: Evidence through a mechanistic approach. *Proc. R. Soc. B: Biol. Sci.* **278**, 3534–3543 (2011).

51. P. G. Falkowski, J. A. Raven, *Aquatic photosynthesis.* (Princeton University Press, 2013).

52. M. J. Behrenfeld, K. H. Halsey, A. J. Milligan, Evolved physiological responses of phytoplankton to their integrated growth environment. *Philosoph. Trans. R. Soc. B: Biol. Sci.* **363**, 2687–2703 (2008).

53. M. Seifert, C. Nissen, B. Rost, M. Vogt, C. Volker, J. Hauck, Interaction matters: Bottom-up driver interdependencies alter the projected response of phytoplankton communities to climate change. *Glob. Chang. Biol.* **29**, 4234–4258 (2023).

54. C. A. E. McKinstry, R. W. Campbell, K. Holderied, Influence of the 2014–2016 marine heatwave on seasonal zooplankton community structure and abundance in the lower Cook Inlet, Alaska. *Deep-Sea Res. II Top. Stud. Oceanogr.* **195**, 105012 (2022).

55. S. D. Batten, C. Ostle, P. Hélaouët, A. W. Walne, Responses of Gulf of Alaska plankton communities to a marine heat wave. *Deep-Sea Res. II Top. Stud. Oceanogr.* **195**, 105002 (2022).

56. U. Işkın, N. Filiz, Y. Cao, É. M. Neif, B. Öğlü, T. L. Lauridsen, T. A. Davidson, M. Søndergaard, Ü. N. Tavşanoğlu, M. Beklioğlu, Impact of nutrients, temperatures, and a heat wave on zooplankton community structure: An experimental approach. *Water* **12**, 3416 (2020).

57. H. Ullah, I. Nagelkerken, S. U. Goldenberg, D. A. Fordham, Climate change could drive marine food web collapse through altered trophic flows and cyanobacterial proliferation. *PLoS Biol.* **16**, e2003446 (2018).

58. F.-X. Fu, B. Tschitschko, D. A. Hutchins, M. E. Larsson, K. G. Baker, A. McInnes, T. Kahlke, A. Verma, S. A. Murray, M. A. Doblin, Temperature variability interacts with mean temperature to influence the predictability of microbial phenotypes. *Glob. Chang. Biol.* **28**, 5741–5754 (2022).

59. S. G. Leles, N. M. Levine, Mechanistic constraints on the trade-off between photosynthesis and respiration in response to warming. *Sci. Adv.* **9**, eadh8043 (2023).

60. M. K. Thomas, M. Aranguren-Gassis, C. T. Kremer, M. R. Gould, K. Anderson, C. A. Klausmeier, E. Litchman, Temperature–nutrient interactions exacerbate sensitivity to warming in phytoplankton. *Glob. Chang. Biol.* **23**, 3269–3280 (2017).

61. E. Bestion, C.-E. Schaum, G. Yvon-Durocher, Nutrient limitation constrains thermal tolerance in freshwater phytoplankton. *Limnol. Oceanogr. Lett.* **3**, 436–443 (2018).

62. A. Knap, A. Michaels, A. Close, D. H. A. E. Dickson, Protocols for the Joint Global Ocean Flux Study (JGOFS) Core Measurements, *JGOFS Report Nr. 19* (UNESCO, 1996).

63. I. M. Bradley, A. J. Pinto, J. S. Guest, Design and evaluation of Illumina MiSeq-compatible, 18S rRNA gene-specific primers for improved characterization of mixed phototrophic communities. *Appl. Environ. Microbiol.* **82**, 5878–5891 (2016).

64. M. Martin, Cutadapt removes adapter sequences from high-throughput sequencing reads. *EMBnet. J.* **17**, 10–12 (2011).

65. B. J. Callahan, P. J. McMurdie, M. J. Rosen, A. W. Han, A. J. A. Johnson, S. P. Holmes, DADA2: High-resolution sample inference from Illumina amplicon data. *Nat. Methods* **13**, 581–583 (2016).

66. N. Schuback, P. D. Tortell, I. Berman-Frank, D. A. Campbell, A. Ciotti, E. Courtecuisse, Z. K. Erickson, T. Fujiki, K. Halsey, A. E. Hickman, Y. Huot, M. Y. Gorbunov, D. J. Hughes, Z. S. Kolber, C. M. Moore, K. Oxborough, O. Prášil, C. M. Robinson, T. J. Ryan-Keogh, G. Silsbe, S. Simis, D. J. Suggett, S. Thomalla, D. R. Varkey, Single-turnover variable chlorophyll fluorescence as a tool for assessing phytoplankton photosynthesis and primary productivity: Opportunities, caveats and recommendations. *Front. Mar. Sci.* **8**, 690607 (2021).

67. Z. S. Kolber, O. Prasil, P. G. Falkowski, Measurements of variable chlorophyll fluorescence using fast repetition rate techniques: Defining methodology and experimental protocols. *Biochem. Biophys. Acta* **1367**, 88–106 (1998).

68. K. Oxborough, C. M. Moore, D. J. Suggett, T. Lawson, H. G. Chan, R. J. Geider, Direct estimation of functional PSII reaction center concentration and PSII electron flux on a volume basis: A new approach to the analysis of Fast Repetition Rate fluorometry (FRRf) data. *Limnol. Oceanogr. Methods* **10**, 142–154 (2012).

69. E. S. Nielsen, The use of radio-active carbon (C14) for measuring organic production in the sea. *J. du Conseil Int. pour l'Explor. de la Mer* **18**, 117–140 (1952).

70. G. B. Gloor, J. M. Macklaim, V. Pawlowsky-Glahn, J. J. Egozcue, Microbiome datasets are compositional: And this is not optional. *Front. Microbiol.* **8**, 2224 (2017).

71. P. Assmy, A. Cecilie Kvernvik, H. Hop, C. J. M. Hoppe, M. Chierici, Seasonal plankton dynamics in Kongsfjorden during two years of contrasting environmental conditions. *Prog. Oceanogr.* **213**, 102996 (2023).

6 Synthesis

6.1. Main findings of this dissertation

This dissertation aimed to understand how Arctic phytoplankton is affected by temperature changes, with a special emphasis on the physiological underpinnings of their overall high plasticity towards ocean warming. I performed detailed physiological assessments of single-strain temperature responses (*Publication I* and *II*), which were then verified in field experiments with Arctic natural communities (*Publication III* and *IV*). This way, I did not only look at direct temperature effects on physiology, but also accounted for ecologically more relevant scales, in which also functional redundancy, species selection and thermal history pay a role.

Physiological processes such as growth rates, biomass production rates or electron transport rates exhibit diverging temperature response patterns due to differences in their thermal sensitivities. *Publication I* assessed response patterns in key Arctic phytoplankton species of different functional groups, i.e. the centric diatom *Thalassiosira hyalina*, the pennate ice algae *Nitzschia frigida* and the mixotrophic pico-eukaryote *Micromonas pusilla*, over large parts of their thermal range under saturating light (100 µmol photons m^{-2} s^{-1}). All investigated species exhibited optimal temperatures for cell division and biomass production higher than what they currently experience in their natural habitat, indicating a stimulation of biomass accumulation at least under moderate warming. Thermal sensitivities and optimal temperatures, however, differed between species and physiological processes. This was also reflected in the temperature response patterns of the respective biomass quotas, which were shown to be a result of the distinct interplay of their underlying physiology, i.e. cell division and biomass production. Overall, this emphasizes the necessity for holistic approaches, including the assessment of different phytoplankton functional groups and functional traits under multiple temperatures, which should be considered for biogeochemically modeling or interpretation of remote sensing data (Riebesell & Gattuso, 2015; Collins *et al.*, 2022).

Publication II aimed to identify physiological bottlenecks potentially arising under warming and to understand how cells adjust their physiology, thereby explaining the observed overall high plasticity and stimulation of biomass production under warming (*Publication I*). To this end, the same *T. hyalina* strain as used in *Publication I* was acclimated to sub-optimal, optimal and supra-optimal temperatures, and photophysiological characteristics as well as photosynthetic O_2 production,

104

photosynthetic C-fixation, respiratory CO_2 release and respiratory O_2 consumption were assessed. It was found that under warming, cells upregulated their light harvesting abilities in order to compensate for a warming-induced light limitation in PSII efficiency, so that cells were able to maintain their gross O_2 production rates. Furthermore, *T. hyalina* employed a metabolic coupling of chloroplasts and mitochondria to dissipate excess reductant into mitochondrial respiration. As a consequence, the TCA cycle, and thereby the respiratory CO_2 loss, was downregulated despite an increased respiratory O_2 consumption. Overall, this coupling between organelles allowed cells to support a sufficient plastidial ATP:NADPH stoichiometry and thereby to maximize net biomass retention under warming.

To also understand temperature responses on Arctic natural communities, I used an incubation approach similar to *Publication II,* also in natural Arctic phytoplankton communities from the open-ocean central Fram strait (*Publication III*) and from a coastal fjord system in Svalbard (*Publication IV*). Both communities exhibited a strongly increasing respiratory O_2 consumption and thus lowered net O_2 production, despite stimulated net biomass retention under warming. In neither of the two studies, responses were accompanied by distinct species shifts towards more heterotrophic communities, indicating that the opposing temperature responses of O_2- and C-fluxes on a community level may result from the same regulatory mechanisms as observed in the single-strain experiment. This highlights that the metabolic coupling of chloroplasts and mitochondria is likely a fundamental mechanism employed across Arctic phytoplankton species in response to ocean warming.

Publication IV aimed to further elucidate the responses to abrupt temperature changes as phytoplankton would experience them in marine heatwaves. To this end, communities' responses were also investigated over short-term temperature fluctuations (warming and cooling) towards their physiology and community composition. Results showed the responses to abrupt temperature changes cannot be predicted from stable warming treatments, especially when combined with subsequent cooling phases. It could be shown that the abrupt cooling at the end of heatwaves impacts the physiology and composition of Arctic phytoplankton communities at least as much as abrupt warming, and especially moderate heatwaves (+4°C) showed most detrimental effects.

Building on the findings of these four *Publications*, I will identify overarching concepts on warming responses of Arctic phytoplankton physiology that allow cells to plastically respond to ocean warming (6.2). Furthermore, findings will be discussed in the context of temperature-light interactions (6.3) of time-scales (abrupt vs. acclimation) on a single-strain and community level (6.4). Lastly, important perspectives for future research will be highlighted (6.5).

6.2. Overarching effects of warming and strategies of physiological regulation

6.2.1. Growth and biomass production benefit from moderate warming

Most physiological processes are generally assumed to be stimulated in response to warming due to increased e.g. diffusion- and reactions rates as well as enzymatic activity, at least until a certain optimum (Raven & Geider, 1988; Padfield *et al.*, 2016; Barton *et al.*, 2020). Findings from all *Publications* indeed reveal stimulatory effects on cell division rates and net biomass production rates, which followed typical optimum curve patterns with a stimulation up to species-specific optimal temperatures and a decline beyond (Thomas *et al.*, 2012; Grimaud *et al.*, 2017). Thereby, all investigated Arctic phytoplankton species exhibited surprisingly high maximal growth and production rates under saturating light conditions (*Publication I*), especially in comparison to temperate phytoplankton species under otherwise similar conditions, which partly exhibit even lower maximal growth rates under much higher temperatures (Baker *et al.*, 2016; Barton & Yvon-Durocher, 2019; Rehder *et al.*, 2024). This not only indicates a high flexibility of Arctic phytoplankton to regulate their underlying physiology and thereby compensate for negative impacts over a wide temperature range, it also suggests that Arctic species will not be unavoidably displaced by temperate species in a warmer Arctic. Arctic phytoplankton will rather engage in ecological competition with poleward advected species from the North Atlantic (Oziel *et al.*, 2020), and the outcome will additionally be affected by the polar photoperiods, i.e. the presence of polar day and night (Giesler *et al.*, 2023). Optimal temperatures of growth and production rates were also consistently above what phytoplankton currently experience in the present Arctic Ocean, indicating a potential for stimulated Arctic primary production under moderate warming and saturated light conditions (*Publication I, III, IV*), and thus likely remain competitive. To robustly predict future primary production,

however, it is essential to identify upcoming physiological bottlenecks and to furthermore understand how cells invest into regulatory mechanisms to achieve metabolic homeostasis, which is discussed in the following section.

6.2.2. Warming impacts PSII efficiency and causes light limitation

Across all investigated species and communities in this dissertation, one potential bottleneck for otherwise not resource-limited (Arctic) phytoplankton under warming was found in the photophysiology of PSII (*Publication I, II, III, IV*; Hancke *et al.*, 2008; Liu *et al.*, 2017). Experiments consistently unraveled detrimental effects on the photosynthetic efficiency of PSII, indicated by decreasing PSII quantum yields (F_v/F_m; *Publication I, II, III, IV*) and relative electron transport rates (rETR; *Publication II, III, IV*). This was surprising because of the simultaneous increase in growth and production rates under warming as well as the assumption of stimulated electron traffic under increasing temperatures due to faster diffusion rates and increased membrane fluidity (Brown *et al.*, 2004; Los *et al.*, 2013). In fact, all investigated single-species (*Publication I, II*), the coastal communities from Svalbard (*Publication IV*) as well as previous studies (Baker *et al.*, 2016; Aardema *et al.*, 2024) exhibited faster re-opening times of PSII, proving a thermodynamically accelerated capacity for electron traffic through the photosynthetic ETC under increased temperatures. *Publication I* showed that PSII re-opening times are highly species-specific, and it has previously been shown that re-opening times in mixed communities cannot be easily interpreted (Suggett *et al.*, 2009), which likely explains the indistinct warming effects on re-opening times in phytoplankton cells from the pelagic community due to a rather high variability of community composition in between treatments (*Publication III*). Hence, despite the lack of significant trends in the latter experiment, the stimulated thermodynamic potential for electron traffic likely remains a fundamental consequence of elevated temperature for phytoplankton. Nonetheless, cells are apparently unable to exploit this, as F_v/F_m and rETR were actually decreasing with warming.

In all experiments, the lowered F_v/F_m and rETRs with increasing temperatures were accompanied by gradually increasing light acclimation indices (I_k; *Publication I, II, III, IV*), which is well in line with other studies on polar and temperate phytoplankton (Hancke *et al.*, 2008; Liu *et al.*, 2017; Camoying & Trimborn, 2023) and indicates a warming-induced light limitation. Hence, under warming, Arctic and temperate phytoplankton would require generally higher light intensities to exhibit saturated

electron transport rates. In other words, cells transition from (close to-) light saturation at low temperatures to light limitation at high temperatures. Thereby, the main bottleneck for electron transport shifts from temperature at cold temperatures to light at high temperatures, proving that light acclimation is ultimately temperature-dependent (Behrenfeld *et al.*, 2008).

6.2.2.1. Upregulated light harvesting compensates the warming-induced light limitation

Despite the decreasing PSII efficiency under warming, phytoplankton cells, however, maintained species-specific homeostatic gross O_2 production rates more or less independent of temperature treatments (*Publication II, III, IV*). This was surprising since the lowered F_v/F_m and rETRs typically indicate an overall lower electron extraction from the water splitting process at the PSII OEC (Suggett *et al.*, 2009; Schuback *et al.*, 2021). Consequently, Arctic phytoplankton must involve physiological regulation to somehow cope with the increasing warming-induced light limitation of PSII. Such a regulation was found in the pigmentation per biomass ratios (Chl *a*:POC) throughout all studies conducted. Except for the ice algae *N. frigida*, all investigated species and communities exhibited increased Chl *a*:POC ratios under warming, which could be seen in increased antenna sizes of the PSII LHCs (*Publication I, II, III, IV*). Depending on the acclimation light intensity, cells were thereby able to compensate the lowered relative ETRs, i.e. PSII efficiencies, so that absolute ETRs per PSII could be maintained (*Publication II*) or even profit from warming (*Publication I*), Consequently, the upregulation of light harvesting abilities, is a central regulatory mechanism to compensate PSII deficiency under warming and thereby maintain homeostatic O_2 production over a large temperature gradient, as illustrated in Fig. 14.
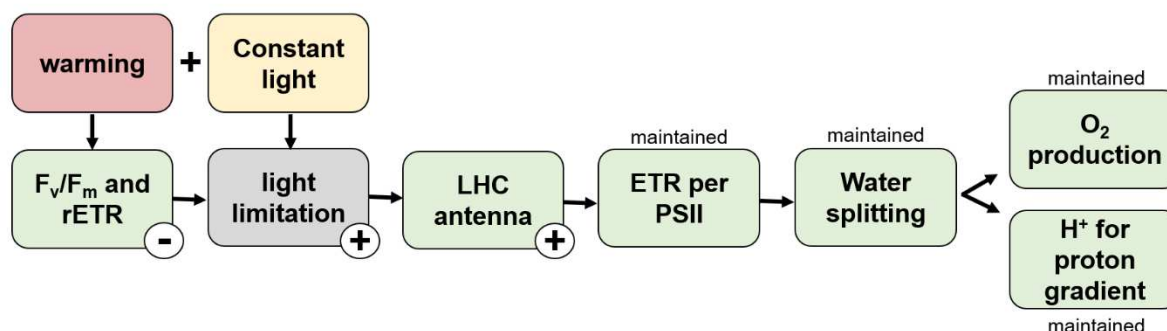
Fig 14. Schematic illustration of warming effects on photosystem II (PSII) under constant light. PSII quantum yields (F_v/F_m) and relative electron transport rates (rETR) decrease under warming, resulting in a warming-induced light limitation. In response, cells upregulate their light harvesting abilities (LHC antenna) to maintain absolute ETRs per PSII. Thereby, photosynthetic water splitting, O_2 production and the provision of protons (H^+) for the thylakoid proton gradient are maintained.

The flexible up- or downregulation of the light harvesting abilities in response to the environmental light conditions is a well-known measure taken by of phototrophic organisms to adjust their photophysiology (e.g. Ballottari *et al.*, 2007; Pi *et al.*, 2019). All *Publications* clearly show that regulation of photophysiological processes is also elicited by thermal cues. The observed upregulation of the antenna size in response to a warming-induced light limitation seems logical, even though this ability is modulated by environmental conditions (see chapter 6.3) and can differ between species (*Publication I*). For instance, *Nitzschia frigida* neither exhibited such a warming-induced light limitation nor increased its pigmentation per biomass. This species remained strongly light limited at acclimation light level throughout their entire thermal range. As an ice alga, *N. frigida* generally thrives under low light conditions, and seems to follow a specialized photophysiological strategy involving comparably low antenna sizes, which is believed to function as a constitutive high-light protection for the case of spontaneous ice break up (Kvernvik *et al.*, 2020; Kvernvik *et al.*, 2021).

Since both, the open-ocean (*Publication III*) as well as the coastal natural communities (*Publication IV*) exhibited responses very similar to those observed in the detailed physiological characterization (*Publication I, II*), it can be assumed that the observed temperature responses in photophysiology are widespread in phytoplankton, whereas ice-algae, as an exception, oppose these general temperature-driven patterns of photo acclimation (Kvernvik *et al.*, 2020; Kvernvik *et al.*, 2021).

6.2.3. The metabolic coupling of chloroplasts and mitochondria

Photosynthetic O_2 production, C-fixation and respiratory O_2 consumption are maintained under higher temperatures

In addition to elucidating photophysiological responses to warming, gas flux measurements of O_2 (and CO_2) were used to identify potentially divergent temperature responses of photosynthetic and respiratory sub-processes (*Publication II, III, IV*). As discussed in chapter 6.2.2, photophysiological adjustments allowed *T. hyalina* to maintain photosynthetic electron transfer as determined fluorometrically as well as O_2 evolution as determined by MIMS (*Publication II*), and O_2 flux data indicated such a regulation also on a phytoplankton community level (*Publication III, IV*). Thus, in all investigated species or communities, gross photosynthetic O_2 production remained mostly unchanged over acclimation timescales, irrespective of acclimation temperature, which is in line with observations of the temperate diatom *Phaeodactylum tricornutum* (Rehder *et al.*, 2023). Up to moderate warming, also gross photosynthetic C-fixation as well as respiratory O_2 consumption in the light and dark were maintained on a constant level (*Publication II*), thereby ensuring physiological homeostasis between these processes. Only under temperatures beyond optimal growth, however, the Calvin cycle and respiratory ETC get out of tune, as indicated by a declining gross C-fixation and increasing respiratory O_2 consumption. Under supra-optimal temperatures, regulatory mechanisms that maintain the physiological homeostasis between processes are apparently partly failing and warming becomes detrimental.

6.2.3.1. Dissipating excess plastidial NADPH is critical to avoid overreduction

Photosynthetic light reactions and the Calvin cycle are physiologically directly dependent from each other, as the former generates the energy and reductants in form of ATP and NADPH to fuel the latter (Falciatore *et al.*, 2022). Therefore, it seems logical that in *T. hyalina* as well as *P. tricornutum* both processes remain homeostatic under moderate warming (*Publication II*; Rehder *et al.*, 2023). The photosynthetic light reactions, however, generally provide excess NADPH relative to ATP with respect to the requirements of the Calvin cycle, N-assimilation and CCM activity even under low temperatures (Allen, 2003; Hahn *et al.*, 2018; Lepetit *et al.*, 2022). Under warming and concomitantly increased diffusion rates, however, more HCO_3^- can diffuse into the thylakoid lumen, i.e. increased CCM activity, which consumes a larger fraction of the PMF that could otherwise be used for ATP generation. Thereby, the plastidial

ATP:NADPH ratio is lowered under warming. This suggests that while CCMs are indispensable for phytoplankton C-fixation, they are also important consumers of the PMF and may therefore be a prime source of the metabolic imbalances occurring under thermal stress. Consequently, cells have evolved mechanisms to adjust the ATP:NADPH stoichiometry in order to prevent plastidial 'overreduction' and concomitant redox stress (Burlacot, 2023; Peltier *et al.*, 2024).

6.2.3.2. Warming increases a metabolic coupling of chloroplasts and mitochondria

To decrease the excess of plastidial NADPH, cells need to either dissipate NADPH, or increase ATP production (Allen, 2003). To this end, cells employ different pathways of photosynthetic AEF (see chapter 1.3.1; e.g. Curien *et al.*, 2016; Burlacot, 2023), such as CEF around PSII (Larkum *et al.*, 2018; Nawrocki *et al.*, 2019), the O_2-consuming Mehler reaction (Mehler, 1951; Asada, 2000), the O_2- consuming plastidial terminal oxidation (Nawrocki *et al.*, 2015) as well as a metabolic coupling of chloroplast and mitochondria. The latter re-routes plastidial reductant into the respiratory processes of the mitochondrial electron transport chain (Bailleul *et al.*, 2015; Burlacot, 2023; Rehder *et al.*, 2023; Peltier *et al.*, 2024).

In line with findings on *P. tricornutum* (Bailleul *et al.*, 2015), also *T. hyalina* exhibited a consistently higher respiratory O_2 consumption in the light than in the dark, which was even more pronounced under warming, indicating a substantial contribution of at least one O_2-consuming AEF pathway (*Publication II*). The significant concomitant decrease of respiratory CO_2 fluxes under moderate and strong warming in *T. hyalina* (*Publication II*), strongly supports the suggestion of a metabolic coupling, in which the additional reductant transported to the mitochondria, shifts the redox state and thereby suppresses the TCA cycle. In line with this, a previous study revealed in response to low acclimation temperatures a transcriptomic upregulation of the TCA cycle in a sub-Arctic *Chaetoceros* strain (Liang, Y *et al.*, 2019). Such a metabolic coupling as a measure to avoid plastidial overreduction is well established in diatoms, green algae and land plants (Cardol *et al.*, 2003; Raghavendra & Padmasree, 2003; Noctor *et al.*, 2004; Rehder *et al.*, 2023). This dissertation shows, however, that the metabolic coupling not only optimizes the plastidial ATP:NADPH stoichiometry for C-fixation, but obviously also controls the flow of carbon and energy through phytoplankton cells as a function of temperature (Fig. 15). Under low temperatures, cells require less

metabolic coupling, likely also because of the relatively lower PMF consumption by the CCM under low temperatures. In this situation, the respiratory ETC seems to be primarily fueled by reductant extracted during the traditional heterotrophic pyruvate respiration in the TCA cycle (Fig. 15a). Under high temperatures, in turn, cells employ the metabolic coupling to fuel plastidial reductant to the mitochondrial ETC more directly, skipping the contribution of carbon-dissimilatory processes for reductant generation (Fig. 15b). This mechanism also explains the stimulation of biomass retention that is widely observed in phytoplankton when grown under increasing temperatures.
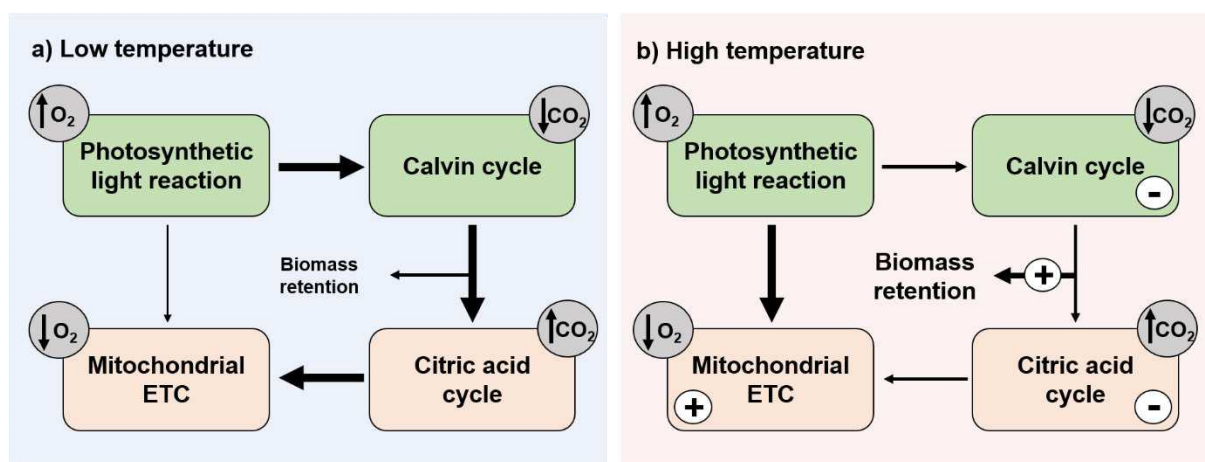
Fig 15. Simplified pathways of reductant flow through phytoplankton cells at low temperatures (a) and high temperatures (b), when the prime alternative electron flow pathway is a re-routing of plastidial reductant into mitochondrial respiration. Arrows indicate reductant flow.

6.2.3.3. Metabolic coupling affects net O_2 production and net C-fixation opposingly

The metabolic coupling of chloroplasts and mitochondria not only regulates PMF and reductant flow through phytoplankton cells, but in further instances also strongly affects net cellular O_2- and C-fluxes. Despite steady gross O_2 production rates across the investigated temperature gradient, net O_2 production rates strongly decreased towards high temperatures, because of the stimulated respiratory O_2 consumption (*Publication II, III, IV*). The downregulation of TCA cycle activity and thus the decrease in respiratory CO_2 loss led, in turn, to massively stimulated net C-fixation rates (*Publication II*).

The described diverging warming responses of O_2- and C-based net photosynthetic rates were also reflected on the community level (*Publication III, IV*). Even though the

open-ocean and coastal communities differed in composition, i.e. *Phaeocytsis-Chaetoceros* and *Navicula-Fragilariopsis* dominance, respectively, communities from both habitats showed the phenomenon of stimulated biomass accumulation despite a lowered net O_2 production. Such a decrease of net O_2 production on a community level under warming has also been observed in benthic communities of Fjord systems in northern Norway and Svalbard (Hancke & Glud, 2004), and a stimulation of biomass accumulation despite decreased net O_2 production was also signified in a mesocosm study with North sea phytoplankton spring bloom communities (Ahme *et al.*, 2024). Apparently, the metabolic coupling as the dominant AEF pathway under warming has not only been verified for *T. hyalina* in this dissertation, but the mechanism is also indicated in different natural phytoplankton community experiments, apparently independent of species composition. Consequently, it appears to be a fundamental physiological regulation strategy of phytoplankton from polar and temperate habitats under warming.

6.3. How light modulates phytoplankton temperature responses

Phytoplankton physiology is controlled not only by temperature but also by other environmental drivers such as light and nutrient availability, which are also affected by climate change (e.g. Doney *et al.*, 2012; Cooley *et al.*, 2022). Several studies have already shown that these different environmental drivers modulate each other's responses in phytoplankton. Therefore, to understand how temperature affects phytoplankton physiology on a broader level, it is also essential to elucidate how thermal sensitivities of physiological processes are modulated by e.g. variations in light intensity (e.g. Geider, 1987; Behrenfeld *et al.*, 2008; Chen *et al.*, 2015; Edwards *et al.*, 2016; Anderson *et al.*, 2022). After discussing overarching temperature responses and physiological regulation strategies in general (see chapter 6.2), the following chapter will unravel how light levels may have modulated these findings by explicitly comparing temperature responses under saturating light (100 µmol photons m^{-2} s^{-1}; *Publication I*) and limiting light (30 µmol photons m^{-2} s-1; *Publication II, III, IV*).

6.3.1. Temperature-light interaction modulates the interplay of cell division and biomass production

Differences in light intensities affect the shape of temperature response patterns for growth rates in phytoplankton. While all investigated species showed typical unimodal growth rate responses towards the applied temperature gradient under saturating light (*Publication I*), cells did not exhibit any stimulation in growth rates under warming when light-limited (*Publication II*). This temperature-light interaction has previously been observed in several phytoplankton species, where lower light intensities generally decreased optimal growth temperatures, and light-limited cultures did not exhibit stimulated growth rates under warming at all (Edwards *et al.*, 2016). In turn, under saturating light intensities, warming can increase growth rates, when both, light intensity and temperature increase, so that phytoplankton may exhibit higher optimal growth temperatures and reach higher maximal growth rates (Chen *et al.*, 2015; Edwards *et al.*, 2016; Coyne *et al.*, 2021).

Under saturating light, biomass production rates of all investigated single-strains responded similarly as the growth rates, i.e. they followed unimodal temperature response patterns (*Publication I*), whereas optimal temperatures and temperature sensitivities were also likely lowered under limiting light (*Publication II*). *Publication I* showed that the thermal sensitivities, i.e. the slope of warming-induced stimulation as well as the optimal temperatures of specifically the processes of cell division and biomass production diverged, leading to different patterns of cellular biomass quotas (Morel, 1987). In that study, *T. hyalina* exhibited a higher temperature sensitivity in cell division than in biomass production with warming, resulting in a U-shaped response pattern of biomass quotas (Fig. 16a). Under limiting light (*Publication II*), however, *T. hyalina* experienced the above described suppression on cell division under higher temperatures whereas net C-fixation rates indicated an optimum curve of biomass production. Thus, biomass production exhibited a higher temperature sensitivity as well as a higher optimal temperature than cell division, which is also reflected in a more or less linearly decreasing temperature response pattern of the resulting biomass quotas (Fig. 16b). Consequently, temperature responses of underlying physiological processes such as cell division or biomass production are modulated by light, and also the resulting biomass quotas are shaped by this interaction.
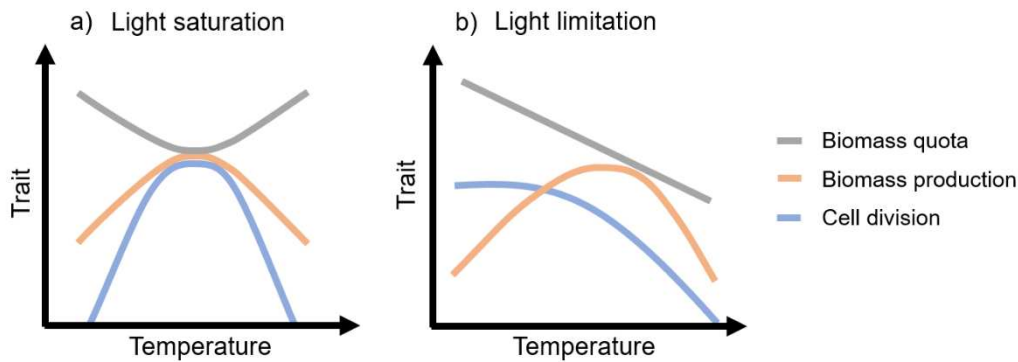
Fig 16. Schematic illustration of the interplay of the temperature response patterns of cell division (blue) and biomass production (orange), which shape the response patterns of biomass quotas (grey) in *Thalassiosira hyalina* under (a) light saturation and (b) light limitation. Modified after *Publication I*.

6.3.2. Temperature and light can synergistically increase maximum photosynthetic efficiencies of PSII

The photophysiological data revealed a similar temperature-light interaction on electron transport as in growth and biomass production: As postulated above *T. hyalina* as well as both, the open-ocean and coastal natural communities experienced gradually decreased rETRs with warming at a limiting incubation light intensity, which cells compensated by an upregulation of light harvesting abilities and thereby achieved maintained absETRs per PSII (*Publication II, III, IV,* see chapter 6.2.2). Under saturating light, however, all investigated single-strains including the same strain of *T. hyalina* showed more or less unchanged rETRs in response to warming, but still increased light harvesting abilities, so that cells experienced even a stimulation in absETRs under warming up to a species-specific optimum (*Publication I*). Even though it might not be surprising that light intensity has a huge effect on light harvesting abilities (e.g. MacIntyre *et al.*, 2002; Graff *et al.*, 2016; Hoppe *et al.*, 2018; Campbell & Serôdio, 2020), it underlines the close interaction of temperature and light on the photosynthetic efficiency.

Furthermore, when cells become increasingly light limited with warming, this also has the potential to "unleash" photosynthesis: Under increasing temperatures, also higher maximum ETRs (relative and absolute) can be achieved (*Publication I, II, III*), especially under abrupt high-light exposure (Rehder 2023). Thus, higher temperatures

enable phytoplankton to exploit higher light intensities, underlining synergistic beneficial interaction of elevated temperature and light on photosynthetic efficiency of PSII (Rehder *et al.*, 2023; Rokitta *et al.*, 2023).

6.4. A matter of time and company – abrupt versus acclimation temperature responses in single-strain or community incubations

Temperature responses on phytoplankton strongly depend on exposure time-scales, i.e. abrupt vs. acclimation effects (Strock & Menden-Deuer, 2021; Rehder *et al.*, 2023), but also on potential intra- or inter-specific competition (Irwin *et al.*, 2006; Marinov *et al.*, 2010; Wolf *et al.*, 2018).

Abrupt temperature increases typically result in a stimulation of photosynthetic and respiratory rates until a process-specific optimum (Barton *et al.*, 2020; Rehder *et al.*, 2023). Over the course of acclimation, however, phytoplankton apparently seeks to adjust their *photosynthetic* processes on constant levels across large parts of their thermal range, while *respiratory* processes are a fundamental part of the regulation inventory to plastically respond to ocean warming and do not approach constant rates irrespective of temperature (see chapter 6.2; *Publication II*). Especially the observed downregulation of TCA cycle activity in response to increasing temperatures on acclimation time-scales (*Publication II*) has been confirmed as a direct response to abrupt temperature increases in *P. tricornutum* (Rehder *et al.*, 2023). This indicates that the metabolic coupling instantaneously responds to temperature, and sustains under acclimation. Consequently, net C-fixation rates, likely exhibit distinct temperature response patterns on both, abrupt as well as acclimation time-scales, whereas the temperature sensitivity on short time-scales is likely higher than on acclimations time-scales due to the stimulatory response of gross C-fixation (Fig. 17a and b; *Publication II*; Rehder *et al.*, 2023).

In natural phytoplankton communities, differences of abrupt and "acclimation" responses can be expected to be more complex than in single-strain incubations. Next to the continuous acclimatory adjustments of cells, also competition for resource availability and species selection processes affect community structure and thus the overall physiological output in terms of net biomass accumulation or net O_2 production (Sommer, 1996; Descamps-Julien & Gonzalez, 2005; Wolf *et al.*, 2018). Thereby, the

sum of individual physiological responses is directly depending on community composition, which is amplified by the aspect of community shifts towards best adapted strains and species.

Even though, single-strain incubations revealed an optimum curve temperature response pattern of net C-fixation over the course of acclimation (Fig. 17b; *Publication I, II*), the investigated natural communities from both habitats seemed to exhibit a gradual stimulation of net C-fixation over the same temperature gradient, indicated by the responses of biomass accumulation rates (Fig. 17c; *Publication III, IV*). This was likely a result of species-selection for highest growth rates and may have thereby masked detrimental temperature effects on the Calvin cycle in typical Arctic phytoplankton species, because communities develop in a way that in sum, they can maintain gross C-fixation also under higher temperatures than the applied warming treatment of 9°C. The metabolic coupling, however, was also indicated on a community level, so that the respiratory CO_2 loss was probably still lowered under higher temperatures, which overall explains the observed gradually increasing net biomass accumulation (Fig. 17c; *Publication III, IV*).
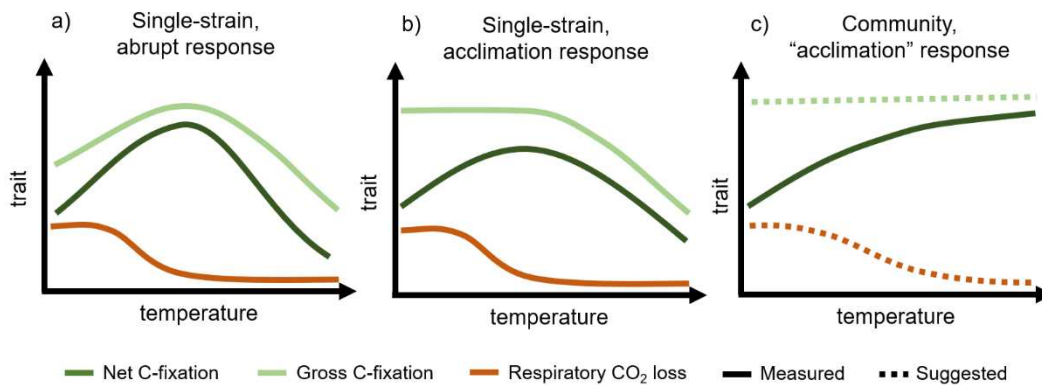
Fig 17. Schematic illustration of temperature responses of net C-fixation (dark green), gross C-fixation (light green) and respiratory CO_2 loss (orange), (a) when a low temperature acclimated single-strain culture is abruptly exposed to increasing temperatures, (b) when this single-strain culture is acclimated to the higher temperatures and (c) when a community was exposed to increasing temperatures over weekly time-scales and underwent selection for better-adapted species and strains. Solid-lines indicate measured temperature responses, the dashed lines indicate suggested temperature response patterns assuming more or less constant gross C-fixation and lowered respiratory CO_2 loss, due to the metabolic coupling (see chapter 6.2).

6.4.1. Abrupt cooling impacts phytoplankton communities at least as much as abrupt warming

Publication IV revealed that short-term temperature responses in the context of heatwaves cannot be directly predicted, neither by community composition nor by physiology, which seems to originate especially from the cooling phase in the end of a marine heatwave. Under the first initial abrupt warming, communities that were exposed to the heatwave scenario, responded similar as under the control treatment which was close to in-situ temperature. The abrupt cooling after the heatwave scenario, however, inhibited net primary production so strongly (NPP; measured using the ^{14}C method), that communities experienced lower NPP rates than the control treatment at the same temperature, very similar to abrupt cooling responses of *P. tricornutum* (Rehder *et al.*, 2023). Especially the moderate heatwave scenario (+4°C) exhibited distinct shifts in community composition after the abrupt cooling, indicating a stronger selection pressure than under stable warming treatments, which may have also affected the overall physiology. A physiological reason for detrimental effects instead of a relief from acute temperature stress after both heatwave scenarios (+4°C and + 7°C) could furthermore be found in the photophysiological adjustments of the light harvesting abilities. During the heatwave scenario, communities upregulated their light harvesting abilities to compensate for a temporal warming-induced light limitation as physiologically resolved in detail in *Publication II* (see chapter 6.2.2). When temperature was afterwards abruptly decreased at the end of the heatwave, communities were apparently unable to quickly downregulate light harvesting abilities as indicated by unaltered high antenna sizes (*Publication IV*), even though the lower temperatures likely alleviate the warming-induced light limitation. Thus, communities likely experienced cold-induced high-light stress, in turn, because of the abrupt inhibition of thermodynamic processes, indicated by slower re-opening times of PSII, despite unchanged high light harvest. This may explain the more severe effects on the photosynthetic light reactions from abrupt cooling than abrupt warming, which potentially also resulted in a higher species selection pressure, as a fast and efficient light harvesting regulation is likely favorable under fluctuating temperatures.

6.5. Future perspectives

6.5.1. Further elucidation of the metabolic coupling

The metabolic coupling of chloroplast and mitochondria (see chapter 6.2.3) seemed to be fundamental across all investigated species and communities under limiting light conditions (*Publication II, III, IV*). However, the magnitude of reductant re-routing is most likely modulated by acclimation light intensities, as it is strongly depending on an 'overreduction' of the chloroplasts (Burlacot, 2023). This suggests an even stronger need of cells to fuel plastidial reductant directly into mitochondrial ETC under warming when acclimation light intensities are higher, as they likely cause a more pronounced 'overreduction' of the photosynthetic ETC. Temperature responses of the respiratory O_2 consumption in the light under abrupt high light exposure, indicate a temporal stimulation of O_2 consuming AEFS, especially under warming (*Publication II*). If an NADPH dissipation is, however, facilitated by a stronger operation of the metabolic coupling or if other AEF pathways, such as Mehler reaction or PTOX additionally contribute (Curien *et al.*, 2016; Burlacot, 2023), remains puzzling. Furthermore, it also remains unknown, if a combined warming and high light exposure over acclimation time-scales would actually even intensify the need to dissipate reductant or if cells involve other regulatory inventory to adjust physiology. Since the downregulation of respiratory CO_2 loss highly effects cellular C biomass retention, which may even have effects on an ecosystem level, further experiments on the metabolic coupling and other potential AEFs should put special emphasis on the following aspects, especially in regards of combined increases in temperature and light intensity: (1) an elucidation of the plastidial overreduction using e.g. electrochromic shift measurements (Bailleul *et al.*, 2015), (2) a quantification of a potential further downregulation of the TCA cycle using MIMS approaches including isotopic labelling of CO_2 to distinguish between respiratory CO_2 loss in the light and dark and ultimately confirm a light-depending regulation of the TCA activity (3) and the verification of reductant shuttling using e.g. proteomics.

6.5.2. Possible warming effects on photosystem I

The regulation of PSII light harvesting abilities was found to be essential as a compensation strategy for the increasing warming-induced light limitation, but also seemed to be a reason for severe impacts in response to abrupt cooling in the end of marine heatwave scenarios. This dissertation elucidated PSII photophysiology on a detailed level, however, it remains open how temperature actually affects PSI and its associated antenna complex. Although PSI is often considered more stable towards environmental stressors than PSII (Scheller & Haldrup, 2005), a protection of PSI under temperature- or light-stress seems essential because of its time- and energy-expensive recovery in comparison to PSII (Bernhard Teicher *et al.*, 2000; Sonoike, 2011). To this end, future studies on mechanistic physiological temperature responses, especially on abrupt time-scales, should also investigate PSI responses. In regard of increasing temperatures, there are different possibilities, how PSI may be affected (Fig. 18): It could respond similar to warming as PSII, i.e. PSI experiences a warming-induced light limitation, which cells compensate by upregulating PSI light harvesting abilities. This would likely maintain a balance between PSII and PSI, thereby ensuring stable NADPH generation and avoiding redox stress due to "electron traffic jams" during the photosynthetic ETC (Fig. 18a). PSI could, however, also experience warming-induced light limitation, but cells cannot invest into a regulatory compensation of the LHC. This would likely result in a less efficient PSI electron excitation and a reduced electron transfer to FNR. As a consequence, cells would likely experience lowered NADPH generation, but also an accumulation of electrons between PSII and PSI. Such an "electron traffic jam" would require electron dissipation between PSII and PSI, for instance involving PTOX, to avoid redox stress in the ETC, rather than employing the metabolic coupling (Fig. 18b). To compensate for a warming-induced light limitation of PSI without upregulation of LHC, cells could furthermore also decrease the PSII:PSI stoichiometry. A higher relative abundance of PSI could thus ensure maintained NADPH generation and avoid redox stress (Fig. 18c). Finally, PSI may actually be stimulated by warming instead of inhibited. This would probably have no effect on NADPH generation, as PSII and PSI efficiency would scale in balance (Fig. 18d).
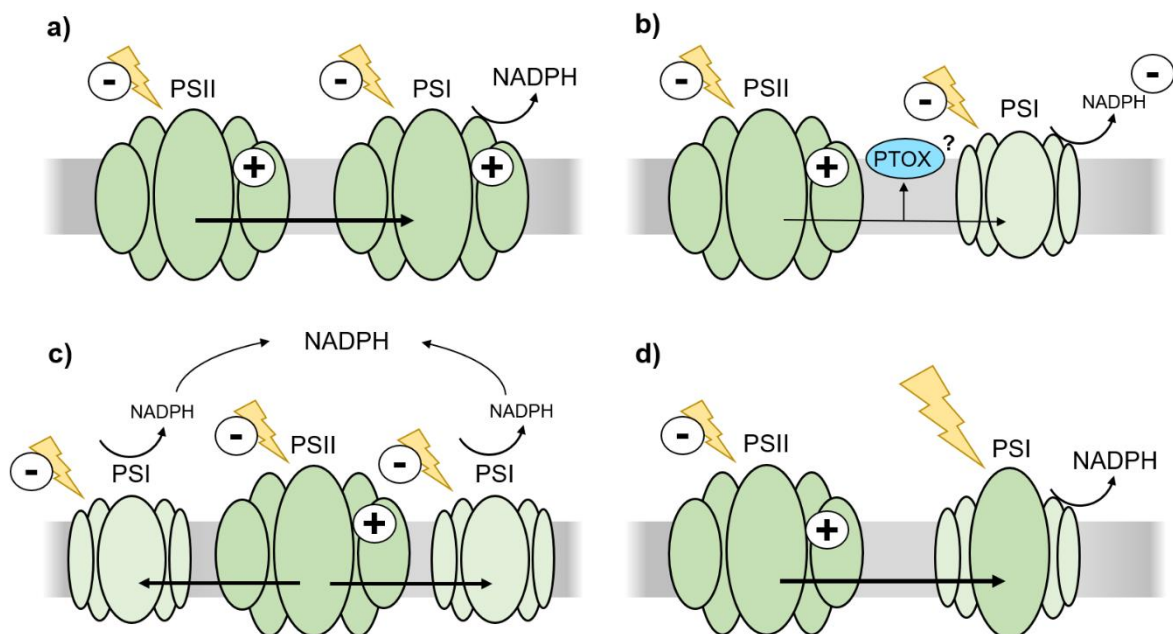
Fig 18. Different possibilities of photosystem I (PSI) responses to increasing temperatures, when photosystem II (PSII) exhibits upregulated light harvesting complexes (LHCs) under warming. (a) PSI responses similar as PSII, i.e. PSI experiences thermal-induced light limitation and exhibits upregulated LHCs, (b) PSI experiences thermal-induced light limitation, but does not upregulation LHCs. As a consequence, less NADPH is generated and electrons are dissipated into plastidial terminal oxidation (PTOX), (c) PSI experiences thermal-induced light limitation, but does not upregulation LHCs. As a compensation, cells increase PSI abundances to maintain the NADPH pool, and (d) PSI does not experience thermal-induced light limitation, i.e. no compensation is necessary.

To this end, in future experiments absorption cross sections of PSI as a proxy for antenna size by means of pulse amplitude modulation (PAM) and combined spectrophotometric assessments of PSI photo-oxidation kinetics (Zipfel & Owens, 1991; Ryan-Keogh *et al.*, 2012) should be investigated. PSI:PSII stoichiometry can also be assessed spectrophotometrically (Falkowski & Owens, 1980; Falkowski *et al.*, 1981) and could further be quantified using proteomic analysis (Kranz *et al.*, 2010; Levitan *et al.*, 2010; Schober *et al.*, 2019). This would allow a more holistic view on the photosynthetic light reaction under temperature changes and should also include marine heatwave simulation experiments, as here a proper regulation mechanism of PSI would be most essential, especially in response to cooling phases.

6.6. Conclusion – resolving the elephant

This dissertation aimed to dissect temperature responses in Arctic microalgae on a detailed physiological level. Temperature response patterns diverged between functional traits as well as species, especially the ones of cellular quotas. This may remind one to the parable of "The elephant in the dark" (Shah, 1974), in which blind people experience an elephant differently according to their subjectivities (Fig. 19). If only bits and pieces are investigated separately, we risk to miss the whole picture or even come up with a wrong assumption. Thus, holistic experiments on multiple functional traits at numerous temperatures in several taxonomic groups are necessary to "resolve the phytoplankton" and understand temperature effects on phytoplankton physiology on a broader view.
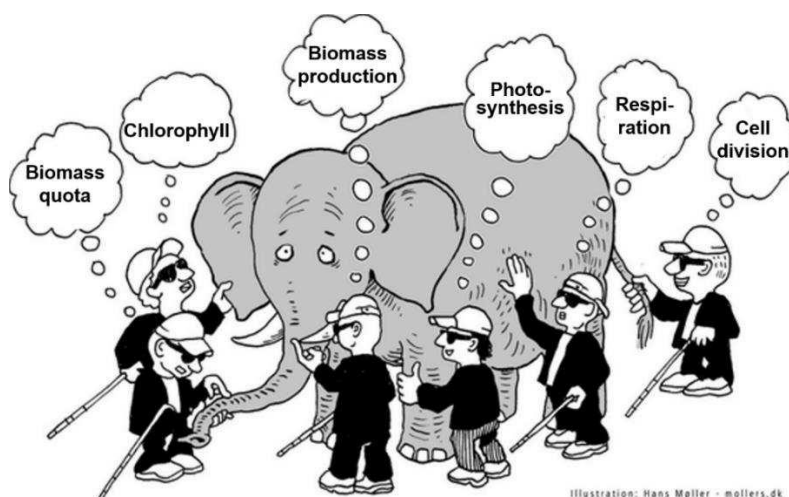
Fig 19. Illustration of the parable "The elephant in the dark", modified after Hans Møller.

Despite the many diverging functional trait responses, the combined approach of detailed single-strain characterizations as well as ecologically more relevant community experiments enabled me to identify fundamental mechanisms how cells adjust their physiology over a wide temperature gradient and thereby maintain metabolic homeostasis. Especially, the upregulation of light harvesting abilities and the metabolic coupling seems fundamental for Arctic phytoplanktons` high plasticity towards ocean warming. This was reflected in the optimal temperatures for growth and biomass production, which exceeded those in the present Arctic Ocean, suggesting a stimulation of biomass accumulation at least under moderate warming. Data of photophysiological assessments further signify synergistic beneficial effects on photosynthetic processes under a combined increase of temperature and light intensity, as it is projected for the future Arctic Ocean.

7 References

References

Aardema HM, Slagter HA, Hrabe de Angelis I, Calleja ML, Dragoneas A, Moretti S, Schuback N, Heins L, Walter D, Weis U, et al. 2024. On the variability of phytoplankton photophysiology along a latitudinal transect in the North Atlantic Surface Ocean. *Journal of Geophysical Research: Biogeosciences* 129(9): e2023JG007962.

Ahme A, Happe A, Striebel M, Cabrerizo MJ, Olsson M, Giesler J, Schulte-Hillen R, Sentimenti A, Kühne N, John U. 2024. Warming increases the compositional and functional variability of a temperate protist community. *Science of The Total Environment*: 171971.

Ahme A, Von Jackowski A, McPherson RA, Wolf KK, Hoppmann M, Neuhaus S, John U. 2023. Winners and losers of Atlantification: the degree of ocean warming affects the structure of Arctic microbial communities. *Genes* 14(3): 623.

Allen JF. 2002. Photosynthesis of ATP, Electrons, proton pumps, rotors, and poise. *Cell* 110(3): 273-276.

Allen JF. 2003. Cyclic, pseudocyclic and noncyclic photophosphorylation: new links in the chain. *Trends in Plant Science* 8(1): 15-19.

Alric J. 2010. Cyclic electron flow around photosystem I in unicellular green algae. *Photosynthesis research* 106: 47-56.

Anderson SI, Franzè G, Kling JD, Wilburn P, Kremer CT, Menden-Deuer S, Litchman E, Hutchins DA, Rynearson TA. 2022. The interactive effects of temperature and nutrients on a spring phytoplankton community. *Limnology and Oceanography* 67(3): 634-645.

Arrigo KR, Perovich DK, Pickart RS, Brown ZW, van Dijken GL, Lowry KE, Mills MM, Palmer MA, Balch WM, Bahr F, et al. 2012. Massive phytoplankton blooms under Arctic sea ice. *Science* 336(6087): 1408-1408.

Arrigo KR, van Dijken G, Pabi S. 2008. Impact of a shrinking Arctic ice cover on marine primary production. *Geophysical Research Letters* 35(19).

Asada K. 2000. The water–water cycle as alternative photon and electron sinks. *Philosophical Transactions of the Royal Society of London. Series B: Biological Sciences* 355(1402): 1419-1431.

Assmy P, Fernández-Méndez M, Duarte P, Meyer A, Randelhoff A, Mundy CJ, Olsen LM, Kauko HM, Bailey A, Chierici M, et al. 2017. Leads in Arctic pack ice enable early phytoplankton blooms below snow-covered sea ice. *Scientific Reports* 7(1): 40850.

Assmy P, Henjes J, Klaas C, Smetacek V. 2007. Mechanisms determining species dominance in a phytoplankton bloom induced by the iron fertilization experiment EisenEx in the Southern Ocean. *Deep Sea Research Part I: Oceanographic Research Papers* 54(3): 340-362.

Atkinson D, Ciotti BJ, Montagnes DJ. 2003. Protists decrease in size linearly with temperature: ca. 2.5% C− 1. *Proceedings of the Royal Society of London. Series B: Biological Sciences* 270(1533): 2605-2611.

References

Bailleul B, Berne N, Murik O, Petroutsos D, Prihoda J, Tanaka A, Villanova V, Bligny R, Flori S, Falconet D. 2015. Energetic coupling between plastids and mitochondria drives CO2 assimilation in diatoms. *Nature* 524(7565): 366-369.

Baker KG, Robinson CM, Radford DT, McInnes AS, Evenhuis C, Doblin MA. 2016. Thermal performance curves of functional traits aid understanding of thermally induced changes in diatom-mediated biogeochemical fluxes. *Frontiers in Marine Science* 3.

Ballottari M, Dall'Osto L, Morosinotto T, Bassi R. 2007. Contrasting behavior of higher plant photosystem i and ii antenna systems during acclimation. *Journal of Biological Chemistry* 282(12): 8947-8958.

Barton S, Jenkins J, Buckling A, Schaum C-E, Smirnoff N, Raven JA, Yvon-Durocher G. 2020. Evolutionary temperature compensation of carbon fixation in marine phytoplankton. *Ecology Letters* 23(4): 722-733.

Barton S, Yvon-Durocher G. 2019. Quantifying the temperature dependence of growth rate in marine phytoplankton within and across species. *Limnology and Oceanography* 64(5): 2081-2091.

Bauwe H, Hagemann M, Fernie AR. 2010. Photorespiration: players, partners and origin. *Trends in Plant Science* 15(6): 330-336.

Behrenfeld MJ, Halsey KH, Milligan AJ. 2008. Evolved physiological responses of phytoplankton to their integrated growth environment. *Philosophical Transactions of the Royal Society B: Biological Sciences* 363(1504): 2687-2703.

Benedetti F, Vogt M, Elizondo UH, Righetti D, Zimmermann NE, Gruber N. 2021. Major restructuring of marine plankton assemblages under global warming. *Nature communications* 12(1): 5226.

Berge J, Renaud PE, Darnis G, Cottier F, Last K, Gabrielsen TM, Johnsen G, Seuthe L, Weslawski JM, Leu E. 2015. In the dark: a review of ecosystem processes during the Arctic polar night. *Progress in Oceanography* 139: 258-271.

Bernhard Teicher H, Lindberg Møller B, Vibe Scheller H. 2000. Photoinhibition of photosystem I in field-grown barley (*Hordeum vulgare* L.): induction, recovery and acclimation. *Photosynthesis research* 64: 53-61.

Boardman N 1977. Development of chloroplast structure and function. *Photosynthesis I: Photosynthetic Electron Transport and Photophosphorylation*: Springer, 583-600.

Boscolo-Galazzo F, Crichton KA, Barker S, Pearson PN. 2018. Temperature dependency of metabolic rates in the upper ocean: A positive feedback to global climate change? *Global and Planetary Change* 170: 201-212.

Brown JH, Gillooly JF, Allen AP, Savage VM, West GB. 2004. Toward a metabolic theory of ecology. *Ecology* 85(7): 1771-1789.

Bruhn CS, Wohlrab S, Krock B, Lundholm N, John U. 2021. Seasonal plankton succession is in accordance with phycotoxin occurrence in Disko Bay, West Greenland. *Harmful algae* 103: 101978.

References

Buick R. 2008. When did oxygenic photosynthesis evolve? *Philosophical Transactions of the Royal Society B: Biological Sciences* 363(1504): 2731-2743.

Burlacot A. 2023. Quantifying the roles of algal photosynthetic electron pathways: a milestone towards photosynthetic robustness. *New Phytologist* 240(6): 2197-2203.

Burlacot A, Burlacot F, Li-Beisson Y, Peltier G. 2020. Corrigendum: Membrane Inlet Mass Spectrometry: A Powerful Tool for Algal Research. *Frontiers in Plant Science* 11.

Calvin M. 1962. The Path of Carbon in Photosynthesis: The carbon cycle is a tool for exploring chemical biodynamics and the mechanism of quantum conversion. *Science* 135(3507): 879-889.

Camoying MG, Trimborn S. 2023. Physiological response of an Antarctic cryptophyte to increasing temperature, CO_2, and irradiance. *Limnology and Oceanography* 68(8): 1880-1894.

Campbell DA, Serôdio J 2020. Photoinhibition of photosystem II in phytoplankton: processes and patterns. *Photosynthesis in algae: Biochemical and physiological mechanisms*: Springer, 329-365.

Cardol P, Gloire G, Havaux M, Remacle C, Matagne R, Franck F. 2003. Photosynthesis and state transitions in mitochondrial mutants of *Chlamydomonas reinhardtii* affected in respiration. *Plant Physiology* 133(4): 2010-2020.

Carlson CA, Hansell DA, Nelson NB, Siegel DA, Smethie WM, Khatiwala S, Meyers MM, Halewood E. 2010. Dissolved organic carbon export and subsequent remineralization in the mesopelagic and bathypelagic realms of the North Atlantic basin. *Deep Sea Research Part II: Topical Studies in Oceanography* 57(16): 1433-1445.

Carmack EC, Yamamoto-Kawai M, Haine TW, Bacon S, Bluhm BA, Lique C, Melling H, Polyakov IV, Straneo F, Timmermans ML. 2016. Freshwater and its role in the Arctic Marine System: Sources, disposition, storage, export, and physical and biogeochemical consequences in the Arctic and global oceans. *Journal of Geophysical Research: Biogeosciences* 121(3): 675-717.

Chakraborty S, Nielsen LT, Andersen KH. 2017. Trophic strategies of unicellular plankton. *The American Naturalist* 189(4): E77-E90.

Chen M, Fan M, Liu R, Wang X, Yuan X, Zhu H. 2015. The dynamics of temperature and light on the growth of phytoplankton. *Journal of theoretical biology* 385: 8-19.

Cheng L, Trenberth KE, Gruber N, Abraham JP, Fasullo JT, Li G, Mann ME, Zhao X, Zhu J. 2020. Improved estimates of changes in upper ocean salinity and the hydrological cycle. *Journal of Climate* 33(23): 10357-10381.

Chisholm SW 1992. Phytoplankton Size. In: Falkowski PG, Woodhead AD, Vivirito K eds. *Primary Productivity and Biogeochemical Cycles in the Sea*. Boston, MA: Springer US, 213-237.

References

Chivers WJ, Edwards M, Hays GC. 2020. Phenological shuffling of major marine phytoplankton groups over the last six decades. *Diversity and Distributions* 26(5): 536-548.

Coello-Camba A, Agustí S, Vaqué D, Holding J, Arrieta JM, Wassmann P, Duarte CM. 2015. Experimental assessment of temperature thresholds for Arctic phytoplankton communities. *Estuaries and Coasts* 38(3): 873-885.

Collins S, Whittaker H, Thomas MK. 2022. The need for unrealistic experiments in global change biology. *Current Opinion in Microbiology* 68: 102151.

Constable AJ, Harper S, Dawson J, Holsman K, Mustonen T, Piepenburg D, Rost B, Bokhorst S, Boike J, Cunsolo A 2022. Cross-chapter paper 6: Polar regions. *IPCC AR WGII*: Cambridge University Press.

Cooley S, Schoeman D, Bopp L, Boyd P, Donner S, Ito S-i, Kiessling W, Martinetto P, Ojea E, Racault M-F 2022. Oceans and coastal ecosystems and their services. *IPCC AR6 WGII*: Cambridge University Press.

Coyne KJ, Salvitti LR, Mangum AM, Ozbay G, Main CR, Kouhanestani ZM, Warner ME. 2021. Interactive effects of light, CO_2 and temperature on growth and resource partitioning by the mixotrophic dinoflagellate, Karlodinium veneficum. *PloS one* 16(10): e0259161.

Cruz JA, Avenson TJ, Kanazawa A, Takizawa K, Edwards GE, Kramer DM. 2004. Plasticity in light reactions of photosynthesis for energy production and photoprotection. *Journal of experimental botany* 56(411): 395-406.

Curien G, Flori S, Villanova V, Magneschi L, Giustini C, Forti G, Matringe M, Petroutsos D, Kuntz M, Finazzi G. 2016. The water to water cycles in microalgae. *Plant and Cell Physiology* 57(7): 1354-1363.

Dahlke FT, Butzin M, Nahrgang J, Puvanendran V, Mortensen A, Pörtner H-O, Storch D. 2018. Northern cod species face spawning habitat losses if global warming exceeds 1.5 C. *Science Advances* 4(11): eaas8821.

Danielsdottir MG, Brett MT, Arhonditsis GB. 2007. Phytoplankton food quality control of planktonic food web processes. *Hydrobiologia* 589: 29-41.

Descamps-Julien B, Gonzalez A. 2005. Stable coexistence in a fluctuating environment: an experimental demonstration. *Ecology* 86(10): 2815-2824.

Descolas-Gros C, de Billy G. 1987. Temperature adaptation of RuBP carboxylase: kinetic properties in marine Antarctic diatoms. *Journal of experimental marine biology and ecology* 108(2): 147-158.

Devos N, Ingouff M, Loppes R, Matagne RF. 1998. RuBisCO adaptation to low temperatures: a comparative study in psychrophilic and mesophilic unicellular algae. *Journal of Phycology* 34(4): 655-660.

Dezutter T, Lalande C, Dufresne C, Darnis G, Fortier L. 2019. Mismatch between microalgae and herbivorous copepods due to the record sea ice minimum extent of 2012 and the late sea ice break-up of 2013 in the Beaufort Sea. *Progress in Oceanography* 173: 66-77.

Doney SC, Fabry VJ, Feely RA, Kleypas JA. 2009. Ocean acidification: the other CO2 problem. *Annual review of marine science* 1(1): 169-192.

References

Doney SC, Ruckelshaus M, Emmett Duffy J, Barry JP, Chan F, English CA, Galindo HM, Grebmeier JM, Hollowed AB, Knowlton N. 2012. Climate change impacts on marine ecosystems. *Annual review of marine science* 4: 11-37.

Edwards KF, Thomas MK, Klausmeier CA, Litchman E. 2016. Phytoplankton growth and the interaction of light and temperature: A synthesis at the species and community level. *Limnology and Oceanography* 61(4): 1232-1244.

Falciatore A, Bailleul B, Boulouis A, Bouly J-P, Bujaldon S, Cheminant-Navarro S, Choquet Y, de Vitry C, Eberhard S, Jaubert M. 2022. Light-driven processes: key players of the functional biodiversity in microalgae. *Comptes Rendus. Biologies* 345(2): 1-24.

Falkowski P, Scholes RJ, Boyle E, Canadell J, Canfield D, Elser J, Gruber N, Hibbard K, Högberg P, Linder S, et al. 2000. The Global carbon cycle: a test of our knowledge of earth as a system. *Science* 290(5490): 291-296.

Falkowski PG, Owens TG. 1980. Light—Shade Adaptation 1: Two strategies in marine phytoplankton. *Plant Physiology* 66(4): 592-595.

Falkowski PG, Owens TG, Ley AC, Mauzerall DC. 1981. Effects of growth irradiance levels on the ratio of reaction centers in two species of marine phytoplankton 1. *Plant Physiology* 68(4): 969-973.

Falkowski PG, Raven JA. 2013. *Aquatic photosynthesis*: Princeton University Press.

Feng H, Guan D, Sun K, Wang Y, Zhang T, Wang R. 2013. Expression and signal regulation of the alternative oxidase genes under abiotic stresses. *Acta Biochim Biophys Sin* 45(12): 985-994.

Field CB, Barros VR. 2014. *Climate change 2014–Impacts, adaptation and vulnerability: Regional aspects*: Cambridge University Press.

Field CB, Behrenfeld MJ, Randerson JT, Falkowski P. 1998. Primary production of the biosphere: integrating terrestrial and oceanic components. *Science* 281(5374): 237-240.

Flori S, Jouneau P-H, Bailleul B, Gallet B, Estrozi LF, Moriscot C, Bastien O, Eicke S, Schober A, Bártulos CR. 2017. Plastid thylakoid architecture optimizes photosynthesis in diatoms. *Nature Communications* 8(1): 15885.

Fock H, Sültemeyer D 1989. O_2 evolution and uptake measurements in plant cells by mass spectrometry. *Gases in plant and microbial cells*: Springer, 3-18.

Friedlingstein P, O'Sullivan M, Jones MW, Andrew RM, Bakker DCE, Hauck J, Landschützer P, Le Quéré C, Luijkx IT, Peters GP, et al. 2023. Global Carbon Budget 2023. *Earth Syst. Sci. Data* 15(12): 5301-5369.

Frölicher TL, Fischer EM, Gruber N. 2018. Marine heatwaves under global warming. *Nature* 560(7718): 360-364.

Galmés J, Hermida-Carrera C, Laanisto L, Niinemets Ü. 2016. A compendium of temperature responses of Rubisco kinetic traits: variability among and within photosynthetic groups and impacts on photosynthesis modeling. *Journal of experimental botany* 67(17): 5067-5091.

Garrabou J, Gómez-Gras D, Medrano A, Cerrano C, Ponti M, Schlegel R, Bensoussan N, Turicchia E, Sini M, Gerovasileiou V, et al. 2022. Marine

References

heatwaves drive recurrent mass mortalities in the Mediterranean Sea. *Global Change Biology* 28(19): 5708-5725.

Gattuso J-P, Heymans S, Natalie H, Neukermans G, Landschützer P, Pörtner H-O. 2023. *Blue Carbon: Challenges and opportunities to mitigate the climate and biodiversity crises.* European Marine Board.

Geider RJ. 1987. Light and temperature dependence of the carbon to chlorophyll *a* ratio in microalgae and cyanobacteria: implications for physiology and growth of phytoplankton. *New Phytologist*: 1-34.

Giesler JK, Harder T, Wohlrab S. 2023. Microbiome and photoperiod interactively determine thermal sensitivity of polar and temperate diatoms. *Biology Letters* 19(11): 20230151.

Graff JR, Westberry TK, Milligan AJ, Brown MB, Olmo GD, Reifel KM, Behrenfeld MJ. 2016. Photoacclimation of natural phytoplankton communities. *Marine Ecology Progress Series* 542: 51-62.

Grimaud GM, Mairet F, Sciandra A, Bernard O. 2017. Modeling the temperature effect on the specific growth rate of phytoplankton: a review. *Reviews in Environmental Science and Bio/Technology* 16(4): 625-645.

Guo R, Gu J, Zong S, Wu M, Yang M. 2018. Structure and mechanism of mitochondrial electron transport chain. *Biomedical journal* 41(1): 9-20.

Hahn A, Vonck J, Mills D, Meier T, Kuhlbrandt W 2018. Structure, mechanism, and regulation of the chloroplast ATP synthase. Science 360: eaat4318.

Hancke K, Glud RN. 2004. Temperature effects on respiration and photosynthesis in three diatom-dominated benthic communities. *Aquatic Microbial Ecology* 37(3): 265-281.

Hancke K, Hancke TB, Olsen LM, Johnsen G, Glud RN. 2008. Temperature effects on microalgal photosynthesis-light responses measured by O_2 production, pulse-amplitude-modulated fluorescence, and ^{14}C assimilation. *Journal of Phycology* 44(2): 501-514.

Harrison K, Sundstrom LM. 2007. The comparative politics of climate change. *Global Environmental Politics* 7(4): 1-18.

Hartmann D, Ramanathan V, Berroir A, Hunt G. 1986. Earth radiation budget data and climate research. *Reviews of Geophysics* 24(2): 439-468.

Hattich G, Jokinen S, Sildever S, Gareis M, Heikkinen J, Junghardt N, Segovia M, Machado M, Sjöqvist C. 2024. Temperature optima of a natural diatom population increases as global warming proceeds. *Nature Climate Change*: 1-8.

Hegarty T. 1973. Temperature coefficient (Q_{10}), seed germination and other biological processes. *Nature* 243(5405): 305-306.

Henson S, Le Moigne F, Giering S. 2019. Drivers of carbon export efficiency in the global ocean. *Global biogeochemical cycles* 33(7): 891-903.

Hermida-Carrera C, Kapralov MV, Galmés J. 2016. Rubisco catalytic properties and temperature response in crops. *Plant Physiology* 171(4): 2549-2561.

References

Hobbs JK, Jiao W, Easter AD, Parker EJ, Schipper LA, Arcus VL. 2013. Change in heat capacity for enzyme catalysis determines temperature dependence of enzyme catalyzed rates. *ACS Chemical Biology* 8(11): 2388-2393.

Hobday AJ, Alexander LV, Perkins SE, Smale DA, Straub SC, Oliver EC, Benthuysen JA, Burrows MT, Donat MG, Feng M. 2016. A hierarchical approach to defining marine heatwaves. *Progress in Oceanography* 141: 227-238.

Hoham RW, Remias D. 2020. Snow and glacial algae: a review1. *Journal of Phycology* 56(2): 264-282.

Holding JM, Duarte CM, Arrieta JM, Vaquer-Sunyer R, Coello-Camba A, Wassmann P, Agustí S. 2013. Experimentally determined temperature thresholds for Arctic plankton community metabolism. *Biogeosciences* 10(1): 357-370.

Hoppe CJ, Fuchs N, Notz D, Anderson P, Assmy P, Berge J, Bratbak G, Guillou G, Kraberg A, Larsen A. 2024. Photosynthetic light requirement near the theoretical minimum detected in Arctic microalgae. *Nature Communications* 15(1): 7385.

Hoppe CJM, Flintrop CM, Rost B. 2018. The Arctic picoeukaryote *Micromonas pusilla* benefits synergistically from warming and ocean acidification. *Biogeosciences* 15(14): 4353-4365.

Horwath M, Gutknecht BD, Cazenave A, Palanisamy HK, Marti F, Marzeion B, Paul F, Le Bris R, Hogg AE, Otosaka I. 2021. Global sea-level budget and ocean-mass budget, with focus on advanced data products and uncertainty characterisation. *Earth System Science Data Discussions* 2021: 1-51.

Irwin AJ, Finkel ZV, Schofield OME, Falkowski PG. 2006. Scaling-up from nutrient physiology to the size-structure of phytoplankton communities. *Journal of Plankton Research* 28(5): 459-471.

Iversen MH. 2023. Carbon Export in the Ocean: A Biologist's Perspective. *Annual review of marine science* 15(Volume 15, 2023): 357-381.

Iversen MH, Robert ML. 2015. Ballasting effects of smectite on aggregate formation and export from a natural plankton community. *Marine Chemistry* 175: 18-27.

Jensen PE, Leister D. 2014. Chloroplast evolution, structure and functions. *F1000prime reports* 6.

John EH, Wilson JD, Pearson PN, Ridgwell A. 2014. Temperature-dependent remineralization and carbon cycling in the warm Eocene oceans. *Palaeogeography, Palaeoclimatology, Palaeoecology* 413: 158-166.

Kahru M, Lee Z, Mitchell BG, Nevison CD. 2016. Effects of sea ice cover on satellite-detected primary production in the Arctic Ocean. *Biology Letters* 12(11): 20160223.

Keeling RF, Körtzinger A, Gruber N. 2010. Ocean deoxygenation in a warming world. *Annual review of marine science* 2(1): 199-229.

Kirst GO, Wiencke C. 1995. Ecophysiology of polar algae. *Journal of Phycology* 31(2).

Klaas C, Archer DE. 2002. Association of sinking organic matter with various types of mineral ballast in the deep sea: Implications for the rain ratio. *Global biogeochemical cycles* 16(4): 63-61-63-14.

Klenke M, Schenke HW. 2002. A new bathymetric model for the central Fram Strait. *Marine Geophysical Researches* 23(4): 367-378.

Koeve W. 2005. Magnitude of excess carbon sequestration into the deep ocean and the possible role of TEP. *Marine Ecology Progress Series* 291: 53-64.

Kok B, Forbush B, McGloin M. 1970. Cooperation of charges in photosynthetic O_2 evolution–I. A linear four step mechanism. *Photochemistry and Photobiology* 11(6): 457-475.

Kolber ZS, Prášil O, Falkowski PG. 1998. Measurements of variable chlorophyll fluorescence using fast repetition rate techniques: defining methodology and experimental protocols. *Biochimica et Biophysica Acta (BBA)-Bioenergetics* 1367(1-3): 88-106.

Kranz SA, Levitan O, Richter K-U, Prá¡ il O, Berman-Frank I, Rost B. 2010. Combined effects of CO_2 and light on the N_2-fixing cyanobacterium Trichodesmium IMS101: physiological responses. *Plant Physiology* 154(1): 334-345.

Krebs H. 1970. The history of the tricarboxylic acid cycle. *Perspectives in biology and medicine* 14(1): 154-172.

Kroth PG. 2015. The biodiversity of carbon assimilation. *Journal of Plant Physiology* 172: 76-81.

Kroth PG, Matsuda Y 2022. Carbohydrate metabolism. *The molecular life of diatoms*: Springer, 465-492.

Kumar S, Himanshu S, Gupta K. 2012. Effect of global warming on mankind-a review. *Int Res J Environ Sci* 1(4): 56-59.

Kvernvik AC, Hoppe CJM, Greenacre M, Verbiest S, Wiktor JM, Gabrielsen TM, Reigstad M, Leu E. 2021. Arctic sea ice algae differ markedly from phytoplankton in their ecophysiological characteristics. *Marine Ecology Progress Series* 666: 31-55.

Kvernvik AC, Rokitta SD, Leu E, Harms L, Gabrielsen TM, Rost B, Hoppe CJ. 2020. Higher sensitivity towards light stress and ocean acidification in an Arctic sea-ice-associated diatom compared to a pelagic diatom. *New Phytologist* 226(6): 1708-1724.

Kwok R. 2018. Arctic sea ice thickness, volume, and multiyear ice coverage: losses and coupled variability (1958–2018). *Environmental Research Letters* 13(10): 105005.

Lana A, Bell TG, Simó R, Vallina SM, Ballabrera-Poy J, Kettle AJ, Dachs J, Bopp L, Saltzman ES, Stefels J, et al. 2011. An updated climatology of surface dimethylsulfide concentrations and emission fluxes in the global ocean. *Global biogeochemical cycles* 25(1).

Larkum A, Szabó M, Fitzpatrick D, Raven J 2018. Cyclic electron flow in cyanobacteria and eukaryotic algae. *Photosynthesis and bioenergetics*: World Scientific, 305-343.

References

Laufkötter C, Vogt M, Gruber N, Aita-Noguchi M, Aumont O, Bopp L, Buitenhuis E, Doney SC, Dunne J, Hashioka T, et al. 2015. Drivers and uncertainties of future global marine primary production in marine ecosystem models. *Biogeosciences* 12(23): 6955-6984.

Le Moigne FA. 2019. Pathways of organic carbon downward transport by the oceanic biological carbon pump. *Frontiers in Marine Science* 6: 634.

Le Treut H, Somerville R, Cubasch U, Ding Y, Mauritzen C, Mokssit A, Peterson T, Prather M. 2007. Historical overview of climate change science. Chapter 1.

Lee H, Calvin K, Dasgupta D, Krinner G, Mukherji A, Thorne P, Trisos C, Romero J, Aldunce P, Barret K. 2023. IPCC, 2023: Climate Change 2023: Synthesis Report, Summary for Policymakers. Contribution of Working Groups I, II and III to the Sixth Assessment Report of the Intergovernmental Panel on Climate Change [Core Writing Team, H. Lee and J. Romero (eds.)]. IPCC, Geneva, Switzerland.

Lee Y, Min J-O, Yang EJ, Cho K-H, Jung J, Park J, Moon JK, Kang S-H. 2019. Influence of sea ice concentration on phytoplankton community structure in the Chukchi and East Siberian Seas, Pacific Arctic Ocean. *Deep Sea Research Part I: Oceanographic Research Papers* 147: 54-64.

Legg S. 2021. IPCC, 2021: Climate change 2021-the physical science basis. *Interaction* 49(4): 44-45.

Lepetit B, Campbell DA, Lavaud J, Büchel C, Goss R, Bailleul B 2022. Photosynthetic light reactions in diatoms. II. The dynamic regulation of the various light reactions. *The molecular life of diatoms*: Springer, 423-464.

Levitan O, Kranz SA, Spungin D, Prásil O, Rost B, Berman-Frank I. 2010. Combined Effects of CO_2 and light on the N_2-fixing cyanobacterium *Trichodesmium* IMS101: A Mechanistic View. *Plant Physiology* 154(1): 346-356.

Liang S, Wang D, He T, Yu Y. 2019. Remote sensing of earth's energy budget: synthesis and review. *International Journal of Digital Earth* 12(7): 737-780.

Liang Y, Koester JA, Liefer JD, Irwin AJ, Finkel ZV. 2019. Molecular mechanisms of temperature acclimation and adaptation in marine diatoms. *The ISME Journal* 13(10): 2415-2425.

Litchman E, de Tezanos Pinto P, Edwards KF, Klausmeier CA, Kremer CT, Thomas MK. 2015. Global biogeochemical impacts of phytoplankton: a trait-based perspective. *Journal of ecology* 103(6): 1384-1396.

Liu C, Zou D, Yang Y, Chen B, Jiang H. 2017. Temperature responses of pigment contents, chlorophyll fluorescence characteristics, and antioxidant defenses in *Gracilariopsis lemaneiformis* (Gracilariales, Rhodophyta) under different CO_2 levels. *Journal of Applied Phycology* 29(2): 983-991.

Los DA, Mironov KS, Allakhverdiev SI. 2013. Regulatory role of membrane fluidity in gene expression and physiological functions. *Photosynthesis research* 116(2): 489-509.

Lowenstein JM 1967. The tricarboxylic acid cycle. *Metabolic pathways*: Elsevier, 146-270.

References

Lund-Hansen LC, Søgaard DH, Sorrell BK, Gradinger R, Meiners KM, Lund-Hansen LC, Søgaard DH, Sorrell BK, Gradinger R, Meiners KM. 2020. Sea ice in a climate change context. *Arctic Sea Ice Ecology: Seasonal Dynamics in Algal and Bacterial Productivity*: 103-130.

MacIntyre HL, Kana TM, Anning T, Geider RJ. 2002. Photoacclimation of photosynthesis irradiance response curves and photosynthetic pigments in microalgae and cyanobacteria 1. *Journal of Phycology* 38(1): 17-38.

Marinov I, Doney SC, Lima ID. 2010. Response of ocean phytoplankton community structure to climate change over the 21st century: partitioning the effects of nutrients, temperature and light. *Biogeosciences* 7(12): 3941-3959.

Martin-Jézéquel V, Hildebrand M, Brzezinski MA. 2000. Silicon metabolism in diatoms: implications for growth. *Journal of Phycology* 36(5): 821-840.

Martin R. 2017. Basic structures of prokaryotic and eukaryotic cells. *Microreviews in Cell and Molecular Biology* 2(2).

Maxwell DP, Wang Y, McIntosh L. 1999. The alternative oxidase lowers mitochondrial reactive oxygen production in plant cells. *Proceedings of the National Academy of Sciences* 96(14): 8271-8276.

McLeod DJ, Hallegraeff GM, Hosie GW, Richardson AJ. 2012. Climate-driven range expansion of the red-tide dinoflagellate *Noctiluca scintillans* into the Southern Ocean. *Journal of Plankton Research* 34(4): 332-337.

Mehler AH. 1951. Studies on reactions of illuminated chloroplasts: I. Mechanism of the reduction of oxygen and other hill reagents. *Archives of Biochemistry and Biophysics* 33(1): 65-77.

Mitchell P. 1966. Chemiosmotic coupling in oxidative and photosynthetic phosphorylation. *Biological reviews* 41(3): 445-501.

Mitra A, Flynn KJ, Burkholder JM, Berge T, Calbet A, Raven JA, Granéli E, Glibert PM, Hansen PJ, Stoecker DK. 2014. The role of mixotrophic protists in the biological carbon pump. *Biogeosciences* 11(4): 995-1005.

Morel FM. 1987. Kinetics of nutrient uptake and growth in phytoplankton 1. *Journal of Phycology* 23(1): 137-150.

Moreno HD, Rokitta S, Tremblay N, Boersma M, Groß E, Klip HC, Wiltshire KH, Meunier CL. 2024. Higher temperature, increased CO_2, and changing nutrient ratios alter the carbon metabolism and induce oxidative stress in a cosmopolitan diatom. *Limnology and Oceanography* 69(1): 121-139.

Mundim KC, Baraldi S, Machado HG, Vieira FM. 2020. Temperature coefficient (Q_{10}) and its applications in biological systems: Beyond the Arrhenius theory. *Ecological Modelling* 431: 109127.

Murata N, Los DA. 1997. Membrane fluidity and temperature perception. *Plant Physiology* 115(3): 875.

Murik O, Tirichine L, Prihoda J, Thomas Y, Araújo WL, Allen AE, Fernie AR, Bowler C. 2019. Downregulation of mitochondrial alternative oxidase affects chloroplast function, redox status and stress response in a marine diatom. *New Phytologist* 221(3): 1303-1316.

References

Napiórkowska-Krzebietke A. 2017. Phytoplankton as a basic nutritional source in diets of fish. *Journal of Elementology* 22(3).

Naselli-Flores L, Padisák J, Albay M. 2007. Shape and size in phytoplankton ecology: do they matter? *Hydrobiologia* 578: 157-161.

Nawrocki WJ, Bailleul B, Picot D, Cardol P, Rappaport F, Wollman F-A, Joliot P. 2019. The mechanism of cyclic electron flow. *Biochimica et Biophysica Acta (BBA)-Bioenergetics* 1860(5): 433-438.

Nawrocki WJ, Tourasse NJ, Taly A, Rappaport F, Wollman F-A. 2015. The plastid terminal oxidase: its elusive function points to multiple contributions to plastid physiology. *Annual Review of Plant Biology* 66(1): 49-74.

Nicolaus M, Katlein C, Maslanik J, Hendricks S. 2012. Changes in Arctic sea ice result in increasing light transmittance and absorption. *Geophysical Research Letters* 39(24).

Niemi A, Bluhm BA, Juul-Pedersen T, Kohlbach D, Reigstad M, Søgaard DH, Amiraux R. 2024. Ice algae contributions to the benthos during a time of sea ice change: a review of supply, coupling, and fate. *Frontiers in Environmental Science* 12: 1432761.

Nikolova D, Weber D, Scholz M, Bald T, Scharsack JP, Hippler M. 2017. Temperature-induced remodeling of the photosynthetic machinery tunes photosynthesis in the thermophilic alga C*yanidioschyzon merolae. Plant Physiology* 174(1): 35-46.

Noctor G, Dutilleul C, De Paepe R, Foyer CH. 2004. Use of mitochondrial electron transport mutants to evaluate the effects of redox state on photosynthesis, stress tolerance and the integration of carbon/nitrogen metabolism. *Journal of experimental botany* 55(394): 49-57.

Noctor G, Foyer CH. 1998. Ascorbate and glutathione: keeping active oxygen under control. *Annual Review of Plant Biology* 49(1): 249-279.

Oliver EC, Burrows MT, Donat MG, Sen Gupta A, Alexander LV, Perkins-Kirkpatrick SE, Benthuysen JA, Hobday AJ, Holbrook NJ, Moore PJ. 2019. Projected marine heatwaves in the 21st century and the potential for ecological impact. *Frontiers in Marine Science* 6: 734.

Olson JM. 2006. Photosynthesis in the Archean Era. *Photosynthesis research* 88(2): 109-117.

Oxborough K. 2012. FastPro8 GUI and FRRf3 systems documentation. *Chelsea Technologies Group Ltd, West Molesey, UK*.

Oziel L, Baudena A, Ardyna M, Massicotte P, Randelhoff A, Sallée J-B, Ingvaldsen RB, Devred E, Babin M. 2020. Faster Atlantic currents drive poleward expansion of temperate phytoplankton in the Arctic Ocean. *Nature Communications* 11(1): 1705.

Padfield D, Yvon-Durocher G, Buckling A, Jennings S, Yvon-Durocher G. 2016. Rapid evolution of metabolic traits explains thermal adaptation in phytoplankton. *Ecology Letters* 19(2): 133-142.

Pearle P, Collett B, Bart K, Bilderback D, Newman D, Samuels S. 2010. What Brown saw and you can too. *American Journal of Physics* 78(12): 1278-1289.

References

Peltier G, Stoffel C, Findinier J, Madireddi SK, Dao O, Epting V, Morin A, Grossman A, Li-Beisson Y, Burlacot A. 2024. Alternative electron pathways of photosynthesis power green algal CO_2 capture. *The Plant Cell* 36(10): 4132-4142.

Peltier G, Tolleter D, Billon E, Cournac L. 2010. Auxiliary electron transport pathways in chloroplasts of microalgae. *Photosynthesis research* 106(1): 19-31.

Perovich DK, Polashenski C. 2012. Albedo evolution of seasonal Arctic sea ice. *Geophysical Research Letters* 39(8).

Petrou K, Kranz SA, Trimborn S, Hassler CS, Ameijeiras SB, Sackett O, Ralph PJ, Davidson AT. 2016. Southern Ocean phytoplankton physiology in a changing climate. *Journal of Plant Physiology* 203: 135-150.

Pi X, Zhao S, Wang W, Liu D, Xu C, Han G, Kuang T, Sui S-F, Shen J-R. 2019. The pigment-protein network of a diatom photosystem II–light-harvesting antenna supercomplex. *Science* 365(6452): eaax4406.

Priest T, von Appen W-J, Oldenburg E, Popa O, Torres-Valdés S, Bienhold C, Metfies K, Boulton W, Mock T, Fuchs BM. 2023. Atlantic water influx and sea-ice cover drive taxonomic and functional shifts in Arctic marine bacterial communities. *The ISME Journal* 17(10): 1612-1625.

Raghavendra AS, Padmasree K. 2003. Beneficial interactions of mitochondrial metabolism with photosynthetic carbon assimilation. *Trends in Plant Science* 8(11): 546-553.

Rantanen M, Karpechko AY, Lipponen A, Nordling K, Hyvärinen O, Ruosteenoja K, Vihma T, Laaksonen A. 2022. The Arctic has warmed nearly four times faster than the globe since 1979. *Communications Earth & Environment* 3(1): 168.

Raven JA, Beardall J. 2016. Dark respiration and organic carbon loss. *The physiology of microalgae*: 129-140.

Raven JA, Geider RJ. 1988. Temperature and algal growth. *New Phytologist* 110(4): 441-461.

Rehder L, Rokitta SD, Hoppe CJ, Buschmann I, Jasper L, Rost B. 2024. Different temperature sensitivities of key physiological processes lead to divergent trait response patterns in Arctic phytoplankton. *Limnology and Oceanography*.

Rehder L, Rost B, Rokitta SD. 2023. Abrupt and acclimation responses to changing temperature elicit divergent physiological effects in the diatom *Phaeodactylum tricornutum*. *New Phytologist* 239(3): 1005-1013.

Riebesell U, Gattuso J-P. 2015. Lessons learned from ocean acidification research. *Nature Climate Change* 5(1): 12-14.

Riebesell U, Zondervan I, Rost B, Tortell PD, Zeebe RE, Morel FM. 2000. Reduced calcification of marine plankton in response to increased atmospheric CO_2. *Nature* 407(6802): 364-367.

Rokitta SD, Grossmann CH, Werner E, Moye J, Castellani G, Nöthig E-M, Rost B. Future warming stimulates growth and photosynthesis in an Arctic microalga more strongly than changes in light intensity or pCO_2. *Limnology and Oceanography*.

References

Rokitta SD, Grossmann CH, Werner E, Moye J, Castellani G, Nöthig EM, Rost B. 2023. Future warming stimulates growth and photosynthesis in an Arctic microalga more strongly than changes in light intensity or pCO_2. *Limnology and Oceanography* 68(12): 2789-2799.

Rokitta SD, Kranz SA, Rost B. 2022. Inorganic carbon acquisition by aquatic primary producers. *Blue Planet, Red and Green Photosynthesis: Productivity and Carbon Cycling in Aquatic Ecosystems*: 81-132.

Ryan-Keogh TJ, Macey AI, Cockshutt AM, Moore CM, Bibby TS. 2012. The cyanobacterial chlorophyll-binding-protein isia acts to increase the in vivo effective absorption cross-section of PSI under iron limitation. *Journal of Phycology* 48(1): 145-154.

Sage RF. 2002. Variation in the k_{cat} of Rubisco in C3 and C4 plants and some implications for photosynthetic performance at high and low temperature. *Journal of Experimental Botany* 53(369): 609-620.

Schaum CE, Barton S, Bestion E, Buckling A, Garcia-Carreras B, Lopez P, Lowe C, Pawar S, Smirnoff N, Trimmer M, et al. 2017. Adaptation of phytoplankton to a decade of experimental warming linked to increased photosynthesis. *Nature Ecology & Evolution* 1(4): 0094.

Scheller HV, Haldrup A. 2005. Photoinhibition of photosystem I. *Planta* 221(1): 5-8.

Schober AF, Rio Bartulos C, Bischoff A, Lepetit B, Gruber A, Kroth PG. 2019. Organelle studies and proteome analyses of mitochondria and plastids fractions from the diatom *Thalassiosira pseudonana*. *Plant and Cell Physiology* 60(8): 1811-1828.

Schuback N, Tortell PD, Berman-Frank I, Campbell DA, Ciotti A, Courtecuisse E, Erickson ZK, Fujiki T, Halsey K, Hickman AE. 2021. Single-turnover variable chlorophyll fluorescence as a tool for assessing phytoplankton photosynthesis and primary productivity: opportunities, caveats and recommendations. *Frontiers in Marine Science* 8: 690607.

Shah I. 1974. *The elephant in the dark*: Octagon Press Ltd.

Sharpe PJ, DeMichele DW. 1977. Reaction kinetics of poikilotherm development. *Journal of theoretical biology* 64(4): 649-670.

Simon N, Cras A-L, Foulon E, Lemée R. 2009. Diversity and evolution of marine phytoplankton. *Comptes rendus biologies* 332(2-3): 159-170.

Smith KE, Burrows MT, Hobday AJ, Sen Gupta A, Moore PJ, Thomsen M, Wernberg T, Smale DA. 2021. Socioeconomic impacts of marine heatwaves: Global issues and opportunities. *Science* 374(6566): eabj3593.

Søgaard DH, Sorrell BK, Sejr MK, Andersen P, Rysgaard S, Hansen PJ, Skyttä A, Lemcke S, Lund-Hansen LC. 2021. An under-ice bloom of mixotrophic haptophytes in low nutrient and freshwater-influenced Arctic waters. *Scientific Reports* 11(1): 2915.

Solomon A, Heuzé C, Rabe B, Bacon S, Bertino L, Heimbach P, Inoue J, Iovino D, Mottram R, Zhang X. 2021. Freshwater in the Arctic Ocean 2010–2019. *Ocean Science* 17(4): 1081-1102.

References

Somero GN. 1978. Temperature adaptation of enzymes: biological optimization through structure-function compromises. *Annual Review of Ecology and Systematics* 9: 1-29.

Sommer U. 1996. Nutrient competition experiments with periphyton from the Baltic Sea. *Marine Ecology Progress Series* 140: 161-167.

Sommer U, Paul C, Moustaka-Gouni M. 2015. Warming and ocean acidification effects on phytoplankton—from species shifts to size shifts within species in a mesocosm experiment. *PloS one* 10(5): e0125239.

Sonoike K. 2011. Photoinhibition of photosystem I. *Physiologia Plantarum* 142(1): 56-64.

Søreide JE, Leu EV, Berge J, Graeve M, Falk-Petersen S. 2010. Timing of blooms, algal food quality and *Calanus glacialis* reproduction and growth in a changing Arctic. *Global Change Biology* 16(11): 3154-3163.

Sournia A. 1982. Form and function in marine phytoplankton. *Biological reviews* 57(3): 347-394.

Stoecker DK, Hansen PJ, Caron DA, Mitra A. 2017. Mixotrophy in the marine plankton. *Annual review of marine science* 9(1): 311-335.

Strock JP, Menden-Deuer S. 2021. Temperature acclimation alters phytoplankton growth and production rates. *Limnology and Oceanography* 66(3): 740-752.

Stroeve J, Notz D. 2018. Changing state of Arctic sea ice across all seasons. *Environmental Research Letters* 13(10): 103001.

Strotmann H, Murakami S 1976. Energy transfer between cell compartments. *Transport in Plants III: Intracellular Interactions and Transport Processes*: Springer, 398-416.

Suggett DJ, MacIntyre HL, Kana TM, Geider RJ. 2009. Comparing electron transport with gas exchange: parameterising exchange rates between alternative photosynthetic currencies for eukaryotic phytoplankton. *Aquatic Microbial Ecology* 56(2-3): 147-162.

Taiz L, Zeiger E. 2006. *Fisiologia vegetal*: Universitat Jaume I.

Tang J, Riley WJ. 2024. A chemical kinetics theory for interpreting the non-monotonic temperature dependence of enzymatic reactions. *Biogeosciences* 21(5): 1061-1070.

Thomas MK, Kremer CT, Klausmeier CA, Litchman E. 2012. A Global Pattern of Thermal Adaptation in Marine Phytoplankton. *Science* 338(6110): 1085-1088.

Thompson PA, Guo Mx, Harrison PJ, Whyte JN. 1992. Effects of variation in temperature. II. On the fatty acid composition of eight species of marine phytoplankton 1. *Journal of Phycology* 28(4): 488-497.

Tikhonov AN. 2014. The cytochrome b6f complex at the crossroad of photosynthetic electron transport pathways. *Plant Physiology and Biochemistry* 81: 163-183.

Toseland A, Daines SJ, Clark JR, Kirkham A, Strauss J, Uhlig C, Lenton TM, Valentin K, Pearson GA, Moulton V, et al. 2013. The impact of temperature on marine phytoplankton resource allocation and metabolism. *Nature Climate Change* 3(11): 979-984.

References

Trainer VL, Moore SK, Hallegraeff G, Kudela RM, Clement A, Mardones JI, Cochlan WP. 2020. Pelagic harmful algal blooms and climate change: Lessons from nature's experiments with extremes. *Harmful algae* 91: 101591.

Van Donk E, Ianora A, Vos M. 2011. Induced defences in marine and freshwater phytoplankton: a review. *Hydrobiologia* 668: 3-19.

van Vuuren DP, Edmonds J, Kainuma M, Riahi K, Thomson A, Hibbard K, Hurtt GC, Kram T, Krey V, Lamarque J-F, et al. 2011. The representative concentration pathways: an overview. *Climatic Change* 109(1): 5.

Vellai T, Vida G. 1999. The origin of eukaryotes: the difference between prokaryotic and eukaryotic cells. *Proceedings of the Royal Society of London. Series B: Biological Sciences* 266(1428): 1571-1577.

Visser AW, Kiørboe T. 2006. Plankton motility patterns and encounter rates. *Oecologia* 148: 538-546.

Volk T, Hoffert MI. 1985. Ocean carbon pumps: Analysis of relative strengths and efficiencies in ocean-driven atmospheric CO_2 changes. *The carbon cycle and atmospheric CO_2: Natural variations Archean to present* 32: 99-110.

Wagner H, Jakob T, Wilhelm C. 2006. Balancing the energy flow from captured light to biomass under fluctuating light conditions. *New Phytologist* 169(1).

Walter B, Peters J, van Beusekom JE. 2017. The effect of constant darkness and short light periods on the survival and physiological fitness of two phytoplankton species and their growth potential after re-illumination. *Aquatic Ecology* 51: 591-603.

Watson AJ, Liss PS. 1998. Marine biological controls on climate via the carbon and sulphur geochemical cycles. *Philosophical Transactions of the Royal Society of London. Series B: Biological Sciences* 353(1365): 41-51.

Weber EU. 2010. What shapes perceptions of climate change? *WIREs Climate Change* 1(3): 332-342.

Wolf KK, Hoppe CJ, Rost B. 2018. Resilience by diversity: Large intraspecific differences in climate change responses of an Arctic diatom. *Limnology and Oceanography* 63(1): 397-411.

Young JN, Goldman JA, Kranz SA, Tortell PD, Morel FM. 2015. Slow carboxylation of Rubisco constrains the rate of carbon fixation during Antarctic phytoplankton blooms. *New Phytologist* 205(1): 172-181.

Young JN, Schmidt K. 2020. It's what's inside that matters: physiological adaptations of high-latitude marine microalgae to environmental change. *New Phytologist* 227(5): 1307-1318.

Zeebe RE, Wolf-Gladrow D. 2001. *CO_2 in seawater: equilibrium, kinetics, isotopes*: Gulf Professional Publishing.

Zipfel W, Owens TG. 1991. Calculation of absolute photosystem I absorption cross-sections from P700 photo-oxidation kinetics. *Photosynthesis research* 29: 23-35.

Appendix

Supporting Information of *Publication I*

Table S1 Photosynthesis-irradiance- (PI-) parameters of *Thalassiosira hyalina*, *Micromonas pusilla* and *Nitzschia frigida*.

Table S2 Statistical parameters of linear and quadratic least squares regressions of *Thalassiosira hyalina*.

Table S3 Statistical parameters of linear and quadratic least squares regressions of *Micromonas pusilla*.

Tab. S4 Statistical parameters of linear and quadratic least squares regressions of *Nitzschia frigida*.

Fig. S1 Exemplary micrographs of cultivated *Nitzschia frigida*.

Fig. S2 Non-photochemical quenching (NPQ) of *Thalassiosira hyalina*, *Micromonas pusilla* and *Nitzschia frigida*.

Tab S1 Photosynthesis-irradiance- (PI-) parameters of *Thalassiosira hyalina, Micromonas pusilla* and *Nitzschia frigida.*

	Thalassiosira hyalina		*Micromonas pusilla*			*Nitzschia frigida*	
Temp	**α**	**ETR_{max}**	**α**	**ETR_{max}**	**Temp**	**α**	**ETR_{max}**
°C	µmol photons $m^{-2}\,s^{-1}$	$e^-\,PSII^{-1}\,s^{-1}$	µmol photons $m^{-2}\,s^{-1}$	$e^-\,PSII^{-1}\,s^{-1}$	°C	µmol photons $m^{-2}\,s^{-1}$	$e^-\,PSII^{-1}\,s^{-1}$
1.5	4.91±0.06	532±35	10.85±0.13	386±17	0	7.42±0.12	763±31
2.5	4.25±0.16	443±0.1	8.65±0.3	425±6	1.5	7.52±0.17	853±26
4	4.42±0.12	481±16	9.09±0.41	539±207	2.5	6.61±0.55	727±131
6	5.72±0.14	535±33	10.45±0.14	595±41	4		
8	5.44±0.40	654±71	9.52±0.29	440±68	5	7.73±0.27	1657±20
10	5.21±0.2	941±118	12.39±0.31	672±27	7	7.60±0.13	985±154
12	4.46	774	12.33±0.31	681±29	8.5	7.14±0.33	939±141
14			8.45	602	11	7.9±0.17	465±39

Tab S2 Statistical parameters obtained from linear or quadratic least squares regressions of functional trait parameters of *Thalassiosira hyalina*.

	POC	Chl *a*	μ*POC	sigma PSII	tau	F_v/F_m	ETR	E_k
				Thalassiosira hyalina				
fit	quadratic	quadratic	quardratic	quardratic	linear	quardratic	quadratic	quadratic
R²	0.68	0.5	0.7	0.65	0.98	0.68	0.52	0.73
SD	25.68	0.77	75.05	0.11	75.87	0.01	30.52	18.7
N	16	16	23	21	21	21	18	18
P	0.004	0.011	>0.0001	>0.0001	>0.0001	>0.0001	0.00424	>0.0001
T_{low}	2.5	2.5	1	1	1	1	1	1
T_{high}	10	10	12	12	12	12	12	12
Shape	U (between 2.5°C and 10°C)	U (between 2.5°C and 10°C)	bell	bell	linear decrease	bell	bell	increase beyond 8°C

Tab S3 Statistical parameters obtained from linear or quadratic least squares regressions of functional trait parameters of *Micromonas pusilla*.

	POC	Chl *a*	μ*POC	sigma PSII	tau	F_v/F_m	ETR	E_k
				Micromonas pusilla				
fit	quadratic	linear	quadratic	quadratic	linear	quadratic	quadratic	linear
R²	0.64	0.01	0.91	0.53	0.91	0.8	0.52	0.68
SD	2.56	3.19	1.87	0.43	284	0.02	65.14	7.79
N	18	21	18	22	22	22	22	21
P	0.0004	0.98	<0.0001	0.0007	<0.0001	<0.0001	0.001	0.0006
T_{low}	1	1	1	1	1	1	1	1
T_{high}	14	12	14	14	14	14	12	14
Shape	bell	none	bell	increase beyond 6°C	linear decrease	bell	bell	linear increase

Tab S4 Statistical parameters obtained from linear or quadratic least squares regressions of functional trait parameters of *Nitzschia frigida*.

	POC	Chl *a*	μ*POC	sigma PSII	tau	F_v/F_m	ETR	E_k
				Nitzschia frigida				
fit	linear	linear	quadratic	quadratic	linear	cubic	quadratic	quadratic
R²	0.84	0.41	0.41	0.45	0.93	0.98	0.53	0.63
SD	51.38	0.97	15.98	0.21	166	0.007	48.93	29.67
N	17	18	17	18	18	18	18	18
P	<0.0001	0.09	0.025	0.012	<0.0001	<0.0001	0.0034	0.0006
T_{low}	2	2	2	0	0	0	0	0
T_{high}	11	11	11	11	11	11	11	11
Shape	linear increase	none	bell	bell	linear decrease	decrease with plateau	bell	increase until 5.5°C
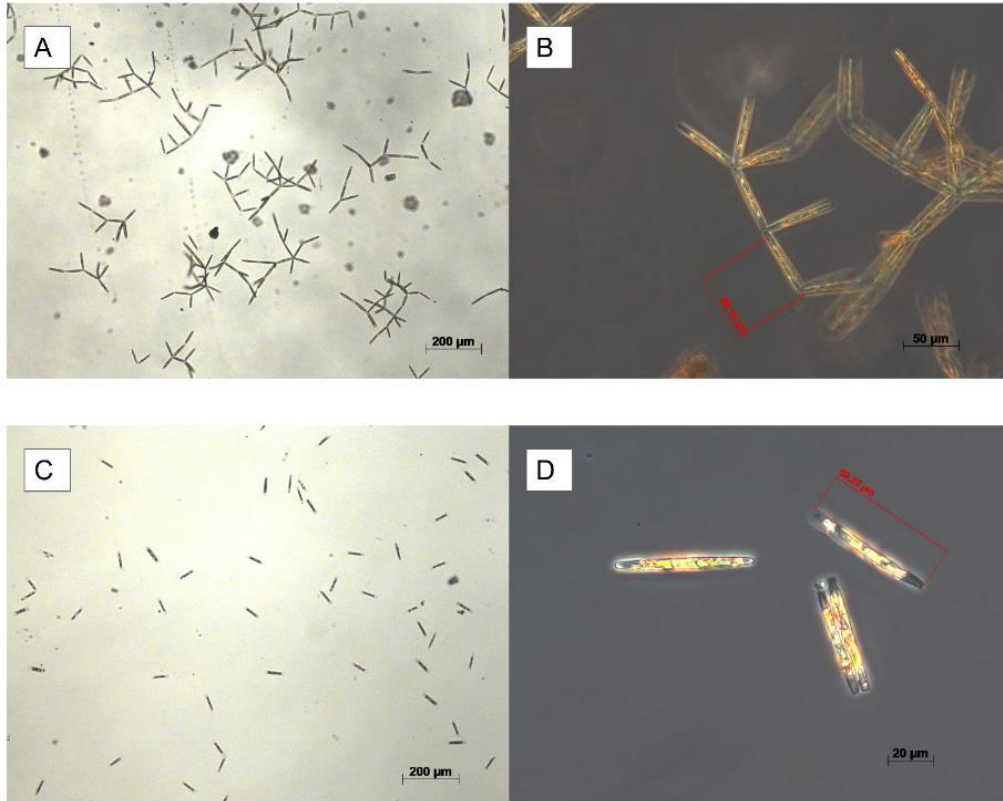
Fig. S1 Exemplary micrographs of cultivated *Nitzschia frigida*, 0°C (A and B) and 11°C (C and D), black bars indicate 200 µm (A, C), 50 µm (B) and 20 µm (D).
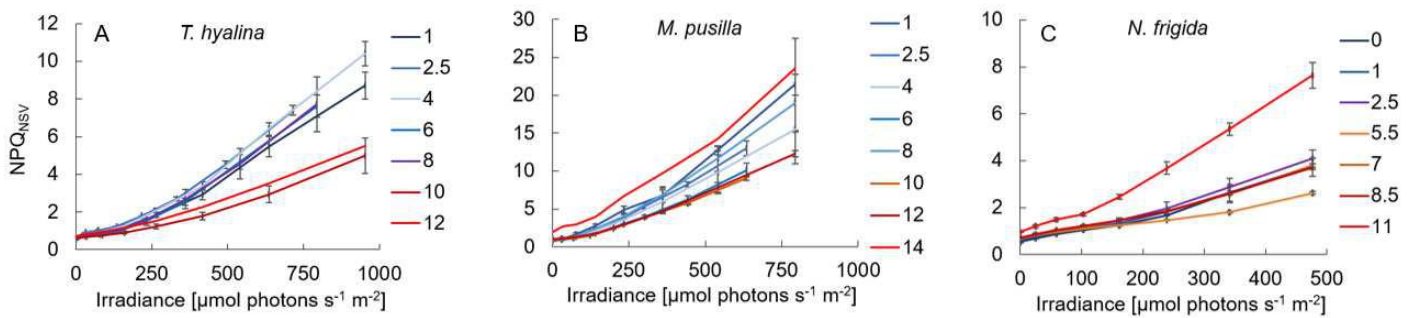

Fig. S2 Non-photochemical quenching (NPQ) of *Thalassiosira hyalina* (A), *Micromonas pusilla* (B) and *Nitzschia frigida* (C) at increasing irradiances obtained from a fluorescence light curve. Colors indicate acclimation temperatures, whereof blue reflects temperatures below growth optimum, purple reflects the optimum growth temperature and red reflects temperatures beyond growth optimum.
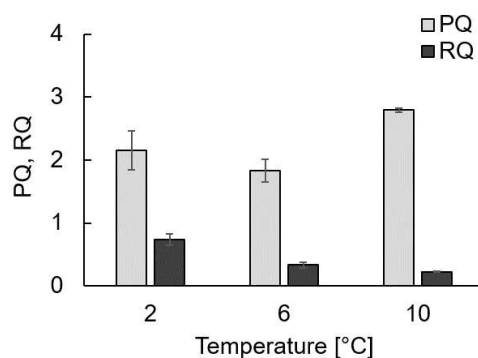
Supporting Information of *Publication II*

Fig S1. Relative electron transport rates (rETR) at in-situ light intensity of 30 µmol photons m^{-2} s^{-1} at different acclimation temperatures (2°C, 6°C and 10°C) in *Thalassiosira hyalina*.

Fig S2. Photosynthetic (PQ) and respiratory (RQ) quotients at in-situ light intensity of 30 µmol photons m^{-2} s^{-1} at different acclimation temperatures (2°C, 6°C and 10°C) in *Thalassiosira hyalina*.
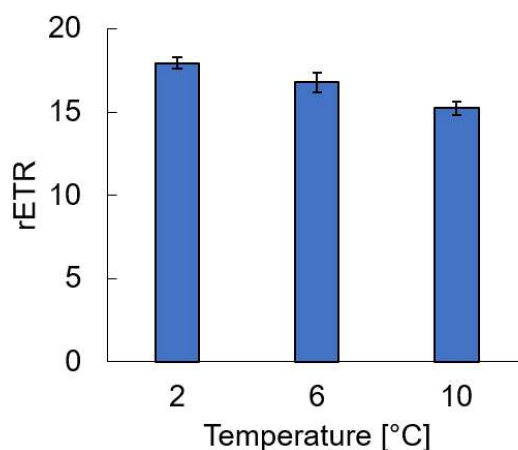
Fig S1. Relative electron transport rates (rETR) at in-situ light intensity of 30 µmol photons m^{-2} s^{-1} at different acclimation temperatures (2°C, 6°C and 10°C) in *Thalassiosira hyalina*.

Fig S2. Photosynthetic (PQ) and respiratory (RQ) quotients at in-situ light intensity of 30 µmol photons m^{-2} s^{-1} at different acclimation temperatures (2°C, 6°C and 10°C) in *Thalassiosira hyalina*.

Supporting Information of *Publication IV*

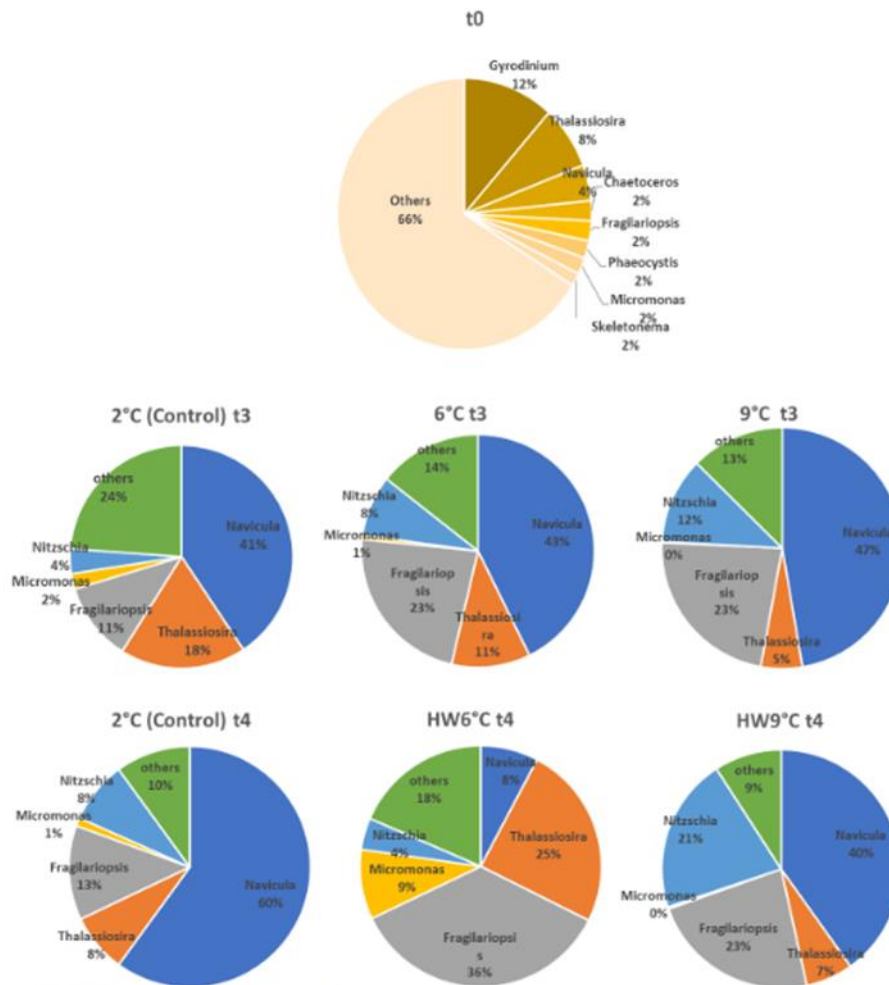**Fig S1.** Weighted means over time of additional parameters.

Fig S2. Relative composition of top 5 genera by treatments at initial timepoint and final timepoint.

Fig S3. Rates of Net primary production (NP; 14C), gross O_2 production (GP) and respiratory O_2 consumption in the dark (DR) at timepoint (t) 2 and 3 of the stable temperature treatments*.*
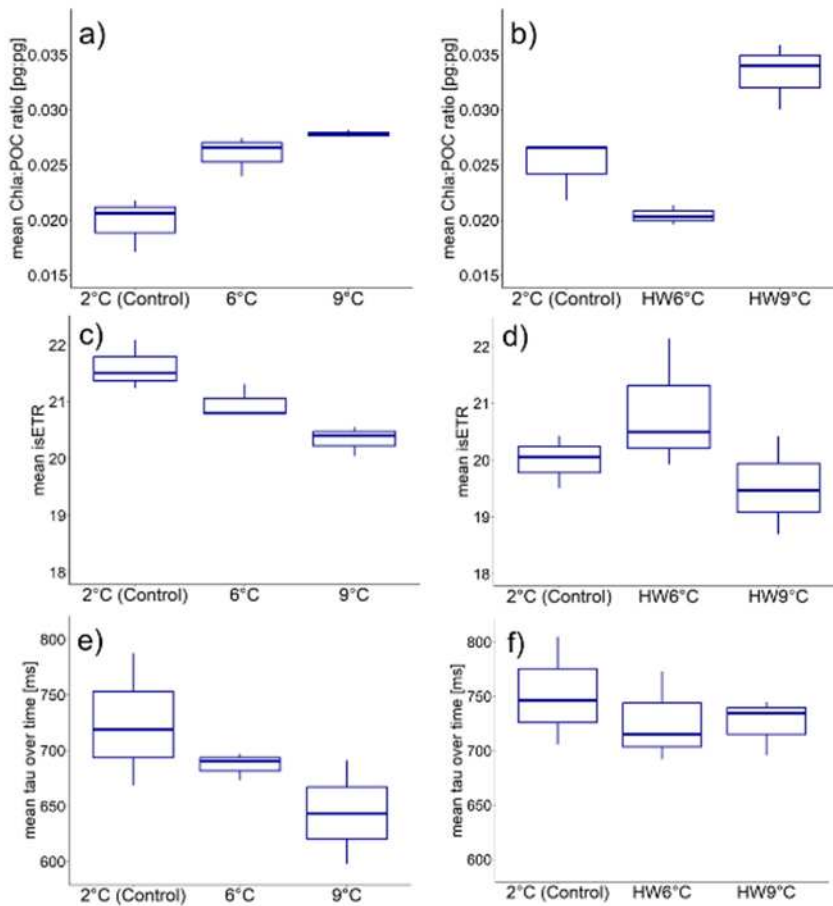

Fig S1. Weighted means over time of additional parameters. a) and b) Chl a:POC ratios, c) and d) relative electron transport rates at experimental light intensity, e) and f) PSII re-opening time. Left: stable temperature treatments, right: heatwave treatments.

Figure S2: Relative composition of top 5 genera by treatment
Relative composition of top 5 genera by treatment at the initial and final timepoint (t0: top 8 genera). Numbers describe relative abundance of assigned ASVs in percent.

Fig S2. Relative composition of top 5 genera by treatments at initial timepoint and final timepoint. Numbers describe relative abundance of assigned ASVs in percent.
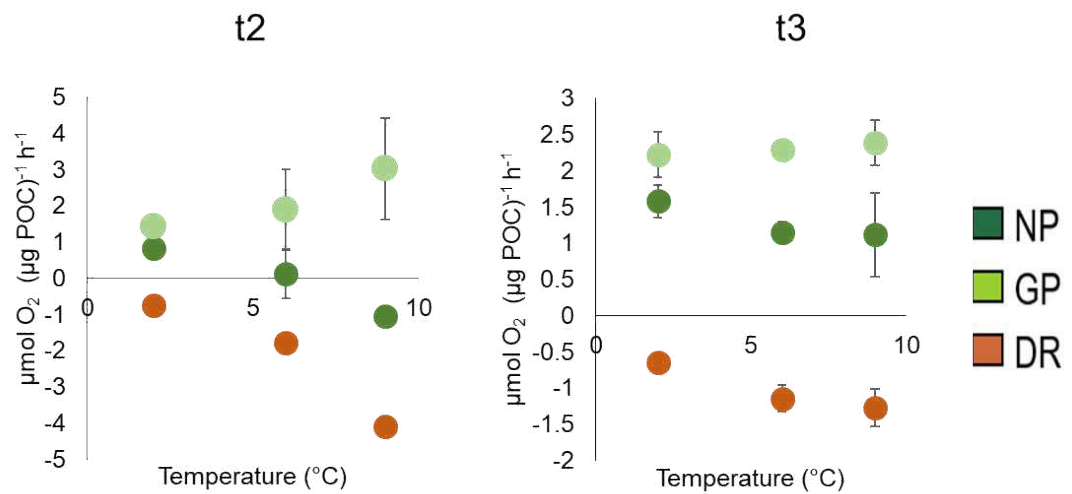
Fig S3. Rates of Net primary production (NP; 14C), gross O_2 production (GP) and respiratory O_2 consumption in the dark (DR) at timepoint 2 and 3 of the stable temperature treatments.

Declaration

Versicherung an Eides Satt

Name, Vorname	Rehder, Linda
Straße	███████████
Ort, PLZ	███████████

Ich, Linda Rehder,

versichere an Eides Statt durch meine Unterschrift, dass ich die vorstehende Arbeit selbständig und ohne fremde Hilfe angefertigt und alle Stellen, die ich wörtlich dem Sinne nach aus Veröffentlichungen entnommen habe, als solche kenntlich gemacht habe, mich auch keiner anderen als der angegebenen Literatur oder sonstiger Hilfsmittel bedient habe.

Ich versichere an Eides Statt, dass ich die vorgenannten Angaben nach bestem Wissen und Gewissen gemacht habe und dass die Angaben der Wahrheit entsprechen und ich nichts verschwiegen habe.

Die Strafbarkeit einer falschen eidesstattlichen Versicherung ist mir bekannt, namentlich die Strafandrohung gemäß §156 StGB bis zu drei Jahren Freiheitsstrafe oder Geldstrafe bei vorsätzlicher Begehung der Tat bzw. gemäß §161 Abs. 1 StGB bis zu einem Jahr Freiheitsstrafe oder Geldstrafe bei fahrlässiger Begehung.

_____	_____
Ort, Datum	Unterschrift

Contribution

Declaration on the contribution of the candidate to a multi-author article/manuscript. Contribution of the candidate in % of the total workload (up to 100% for each of the following categories).

Chapter 2, *Publication I*

Experimental concept and design: ca. 70%

Experimental work and/or acquisition of (experimental) data: ca. 70%

Data analysis and interpretation: ca. 80%

Preparation of Figures and Tables: ca. 95%

Drafting of the manuscript: ca. 85%

Chapter 3, *Publication II*

Experimental concept and design: ca. 90%

Experimental work and/or acquisition of (experimental) data: ca. 100%

Data analysis and interpretation: ca. 80%

Preparation of Figures and Tables: ca. 100%

Drafting of the manuscript: ca. 85%

Chapter 4, *Publication III*

Experimental concept and design: ca. 95%

Experimental work and/or acquisition of (experimental) data: ca. 100%

Data analysis and interpretation: ca. 75%

Preparation of Figures and Tables: ca. 75%

Drafting of the manuscript: ca. 85%

Chapter 5, *Publication IV*

Experimental concept and design: ca. 10%

Experimental work and/or acquisition of (experimental) data: ca. 50%

Data analysis and interpretation: ca. 10%

Preparation of Figures and Tables: ca. 10%

Drafting of the manuscript: ca. 10%